Solid-state nuclear magnetic resonance studies at ambient and cryogenic temperatures

Espidel M. Youssef Evelio,

SOLID-STATE NUCLEAR MAGNETIC RESONANCE STUDIES AT AMBIENT AND CRYOGENIC TEMPERATURES

BY

YOUSSEF EVELIO ESPIDEL M.

(GRADUATE SOCIETY)

B.Sc. Essex University (1978)

M.Sc. University of East Anglia (1982)

A thesis submitted for the degree of

Doctor of Philosophy

of the University of Durham

March 1990

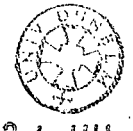

I dedicate this thesis to my very supportive family, and especially to my lovely daughter, Anita, for her patience and understanding during the last three and a half (and sometimes) difficult years. Also to my wife, Aída, for all her encouragement, hard work, and love which help me through all this time.

MEMORANDUM

The research presented in this thesis has been carried out at the Department of Chemistry of the University of Durham between October 1986 and February 1990. It is the original work of the author unless stated otherwise. None of this work has been submitted for any other degree.

SOLID-STATE NUCLEAR MAGNETIC RESONANCE STUDIES AT AMBIENT AND CRYOGENIC TEMPERATURES

by
YOUSSEF EVELIO ESPIDEL M.

Abstract

The research work presented in this thesis was concentrated on the study of solid materials at ambient temperature, and the study of matrix-isolated materials at cryogenic temperatures.

The first was directed to the examination of organolithium and organocopper compounds with particular interest in nuclear quadrupolar effects and their relation to molecular structure. All the compounds studied were air and moisture sensitive, which made necessary the design and construction of special rotor inserts to prevent the decomposition of these materials. A series of $LiBH_4X_n$ compounds were studied. They showed a good correlation between the symmetry of the Li-X bonds and the quadrupole coupling constants, which allows the prediction of molecular structures for some of the complexes.

The design and construction of an integrated NMR-cryogenic system was carried out for the deposition and study of matrix-isolated materials. A full description of the system and the way it is assembled is presented. A method to determine the sample temperature is introduced where the NMR signal from the deposited sample is used as a probe. CH_2Cl_2 and C_2H_4 in Ar matrices at different molar fractions were studied . The inter-proton distance was obtained for the CH_2Cl_2 case. This work also shows a relation between the degree of isolation and the multi-exponential T_1 behaviour.

ACKNOWLEDGEMENTS

I would like to thank my supervisor Prof. Robin K. Harris for all the guidance and support that kept me going during the period of this research.

I would like to thank "Funfación Gran Mariscal de Ayacucho" from the Venezuelan goverment for their financial support over the past three years and the six months extention period needed for the completion of this work, as well as Prof. Robin K. Harris for the financial support during the last six months.

I would like to express my gratitude to Prof. K. Wade from Durham University and Prof O. Stelzer for supplying the organolithium and organocopper complexes used in the investigation of samples at ambient temperatures.

I would also like to thank Prof. I. Beattie from the University of Southamptom for the technical support given in the area of high vacuum and matrix isolation.

The construction of the cryogenic could not have been done without the very important work done by the glass blower and engineering workshop to whom I give my thanks.

I am grateful to Barry Say and Alan Kenwright for the construction of the Wrac spectrometer system which was so important for the detection of the signals from the matrix-isolated material and for the long discussions related to this work. My thanks go also to Peter Clark for providing all the plotting routines used on the matrix-isolated data.

I thank all of the past and present members of the NMR research group at Durham for all the interesting discussions on general aspects of the related subject. In particular my thanks go to Peter Jackson for his contribution to my

understanding of the practical aspect of NMR and his personal support.

Finally, I would like to thank my parents, and Fozie and Nelson, for all their support over this period of time.

ABBREVIATIONS

The following have been used:

NMR	Nuclear Magnetic Resonance
B_o	External Magnetic Field
EFG	Electric Field Gradient
B_1	Radio Frequency Magnetic Field
RF	Radio Frequency
T_1	Spin-lattice Relaxation Time
T_2	Transverse Relaxation Time
Q_{cc}	Quadrupole Coupling Constant
MAS	Magic Angle Spining
HPPD	High Power Proton Decoupling
ω_R	Spinning Frequency
CP	Cross Polarization
TMS	Tetramethylsilane
STP	Spin Temperature Inversion
IR	Infra-red
UV	Ultra-violet
ESR	Electron Spin Resonance
psi	pound per square inch
K	Kelvin
T_m	Melting Point Temperature
fcc	face centred cubic
$\varkappa$	molar fraction
ppm	par per million
OFHP	Oxygen-Free, High-Purity
T	Temperature
CT	Contact Time

FID	Free Induction Decay
PAS	Principal Axis System
SE	Solid Echo

MEMORANDUM		i
ABSTRACT		ii
ACKNOWLEDGEMENTS		iii
ABBREVIATIONS		v
CHAPTER 1	INTRODUCTION	1
	INTRODUCTION	2
CHAPTER 2	THEORY OF NMR	7
2.1	CLASSICAL DESCRIPTION	8
2.2	QUANTUM MECHANIC DESCRIPTION	11
2.3	NUCLEAR SPIN HAMILTONIAN	13
2.3.1	INTERNAL HAMILTONIAN AXIS ROTATION	16
2.3.2	DIPOLAR INTERACTION	18
2.3.3	QUADRUPOLAR INTERACTION	23
2.4	HIGH RESOLUTION NMR IN SOLIDS	27
CHAPTER 3	SAMPLES AT AMBIENT TEMPERATURE	
	EXPERIMENTAL	32
3.1	NUCLEUS OF INTEREST	33
3.2	REFERENCE SAMPLES	34
3.2.1	PROTON	34
3.2.2	LITHIUM-7	35
3.2.3	LITHIUM-6	35
3.2.4	PHOSPHORUS-31	36
3.2.5	CARBON-13	36
3.3	SPECTROMETER DESCRIPTION	36
3.4	SAMPLE MANIPULATION	38
3.4.1	SPECIAL CONSIDERATIONS	38
3.4.2	CAPSULE DESIGN FOR ANDREW-BEAMS PROBES	41

3.4.3	CAPSULE DESIGN FOR DOUBLE-BEARING PROBES	42
3.5	PULSE SEQUENCES	53
3.5.1	SINGLE PULSE ACQUISITION	54
3.5.2	CROSS-POLARIZATION	54
CHAPTER 4	AMBIENT TEMPERATURE STUDIES: QUADRUPOLAR EFFECTS IN AIR SENSITIVE SAMPLES	59
4.1	INTRODUCTION	60
4.2	DIRECT QUADRUPOLAR EFFECTS	61
4.2.1	REFERENCE COMPOUNDS AND 90° PULSE SETTING	62
4.2.2	NMR STUDY OF $LiBH_4X$ COMPLEXES	63
4.2.2.1	NMR INVESTIGATON OF $[LiBH_4TMEDA]_2$	66
4.2.2.2	NMR INVESTIGATION OF $LiBH_4PMDETA$	83
4.2.2.3	NMR INVESTIGATION OF $LiBH_4PYR_4$ AND $LiBH_4HMPA_4$ COMPLEXES	94
4.3	INDIRECT QUADRUPOLAR EFFECTS	101
4.4	CONCLUSIONS	111
CHAPTER 5	MATRIX ISOLATION	115
5.1	INTRODUCTION	116
5.2	DESCRIPTION OF MATRIX ISOLATION	118
5.2.1	VACCUM SYSTEM	118
5.2.2	CRYOGENIC UNIT	120
5.2.3	TEMPERATURE MEASUREMENTS	124
5.3	DESCRIPTION OF MATRIX MATERIALS	125
5.3.1	MATRIX CHARACTERISTICS	125
5.3.2	STRUCTURE OF MATRIX MATERIALS	128
5.4	LITERATURE REVIEW OF NMR MATRIX ISOLATION	131

5.4.1	PROTON MATRIX ISOLATION STUDIES	132
5.4.2	CARBON-13 MATRIX ISOLATION STUDIES	136
5.4.2.1	C-13 MATRIX-ISOLATION STUDIES OF SMALL ORGANIC MOLECULES	137
5.4.2.3	OTHER CARBON-13 STUDIES	143
5.5	CONCLUSIONS	145
APPENDIX 5-A		151
CHAPTER 6	MATRIX ISOLATION: EXPERIMENTAL	155
6.1	NMR-CRYOGENIC SYSTEM DESIGN CONSIDERATIONS	156
6.2	NMR-CRYOGENIC SYSTEM-DESCRIPTION OF COMPONENTS	157
6.2.1	CRYOGENIC SYSTEM	157
6.2.2	VACUUM SYSTEM	167
6.2.3	NMR PROBE AND SAMPLE ACCESS	171
6.3	CRYOGENIC SYSTEM ASSEMBLY	176
6.4	SYSTEM TESTING AND ROUTINE RUNNING	185
6.4.1	VACUUM SYSTEM TESTING	185
6.4.2	CRYOGENIC SYSTEM TESTING	186
6.5	SAMPLE PREPARATION AND DEPOSITION	190
6.6	SPECTROMETER DESCRIPTION AND DATA ACQUISITION	193
CHAPTER 7	MATRIX ISOLATION: APPLICATION PROTON STUDIES	198
7.1	INTRODUCTION	199
7.2	SPECTROMETER EXPERIMENTAL CONDITIONS	200
7.2.1	MAGNETIC FIELD HOMOGENEITY	200

7.2.2	PULSE SEQUENCES	203
7.2.3	SIGNAL INTENSITY AND LINE-SHAPE DISTORTIONS	207
7.3	DETERMINATION OF SAMPLE TEMPERATURE	208
7.3.1	T_1 MEASUREMENTS AND MOLECULAR MOTION	223
7.4.	STUDY OF DICHLOROMETHANE AND ETHYLENE IN ARGON MATRIX	227
7.4.1	MATRIX ISOLATION STUDY OF CH_2Cl_2	227
7.4.1.1	LINE-SHAPE AND INTER PROTON DISTANCE	230
7.4.1.2	SPIN-LATTICE RELAXATION STUDY	244
7.4.2	MATRIX ISOLATION STUDY OF C_2H_4	251
7.5	IMPROVEMENT TO THE NMR-CRYOGENIC SYSTEM	257
7.5.1	VACUUM SYSTEM MODIFICATIONS	257
7.5.2	SAPPHIRE COLD FINGER MODIFICATION	260
7.5.3	OTHER NUCLEI	261
7.6	CONCLUSIONS	262
APPENDIX 7-A		265
APPENDIX 7-B		277

CHAPTER 1

INTRODUCTION

INTRODUCTION:

The research work presented in this thesis has been concentrated in two main areas of solid-state nuclear magnetic resonance. First, solid materials at ambient temperature were studied with special interest in the nuclear quadrupole interaction observed in some organolithium and organocopper complexes. In the past, it was difficult to carry out this type of study in systems such as these, due to the fact that they are very air and moisture sensitive, especially in the case of organolithium complexes. The manipulation of air sensitive material has been addressed by several authors in the past and in all cases the solution involves the use of glass sealed capsules. They are very difficult to use in commercially available spectrometers and in particular for high-resolution NMR systems. This problem has been made easier by the introduction of a new rotor insert design made during the period of this investigation from polymeric materials. Such inserts ensure the integrity of the samples for long periods of time. In this way, a series of $LiBH_4X_n$ complexes was studied for the first time using high-resolution NMR spectroscopy with the particular interest of observing signals from ^6Li and ^7Li isotopes.

Secondly, matrix-isolated materials at cryogenic temperature were also studied by solid-state NMR. To this end, an integrated NMR-cryogenic system was designed and constructed for the deposition of such matrix materials. The main characteristic of this system is the ability of being able to deposit one sample after another without dismantling

the system, i.e. it is always under a dynamic vacuum. This will allow a considerable reduction in the time between the evaporation of one sample and the deposition of the next. Two samples at different molar concentrations were studied with this system, namely dichloromethene and ethylene. The intra-molecular dipolar interaction present in this type of system was studied and values of inter-proton distance were obtained from the well-known 'Pake' pattern observed.

The Thesis has been divided into six chapters and a short description of their contents is now presented.

Chapter two will be dedicated to a general description of the relevant NMR theory for the solid-state. A description of the different nuclear spin interactions will be presented, in particular the dipolar interaction (homonuclear and heteronuclear) as well as the quadrupolar interaction. Some description will also be presented in respect to the techniques used in high-resolution NMR.

Chapter three will introduce the experimental conditions needed for the study of the samples at ambient temperature. NMR properties for the different nuclei will be presented as well as the reference compounds used in each case. This chapter will also include the steps followed in the design and testing of the new rotor inserts which play an important part in the study of air sensitive materials. This will be followed by a description of the different pulse sequences used in the investigation of this type of sample.

Chapter four will contain the discussion of the results obtained from the organolithium and organocopper complexes. In particular, direct and indirect nuclear quadrupolar interaction effects are observed in these systems. For the direct case, four $LiBH_4X_n$ complexes were studied with the aid of the new rotor inserts. Crystallographic data were used in some cases to estimate the dipolar interactions between the lithium nucleus and its near neighbours in an effort to predict the effect that such interactions may produce in the Li spectra. The relation between the symmetry of the lithium environment and the quadrupole coupling constant are also discussed.

The indirect quadrupolar interaction between ^{31}P and Cu was investigated in two organocopper complexes, and a description of this effect is also presented. It was possible to measure the indirect or 'scalar' coupling constant between the two nuclei as well as to predict the value of the true chemical shift for the ^{31}P spectra.

Chapter five will be divided into two main parts. The first will be dedicated to a detailed description of the matrix isolation technique. This will include a description of the minimum system requirements needed for the isolation of the material, such as vacuum system, and ways of obtaining the cryogenic temperatures. A description of the matrix materials is presented, which includes their characteristics and expected structures. The second part of the chapter will be dedicated to a literature review of the NMR matrix-isolated studies made up to present time. The review will cover the

studies carried out in ^{1}H and ^{13}C nuclei in both stable molecules as well as in reaction intermediate.

Chapter six will present a detailed description of the new NMR-cryogenic system needed for the isolation of matrix materials. This will include the design and construction of the vacuum and cryogenic facilities, NMR probe system capable of being coupled directly to the vacuum system, and the way of introducing the matrix samples to the probe area. The chapter will also contain a step-by-step description of the assembly of the system, as well as the testing carried out to the system. A description of the NMR spectrometer for data acquisition is presented.

Finally, chapter seven will contain the results and discussion of the data obtained from the matrix-isolation of materials using the NMR-cryogenic system described in chapter six. It will include the spectrometer conditions like magnetic field homogeneity and the different pulse sequences used in this study. The distortions of the NMR signal obtained from strongly coupled proton systems is discussed as well as methods to prevent them.

A new method to determine the sample temperature is presented in which the proton NMR signal from a deposited sample is used as a probe. The linear correlation of the signal intensity as a function of the inverse temperature is used to determine the temperature gradient between the sample location and the position of the temperature measuring device.

Finally, the effect of sample dilution and method of

deposition on the NMR line-shape were studied for the cases of dichloromethene and ethylene. The line-shape from the CH_2Cl_2, matrices show the well-known 'Pake' doublet pattern. The value for the splitting of the doublet was used to calculate the inter-proton distance and the results were compared with those from the literature. A relationship was established between the degree of isolation of the CH_2Cl_2 molecules inside the matrix and the multi-component behaviour of the spin-lattice relaxation time, T_1.

CHAPTER 2

THEORY OF NMR

2.1 CLASSICAL DESCRIPTION:

The presence of a nuclear spin in a nucleus could be regarded as one of the fundamental properties as far as nuclear magnetic resonance (NMR) is concerned . The range of values that it can have depends upon the mass and the atomic number, i.e. odd mass and even or odd atomic number gives half integer nuclear spins, whereas even mass and odd atomic number gives as a result integer spin; the remaining combination gives I=0. The presence of I=0 is a very important fact because nuclei like ^{12}C, ^{16}O, and ^{32}S have it. Therefore, NMR signals are not observed from them which makes very much simpler the study of organic material . Nuclei with I=1/2 have dipolar moments whereas those with I≥1 also possess electrical quadrupole moments. This effect is produced by the presence of a non-spherical distribution of charges around the nucleus which can interact with electric field gradients (EFG) giving rise to very broad lineshapes even in the liquid state.

So, all nuclei that have a nuclear spin have a magnetic moment, μ, associated to them given by

$$\mu = \gamma \hbar I \qquad 2.1$$

where $\hbar$ is Planck's constant divided by 2π

γ is the magnetogyric ratio, particular for each nucleus.

In the presence of a strong external magnetic field, B_o, the magnetic moment will precess along the field direction at a characteristic frequency for each nucleus known as the Larmor frequency and it can be expressed as

$$\omega_o = -\gamma B_o \qquad 2.2$$

or

$$\nu_o = -\gamma B_o/2\pi \quad \text{(in Hz)}$$

In the case I=1/2, there are two possible orientations for the nuclear spin, i.e. ± 1/2. In an ensemble of like nuclei and because of the Boltzmann distribution of spins, there will be more spins in the lower state than in the upper state, and a net magnetization, $M=\sum_i \mu_i$, will be formed in the direction of the external magnetic field. It is the behaviour of this magnetization when manipulated by an additional radio frequency field, B_1, rotating in the plane (xy) perpendicular to M_o (in the z direction) with a frequency ω, that is of very important interest in NMR.

The effects of these two fields on the magnetization were studied phenomenologically by Bloch[1] where the torque experienced by magnetic moment from B_o field was expressed as the solution of the classical equation of motion

$$dp/dt = \mu \times B \qquad 2.3$$

where $dp/dt=(d\mu/dt)/\gamma$ is the rate of change of the angular momentum.

The external magnetic field is composed of the static and the RF magnetic field, so that

$$B = B_x + B_y + B_z \qquad 2.4$$
$$= B_1\cos\omega t - B_1\sin\omega t + B_o$$

For a macroscopic sample, it is necessary to express eq. 2.3 in terms of the total magnetization, and if its

vectorial product is also expanded it gives

$$\begin{aligned} dM_x/dt &= \gamma(M_y B_o + M_z B_1 \sin \omega t), \\ dM_y/dt &= \gamma(M_z B_1 \cos \omega t - M_z B_o) \\ dM_z/dt &= -\gamma(M_x B_1 \sin \omega t + M_y B_1 \cos \omega t) \end{aligned} \qquad 2.5$$

There is an extra factor that needs to be considered for the completion of the expression of the magnetization . This comes from the fact that after the magnetization has been displaced from equilibrium by the radio frequency field (RF) and this field has been turned off, the magnetization has to relax back to the original state . Two different mechanisms are involved in this process, each one having its own time constant. The first is the one that controls the magnetization's dephasing in the xy plane perpendicular to B_o, known as spin-spin or transverse relaxation time, T_2. The second is that determining the return of M_z to its equilibrium values of M_o along the direction of B_o, known as spin-lattice relaxation time T_1. Introducing these two time constants into the equation 2.5 gives as a result

$$\begin{aligned} dM_x/dt &= \gamma(M_y B_o + M_z B_1 \sin \omega t) - M_x/T_2, \\ dM_y/dt &= \gamma(M_z B_1 \cos \omega t - M_z B_o) - M_y/T_2, \\ dM_z/dt &= -\gamma(M_x B_1 \sin \omega t + M_y B_1 \cos \omega t) \\ &\quad -(M_z - M_o)/T_1. \end{aligned} \qquad 2.6$$

The solutions of these coupled differential equations give the well-known Lorentzian absorption lineshape which is in phase with the excitation RF field, and the dispersion lineshape which is 90° out of phase with respect to the previous one. The observed half width at half height, $\Delta\nu_{1/2}$,

of the absorption line is given by

$$\Delta\nu_{1/2} = (\pi T_2^*)^{-1} \qquad 2.7$$

where $1/T_2^*$ is the sum of the natural relaxation rate $1/T_2$ and the relaxation produced by magnetic field inhomogeneity.

It is important to bring up some points at this moment. The above equations (2.6) are good representations for the behaviour of the magnetization in the liquid phase but not in the solid. This is because in isotropic liquids molecular motion averages out almost all interactions and allows sharp lines to be observed. Also in liquids, the two relaxation constants usually have the same values whereas in the solid they have markedly different values, with T_2 being the shorter time , as low as 10's of microseconds. In the solid, molecular interactions are very strong, and as a result, they give very broad spectral lines that can run for 100's of ppm.

2.2 QUANTUM MECHANICS DESCRIPTION:

As mentioned in the above section, the classical description of the NMR phenomena is not adequate to explain what is really happening in the solid state. Thus, it is necessary to use quantum mechanics to have a complete understanding of all the possible interactions present.

For a nucleus with spin quantum number I, the presence of an external magnetic field will result in the splitting of the zero-field energy into different levels[2,3]. As energy is

quantised, only a discrete number levels are possible given by $m_I = 2I+1$; the energy separation of the levels separation can be expressed as $\Delta E = \mu\hbar B_o$. This is shown graphically, for $I=1/2$, in Fig (2.1).

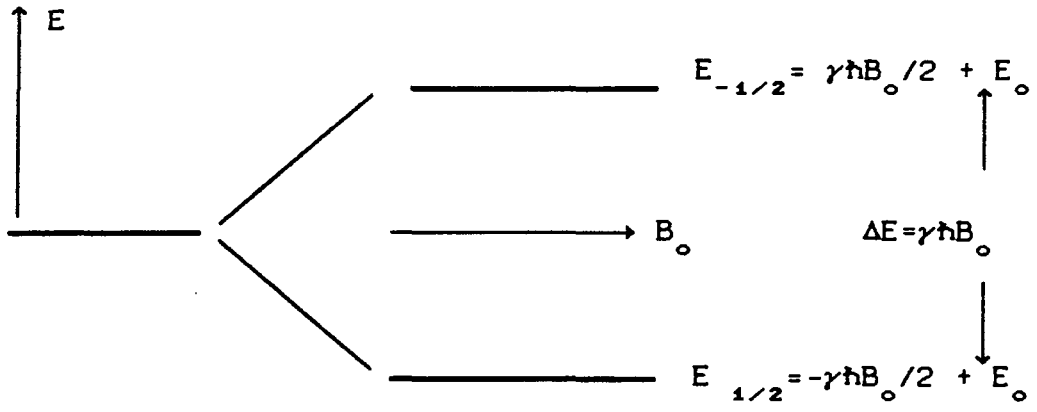

Fig (2.1) Quantum mechanical representation of the energy level diagram for $I=1/2$

In quantum mechanical terms, this is given by the expression

$$\mathcal{H}_z = -\sum_i \gamma_i \hbar B_o I_i \qquad 2.8$$

known as Zeeman Hamiltonian, which has been written to take into account the total number of spin in the sample. This is the simplest and the strongest of all nuclear spins interaction and they will be described in detail in the next section.

2.3 NUCLEAR SPIN HAMILTONIAN:

The total spin Hamiltonian can be divided into a sum of two terms,

$$\mathcal{H}_T = \mathcal{H}_{ext} + \mathcal{H}_{int} \qquad 2.9$$

namely the external and the internal Hamiltonians. The first term is composed of the Zeeman interaction from two external magnetic fields, the static field B_o, and the RF field B_1.

The second term involves all the interactions that come from within the sample. They are smaller than the external interaction and usually treated as perturbation to the Zeeman term. These can be identified as: i) the dipole-dipole interaction between two nuclear magnetic moments, either equal or different, which are separated by distance r; ii) the indirect spin-spin coupling or J coupling (the anisotropy in J can not be distinguished from the dipolar interaction); iii) the shielding interaction which is produced by the screening of the magnetic moment by the surrounding electrons; iv) the quadrupolar interaction between the nuclear quadrupole moment and the electric field gradient around the nucleus.(This is the only type of interaction that can be bigger than the Zeeman interaction and its study is a spectroscopic field in its own right); and finally v) the spin-rotation interaction between the nuclear spin and the magnetic moment produced by the angular momentum. In summary the total spin Hamiltonian can be written as

$$\hat{\mathcal{H}}^{T} = \hat{\mathcal{H}}^{Z} + \hat{\mathcal{H}}^{RF} + \hat{\mathcal{H}}^{D} + \hat{\mathcal{H}}^{J} + \hat{\mathcal{H}}^{S} + \hat{\mathcal{H}}^{Q} + \hat{\mathcal{H}}^{SR} \qquad 2.10$$

where Z =Zeeman
RF= Radio Frequency
D =Dipolar
J =Indirect Spin-Spin
S =Shielding
Q =Quadrupolar
SR=Spin-Rotation

It is important to realize that all these interactions can be represented as second rank Cartesian tensors[3] (R^{λ}) (a 3×3 matrix) so that the individual Hamiltonians can be written as

$$\hbar^{-1}\hat{\mathcal{H}}^{\lambda} = (I_x + I_y + I_z) \begin{bmatrix} R_{xx} & R_{xy} & R_{xz} \\ R_{yx} & R_{yy} & R_{yz} \\ R_{zx} & R_{zy} & R_{zz} \end{bmatrix} \begin{bmatrix} S_x \\ S_y \\ S_z \end{bmatrix} \qquad 2.11$$

where the first term is the spin vector of the nucleus of interest; the second term is the second rank tensor representing the interaction; and the third is a second interacting vector.

After expanding the above product it is possible to express the Hamiltonian in a more compact way as

$$\hbar^{-1}\hat{\mathcal{H}}^{\lambda} = \hat{C}^{\lambda} \sum_{\alpha\beta} I_{\alpha} R^{\lambda}_{\alpha\beta} S^{\lambda}_{\beta} \qquad 2.12$$

where $\alpha,\beta = x,y,z$

where $\hat{I}$ are the nuclear spin operators and S^{λ} is a vector that can be of several kinds: it could be a different nuclear spin as in the case of the dipolar interaction, or the same as I as in the quadrupole case, or even the external magnetic field B_o as in the case of the shielding interaction. C^{λ} is a constant

characteristic of each interaction. It is possible to see that the $\underline{R}_{\alpha\beta}$ is a 9-component tensor. Most tensors are symmetric ($R_{\alpha\beta}=R_{\beta\alpha}$), which gives the possibility of selecting a suitable axis system so that a diagonal tensor can be obtained. This system is known as the principal axis system (PAS). Given this fact, it is important to define three main properties of these tensors. But before this, it is necessary to define the trace of a tensor as

$$Tr\underline{R} = R_{xx} + R_{yy} + R_{zz} \qquad 2.13$$

From this equation it is possible to define the isotropic average as

$$R_{iso} = Tr\underline{R}/3 \qquad 2.14$$

a value that is observed in solution for both the chemical shift and the scalar coupling constant. It is important to label axes of the PAS appropriately and the most common convention is that adopted by Haeberlen[4] where

$$|R_{zz} - R_{iso}| \geq |R_{xx} - R_{iso}| \geq |R_{yy} - R_{iso}| \qquad 2.15$$

This leaves the last two properties to define, namely the anisotropy (δ or ΔR) and the asymmetry (η) given by the expressions

$$\delta = R_{zz} - R_{iso} \qquad 2.16$$

$$\text{and } \eta = (R_{yy} - R_{xx})/\delta \qquad 2.17$$

$$\text{where } 0 \leq \eta \leq 1$$

When $\eta=0$, the tensor is called axially symmetric and its principal components are defined as $R_{xx} = R_{yy} = R_{\perp}$ and $R_{zz} = R_{\parallel}$. A summary of all the interactions and their related tensors is

presented in Table (2.1).

For the remainder of this chapter we will only be concerned with the dipolar, and quadrupole interaction.

Name of the Interaction	λ	C^{λ}	$R^{\lambda}_{\alpha\beta}$	(units)	S^{λ}
Dipolar	D	$\gamma_i\gamma_k\hbar\frac{\mu_o}{4\pi}r^{-3}$	$D_{\alpha\beta}$	(none)	S^1
Indirect Spin-Spin	J	2π	$J_{\alpha\beta}$	(Hz)	S^1
Shielding	S	γ	$\sigma_{\alpha\beta}$	(none)	Bo
Quadrupole	Q	$\frac{e^2Q}{2I(2I-1)\hbar}$	$V_{\alpha\beta}$ $\sum_{\alpha} V_{\alpha\alpha}=0$	(q in Vm^{-2})	I^1
Spin-Rotation	SR	2π	$C_{\alpha\beta}$	(Hz)	J

Table (2.1) Nuclear-spin interactions and their related tensors

2.3.1 INTERNAL HAMILTONIAN AXIS ROTATION:

The two possible vectors interacting with the tensor $\underline{R}$ are defined in the laboratory frame of reference (LAB), so the tensor also needs to be expressed in this way. For this transformation it is best to represent the tensors in spherical form[5], and so they can be reduced to $\underline{R}= R^{(0)}+R^{(1)}+R^{(2)}$ with scalar part

$$R^{(0)}= R_{iso} \qquad 2.18$$

recognizing that this component is invariant to rotation, an antisymmetric tensor, $R^{(1)}$, which is usually ignored, and finally a symmetric tensor, $R^{(2)}$, which has five components defined as

$$\begin{aligned} \rho_2^{(2)} &= \rho_{-2}^{(2)} = (1/2)\eta\delta \\ \rho_1^{(2)} &= \rho_{-1}^{(2)} = 0 \\ \rho_0^{(2)} &= \sqrt{3/2}\,\delta \end{aligned} \qquad 2.19$$

It is also convenient to rewrite eq. 2-12 in the form of

$$\hbar^{-1}\hat{\mathcal{H}}^{\lambda} = C^{\lambda} \sum_{\alpha\beta} R^{\lambda}_{\alpha\beta} T^{\lambda}_{\alpha\beta} \qquad 2.20$$

where $\alpha,\beta = x,y,z$

where $T^{\lambda}_{\alpha\beta}$ is the dyadic product between I and S^{λ}. Table (2-2) shows the irreducible representation of these dyadic products for three of the most important interactions. Now, it is possible to combine eq. 2.19 and 2.20 to express the spin Hamiltonian in spherical tensor form as

$$\hbar^{-1}\hat{\mathcal{H}}^{\lambda} = C^{\lambda} \sum_{\ell} \sum_{m=-\ell}^{\ell} (-1)^m R^{(\ell)\lambda}_{-m}\, T^{(\ell)\lambda}_{m} \qquad 2.21$$

λ	$T_0^{(0)}$	$T_0^{(2)}$	$T_{\pm1}^{(2)}$	$T_{\pm2}^{(0)}$
D, J	$I.S$	$\frac{1}{\sqrt{6}}(3I_oS_o - I.S)$	$\frac{1}{\sqrt{6}}(I_{\pm1}S_o + I_oS_{\pm1})$	$I_{\pm1}S_{\pm1}$
S	I_oB_o	$\sqrt{\frac{2}{3}}\, I_oB_o$	$\frac{1}{\sqrt{2}}\, I_oB_o$	0
Q	$(I)^2$	$\frac{1}{\sqrt{6}}(3(I_o)^2 - (I)^2)$	$\frac{1}{\sqrt{6}}(3(I_o)^2 - (I)^2)$	$(I_{\pm1})^2$

where $I_o \equiv I_z$ and $I_{\pm1} \equiv \pm\frac{1}{\sqrt{2}}\, I_{\pm} = \pm\frac{1}{\sqrt{2}}\left[I_x \pm iI_y\right]$

Table (2-2) Dyadic products irreducible representations

In order to complete the transformation of the tensor R from the PAS to the LAB frame the Wigner rotation matrices, $\mathcal{D}_{m'm}(\alpha,\beta,\gamma)$, are used and the tensor can be represented as

$$R_m^{(2)} = \sum_{m'} \mathcal{D}_{m'm}^{(2)}(\alpha,\beta,\gamma)\ \rho_{m'}^{(2)}$$
$$= \mathcal{D}_{0m}^{(2)}\ \rho_0^{(2)} + \mathcal{D}_{2m}^{(2)}\ \rho_2^{(2)} + \mathcal{D}_{-2m}^{(2)}\ \rho_{-2}^{(2)} \qquad 2.22$$

where α,β,γ are the Euler Angles used to aligned the PAS with the LAB frame. The values of the Wigner rotation matrices are presented in Table (2-3).

Therefore, the spin Hamiltonian 2.21 can be re-written in a general form for any given interaction under these new conditions as

$$\hbar^{-1}\hat{\mathcal{H}}^{\lambda} = C\left[\frac{1}{3}\ \mathrm{Tr}\underline{R}\ T_0^{(0)} + \delta\sum_{m=-2}^{2}(-1)^m\ T_m^{(2)}\left\{\sqrt{\frac{3}{2}}\ \mathcal{D}_{0-m}^{(2)} + \frac{1}{2}\eta\left[\mathcal{D}_{2-m}^{(2)} + \mathcal{D}_{-2-m}^{(2)}\right]\right\}\right] \qquad 2.23$$

Now, It is possible to use the above equation and Tables (2-2) and (2-3) to express any spin interaction in the LAB frame and in this way to try to understand their effect upon the spectrum of the observed nucleus.

2.3.2 DIPOLAR INTERACTION

In the case of the dipolar interaction, the tensor is symmetric and traceless. So, the terms containing ℓ=0 and ℓ=1 are not present in equation 2.21. A definition of orientation of the dipolar vector, r_{IS}, can be represented as shown in

$d^2_{m'm}(\beta)$[b]			
	m		
m'	2	1	0
± 2	$\frac{1}{4}(1 \pm \cos\beta)^2$	$\pm\frac{1}{2}(1\pm\cos\beta)\sin\beta$	$\sqrt{\frac{3}{8}}\sin^2\beta$
± 1	$-\frac{1}{2}(1\pm\cos\beta)\sin\beta$	$\pm\left[\cos^2\beta-\frac{1\mp\cos\beta}{2}\right]$	$\pm\sqrt{\frac{3}{8}}\sin2\beta$
0	$\sqrt{\frac{3}{8}}\sin^2\beta$	$-\sqrt{\frac{3}{8}}\sin2\beta$	$3\cos^2\beta-1$

[a] $\mathcal{D}^2_{om}(\alpha,\beta,\gamma)= \sqrt{\frac{4\pi}{5}}\,Y_{2m}(\beta,\alpha)$, $\mathcal{D}^2_{m'o}(\alpha,\beta,\gamma)= (-1)^{m'}\sqrt{\frac{4\pi}{5}}\,Y_{2m'}(\beta,\alpha)$

[b] For m= -1, -2 use the equation $d^2_{-m'-m}= (-1)^{m'+m}\,d^2_{m'm}$

Table (2.3) Wigner rotation matrices[4]

$$D^2_{m'm}(\alpha,\beta,\gamma)= d^2_{m'm}(\beta)\exp[i(m'\gamma +m\alpha)]^{\alpha}$$

Fig (2.2). In this condition, it is possible to simplify equation 2.23 to take the form

$$\hbar^{-1}\hat{\mathcal{H}}^{D}=C^{D}\sqrt{\frac{3}{2}}\ \delta\sum_{m=-2}^{2}(-1)^{m}\ \mathcal{D}^{(2)}_{o-m}\ T^{(2)}_{m} \qquad 2.24$$

Using Tables (2.2) and (2.3) it is possible to expand the above equation to give as a result the well-known alphabet[6] expression for the dipolar interaction as

$$\hbar^{-1}\hat{\mathcal{H}}^{D}=-\ \frac{\mu_o}{4\pi}\ \frac{\gamma_I\gamma_S\hbar}{r^3_{IS}}\left[A+B+C+D+E+F\right] \qquad 2.25$$

where A to F are given by

$$A=\ I_{Iz}I_{Sz}\ (1-3\cos^2\theta)$$

$$B=-\ \frac{1}{4}\left[\ I_{I+}I_{S-}+I_{I-}I_{S+}\right](1-3\cos^2\theta)$$

$$C=\ \frac{3}{2}\left[\ I_{Iz}I_{S+}+I_{I+}I_{Sz}\right]\sin\theta\cos\theta\ \exp(-i\phi)$$

$$D=\ \frac{3}{2}\left[\ I_{Iz}I_{S-}+I_{I-}I_{Sz}\right]\sin\theta\cos\theta\ \exp(\ i\phi)$$

$$E=\ \frac{3}{4}\ I_{I+}I_{S+}\sin^2\theta\exp(-2i\phi)$$

$$F=\ \frac{3}{4}\ I_{I-}I_{S-}\sin^2\theta\exp(2i\phi)$$

If the dipolar Hamiltonian is considered as a first order perturbation to the Zeeman interaction all but terms A and B can be neglected from equation 2.25. The A term produces no change in spin transitions and it is present when considering both homonuclear and heteronuclear interaction. The B term involves the "flip-flop" operator and describes a simultaneous exchange of spin between two adjacent states. For homonuclear

interactions, energy is conserved so this term is included in the truncated Hamiltonian. In the heteronuclear case, the term is not included because the Zeeman energy between these two states is very different.

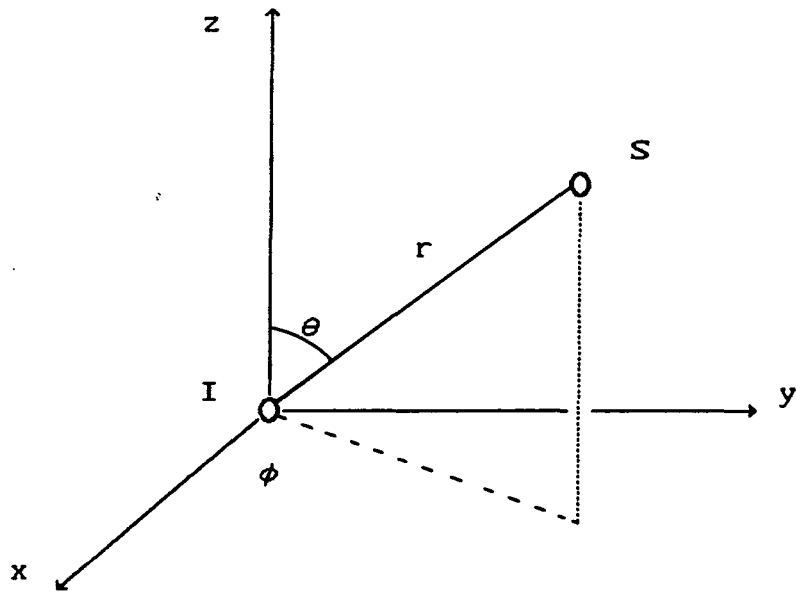

Fig (2.2) Definition of the angles involved in the dipolar interaction

It is possible to notice that each term is composed of a spin part and an angular or spatial term. This last term is the one which can be manipulated experimentally in the pursuit of high resolution spectra. The manipulation of this term will be explained in a later section. In the case homonuclear dipolar interaction, $\gamma_I=\gamma_S$, and in particular for a single crystal where the direction of the internuclear vector, r_{II}, is well defined, it is possible to observe two resonance frequencies at

$$\nu = \nu_o \pm \Delta\nu \ (1 - 3\cos^2\theta_{II}) \qquad 2.26$$

where $\Delta\nu = \frac{1}{2\pi}\frac{3}{4}\frac{\mu_o \gamma_I^2 \hbar}{4\pi r_{II}^3}$

It can be noticed that this separation has an angular dependence of the internuclear distance with respect to the external magnetic field[6]. The separation between the lines is equal to $2\Delta\nu$. So, if this value is determined, it is possible to obtain the distance between e.g. two strongly coupled protons.

In the case of a polycrystalline sample, all possible orientations of the internuclear vector are present due to the random distribution of crystallites in the sample, each giving rise to a pair of lines. The observed signal from such a sample will give a powder pattern, due to the superposition of the different doublets[6], known as "Pake Doublet" first observed by Pake[7] from the proton NMR signal from a sample of $CaSO_4 \cdot 2H_2O$. An analytical representation of this powder distribution is presented in Fig (2.3). For strongly coupled spins the spread of frequencies of this powder pattern can be as wide as 40 Hz. This homonuclear dipolar interaction will be the focus of attention in the application of the matrix isolation technique that will be presented in chapter 7 of this thesis. Matrix-isolation will be used to minimize or eliminate the intermolecular dipolar interaction, reducing line broadening, and therefore obtaining sharper lines. In this way, internuclear distances can be determined in a more accurate way.

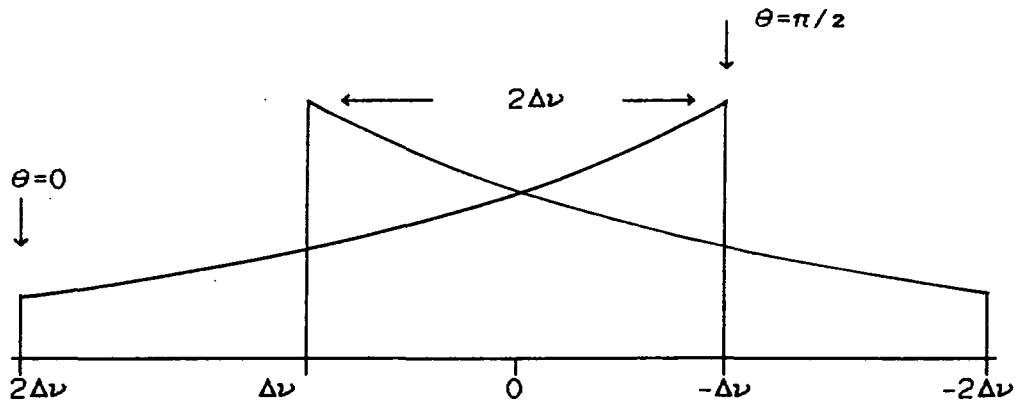

Fig (2.3) Analytical representation of the powder distribution for the homonuclear dipolar interaction case.

In the case of heteronuclear dipolar interaction, $\gamma_I \neq \gamma_S$, two such powder patterns can be observed, one for each nucleus. The value of $\Delta\nu$ is given by

$$\Delta\nu = \frac{1}{2\pi} \frac{\mu_o}{4\pi} \frac{\gamma_I \gamma_S \hbar}{2r_{IS}^3} \qquad 2.27$$

and for the case of ^{13}C-^{1}H interaction $2\Delta\nu$ can be of the order of 30 Hz which can be a major line-broadening factor.

2.3.3 QUADRUPOLAR INTERACTION

As in the case presented above for the dipolar interaction, it is also convenient to choose the principal axis for the electric field gradient tensor so that it is symmetric ($V_{xy} = V_{yx}$) and traceless ($V_{xx}+V_{yy}+V_{zz}=0$). Under this condition, the quadrupolar Hamiltonian can be expressed in the principal axis system as

$$\hbar^{-1}\hat{\mathcal{H}}^{Q} = C^{Q}\left[V_{xx}I_x^2 + V_{yy}I_y^2 + V_{zz}I_z^2\right] \qquad 2.28$$

$$= \frac{1}{2}\, C^{Q}\left[\, V_{zz}\left(3I_z^2 - 1\right) + \eta_Q\left(I_+^2 + I_-^2\right)\right.$$

where C^{Q} is given by $\frac{e^2 Q}{2I(2I-1)\hbar}$, and $\eta = \frac{V_{xx} - V_{yy}}{V_{zz}}$.

If axial symmetry is also assumed, it is possible to express the quadrupolar interaction, in the laboratory frame, in a similar fashion as equation 2.24, where $\delta = q_{zz}$, and $\eta = 0$. The Hamiltonian can now by written as

$$\hbar^{-1}\hat{\mathcal{H}}^{Q} = \sqrt{\frac{3}{2}}\; 2\pi \frac{Q_{cc}}{[2I(2I-1)]} \sum_{m=-2}^{2} (-1)^m\, \mathcal{D}^{(2)}_{0-m}\, T^{(2)}_{m} \qquad 2.29$$

where Q_{cc} is the quadrupole coupling constant.

From the viewpoint of this work, we will only consider the case where the magnitude of the quadrupolar interaction, $|\,\mathcal{H}_Q\,|$, and the splitting it produces in the energy levels is small in comparison to the Zeeman interaction, $|\,\mathcal{H}_Z\,|$. But the quadrupole interaction is usually greater than the chemical shift allowing one to write the truncated Hamiltonian as $\mathcal{H}^{T} = \mathcal{H}^{Z} + \mathcal{H}^{Q}$.

So, it is possible to treat this interaction by perturbation theory. The secular part of the quadrupole Hamiltonian contributes to first order to the total energy[8], and is given by

$$\hbar^{-1}\hat{\mathcal{H}}^{Q}_{sec} = \frac{Q_{cc}}{4I(2I-1)}\left[\, (3\hat{I}_z - \hat{I}^2)\, \frac{1}{2}\, (3\cos^2\theta - 1)\,\right] \qquad 2.30$$

and the corresponding frequency of transition between the different energy levels, m↔ → m+1 is given by

$$\nu_{m\leftrightarrow m+1}=\nu_L + \frac{Q_{cc}}{2I(2I-1)}\left[\frac{1}{2}(3\cos^2\theta-1)\left(m-\frac{1}{2}\right)\right] \qquad 2.31$$

The work presented in this thesis will involve the study of nuclei with both integer spin, I=1 (^{6}Li), and half integer, I=3/2 (^{7}Li). The energy level diagram for the combined Zeeman and quadrupole interaction is presented in Fig (2.4) for both cases. The shift produced for each transition is the same order of magnitude to first order. Two allowed transitions are observed for I=1 giving rise to a doublet in the NMR spectrum for the case of a single crystal. Similarly to the dipolar interaction, the separation of these two lines is given by

$$\Delta\nu=\frac{3}{4}Q_{CC}(3\cos^2\theta-1) \qquad 2.32$$

where θ is the angle between the principal component of the EFG and the static magnetic field B_o. Again an angular dependence is observed for the two transitions. The value of Q_{cc} can be determined directly from the spectrum.

In the case of a powder sample, a random distribution of spins is present giving rise to a powder pattern spectrum with a central doublet and a pair of outer steps as shown in Fig (2.5). As before, the separation of the doublet[9] is given

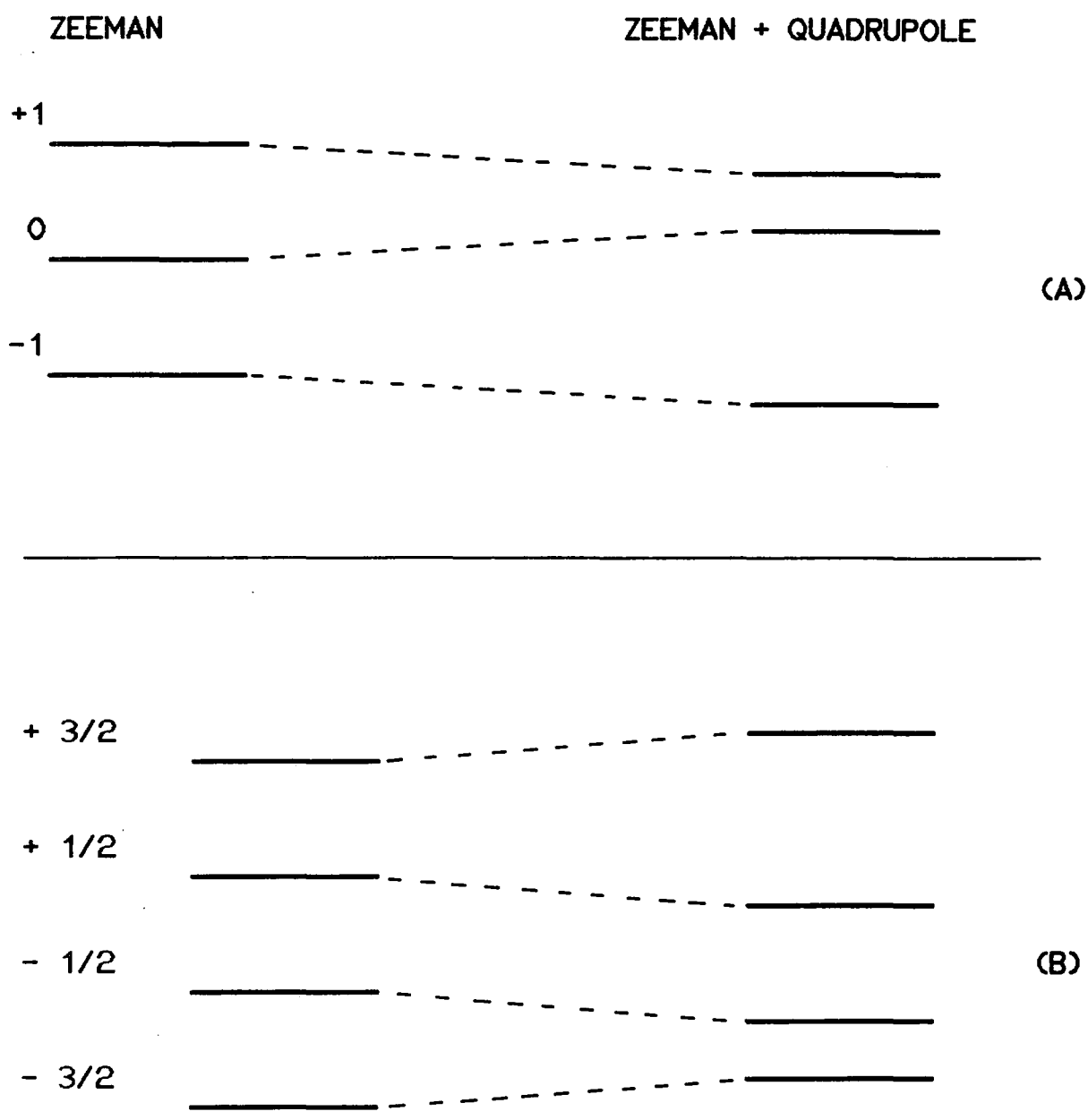

Fig (2.4) Energy level diagram of the spins (A) I=1 and (B) I=3/2 under the influence of Zeeman interaction and quadrupolar interaction to first order .

by $\Delta\nu_1=(3/4)\ Q_{cc}$, and the outer steps by $\Delta\nu_2=(3/2)\ Q_{cc}$.

There are three allowed transitions for the case of I=3/2 as shown by Fig (2.4). The central transition is not shifted to first order and has frequency equal to ν_L. The other two transitions or satellite transitions are shifted to first order and have frequencies equal to $\nu_L \pm \frac{1}{4} Q_{cc}$. In polycrystalline samples, these outer transitions produce powder patterns with the outer step at $\nu_L \pm \frac{1}{2} Q_{cc}$. This type of pattern is also shown in Fig (2.5). So, it is also possible, with well-defined transition frequencies, to estimate the quadrupole coupling constant from such spectra.

The quadrupolar interaction also contributes to a second order frequency shift to the central transition resonance line. The shift is given by

$$\nu_L - \left[(Q_{cc}/(2I(2I-1)))^2/16\nu_L\right]\left[(I(I+1)) - \frac{3}{4}\right](1-\cos^2\theta)(9\cos^2\theta - 1) \qquad 2.33$$

This effect will not play any significant part in the NMR studies presented in this work, and therefore it will not be discussed further.

2.4 HIGH RESOLUTION NMR IN SOLIDS:

As mentioned in section 2.1, NMR spectra from solid materials are broad in comparison to those obtained from liquids. So, different techniques have been developed to

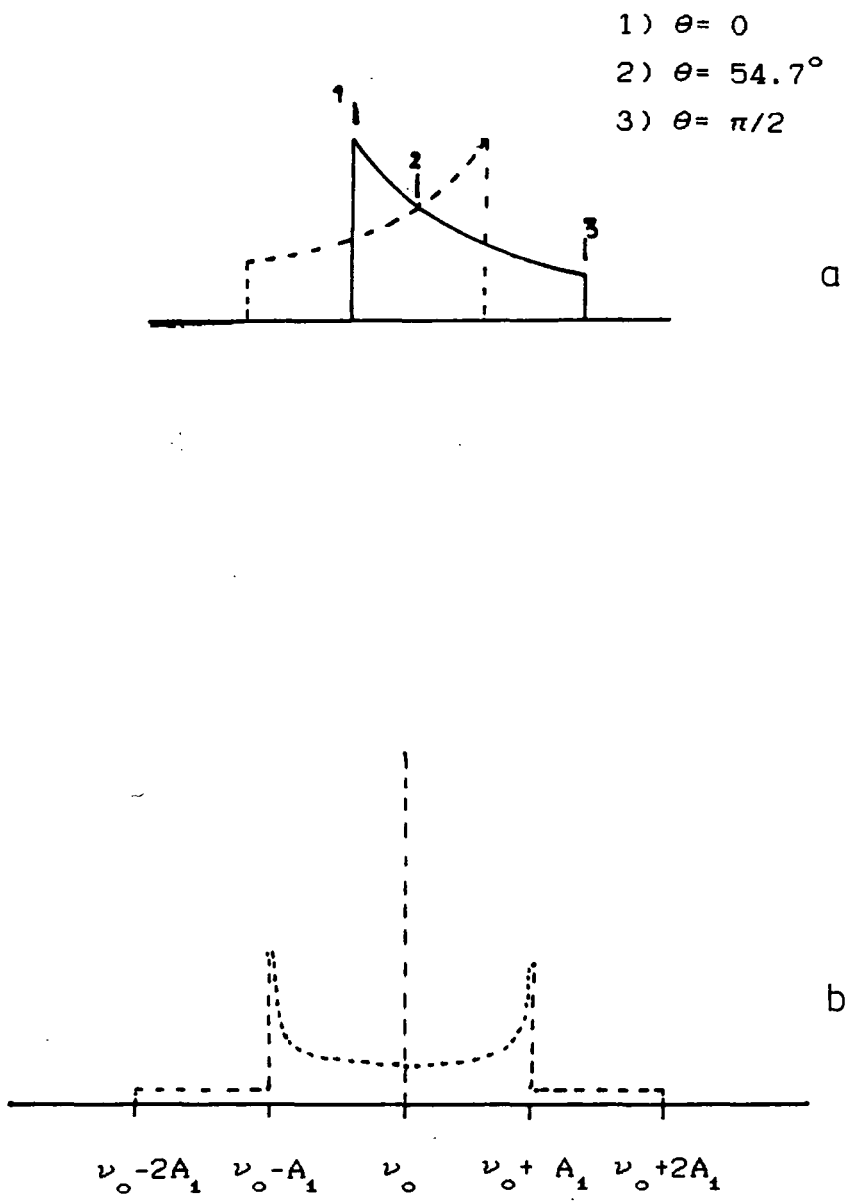

Fig (2.5) Powder pattern representation for the (A) I=1 and (B) I=3/2. (B) is for first order quadrupolar interaction only

overcome this limitation so as to obtain high resolution spectrum. One of these averaging technique is the rapid rotation of powder samples at an angle β with respect to the external magnetic field B_o. This technique is known as magic angle spinning[10] (MAS).

All the interactions that have been presented contain the term $(3\cos^2\theta-1)$ as part of their expressions. In the case of the dipolar interaction, this is the angle between the internuclear distance, r_{IS}, and B_o. It has been shown that $\cos^2\theta$ can be expressed in terms of two angles[2]; the first is χ, the angle between r_{IS} and the rotor axis, and the second is β, that has already been defined. This is shown in Fig (2.6). So, the term $\cos\theta$ at a time t can be written as

$$\cos\theta = \cos\chi\cos\beta + \sin\chi\sin\beta\cos\omega_r t \qquad 2.34$$

where ω_r is the angular rotational frequency of the sample.

It can also be shown[2] that the average of the $(3\cos^2\theta-1)$ term under rotation is given by

$$\langle 3\cos^2\theta-1\rangle = \tfrac{1}{2}(3\cos^2\beta-1)(3\cos^2\chi-1) \qquad 2.35$$

The angle β in the above expression is the only one that can be controlled experimentally. The expression 2.35 can be made equal to zero if the value is $\beta=54.7^\circ$ (known as the magic angle), i.e $\cos\beta=1/\sqrt{3}$ and the first factor on the right hand side is zero, so the average on the left is also zero for all initial orientations θ. So, this interaction can be averaged to zero as in liquids in some cases. However, in general, this can only be so when $2\pi\Delta\nu \ll \omega_r$, where $\Delta\nu$ is the spread of

the interaction. This is true for heteronuclear dipolar interactions giving rise to inhomogeneous line broadening, which can be averaged to zero in this way, as well as the shielding interaction in some cases. In the case of homonuclear dipolar and quadrupolar interactions $\Delta\nu$ can be as big as 10's of kHz and the spectrum will be scaled down and composed of spinning side bands (ssb) separated from the central band by multiples of ω_R that will mimic the static powder pattern.

In the case of dilute spins like ^{13}C or ^{31}P, the above problem can be solved by combining the MAS technique with another powerful averaging technique known as High Power Proton Decoupling (HPPD). In this method, the proton spins are irradiated with high power RF pulses resulting in a time average of $\hat{I}_z$ to zero. This eliminates the heteronuclear dipolar interaction and gives as a result high resolution lines.

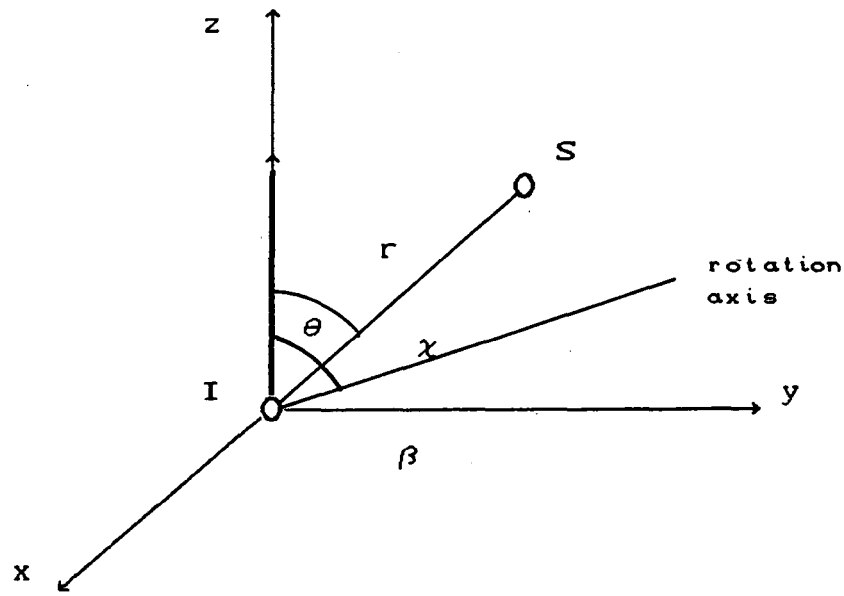

Fig (2.6) Definition of the magic angle of spinning

REFERENCES:

1- Bloch F., Phys. Rev., 70, 460, (1946).

2- Harris R. K., "Nuclear Magnetic Resonance Spectroscopy. A physicochemical view", Pitman Books Limited, Londom, (1983).

3- Mehring M., "High Resolution NMR in Solids", Springer-Verlag, Berlin, Heidelberg, New York, (1983).

4- Haeberlen U., "High-Resolution NMR in Solids - Selective averaging", Suppl. 1, Adv. Mag. Res., 1976, Academic Press.

5- Rose M. E., "Elementary theory of angular momentum", New York, John Wiley, (1967).

6- Abragam A., "The principles of nuclear magnetic resonance", Oxford University Press, (1978).

7- Pake G. E., J. Chem. Phys., 16, 327, (1948).

8- Cohen M. H., Reif F., Sol. State Phys., 5, 321, (1957).

9- Fyfe C. A., "Solid State NMR for Chemistry", C.F.C. Press, (1983).

10- Andrew E. R., Bradbury A., Eades R. G., Nature, London, 184, 1659, (1958).

CHAPTER 3

SAMPLES AT AMBIENT TEMPERATURE:

EXPERIMENTAL

3.1 NUCLEUS OF INTEREST:

The investigation of samples at ambient temperatures was concentrated on several nuclei and their most interesting properties are listed in Table (3.1). Most of the work presented in the next chapter was directed to the lithium and phosphorus nuclei.

NMR PROPERTIES	^{6}Li	^{7}Li	^{31}P	^{13}C	^{1}H
Spin (I)	1	3/2	1/2	1/2	1/2
Natural abundance (%)	7.2	92.58	100	1.11	99.9
Magnetic moment (μ/μ_n)	1.1624	4.2035	1.9602	1.2166	4.8372
Quadrupole moment ($Q/10^{-28}$ m^2)	$-8E^{-4}$	$-4.5E^{-2}$	———	———	———
Magnetogyric ratio (γ /10^{-7}rad $T^{-1}S^{-1}$)	3.9366	10.396	10.841	6.728	26.752
NMR frequency* (νo/ MHz)	29.4310	77.7778	81.0141	50.3227	200.13
Relative receptivity (Dp)	$6.61E^{-4}$	$2.72E^{-1}$	$6.7E^{-2}$	$1.76E^{-4}$	1

TABLE (3.1) NMR PROPERTIES OF NUCLEI OF INTEREST[1]

*The frequencies are relative to that of the protons of TMS that resonate at 200.13 MHz.

The samples studied in the present work were in all cases either air - or moisture - sensitive. This fact presented severe problems for the proper detection of the NMR signals from these samples. The method used to present the samples to the RF coil in the NMR probe head so that the signal could be

detected from this type of sample will be described in full in another section of the present chapter.

3.2 REFERENCE SAMPLES

The resonance frequencies and chemical shift spread obtained from the spectrum of the different samples studied have been measured relative to standard reference compounds and using methods established in the literature. It has been difficult to perform the above referencing using the standard liquid samples in a routine manner . The problem arises from the way the samples are presented to the solid-state NMR probes. It is very difficult to use liquid samples in this type of system without taking the risk of contaminating the RF coil and the stator area. So, secondary references were used in all cases presented in this work. This section will be concerned with the description of the reference samples used for each of the nuclei mentioned above.

3.2.1 PROTON

This is the most important of all nuclei to be referenced. The resonance frequency of the protons in the reference sample determines the setting up of the external static magnetic field B_o. As in liquid-phase NMR spectroscopy, TMS is used as the reference sample. Also, the indirect reference sample is silicone gum which is used in the day-to-day running of the spectrometer. It has a chemical shift of 0.6 ppm from TMS. This sample serves two purposes in

the routine running of the spectrometer; i) in the first instance, it is used to obtain the best homogeneity of B_o field when the shimming operation is done to the magnet; ii) secondly, it is used to set the B_o field so that the NMR signal from the protons in the silicone gum sample are on-resonance when the spectrometer frequency is set to 200.13 MHz.

3.2.2 Lithium-7

Lithium-7 chemical shifts have been referenced indirectly to Li^+ at infinite dilution of LiCl. LiBr has been used as a solid-state reference sample which has a chemical shift of 1.9 ppm relative to the aqueous reference. The reference sample has to be properly dried in an oven and then sealed to avoid hydrolysis so that the spherical environment around the Li^+ is maintained.

3.2.3 Lithium-6

Lithium-6 chemical shifts have been referenced directly to Li^+ in a 1 M solution of LiCl. An indirect reference sample was not needed in this case. For more detail of this procedure see section 4.2.1 in the following chapter.

3.2.4 Phosphorus-31

The chemical shifts of the phosphorus-containing samples were indirectly referenced to 85% aqueous phosphoric acid (H_3PO_4). The solid sample used as a reference compound was $CaHPO_4*2H_2O$, better known as "brushite". It has a chemical shift of 1.2 ppm relative to the liquid standard. This sample was also used in the magic-angle setting of the double-bearing probe.

3.2.5 Carbon-13

Carbon-13 chemical shifts were referenced indirectly to the standard TMS. The high-frequency line detected from adamantane was used as the solid-state reference. The chemical shift of this line is 38.5 ppm relative to TMS.

3.3 SPECTROMETER DESCRIPTION

In the execution of the present work a Bruker CXP-200 spectrometer system was used for the study of the majority of the samples . It uses an Oxford Instruments 4.7 Tesla wide bore (89.5 mm) superconducting magnet with a proton resonance frequency of 200.13 MHz. It was initially fitted with an Aspect 2000 computer system and later up-graded with an Aspect 3000 system with graphic and colour display. A complete description of the system has been provided[2] and it is readily available.

Two different probe systems were used in the course of this investigation. Initial work on lithium was carried out on a dual-channel Cross Polarization and Magic Angle Spining[3], CP/MAS, probes using an Andrew-Beams[4] spinning system. Due to the nature of the spinning system in the Andrew-Beams probe it was very important to check the magic-angle setting of the stator each time a sample was placed in it. This was possible by observing the spinning side pattern from the ^{79}Br nucleus in a sample of KBr. The number of spinning side bands observed are strongly dependent on the accuracy of the magic-angle setting.[5]

One of the problems that was encountered with this probe system was that it was very difficult to study air-sensitive samples without decomposing the actual sample. Special arrangements had to be made in order to work satisfactorily with this type of material. This point will be described fully in the next section.

The second probe system used was a double-bearing (DB) CP/MAS probes from Brucker Spectrospin. They cover the frequency range from ^{15}N to ^{13}C on the low frequency probe and from ^{13}C to ^{31}P at the high frequency range. They offer greater stability in magic-angle setting as well as a very good spinning sample stability. They were very important in the final solution taken for dealing with air-sensitive materials. Another advantage of these probes is the improved sensitivity in signal that can be obtained in comparison with the Andrew-Beams system. The spinning frequency (ω_R)range of these probes goes up to 4500 Hz.

A second spectrometer system was used in the

investigation of the lithium compounds. This was a Varian VXR-300 spectrometer using a 7 Tesla, narrow bore (89 mm), super-conducting magnet. The CP/MAS capability is provided by a dual-channel, double-bearing probe system from Doty Scientific. This spectrometer was used to perform a variable-temperature study of ^{7}Li and to run some ^{6}Li spectra.

3.4 SAMPLE MANIPULATION

As mentioned in section 3.1, all the samples studied under ambient conditions were either air-and/or moisture-sensitive. It is possible to see that this fact will present severe problems when using either of the probe systems mentioned in section 3.3 of this Chapter.

Two type of sample inserts will be described in this section. They were designed and tested during the period of this work, for the two different probehead systems used. The experience obtained during the design of the first type of insert system for the Andrew-Beams probe made it easier to produce a second and better version of this design for the Brucker double-bearing probe.

3.4.1 SPECIAL CONSIDERATIONS

The problem of dealing with air-sensitive sample in solid-state NMR is one that has taken the attention of the NMR community for a long time[6,7]. These attempts had been

concentrated on the sealing of the samples in glass inserts which in turn are placed in the normal spinner for the commercially available probe systems or are used with specially built spinning systems to maximize observed signals from samples in large sealed NMR tubes.

Fig (3-1) show a typical stator-rotor arrangement and a diagram of a 7 mm "broomstick"[8] rotor used in the Andrew-Beams probe system. The use of 7 mm rotors means that if inserts are used to keep the samples in inert conditions they need to be of 5 mm diameter and with a 1 mm constriction at one end to make the sealing possible. The type of sample presentation mentioned above has several immediate problems when it is used with the Andrew-Beams probes. The first problem faced with this arrangement is to introduce enough sample inside the

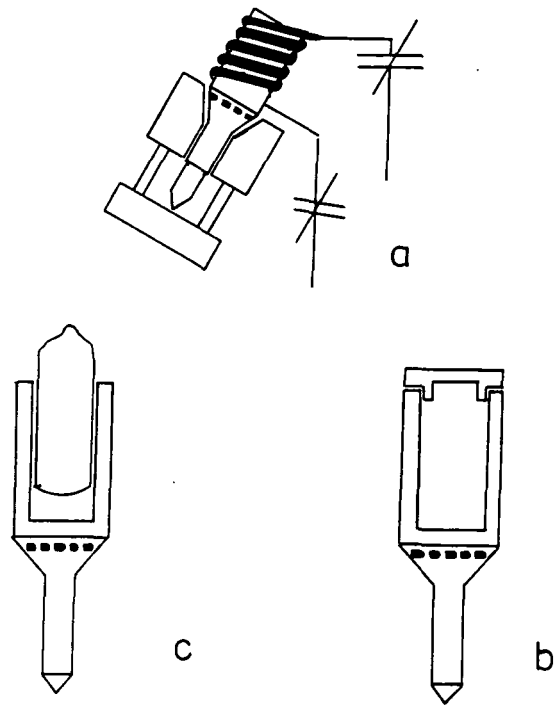

Fig (3-1)(a) Typical stator rotor arrangement for the Andrew-Beams probe.
(b) Typical "broomstick" rotor.
(c) Glass-sealed capsule for the "broomstick" rotors.

insert through the 1 mm constriction, when they were being manipulated inside a glove-box environment. The sample has to be pushed through with a very fine wire and there is no guarantee that the constriction will be clean of sample before sealing. It will also present the problem of packing the sample well enough so that stable spinning can be produced in the NMR probe.

It was found that this configuration is not very appropriate for samples with low melting points. Some attempts to seal inserts with low-melting samples were made by immersing part of the insert inside a nitrogen bath during the sealing process. Even in this conditions it was not possible to guarantee that the sample was not decomposed due to the heat transferred along the body of the insert from the sealing point. Referring to the sealing process, it was very difficult to produce sealed inserts that were symmetrical enough so that they would spin stably in the Andrew-Beams stator. Collision with the RF coil was always the major problem in these cases. All the difficulties mentioned above were very time-consuming and the approach cannot be considered good enough to be used in a routine fashion.

Some of the problems with the sealed insert have been solved and presented in a work by Giammatteo[9]. This method still uses glass inserts with a 1 mm constriction but the sealing is done by blocking the small aperture with a type of epoxy resin. This approach will solve the problem of low-melting point samples and symmetrical sealing but it will still leave the problem of even packing and cleanliness in the neck of the constriction.

3.4.2 CAPSULE DESIGN FOR ANDREW-BEAMS PROBES

An alternative solution for the handling of air-sensitive samples was used in this investigation that makes the manipulation of the samples easier inside the glove-box. It was decided to change the shape of the top of the inserts and leave them with the normal outside diameter of 5 mm (to fit inside rotors). Glass inserts were used with a wall thickness of 2 mm. The tops of the inserts were not sealed but they were closed with a teflon plug which was machined so that it will fit as tightly as possible but without breaking the glass. The final adjustment of the fit was done using teflon film around the plug before it was introduced at the top of the insert. As in the Giammatteo system, the insert has a flat bottom so that it sits properly inside the spinners.

So, the procedure to manipulate the samples and the inserts inside the glove-box will be: i) the inserts are pre-heated under vacuum. This will ensure that no residual moisture is trapped in the inside walls of the glass which can cause the contamination of the sample in the long run; ii) the inserts are introduced in the glove-box and the samples are packed inside them as would be done with a normal ceramic rotor. A glass or teflon packing tool was specially made to facilitate the process; iii) the teflon plug is wrapped with teflon film before being pushed into the insert.

The great advantage of this configuration is that after the insert is inside the glove-box it can be treated as an ordinary rotor. The time needed to properly pack the inserts is not more than a couple of minutes, and they can be used

immediately after they are brought into ambient conditions. Their stability under MAS conditions is very good and no increment in linewidths was observed in any of the samples. They can be spun up to 3.6 kHz. This limitation seems to be more of a problem with the spinning system rather than on the inserts. A diagram of the insert is shown in Fig (3-2).

Tests were carried out on the glass inserts in order to check how important the step ii of the procedure described above was for the samples studied. The results are presented in Fig (3-3). Fig (3-3a) shows a ^{7}Li spectrum of a lithium tetraborohydrate tetra-pyramide inside one of the pre-heated insert, and Fig(3-3b) shows a spectrum of a similar sample inside an untreated inserts. The resonance lines at 5.7 and 6.7 ppm in the first spectrum were thought to correspond to two different isomers for this molecule. The resonance peak at 4.7 ppm in the second spectrum corresponds to the hydrated compound that was formed by contact with the inside walls of the insert. A second spectrum from this sample was taken some days later, showing no further increase in the intensity of the peak at 4.7 ppm relative to the other two. This result indicated that no more hydration occurred inside the insert and that no moisture was getting inside the insert through the teflon plug.

3.4.3 CAPSULE DESIGN FOR THE DOUBLE-BEARING PROBES

The design, construction, testing and routine work with the glass insert for the Andrew-Beams probes gave an enormous

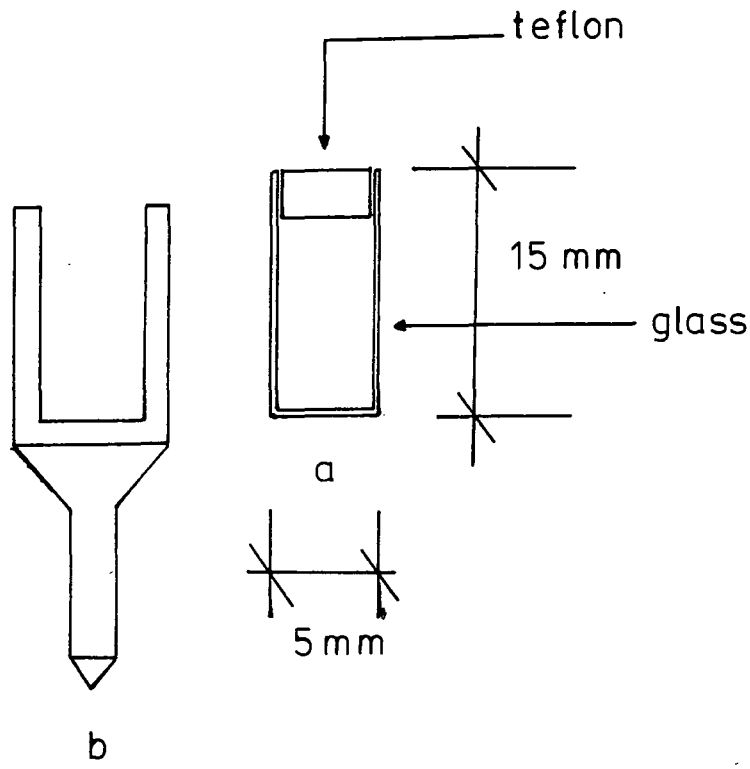

Fig (3-2) Schematic diagram of glass-capsule design for the Andrew-Beams probes.
(a) Glass-capsule dimensions (b) Broomstick rotor.

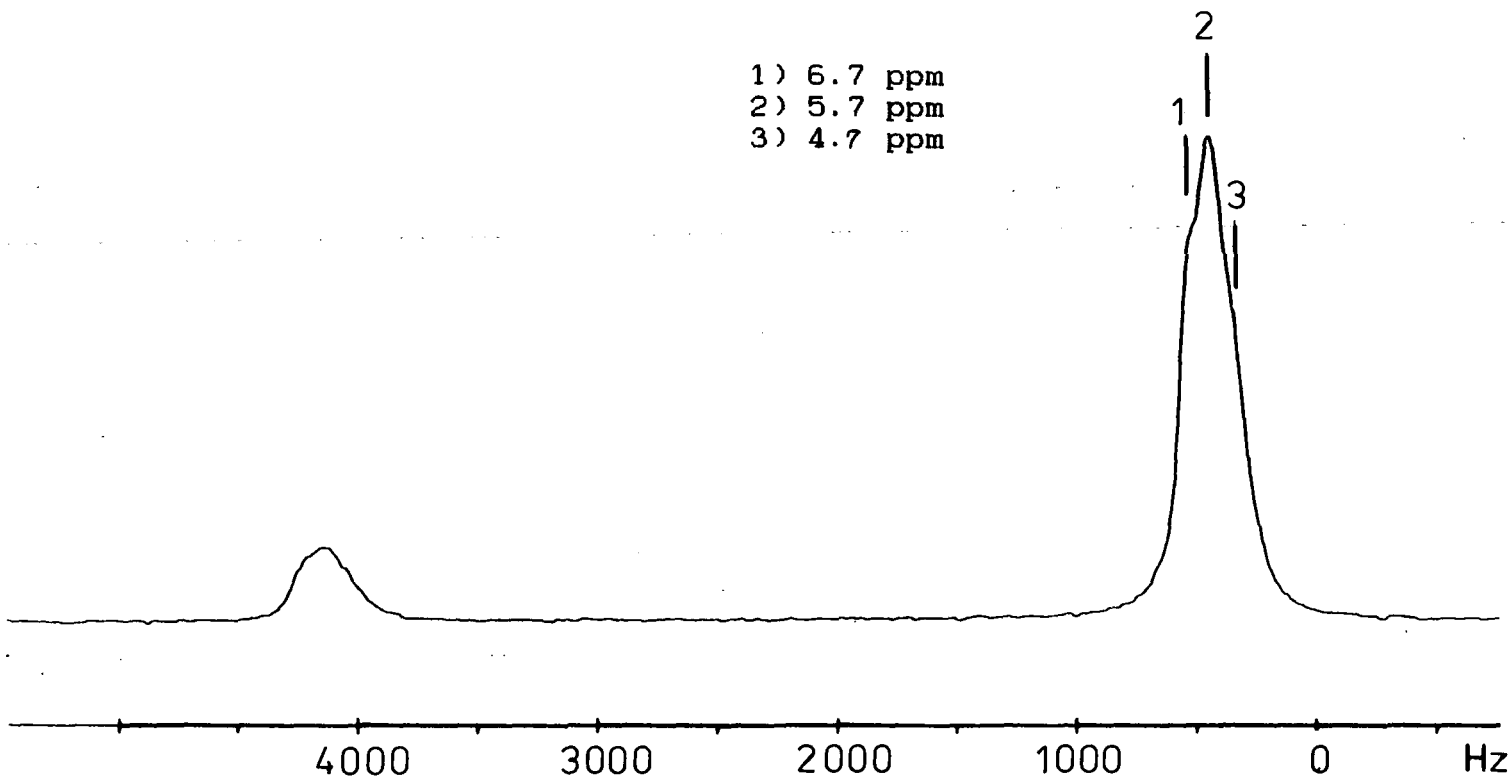

Fig (3-3a) $LiBH_4Py_4$ SP/MAR/HPPD Spectrum from sample inside preheated capsule.

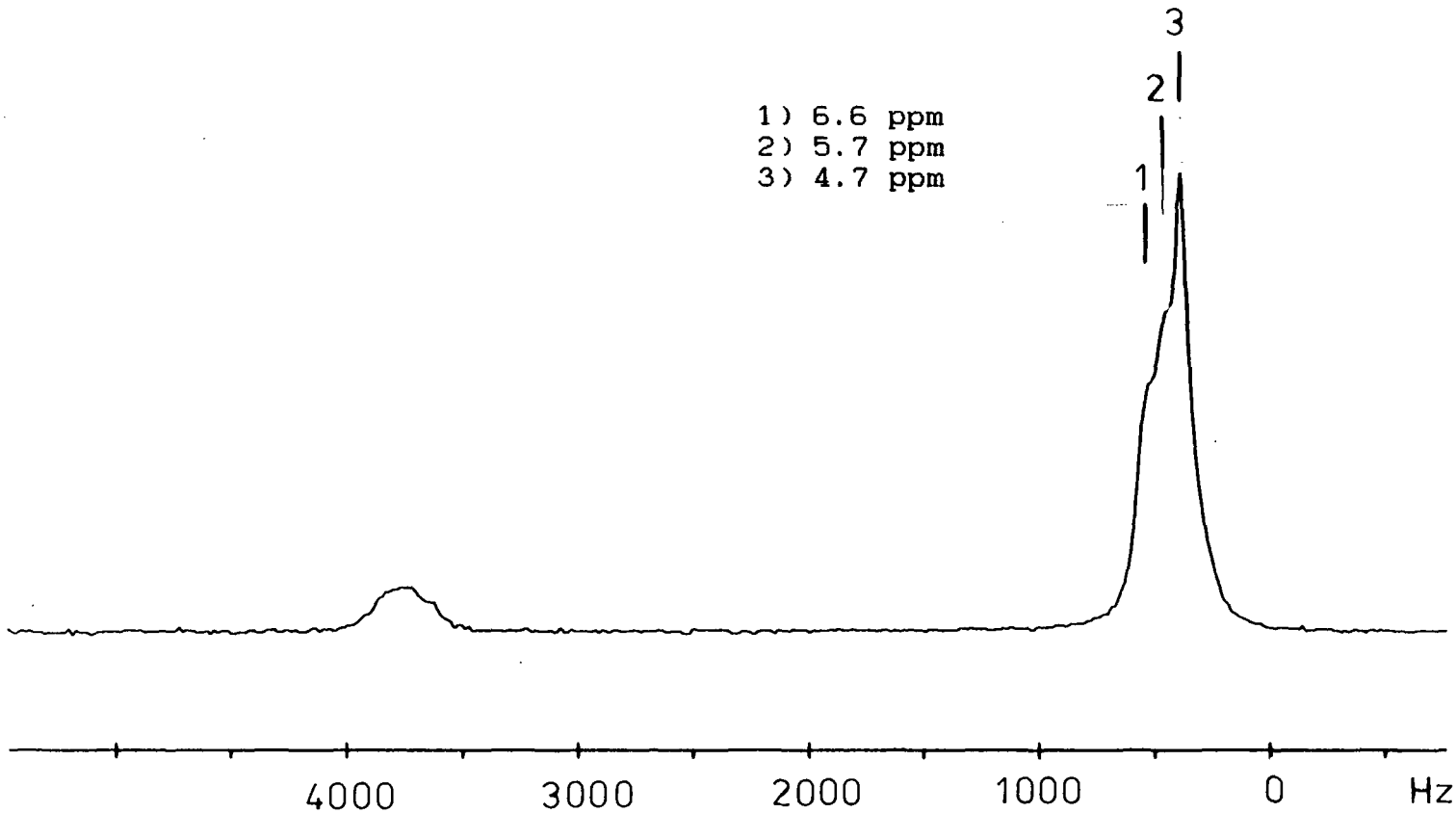

Fig (3-3b) $LiBH_4Py_4$ SP/MAS/HPPD Spectrum from sample inside untreated capsule.

amount of experience in the manipulation of the air/moisture-sensitive materials. One of the advantages that the Andrew-Beams probes presented was the way in which the RF coil is located with respect to the stator, spinner and sample insert (see Fig (3-1)). The fact that the coil was detached from the stator meant that any errors made during the insert's development period, i.e. unstable spinning, would only damage the RF coil and nothing else. The coil was very easy to replace in this type of probe and it could be done in situ. The experience gained prove to be essential when designing an equivalent insert for the double-bearing probes[10a,b,c].

One of the biggest differences between the two types of probe is that in the double-bearing type the RF coil is mounted in a ceramic base and it sits inside the stator. So, in the case of a possible crash of the rotor during spinning it could damage itself as well as the coil and the stator in the process. It is not easy to replace the coil in this probe. It was also important to know that the new stator and ceramic rotor design were more critical to sample packing than the other system. So, stable spinning was more dependent on a well-balanced rotor than before. All these new parameters had to be taken into consideration in the new insert design.

The new inserts keep some of the features of the old design and they have some new modifications. A diagram of the inserts is presented in Fig(3-4). Some of the old features are: i) It keeps the cylindrical shape of the glass capsules, giving the greater stability needed under MAS conditions; ii) As it is an open-top cylinder, it will be very easy to pack properly inside a glove-box used tools made specially for the

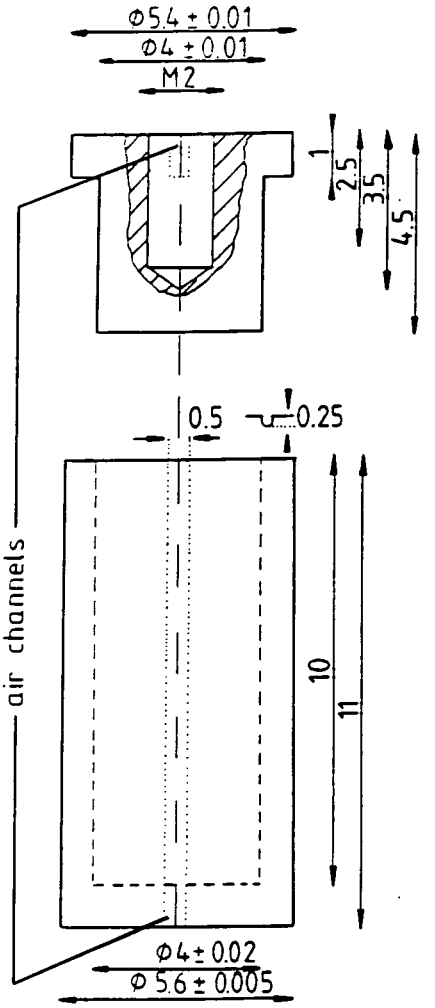

Fig (3-4) Schematic diagram of the new rotor insert used in double-bearing probes. Dimensions in millimeters.

purpose; iii) the diameter and length are maintained the same, i.e. 5.6 mm by 12.0 mm, respectively. The new features are: i) it was decided to make the new inserts of the carbon-based fluoro polymer Kel-F rather than of glass. This reduces the chances of breaking inside the rotor. This material is also very easy to machine using the facilities present at Durham University; ii) the top plug was changed to a very tightly fitting cap which gives all the necessary seal to prevent any air or moisture getting inside the capsule. The cap also has a hole with a screw thread located in its middle. This allows a brass screw to be fitted so that the capsule could be put in or out of the rotor with no great difficulty. The screw is also used to remove the cap from the body of the insert during sample changes inside the glove-box.

It has to be mentioned that the insert has a couple of small drawbacks. The first one is that the Kel-F material used gives a small ^{13}C background in normal single pulse experiments. Having said this, the majority of the ^{13}C work is done under CP/MAS conditions, when no background will be presented. Secondly, it is not possible to use very strong solvents when cleaning the inserts because they react with the polymer material and damage the inserts. Finally, Kel-F is relatively expensive, though it is cheaper that the cost of the ceramic rotors used with the double-bearing probes. Alternative, less-expensive materials could be used to machine the insert when other nuclei rather than ^{13}C are studied.

The inserts have proved to be very efficient to maintain air tightness for long periods of time. Samples have been left under ambient conditions for several weeks and only small

amounts of decomposition have been observed. This small effect would be explained in terms of permeability of air and moisture through the insert wall. This is easily avoided by maintaining the inserts inside a desiccator, when the same samples are not used for long periods of time. The desiccators do not need to be under vacuum but a good supply of dry silica inside them will be enough. As far as low-temperature work is concerned, the inserts have been tested down to -90 ^{o}C without any sign of damage to them. High-temperature work will be difficult to do. If the inserts are packed with a suitable sample, i.e. silicone gum, they could be used to perform the shimming of the magnet prior to the experiment. This is a very important factor because in this way it is guaranteed that the best B_o homogeneity is concentrated at the sample volume, which in this case is believed to be within the RF coil volume.

This brings the point of sensitivity. On one hand, the sample volume is less in this type of insert in comparison with a full capacity rotor and therefore sensitivity is less. On the other hand, homogeneity is concentrated in the small sample region, so some compensation is made. Fig (3-5) shows the spectrum of adamantane obtained with a full-capacity ceramic rotor and another with a sample inside the insert. The spectra were taken under CP/MAS with the following conditions: i) a contact time of 5 ms, ii) recycle time of 5 s, iii) proton $\pi/2$ pulse of 4 μs, iv) spinning speed (ω_R) of 1500Hz and v) a number of scans of 8. In this particular case the homogeneity adjustment was done on a full rotor. The results show a reduction by a factor of 3 in the signal

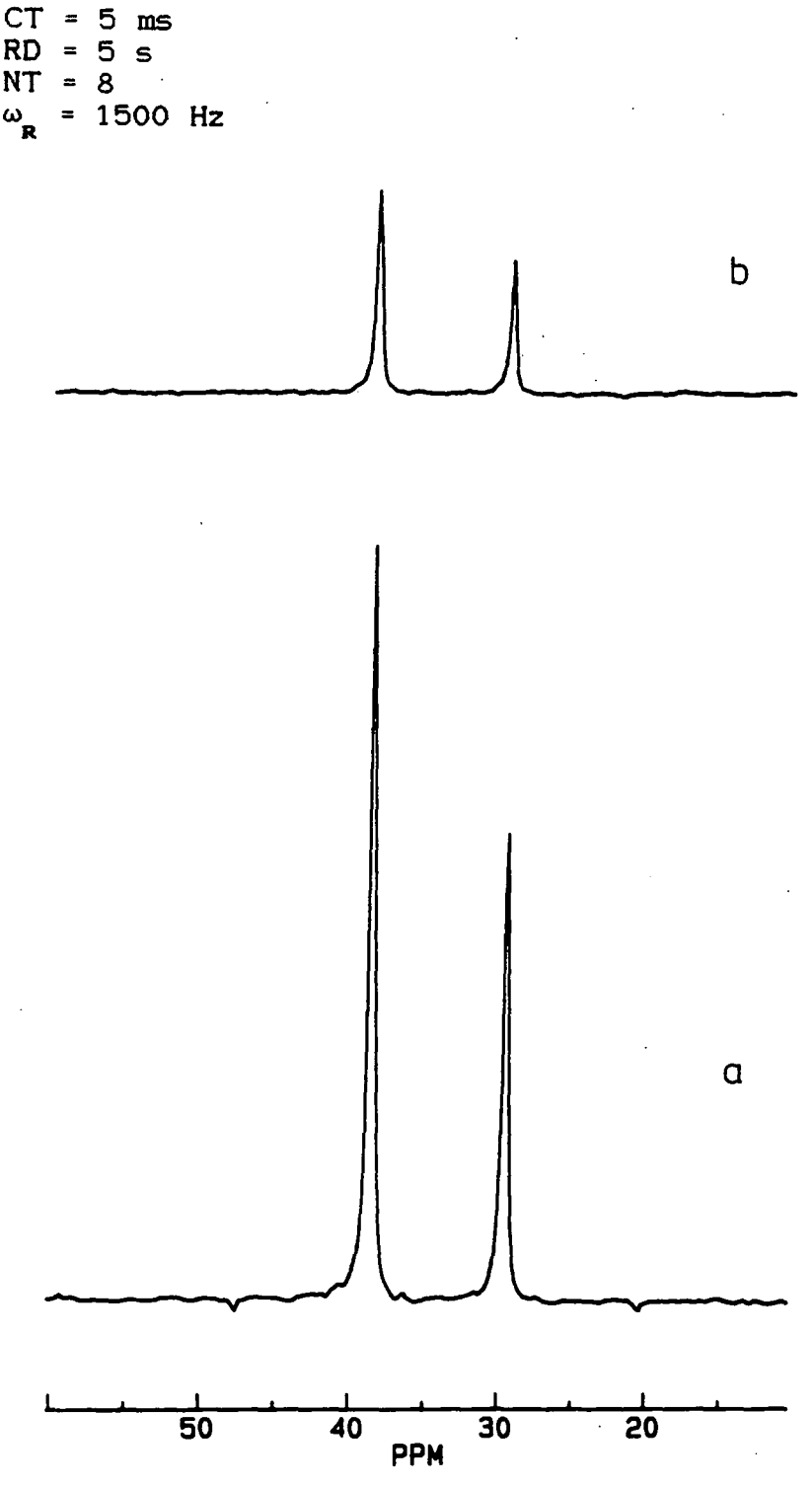

Fig (3-5) ^{13}C CP/MAS Spectrum from adamantane.
(a) full rotor, (b) sample inside new rotor insert

intensity between the full rotor and the insert. This means that there will be an increase of 640 s to obtain the same amount of signal/noise from a sample in the insert using the above conditions.

The capsules were tested for MAS stability over a wide range of spinning frequencies, going from 500 Hz up to 4500 Hz using brushite as a test sample. A summary of the results is presented in Fig (3-6) and Table (3-2). The agreement between the speed read from the optical tachometer and the one measured from the separation of the spinning side-bands (ssb) is very good over the wide range. The values of the line width and half-height ($\Delta\upsilon_{1/2}$) of the ssb do not change significantly over the same range. The average line width was 104.6±4.2 Hz over the range, which is in agreement with the accuracy of optical read out.

ω_R^1 (Hz)	$\Delta\nu_{1/2}$ (Hz)	$\bar{\omega}_R^2$ (Hz)
503	108	502±10
1500	100	1500± 4
2000	104	2000± 6
2500	110	2500± 3
3000	100	3002± 6
4500	106	4505± 6

[1] Values obtained from the ligth meter read out

[2] Average separation between the ssb at the particular frequency.

Table (3.2) Comparison between spinning frequency measured instrumentally and from ssb separation of a brushite spectrum. Sample inside capsule insert.

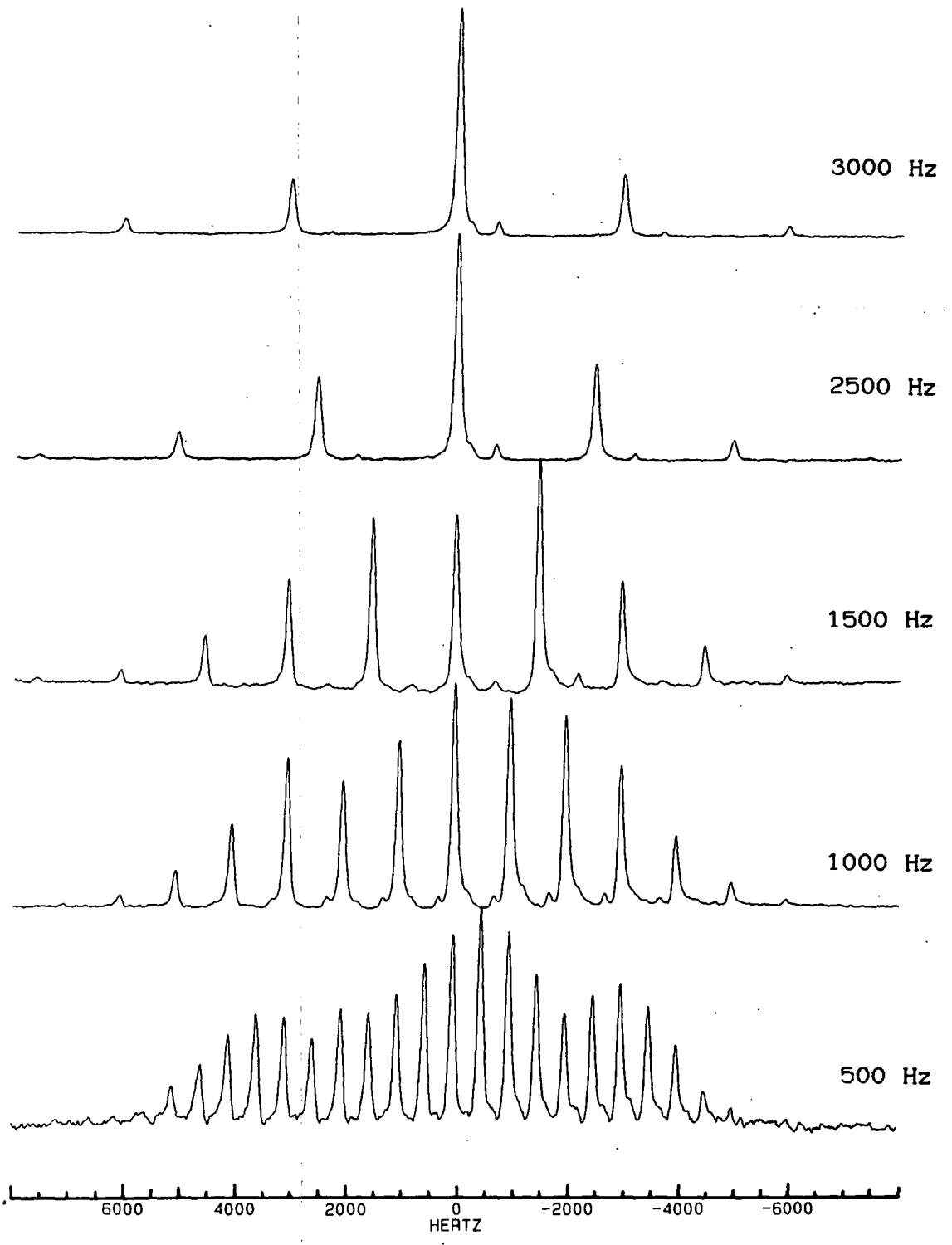

Fig (3-6) ^{31}P CP/MAS Spectrum from $CaHPO_4.2H_2O$ inside the new rotor insert. Comparison at different ω_R values.

In conclusion, it is possible to say with confidence that the stability of this type of insert under MAS condition is very good. This fact opens the possibility to carry out variable spinning speed studies in air- and moisture-sensitive sample.

This design was modified so that the inserts could be fitted inside the sapphire double-end-cap rotors used in the Doty probes for the VXR spectrometer. They proved to be as efficient in their performance in the new configuration as in the one for the Bruker ceramic rotors. The low temperature work mentioned above was carried out with these new modified inserts.

3.5 PULSE SEQUENCES

This section will be dedicated to giving a general description of the different NMR pulse sequences used during the period of this investigation. Several authors have given their attention to the treatment and understanding of the different pulse sequence techniques available to the experimentalist. The reader is directed to these references for a more in-depth treatment. A schematic representation of the pulse sequences used is presented in Fig(3-8).

3.5.1. Single-Pulse Acquisition

This is the simplest of all pulse sequences (Fig.3-8a-8b). It was applied to the observation of the NMR signal from quadrupolar nuclei, i.e. ^{6}Li and ^{7}Li, in samples with and without proton content. Therefore, two variations of this sequence were used, namely single pulse with and without high-power proton decoupling (HPPD). The requirements for both the 90^{o} pulse and HPPD are much greater than those needed in liquid-state NMR studies due to the wider frequency domain that needs to be excited and decoupled. The $\pi/2$ pulses were typically of the order of 3 μs but the actual signals observed from quadrupolar nuclei were obtained using $\pi/4$ pulses in order to excite all possible transitions[11].

3.5.2 Cross-Polarization

The technique of cross polarization [12](CP) combined with magic-angle spinning[13] (MAS) was used to overcome the very difficult task (present in solid-state NMR) of observing resonance signals from nuclei with very low sensitivity (i.e. C-13; X-nucleus) in comparison with proton (^{1}H). The principle involved in this pulse sequence is to transfer magnetization from the great pool of the proton nuclei to the less sensitive one, in the rotating frames of reference. This rapid and efficient magnetization transfer is induced by the flip-flop term in the dipolar Hamiltorian involving the two nuclei. This technique also helps to overcome the problem of long values of T_1 possessed by this low abundance nucleus.

This is because the time need to repeat the pulse sequence does not depend upon the X nucleus's T_1 but on that from the protons. There are two other important aspects of this sequence that need some attention. The first one is the use of flip-back[14] in order to reduce even further the recycle time. The second is the spin temperature inversion[15] (STP) in order to eliminate any artefact coming from the spectrometer electronics. This sequence is shown in Fig(3-8c).

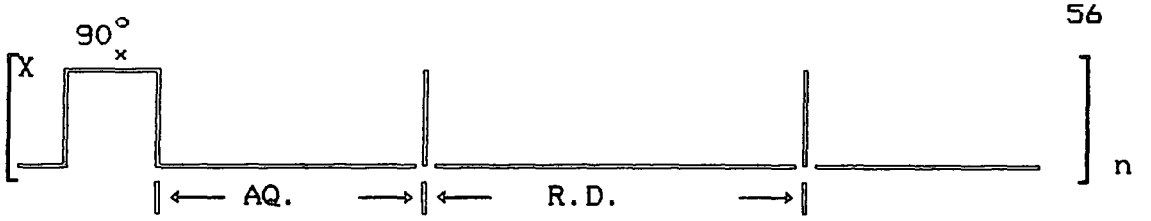

a) Single pulse no decoupler

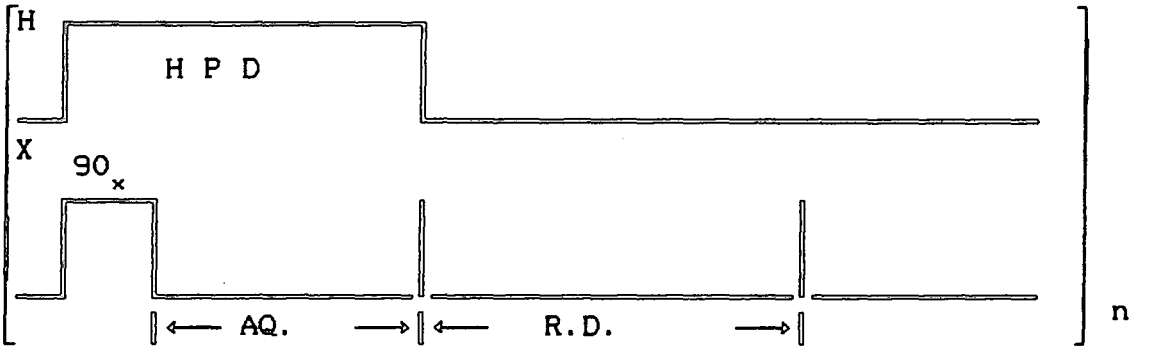

b) Single pulse/High power decoupling

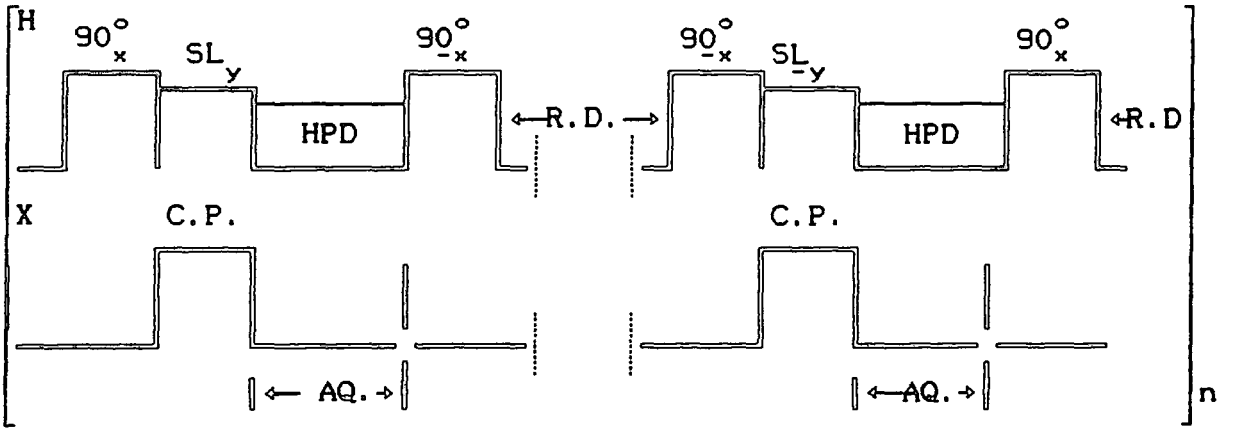

c) Cross Polarization with flip back

Fig (3.8) Schematic diagram of the different pulse sequencies used in this investigation.

REFERENCE:

1- Harris R. K., Mann B. E. . NMR and the Periodic Table, Academic Press, 5-7, (1978).

2- Bruker Spectrospin Ltd., "Pulse NMR Spectrometer CXP User's Manual.

3- Schaefer J., Stejskal E. O., J. Am. Chem. Soc., **98**, 1031, (1976).

4- Andrew E.R., Bradbury A., Eades R.G., Nature, **182**, 1659 (1958).

5- Frye E., Maciel G.E., J. Mag. Res., **48**, 125, (1982)

6- Gay D., J. Mag. Res. **58**, 413, (1984).

7- Geschke D., Quillfeldt E., J. Mag. Res., **65**, (1985).

8- Jackson P., PhD Thesis, Durham University, (1987).

9- Giammateo P.J., Hellmuth W.W., Ticehurst F.G., Cope P.W., J. Mag. Res. **71**, 147, (1987).

10 a- Espidel Y., University of Durham, Chemistry Department, Second Year Ph. D. Report, July (1988). b- Espidel Y., "Air Sensitive Sample Insert", Bruker Users' Meeting, Coventry, England, 14th of November, (1988). c- Merwin L. W., Sebald A., Espidel J., Harris R. K., J. Mag. Res. **84**, 367, (1989).

11- Fukushima E., Roedar S. B. W., "experimental Pulse NMR: a Nuts and Bolts aproach", (Addison-Weslay, London. 1981).

12- Pines A., Gibby M. G., Waugh J. S., J. Chem. phys., **59**, 569, (1973).

13- Schaefer J., Stejskal E. O., J. Amer. Chem. Soc., **98**, 1031, (1976).

14- Haeberlen U., Tegenfeld N., J. Mag. Res.,**36**, 453, (1979).

15- Steskal E. O., Schaefer J., J. Mag. Res., **18**, 560, (1975).

CHAPTER 4

AMBIENT TEMPERATURE STUDIES: QUADRUPOLAR EFFECTS IN AIR SENSITIVE SAMPLES

4.1 INTRODUCTION

This chapter will be dedicated to the investigation of two different types of quadrupolar interaction. In particular, these interactions will be studied in samples that are extremely sensitive to air and moisture.

As far as the interactions are concerned, they can be classified as direct quadrupolar effects and indirect quadrupolar effects. For the first case, the investigation was directed to the observation of NMR signals from a quadrupolar nucleus from which quadrupolar parameters can be extracted to give information about the molecular environment around the nucleus of interest. The investigation concentrated on a series of organolithium complexes using the signals from both ^{7}Li and ^{6}Li isotopes as probe.

In the second type of interaction, the study concentrated on the effects of coupling between a quadrupolar nuclei and a spin 1/2 one in the NMR spectrum of the second nucleus: In particular the observation of scalar coupling between the two type of nucleus. The molecular systems used were transition metal complexes where the interaction between Cu(I) and ^{31}P is the one of interest.

All the above systems are very sensitive to air and moisture, which makes it very difficult to perform solid state NMR studies in normal conditions. This problem has been very much facilitated by the recent introduction of a new rotor insert specially designed during the period of this work to cope with this type of sample (see chapter 3.4.3)[1]. All the results presented in this chapter were obtained with the aid

of these inserts unless otherwise stated.

4.2 DIRECT QUADRUPOLAR EFFECTS

It has already been indicated in chapter 2 that the interaction between the nuclear quadrupole moment in nuclei with I>1/2 and the non-spherical electric field gradient around them gives rise to quadrupolar type of resonance line-shapes. In these cases, different resonance lines can sometimes be detected, arising from the allowed energy transitions[3,4]. The possibility of detecting these transitions depends on the magnitude of the quadrupole coupling constant which is give by $Q_{cc}=\left(e^2 q\ Q/\hbar\right)$.

Thus, it is possible to identify three possible conditions that may be encountered when working with quadrupolar nucleus in solid state NMR. The first two cases correspond to two extreme situations, where on the one hand $\mathcal{H}_Q \ll \mathcal{H}_z$, and on the other $\mathcal{H}_Q \gg \mathcal{H}_z$. In the first case, it is possible to observed all allowed transition whereas for the second only the central transition can be observed. The last possibility involves the intermediate cases where the values of both interactions are comparable. In these cases very complicated line-shapes are observed involving some or all transitions under the influence of both first and second order interactions.

For the particular case concerning this work, the two lithium isotopes posses low quadrupole moments, as indicated in Table (3.1), and if this is combined with high symmetry

around them, it is expected that $\mathcal{H}_Q \ll \mathcal{H}_z$ and therefore all allowed transitions will be observed, i.e three transitions for ^7Li and two for ^6Li. Furthermore, it is also expected that for all the cases presented in this work

$$\omega_a = \frac{e^2 q Q}{8\hbar I(2I-1)} \ll \gamma B_o \qquad 4.1$$

and then only first-order quadrupolar effects will influence the NMR spectrum[5].

Even in these low-limit cases, the observed line-shapes can span for 10's of kHz. Thus, it is important to set the strong 90° pulse properly in order to guarantee uniform irradiation of the total spectrum[6]. This is best achieved by using a reference compound in which the nucleus of interest is present in a highly symmetrical environment, e.g. octahedranal environment.

4.2.1 REFERENCE COMPOUND AND 90° PULSE SETTING

Solid state NMR spectroscopy of lithium compounds is dominated by long T_1 values which in some cases make recycle times very long. Thus, this is also true for the possible candidates that may be chosen as reference sample. For the purpose of this work, LiBr was selected as the reference compound. The value for the T_1 was estimated to be between 30 and 40 s. At the same time, lithium compounds are very moisture sensitive and LiBr is no exception of this rule.

Therefore, they have to be specially handled to avoid hydrolysis. For the case concerned, the LiBr was dried in an oven at 60° C for two days. Then, the sample was transferred to a dry glove-box and packed inside the specially made rotor inserts. In this way it is possible to guarantee the integrity of the sample almost indefinitely if the insert is kept inside a desiccator when it is not used.

The sample prepared in the way described above was used to set the 90° pulse and for the use of the spectrometer system the shortest possible $\pi/2$ was of 3 μs. The resonance signal from the reference sample obtained under these conditions is presented in Fig (4.1). Thus, it will be possible to use a pulse of 1.5 μs for the appropriate detection of the central and satellite transitions for the ^{7}Li (equivalent to a 45° pulse angle). A flip angle of 63° was used for the case of ^{6}Li.

Due to the limited number of rotor inserts available for the VXR system it was not possible to have a sample of LiBr permanently inside one of them. For this reason all the referencing done with this spectrometer was carried out using LiCl solution directly.

4.2.2 NMR STUDY OF $LiBH_4X_y$ COMPLEXES

Organolithium compounds present a vast and interesting chemistry. Their structures are not only of monomeric form but dimer, trimer and other oligomeric structures can also be found among common structures. Even though an ionic bond is

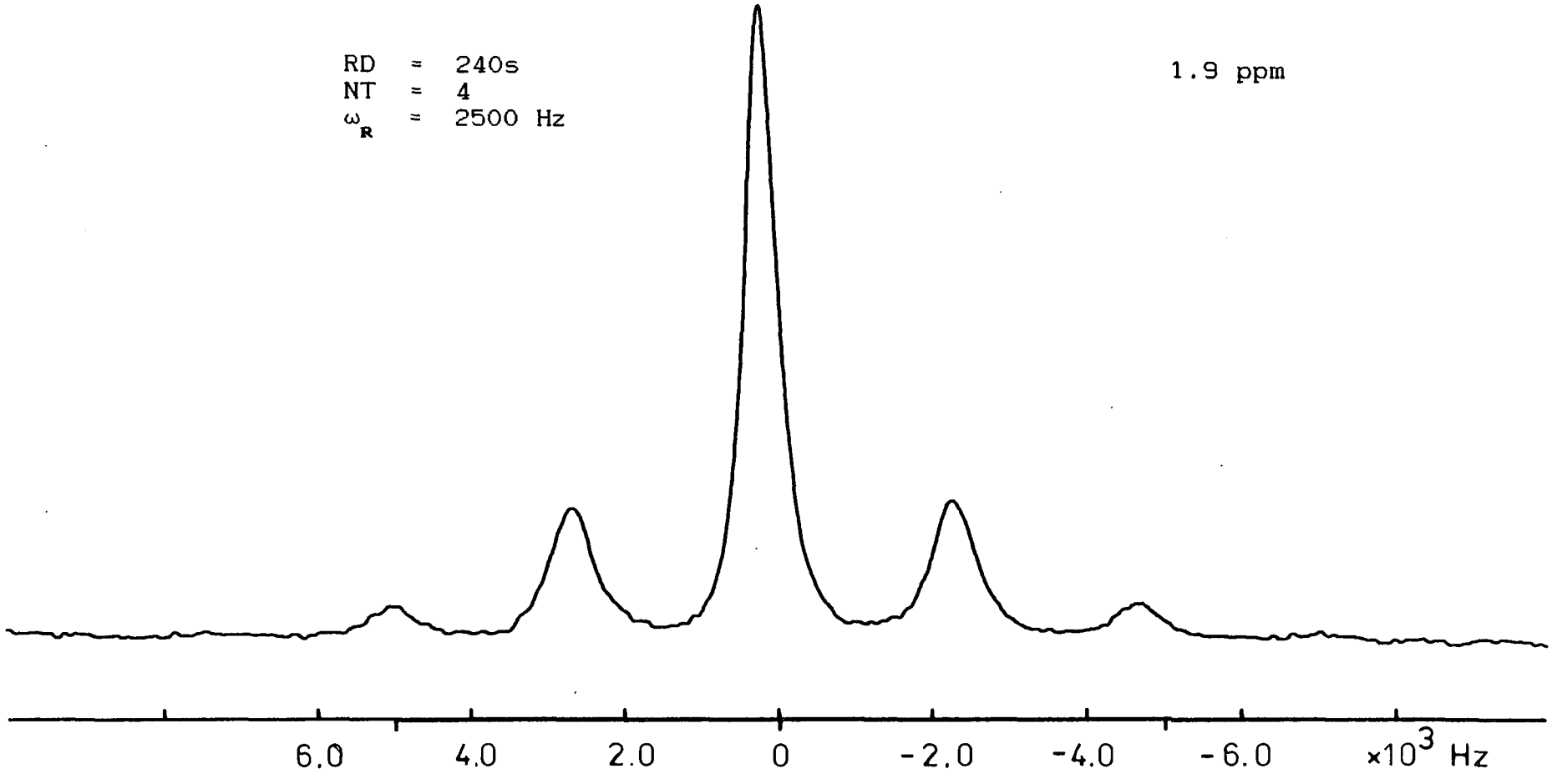

Fig (4-1) ^{7}Li SP/MAS Spectrum of a LiBr sample inside the new rotor insert.

the most representative type of bonding in this type of compound, lithium also has interactions with hydrocarbon π systems and it can be found to engage in multicentre covalent bonding[8].

A great number of organolithium structures have been determined with the use of X-ray crystallography and good compilation reviews have been presented[8]. The use of NMR in the structure elucidation of organolithium compounds has been limited to studies in the liquid phase[9]. These investigations have concentrated on the ^{6}Li isotope, which has always been considered as an "honorary spin 1/2" with sharp resonance lines dominating the spectrum. There are good examples where $J^{(C,Li)}$coupling constants have given valuable information in structure determination[10]. The extent of the NMR application in liquid-state organolithium studies ranges from spin lattice relaxation mechanism, chemical shift studies, scalar spin-spin coupling, to the use of 2-D spectroscopy. The last one has been highlighted in a recent review[11] where the importance of the application of this technique was presented.

However, the application of solid-state NMR has been very limited, even non-existent, in the investigation of organolithium complexes. The one reported case was concentrated on the effects of the quadrupolar interaction from Li upon the ^{13}C NMR spectrum[12]. These limitations have been produced by the large amounts of sample needed and also by the sensitivity of such compounds to air and moisture, already stated.

With the introduction of the new rotor insert, the first of these problems has been greatly reduced, and the second one

eliminated. With these advantages, a family of organolithium complexes was investigated where $LiBH_4$ is the parent compound[13]. The present work could be considered as one of the first attempts to study organometallic compounds by $^7Li/^6Li$ NMR spectroscopy in the solid state to obtain information about the molecular structure of these compounds. In total four complexes were studied, namely: lithium tetrahydroborate-tetramethylethylenediamine $[LiBH_4TMEDA]_2$, lithium tetrahydroborate-di-pentamethyl-diethylenetrianime $LiBH_4PMDETA$, lithium tetrahydroborate tetrapyridine $LiBH_4Pyr_4$, and lithium tetrahydroborate tetra hexamethylphosphoric triamide $LiBH_4HMPA_4$. The first two complexes are the only compounds where full characterization by X-ray crystallography has been done[14,15]. Similarly, they are the only compounds from which both ^6Li, and ^7Li spectra were obtained in this investigation.

4.2.2.1 NMR INVESTIGATION OF $[LiBH_4TMEDA]_2$

$[LiBH_4TMEDA]_2$ was the first compound of this series to be investigated by X-ray crystallography[14], and it was also the first one to be studied in this work by NMR. The X-ray study reveals a very interesting centro symmetric dimer structure in which the two halves of the molecule are linked by the two BH_4 units. From these units, two hydrogen atoms are used in a two centre bonding and one is used in a "three centre bonding" joining the two lithium atoms. At the same time, each of the lithium atoms are bonded to the two nitrogen atoms from the

bidentate TMEDA ligand. These make the lithium atoms 6-coordinate. This uncommon structure can clearly be seen in Fig (4.2)[15].

The crystallographic study gave valuable information about the interatomic distances between the lithium atoms and its surrounding neighbours. With these data in hand, it was possible to estimate the maximum magnitudes of the heteronuclear dipolar interaction , $2\Delta\nu$, experienced by the lithium atom. In this way, it was possible to predict how they might influence the NMR spectrum.

This can be achieved with the aid of equation 2.27 from chapter 2 in which the dipolar breadth, $\Delta\nu$, is given by

$$\Delta\nu = \frac{1}{2\pi} \frac{\mu_o \gamma_I \gamma_S \hbar}{4\pi\ 2r_{IS}^3} \qquad 4.2$$

The results of the calculation using this expression are given in Table (4.1).

It can be seen from the table below that the Li-H interaction is the dominant one in comparison with the rest, but it is also possible to remove its effects with the use of high power proton decoupling (HPPD). As far as the other interactions are concerned, they are small enough to be removed under magic angle spinning (MAS) conditions, and they could be too small to be observed in the static lineshape.

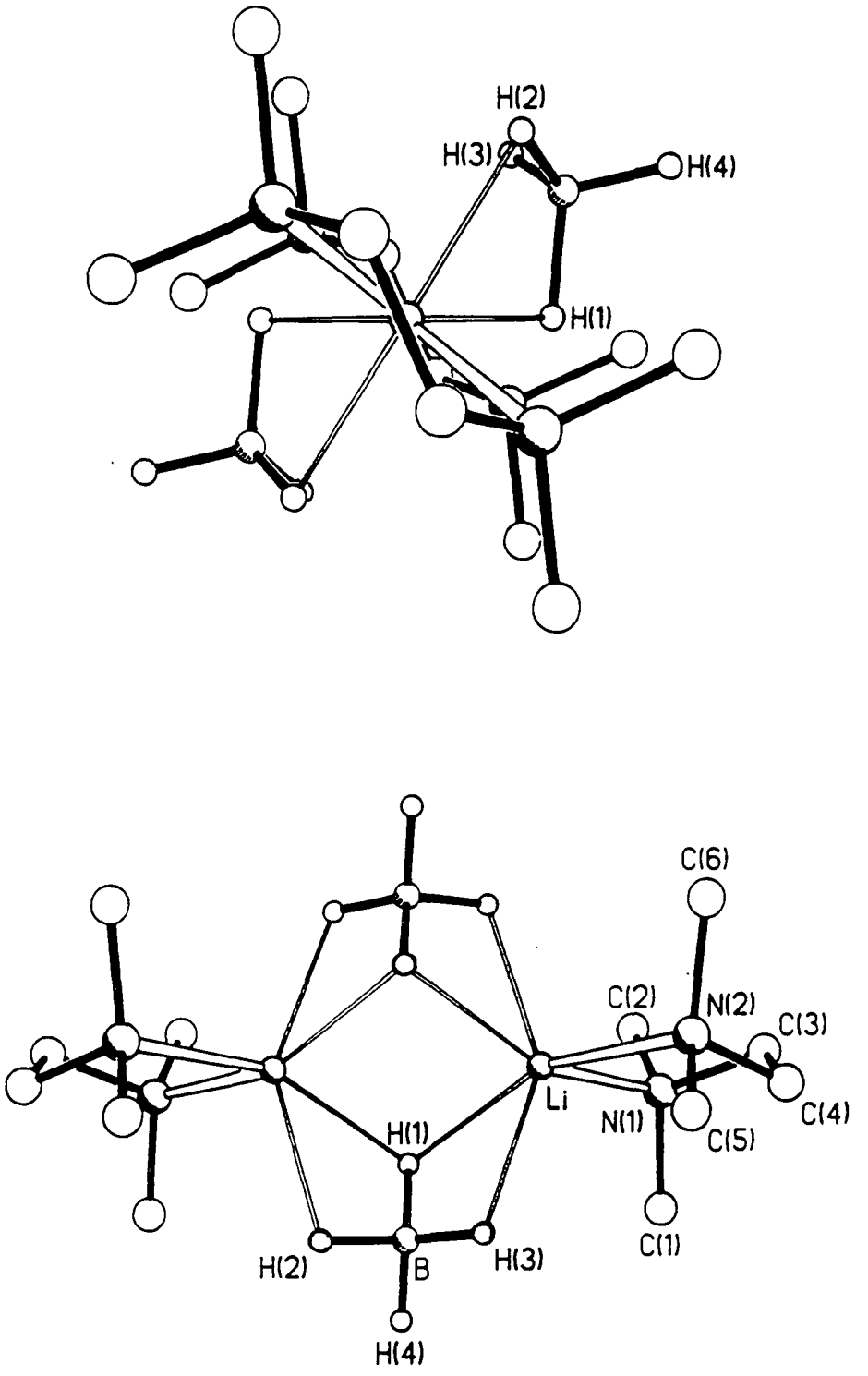

Fig (4-2) $[LiBH_4TMEDA]_2$ molecular structure[14]

S-Nucleus	r_{Li-S} (Å)	$2\Delta\nu$(kHz)
H (1)	2.069	2.632
H (1')	2.116	2.460
H (2')	2.063	2.655
H (3)	2.022	2.819
B	2.467	0.996
B'	2.461	1.0
N (1)	2.115	0.352
N (2)	2.115	0.356

TABLE 4.1 Internuclear distances and dipolar breadth between lithium atoms and its nearest neighbours in [LiBH $_4$ TMEDA] $_2$.

Spectra from this sample were obtained using the Andrew-Beams probe system with the glass capsules described in chapter 3, as well as with the new double-bearing Bruker probes using the new rotor insert already described. A comparison of the spectrum obtained with these systems will be given later.

The ^{13}C spectrum from this sample was taken under CP/MAS conditions with ω_R = 2.4 kHz. This spectrum shows two partially resolved doublets between 45 and 50 ppm and a broad resonance line at 57.3 ppm with an intensity ratio between the doublets and the broad line of 2:1 . After resolution enhancement was applied to the FID the doublet resolved into four lines of equal intensity at 46.5, 46.8, 48.3, and 48.8 ppm, but the broad line at 57 ppm did not show any increase in

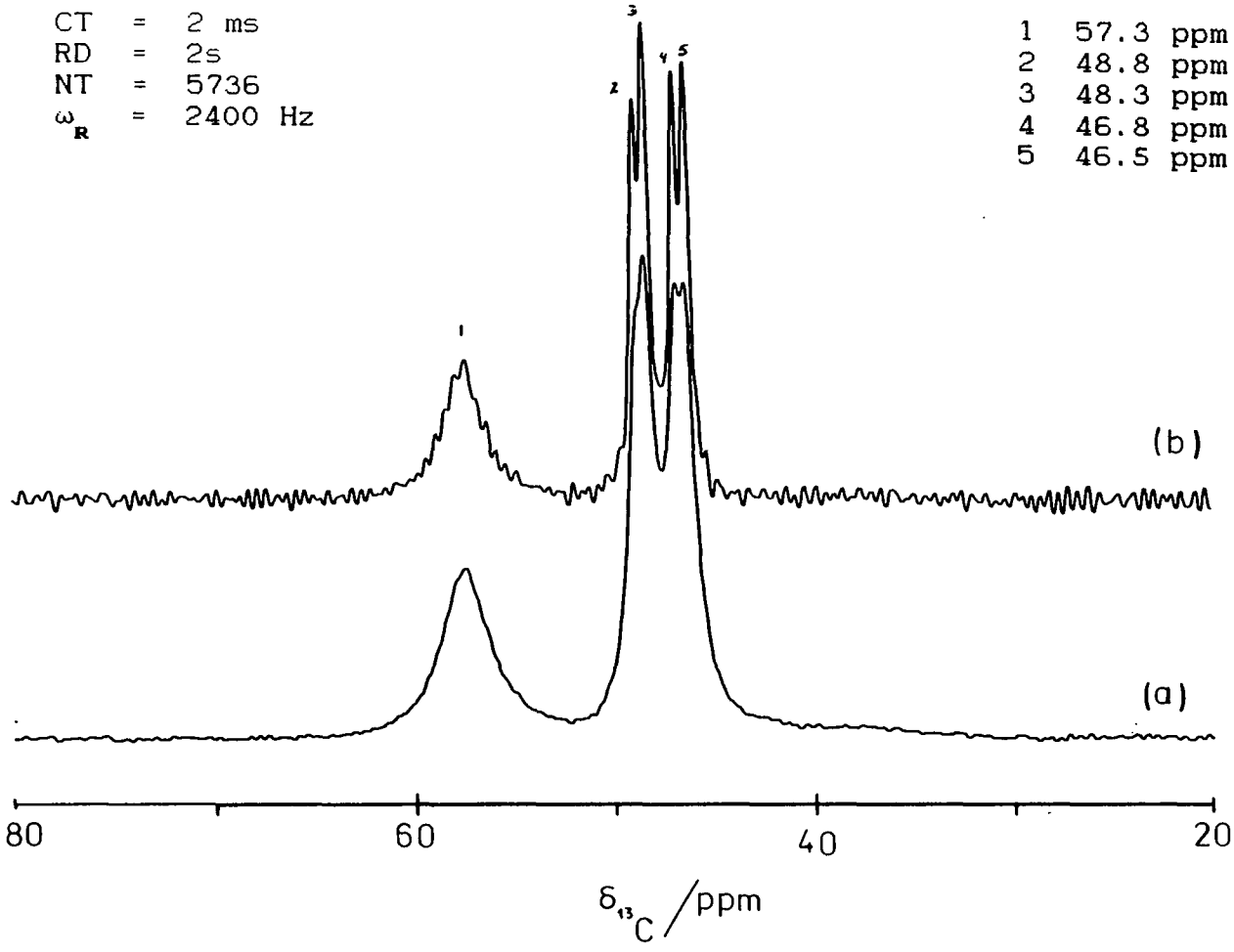

Fig (4-3) ^{13}C CP/MAS Spectrum of $[LiBH_4TMEDA]_2$: (a) normal spectrum, (b) resolution enhance spectrum GB = 0.8, LB = 20.

resolution. These resonance lines can be assigned as follows: the four lines can be attributed to the CH_3 groups attached to the nitrogen in the TMEDA unit; the broad line can be assigned to the two CH_2 groups attached to the nitrogen, having been broadened by the quadrupolar interaction with the N's. The CH_3 groups do not show this effect due to their greater mobility. The eight CH_3 groups are related by the centre of inversion making the four CH_3 in one half of the molecule equivalent to those of the other half. This assignment also agrees with the intensity ratio, i.e. there are twice as many CH_3 as CH_2 per monomeric unit. Fig (4.3) shows the ^{13}C spectrum in both normal conditions and with resolution enhancement.

First, the lithium-7 spectrum was obtained with the sample inside the glass capsule using the Andrew-Beams probe at a magnetic field of 4.6975 T under SP/MAS/HPPD conditions. In these conditions, the spectrum shows a sharp central transition line , $1/2 \longrightarrow -1/2$, at 4.0 ppm with a linewidth, $\Delta\nu_{1/2}$, of 314 Hz. The spinning side band pattern, ssb, spread symmetrically from either side of the central line, covered a frequency range of 80 kHz or the equivalent of 1000 ppm. The overall shape of this set of ssb does not mimic the expected first order quadrupolar pattern, but has a kind of triangular shape.

The SP/MAS/HPPD spectrum was also obtained with the sample inside the new rotor insert used in the double-bearing Bruker probes for the CXP spectrometer. A similar insert was also used with the probe system for the VXR spectrometer, with a resonance frequency at ν_o= 116.571 MHz for ^7Li. The spectrum

obtained under these conditions did not show any difference from the previous one. The chemical shift was the same at both magnetic fields within experimental error. The spread of the ssb pattern was reduced from 1000 ppm to 800 ppm, an expected effect when going from low field to high field. These three spectra are presented in Fig (4.4) indicating the conditions under which they were taken.

Static band shapes were obtained in all probe systems and magnetic fields described above. In the case of the glass capsule the spectrum shows a doublet in the central transition peak with a splitting of 1.58 kHz and a $\Delta\nu_{1/2}$ = 4296 Hz. The spectrum also shows small symmetrical intensity features that spread over the same frequency range as the the one observed in the ssb pattern. These features may be related to outer $\pm 3/2 \longrightarrow \pm 1/2$ transitions. This spectrum was reproduced at the higher magnetic field but showed less sensitivity in the outer transition region of the spectrum.

The static spectrum was also obtained with rotor inserts. This configuration together with the use of the Bruker double-bearing probes gave a dramatic improvement in sensitivity. It shows the same central transition resonance line together with well resolved outer signals in the region where the outer transitions were expected. The maxima of these resonance lines came at 37.0, 28.3, 24.6, and 9.3 kHz respectively. A comparison between the low sensitivity and high sensitivity spectrum is present in Fig (4.5). Close examination of these spectra shows that the better-resolved non-central transition signal shown in Fig (4.5b) reproduces

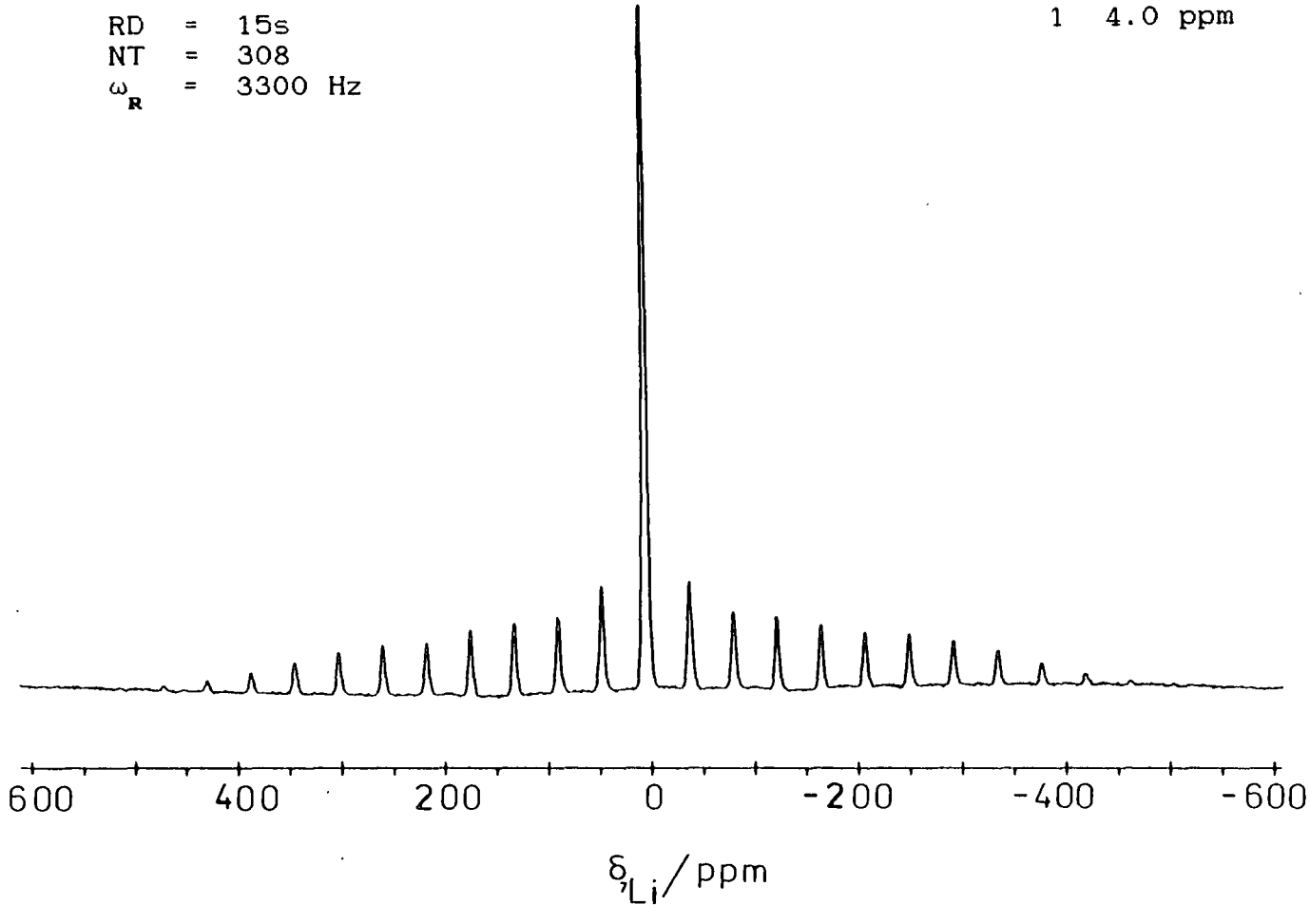

Fig (4-4a) ^{7}Li SP/MAS/HPPD Spectrum of $[LiBH_4TMDA]_2$ with the sample inside a glass capsule using Andrew-Beams probe at 4.6975 T.

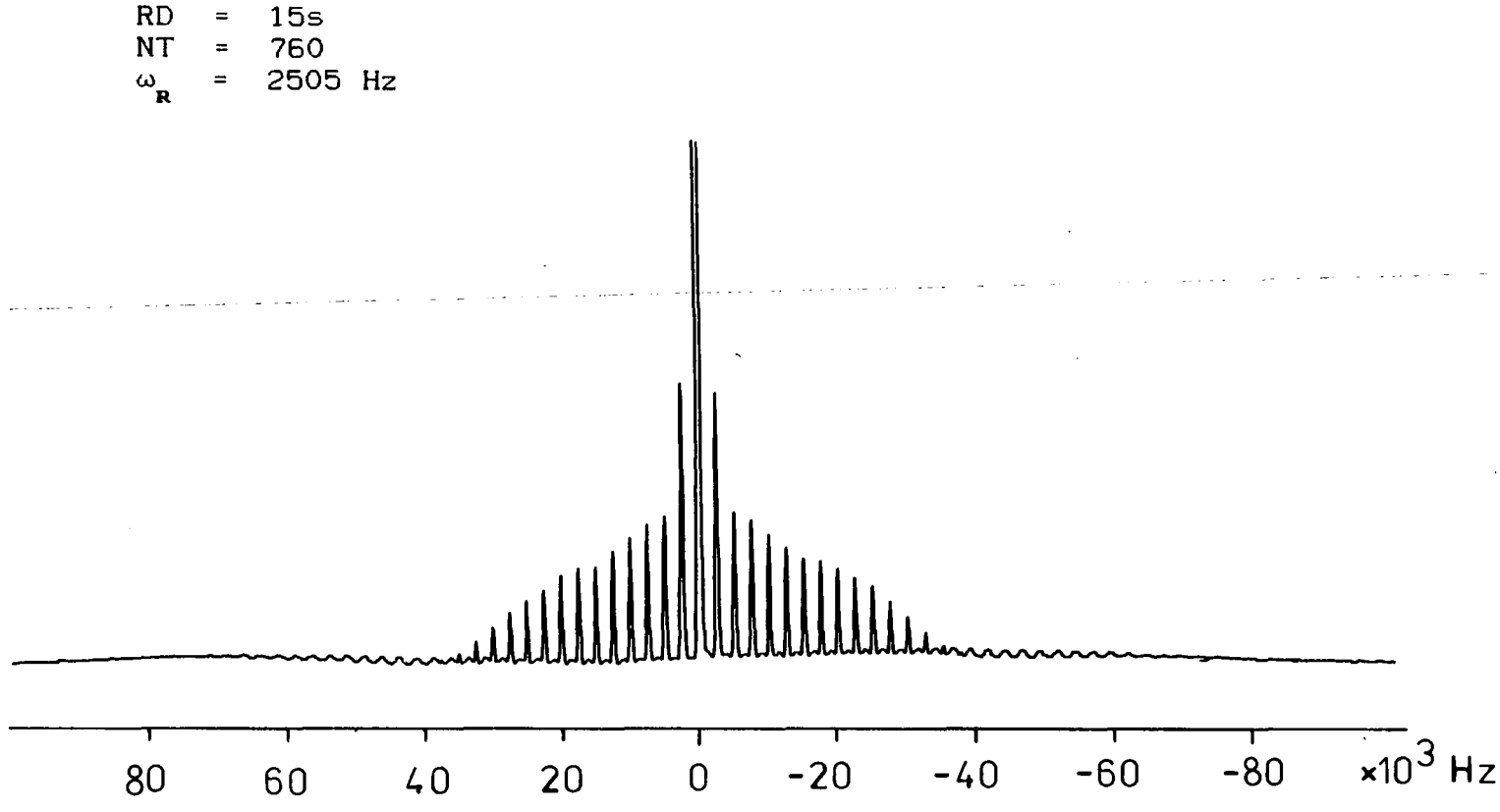

Fig (4.4b) ^{7}Li SP/MAS/HPPD Spectrum of $[LiBH_4TMEDA]_2$ with sample inside the new rotor insert at 4.6475 T.

RD = 15s
NT = 256
ω_R = 4030 Hz

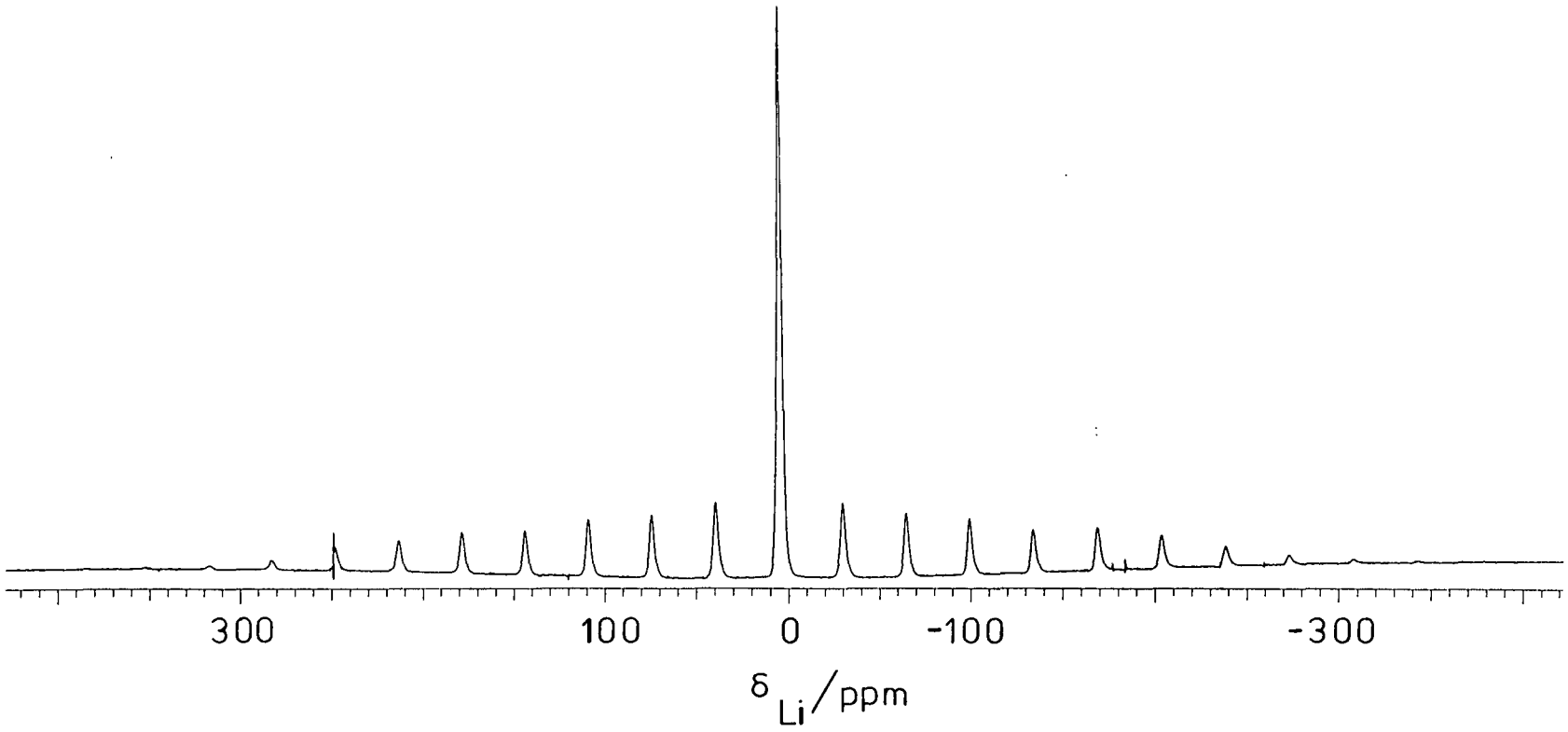

Fig (4-4c) ^{7}Li SP/MAS/HPPD Spectrum of $[LiBH_4TMEDA]_2$ with the sample inside the new insert at 7.0463 T.

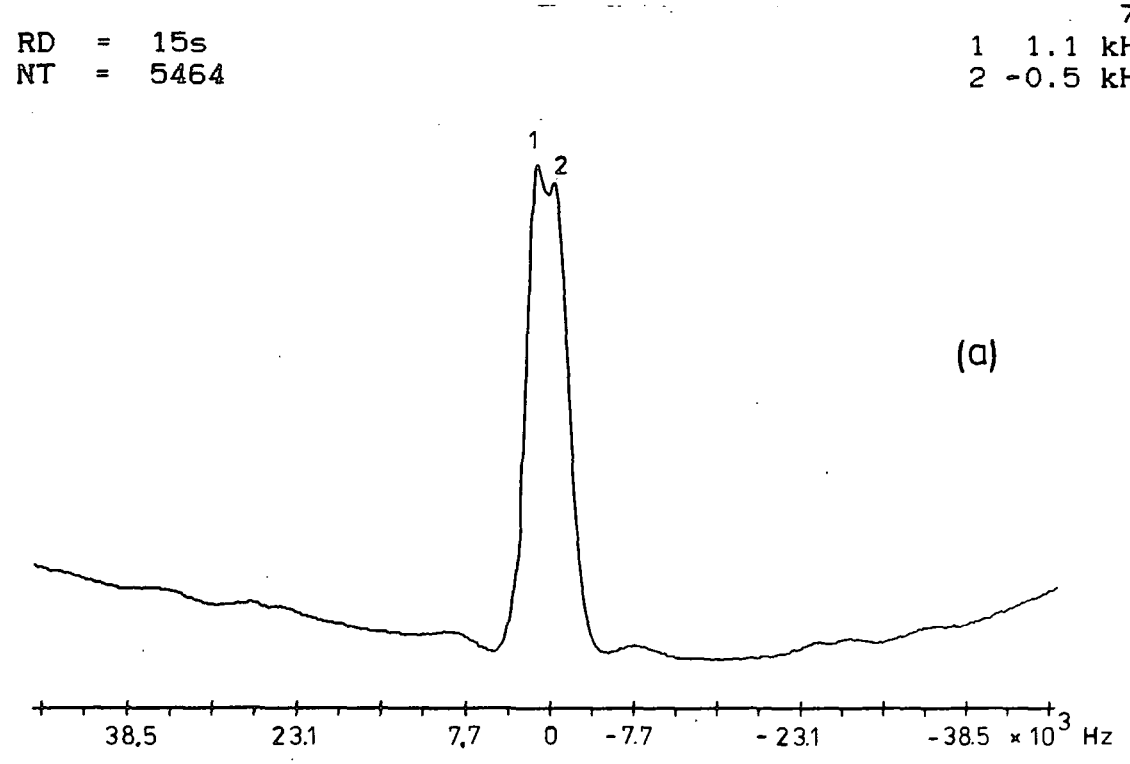

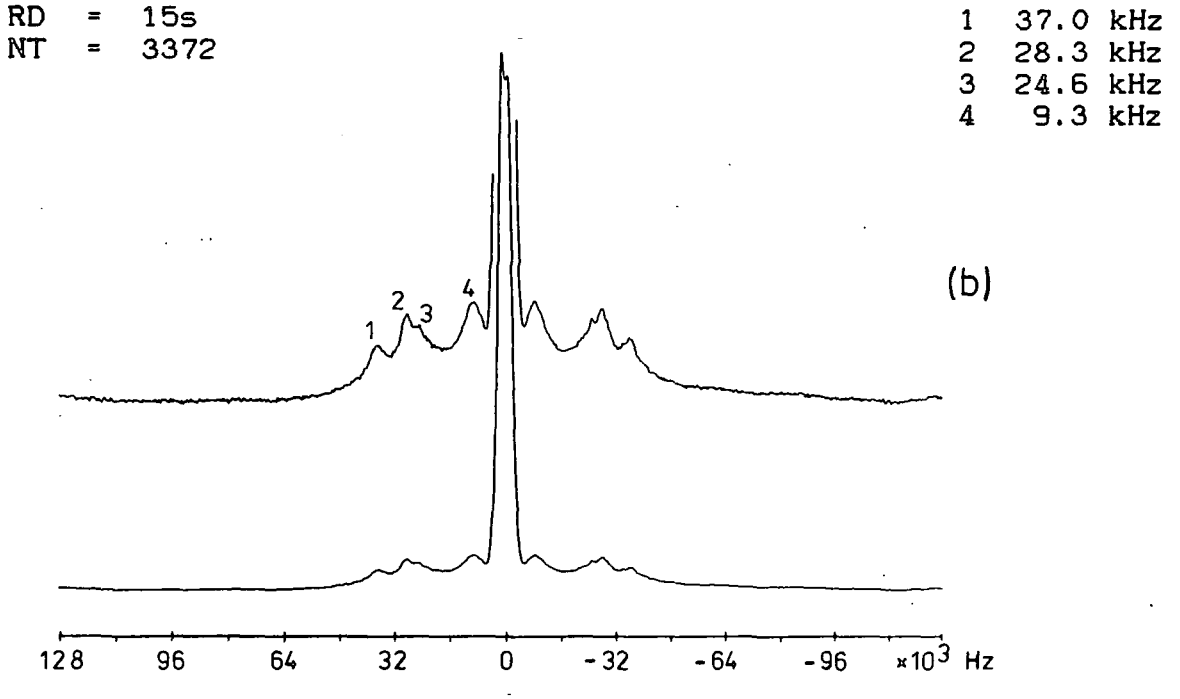

Fig (4-5) ^{7}Li SP/static/HPPD Spectrum of $[LiBH_4TMEDA]_2$: (a) with the sample inside a glass capsule at 4.6975 T, (b) with the sample inside the new rotor insert at 4.6975 T.

those at low intensity seen in Fig (**4.5a**) spectrum even though no precise measurement of their position could be made using the latter spectrum.

As far as the central doublet in the static spectrum is concerned, this splitting cannot be attributed to second order quadrupolar effects because it is not possible to remove this type of interaction with MAS at the values of ω_R used to obtain the spectra in Fig (**4.4**), and only a sharp central resonance line is observed in it. It may be possible to explain this splitting in terms of a dipolar interaction but this is in contradiction with the values of the dipolar breadth reported in Table (**4.1**). It may be possible to believe that this effect can be explained in terms of two different types of lithium atoms within the molecules. However, this cannot easily be correlated considering the fact that the SP/MAS spectrum shows only one resonance line for the central transition, and also no splitting was observed in the ssb pattern, within the resolution of the acquired data. In the same manner as before, this will not agree with the crystallographic information. Fig (**4.6**) shows a comparison between the SP/MAS/HPPD and SP/static/HPPD spectrum obtained from the Bruker double-bearing probes. In the SP/MAS spectrum, it is not possible to distinguish the different structures observed in the static one. But it is possible to see that intensity from the signals at $\approx \pm$ 450 ppm drops off considerably, an effect that would not be expected if this signal comes from an outer transition.

Another possible way of interpreting this spectrum is to consider that some kind of molecular motion is occurring and

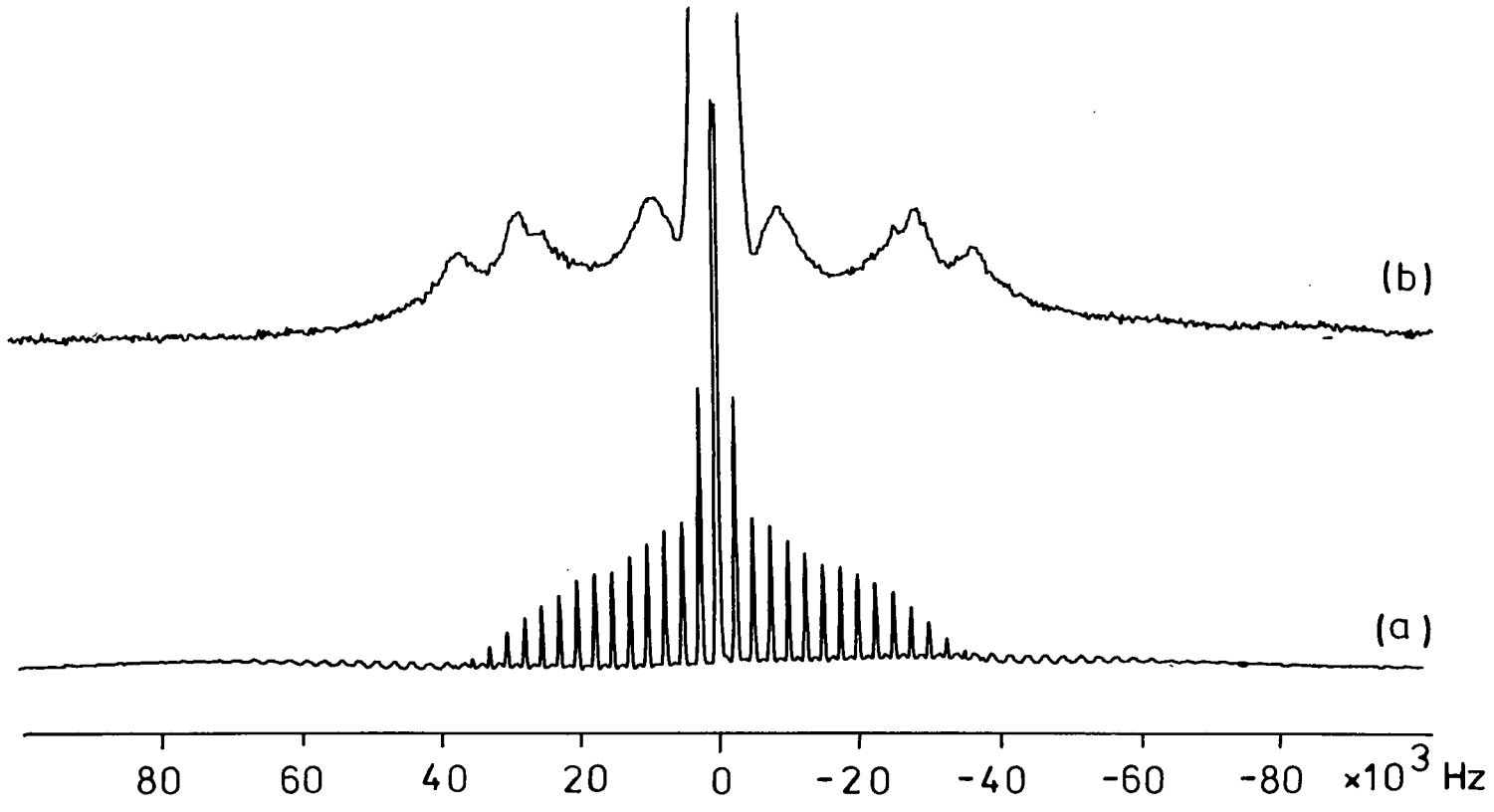

Fig (4-6) ^{7}Li (a) SP/MAS/HPPD and (b) SP/static Spectra of $[LiBH_4TMEDA]_2$ from Fig (4-4c) and Fig (4-5(b)).

producing this type of pattern. In this direction, variable temperature work was carried out at 7.04 T to determine if this was a reasonable explanation. The temperature was varied between room temperature to -110° C (163 K), and the spectra were taken in static conditions using SP/HPPD. It was not possible to observe any appreciable change in the spectrum over this temperature range. The splitting in the central transition line did not change, maintaining its value of 1.58 kHz over all the temperature range. This result may suggest that this splitting can be caused by dipolar interaction but at this point in time it cannot be justified on account of the overall evidence already presented. The results also show that no molecular motion is occurring in this temperature range. There are limitations that do not allowed the performance of the same work at high temperatures, namely the material from which the insert is made, and more important, the low melting point of the actual sample. Therefore, no attempt was made in this direction.

With these unknowns in hand, it was decided to perform a similar type of study looking this time at the ^{6}Li resonance lines. This work could only be carried out using the VXR spectrometer due to sensitive problems encountered with operation of the CXP spectrometer and specially with the low frequency probe. In this case of the VXR, the resonance frequency is at ν_o = 44.15 MHz. The spectra were taken from the sample inside the new rotor insert modify for the VXR system.

Let us assume for a moment that each of the outer signals originate from lithium atoms under the influence of first

order quadrupolar interaction but with different magnitude of Q_{cc}, i.e. different degrees of distortion of the EFG. Under this assumption, it is possible to estimate the magnitude of Q_{cc} of the ^{7}Li isotope from the expression $A_1 = (1/4)\, Q_{cc}^{16}$, where A_1 is the separation between outer transitions and the central one. Table (4.2) shows a summary of the calculation using this expression, indicating the value for A_1 and the corresponding value for $(^{7}Li\text{-}Q_{cc})$.

It is possible to predict the magnitude of $(^{6}Li\text{-}Q_{cc})$ from the fact that it is related to the one from ^{7}Li isotope by the expression

$$\frac{(Q\text{-}^{7}Li)}{(Q\text{-}^{6}Li)} = \frac{(^{7}Li\text{-}Q_{cc})}{(^{6}Li\text{-}Q_{cc})} \qquad 4.3$$

where $(Q\text{-}X)$ = the quadrupole moment of the particular nucleus isotope.

$(X\text{-}Q_{cc})$ = the quadrupole coupling constant of the particular nucleus isotope.

It is therefore possible to use the values of $(^{7}Li\text{-}Q_{cc})$ in Table (4.2) to predict the possible expected values from ^{6}Li. The values obtained with the use of the expression 4.3 are also presented in Table (4.2). So, on the basis of these predictions, it would be expected to see a resonance line with some kind of structure and with a $\Delta\nu_{1/2} > 3kHz$.

The $[^{6}LiBH_4TMEDA]_2$ spectrum gave a very unexpected

result. The SP/MAS spectrum, run with ω_R = 0.5kHz, shows a symmetrical ssb pattern with a central band at 0.22 ppm and spreading over a range of 4 kHz. No splitting was observed in the individual ssb's. The static spectrum shows a single resonance line centred at 0 ppm, with $\Delta\nu_{1/2}$ = 2.2 kHz, and no detectable structures are observed. This linewidth is smaller than the highest expected quadrupolar interaction under the proposed assumption given above. Fig (4.7) shows the plot of the $[^{6}LiBH_4TMEDA]_2$ SP/MAS/HPPD and static spectra.

A_1 (kHz)	(^{7}Li-Q_{cc}) (kHz)	(^{6}Li-Q_{cc}) (kHz)
37.04	145.00	2.57
28.28	109.96	1.96
24.62	95.31	1.70

Table (4.2) Estimated and predicted values for the quadrupolar coupling constant for ^{7}Li and ^{6}Li isotopes.

As a matter of completion, a variable temperature study was also carried out observing the ^{6}Li isotope at 20°C, -50°C, -70°C, and back to 20°C again. These spectra were taken under MAS conditions with ω_R = 0.65 kHz. No increase was observed in the spread of the ssb pattern nor on the linewidth of the individual ssb over the temperature range mentioned above. This result agrees perfectly well with that obtained for the ^{7}Li isotope described earlier in that no molecular motion occurs within the temperature range. But at the same time it

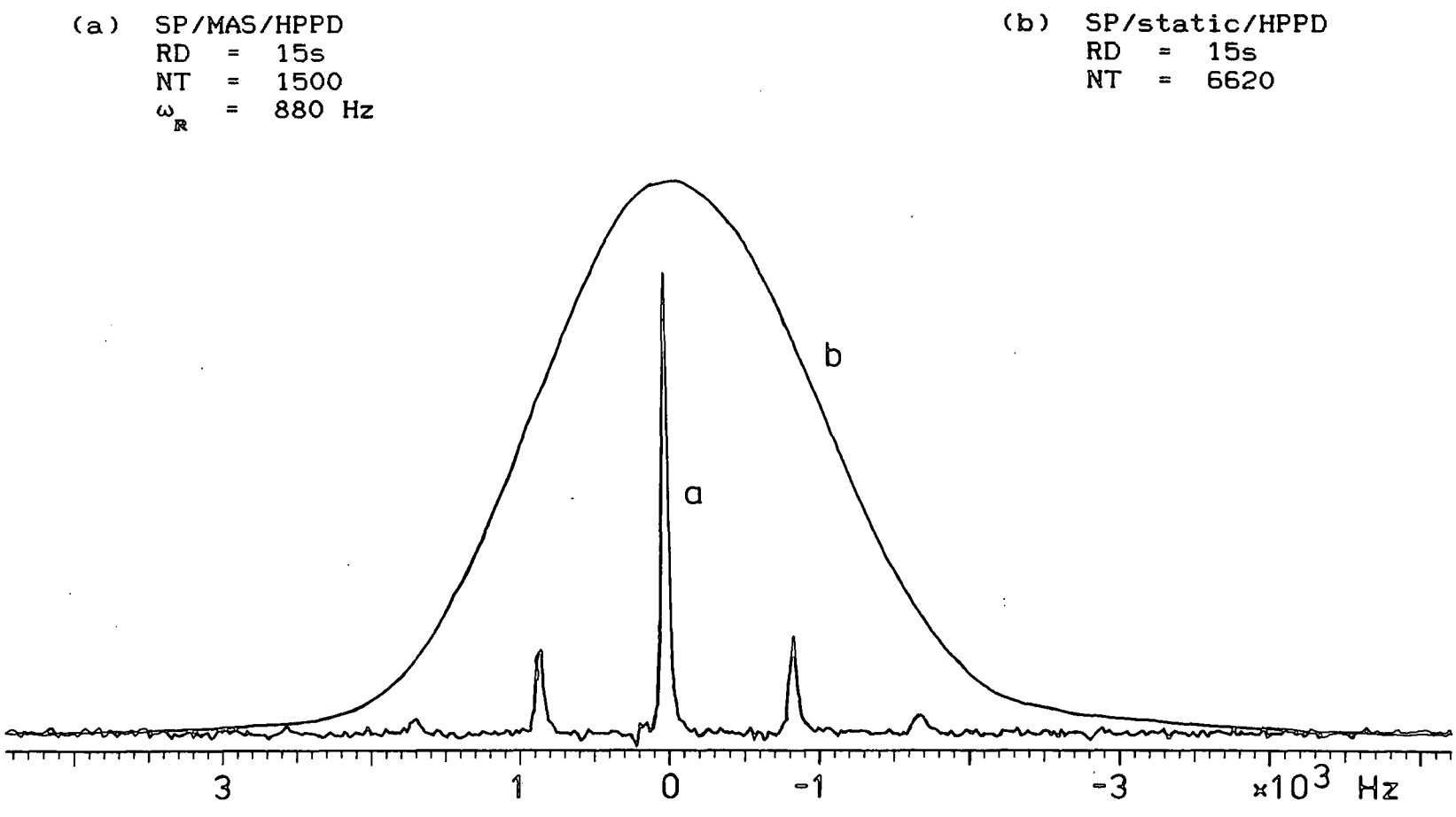

Fig (4-7) ^{6}Li (a) SP/MAS/HPPD and (b) SP/static/HPPD Spectra of $[LiBH_4TMEDA]_2$ with the sample inside new rotor insert at 7.0463 T.

does not give any new information concerning interpretation of the quadrupolar NMR spectra from either or both isotopes.

In conclusion, it is not possible to determine the actual origin giving rise to the static lineshape observed from ^{7}Li isotope spectrum. It can only be said that the quadrupolar coupling constant for this system is in the range between 140 and 90 kHz. It is also possible to say that no molecular motion was observed between room temperature and -110°C and that no extra information was obtained when looking at the NMR resonance signal from the ^{6}Li isotope.

4.2.2.2 NMR INVESTIGATION OF $LiBH_4$PMDETA

At the start of this investigation no crystallographic data was available for this complex and therefore an attempt was made to predict the possible structure.

Based on the crystallographic information known from the previous complex, and with the knowledge of the molecular formula of the present one, it is possible to predict two possible molecular structures for this complex. Both of these possible structures involve the bonding of the lithium with the three nitrogen atoms of the tridentate pmdeta ligand. The difference between the two possible structures will be in the way that BH_4 unit is bonded to the lithium atom. Two possibilities can be considered in this case, namely that i) three hydrogen atoms will be bonded to the lithium or ii) that only two hydrogen atoms are involved in the bonding. It was

thought at the time that the first arrangement for the BH_4 unit was the most likely one.

A recent crystallographic study done on this complex[15] shows that the actual structure involves the second configuration for the BH_4 unit and not the first one as was assumed. The structure of the $LiBH_4$PMDETA complex is presented in Fig (4.8)[15]. This structure presents the (Li-H_2-B) unit in the same plane, with the remaining two H in a plane perpendicular to it. So, the lithium is in a five coordinate environment at the top vertex of a triangular pyramid where the three nitrogens form the base of this pyramid (see Fig (4.8b)). The BH_4 can be said to be looking down towards the top vertex where the lithium is located. Under this condition, it is possible to say that $\eta \neq 0$, but it should be small.

It also shows that the two Me groups, 8 and 9, are symmetrical with respect the (Li-H_2-B) plane whereas the 1,2 Me groups are not, due to the arrangement of the (CH_2-CH_2) unit directly linking N(1) and N(2) atoms.

As in the previous case, the internuclear distance obtained from the crystallographic data was used to determine the value of $2\Delta\nu$ with the help of equation 4.2. The results are presented in Table (4.3). None of the dipolar interactions appear to be important in the interpretation of the NMR spectrum of this complex.

The ^{13}C spectrum reveals the inequivalence of the Me in the $N(CH_3)_2$ groups mentioned in the previous paragraph. It shows four partially resolved resonance lines and a broad asymmetrical resonance. When resolution enhancement is

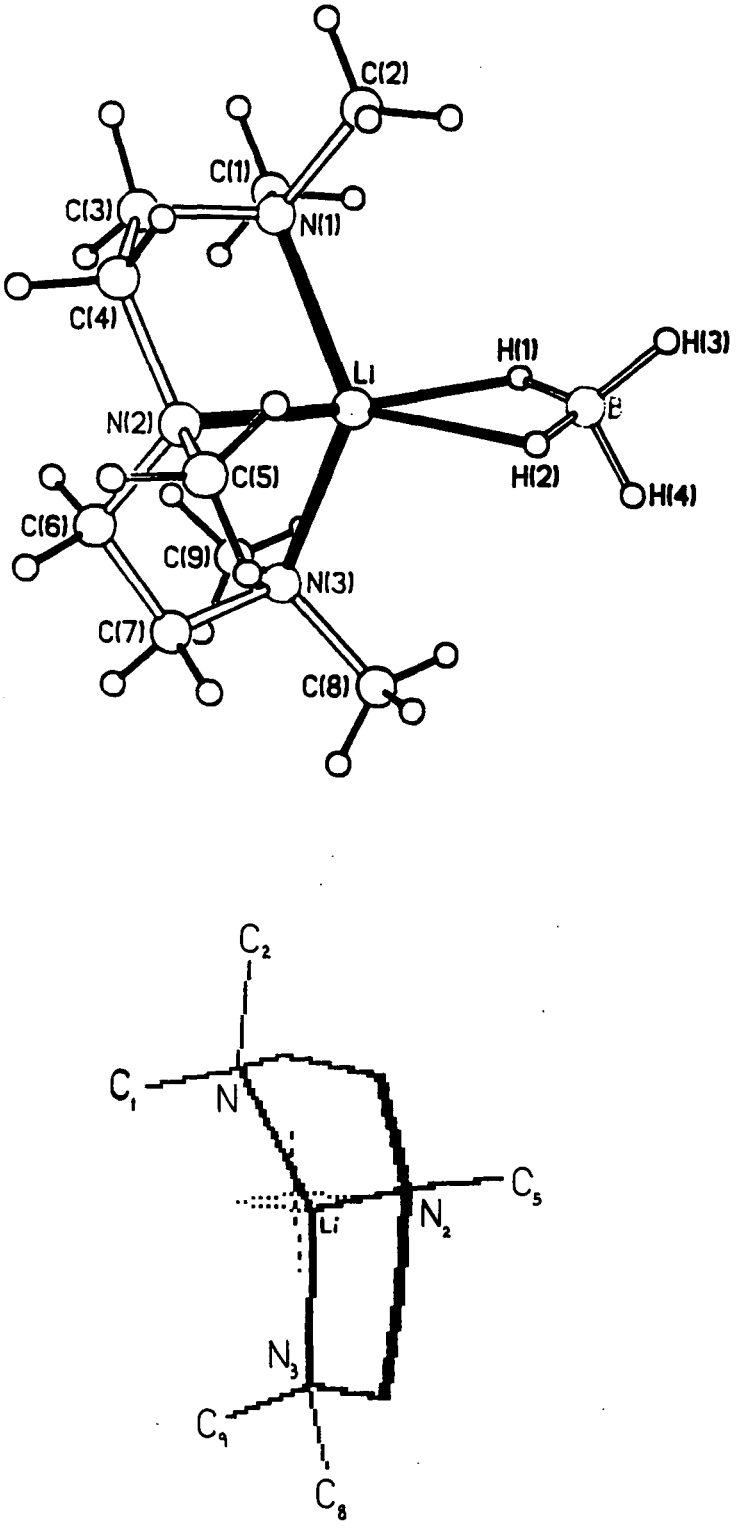

Fig (4-8) $LiBH_4$PMEDTA molecular Structure[15].

applied to the FID, it shows four resonance lines at 45.0, 45.9, 47.0 and 48.1 ppm with intensity ratio of 1:2:1:1. Based on the molecular structure, this resonance could be assigned as: the ones at 45.0 and 46.9 ppm are due to the (1),(2) unsymmetrical Me groups; the double intensity peak at 47.0 ppm due to the symmetric pair of Me groups at positions (8) and (9); and finally the resonance at 48.1 ppm due to the Me group at position (5) bonded to N(2). The broad band between 50 and 60 ppm could not be resolved by this treatment but can be assigned, undoubtedly, to the two (CH_2CH_2) chains from the backbone of the ligand. These units are not equivalent and this is reflected in the spectrum. The ^{13}C spectrum is presented in Fig (4.9).

S-Nucleus	r_{Li-s} (A)	$2\Delta\nu$ (kHz)
H (1)	1.984	2.984
H (1')	1.992	2.948
B	2.327	1.186
N (1)	2.118	0.354
N (2)	2.113	0.356
N (3)	2.103	0.362

TABLE 4.3 Internuclear distances and dipolar breadth between lithium atoms and its nearest neighbours in $LiBH_4$PMDETA.

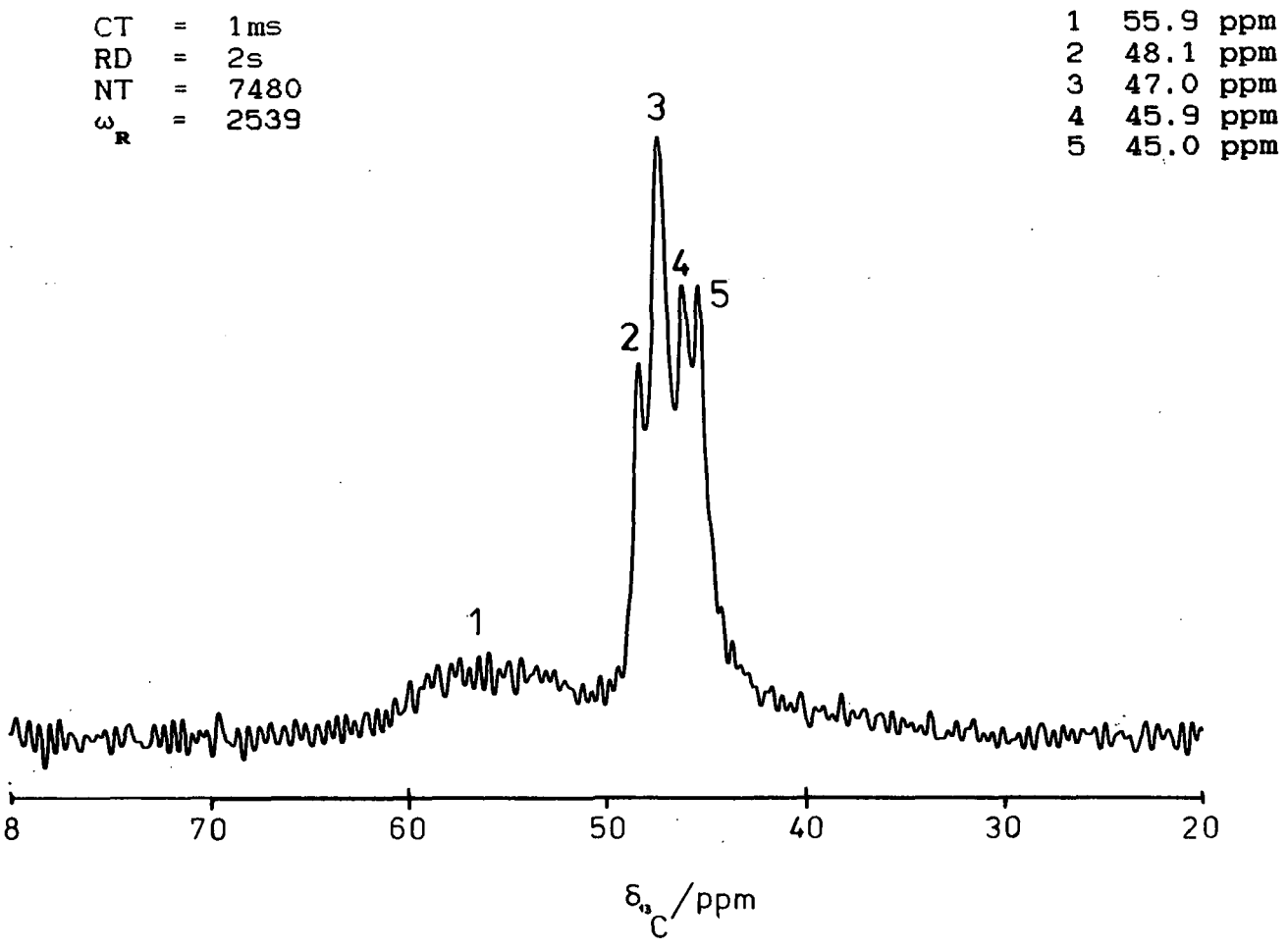

Fig (4-9) ^{13}C CP/MAS Spectrum of $LiBH_4$PMDETA; resolution enhanced. GB = 0.8, LB20.

The $^{7}LiBH_4$PMDETA spectra were obtained under the same conditions as in the case of $[LiBH_4TMEDA]_2$, namely at two different magnetic fields and with the use of both rotor inserts. The SP/MAS/HPPD spectrum shows a sharp central band at 4.2 ppm with a $\Delta\nu_{1/2}$= 97.7 Hz, and a ssb that spreads over 160 kHz or the equivalent of 1800 ppm. The central resonance assigned to the central transition band is almost 3 times sharper in comparison to the one observed in the previous complex. The ssb pattern is a good resemblance of a first order quadrupolar interaction lineshape with the possibility to observe ssb in the region where the outer step from the $\pm 3/2 \longrightarrow \pm 1/2$ are expected, and the individual sidebands do not show any splitting along the spectrum.

The static/SP/HPPD spectrum shows the expected quadrupolar powder pattern, but not as simple as the MAS spectrum may have indicated. The central transition band shows a very distinctive fine structure with feature at 1941, 721, 305, -1013 and -2917 Hz., and with a total $\Delta\nu_{1/2} \approx$ 2kHz. For their part, the outer transition signals show a splitting with a value of 3.7 kHz. The maxima of this splitting are 33.36, 29.67, -29.28, and -33.16 kHz respectively. It is also possible to observe the outer steps from these transitions at 64.19, and -62.8 kHz. A plot of these two spectra is presented in Fig (**4.10a** and **b**). No differences were observed between the spectra obtained at the two magnetic fields

It is evident from these results that no second order quadrupolar interaction affects the ^{7}Li spectrum of this complex. All the fine structures observed in the static

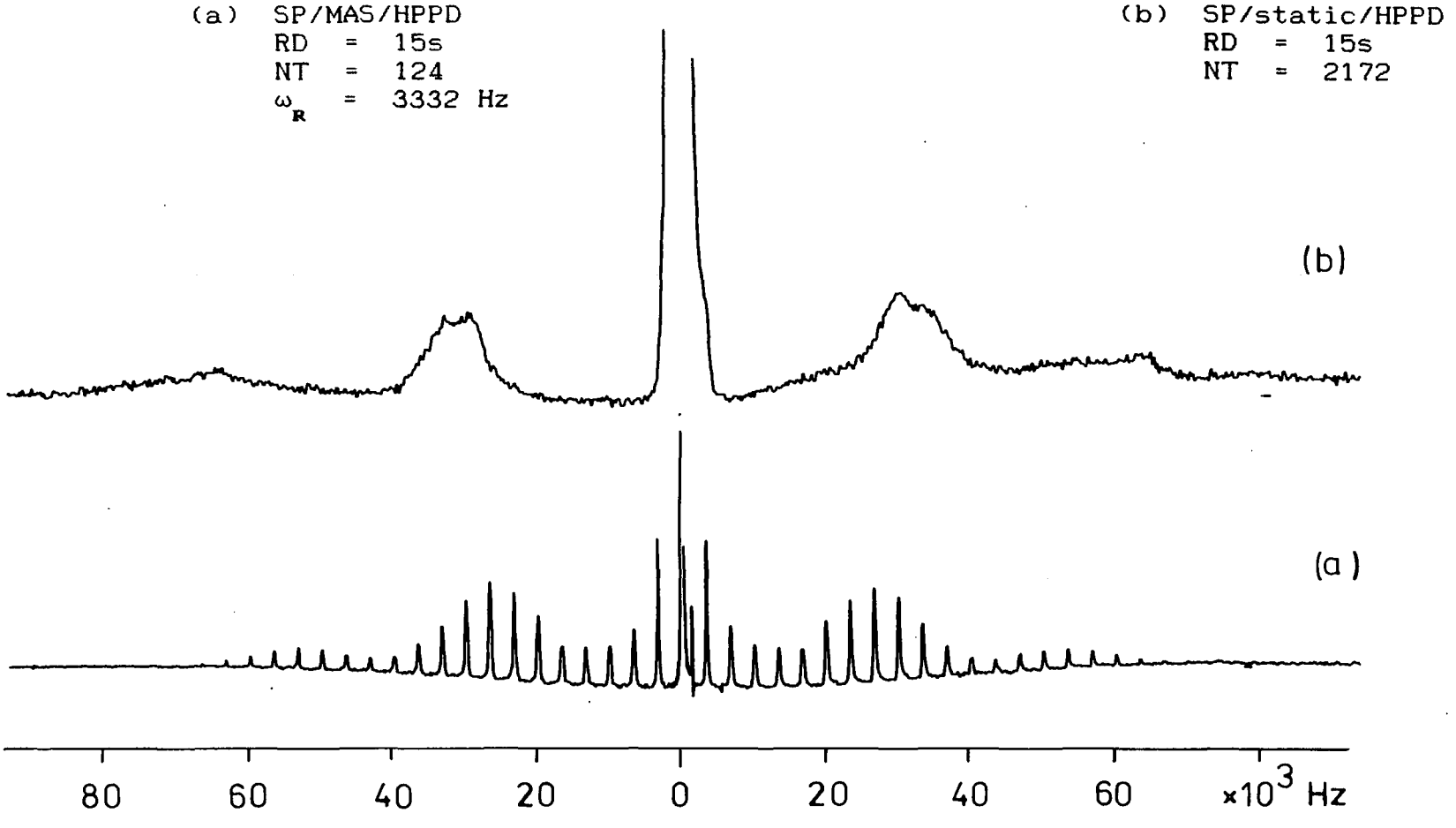

Fig (4-10) ^{7}Li (a) SP/MAS/HPPD and (b) SP/static/HPPD Spectra of $LiBH_4$PMETA using new rotor insert at 4.6975 T.

spectrum of the central transition (see Fig (4.10c)), as well as in the outer transitions, appear to average under MAS conditions, considering the fact of the very sharp central transition line observed in the MAS spectrum. An interesting point is the fact that even when the splitting in the outer transitions is 3.7 kHz, the $\omega_{R=}$3.1 kHz is enough to average whatever effect is producing the observed splitting in the static band shape, i.e. no splitting is observed in the ssb pattern in this or any region of the spectrum. A possible explanation for these fine structures in the central transition line could be that they result from dipolar interaction between Li and B combined with some possible chemical shift interaction. This may also have applied for the outer transition band.

If it is assumed that the splitting in the outer transitions is a symmetrical one and that under MAS condition it will coalesce in its centre (as they actually do), it is possible to estimate the value of A_1 from the average of the splitting. If the average value of the two A_1 values is also taken, it is possible to calculate the value for the $^{7}Li\text{-}Q_{cc}$, as has already been described, to be equal to 124.75 kHz. Under these conditions, it is possible to estimate the value of $^{6}Li\text{-}Q_{cc}$ obtaining a value of 2.22 kHz.

As has already been indicated, the ^{6}Li spectra for this sample was only obtained at the higher magnetic field using the new rotor inserts. The SP/HPPD/MAS spectrum shows a sharp central line at 0 ppm with ssb spreading over 5 kHz or the equivalent of 113 ppm. The first ssb to either side of the central band have almost the same intensity as the centre band

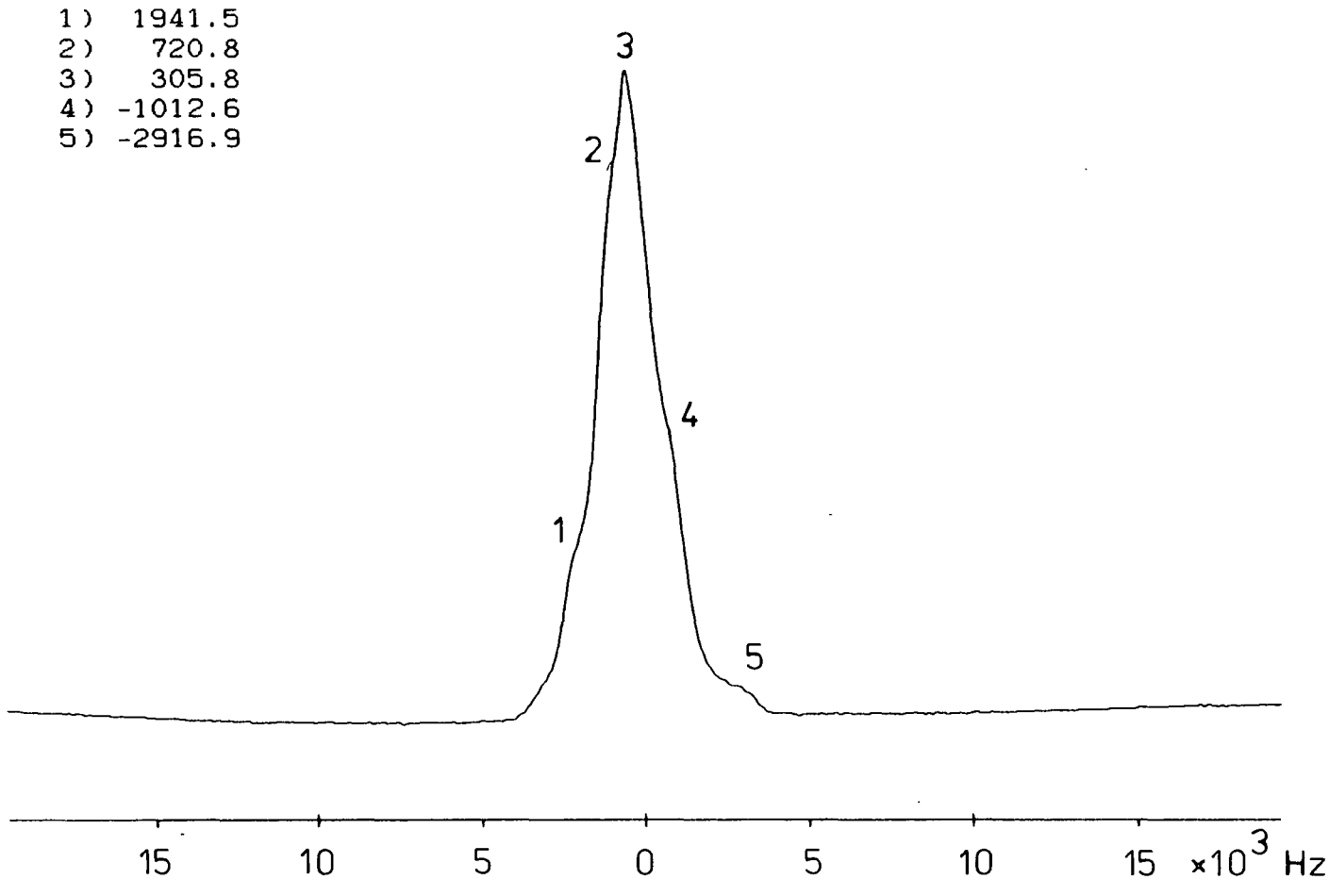

Fig (4-10c) $LiBH_4$PMDETA Spectrum; expansion of Fig (4-10(b)).

and the intensity of remaining ssb drop rapidly to zero intensity. The static spectrum is more informative than the MAS one. It shows a well resolved doublet characteristic of a quadrupolar powder pattern for spin 1 nucleus. The maxima of the doublet are at 593 Hz(13.4 ppm) and -837 Hz(-18.9 ppm), which gives a total splitting of 1.43 kHz. The spectrum also shows some extra structure from the outer step of the transition at about 1.6, -1.5 and -2.0 kHz. Plots of both the MAS and static band shape from $^{6}LiBH_4$PMDETA are presented in Fig (4.11).

It is possible to calculate the ^{6}Li-Q_{cc} from the value of this splitting with the aid of the expression $\Delta\nu = (3/4)Q_{cc}$[16]. The value obtained using this expression was equal to 1.91 kHz. This value is in very good agreement with respect to the prediction made from the information given by the ^{7}Li spectrum, within experimental error. This result seems to indicate that the assumption under which the ^{6}Li quadrupole coupling constant was calculated from the one from ^{7}Li may be correct giving a high degree of confidence in the results presented. This is taking into account that the measurements used in the calculations were taken directly from the static spectrum and not from line-fittings to experimental spectrum.

As far as the structure observed in the ^{6}Li static powder pattern is concerned, it could also be explained in terms of the dipolar interaction between Li-B or chemical shift interaction as it was observed for the case of ^{7}Li. But in this case, the dipolar breadth is 3 time smaller. So, it is possible that the chemical shift interaction may be dominant

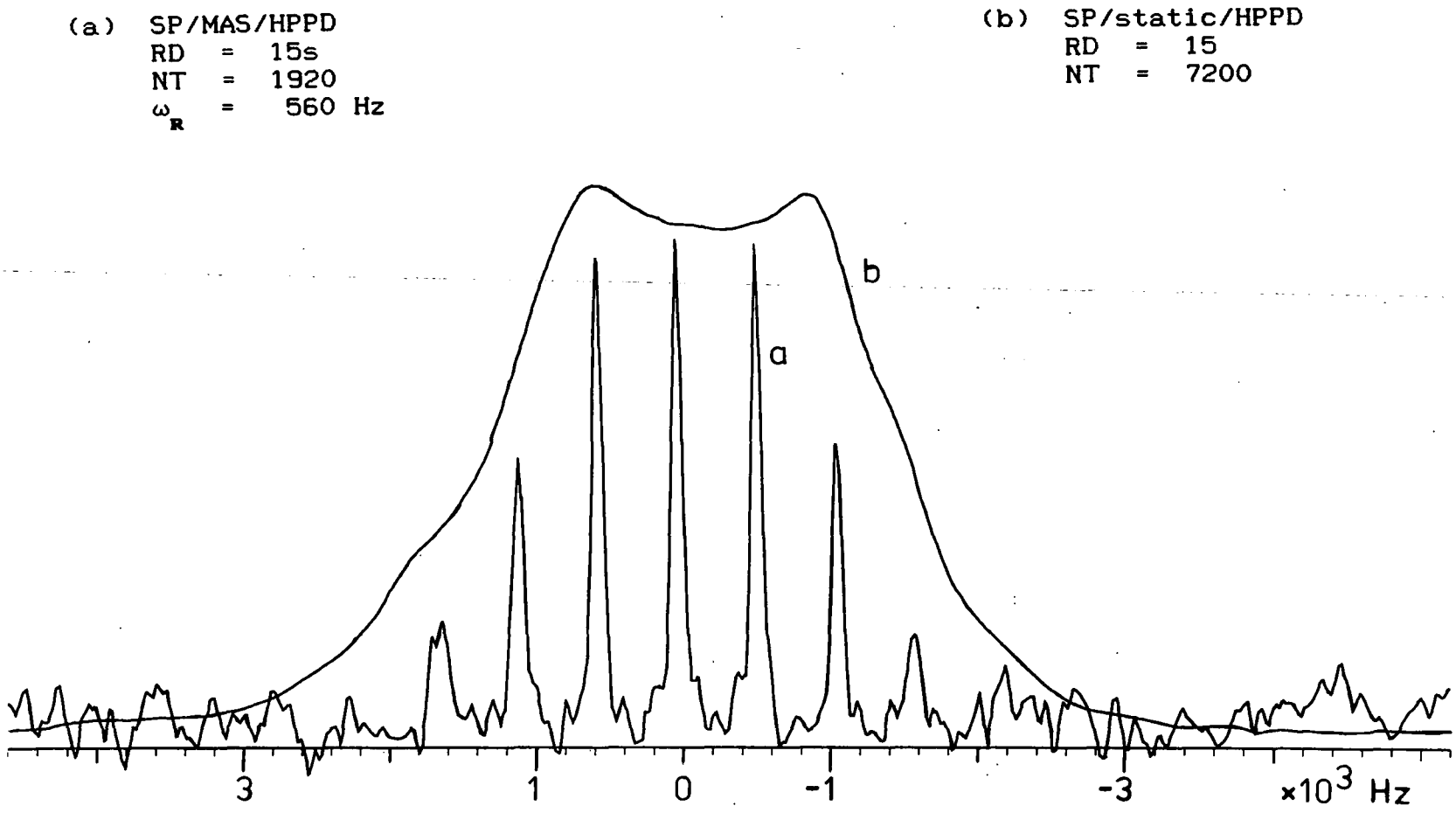

Fig (4-11) ^{6}Li (a) SP/MAS/HPPD and (b) SP/static/HPPD Spectra of $LiBH_4$PMDETA using the new rotor insert at 7.0463 T.

over the dipolar interaction.

4.2.2.3 NMR INVESTIGATION OF $LiBH_4PYR_4$ AND $LiBH_4HMPA_4$ COMPLEXES

These two samples complete the study of organolithium complexes from the $LiBH_4X_y$ family. There are no crystallographic data available for either of these complexes. The NMR spectra were only possible to record at the low magnetic field. In the case of $LiBH_4Pyr_4$, the spectrum was obtained using the Andrew-Beams probe with the sample inside the glass insert. In the case of $LiBH_4HPMA_4$, the NMR spectrum was only taken using the double-bearing probe with the sample inside the new rotor insert

The ^7Li SP/MAS/HPPD spectrum from $LiBH_4Pyr_4$ shows the expected pattern (see Fig (**4.11a**)which resembles the static quadrupolar powder pattern with the central transition line centred at 5.7 ppm. The spread of the full ssb pattern covers a range of about 60 kHz. The central transition line presents fine structure with peaks at 6.7, 5.6, and 4.7 ppm. The last one has been identified to come from slight hydration of the main complex. The presence of the other two signals seems to indicate the possibility to observe the main complex plus some dissociation product that may be formed with the liberation of Pyr. It was not possible to observe these structures in the individual ssb. This lack of structure in the ssb was due to a small instability in the spinning frequency of the sample when using the glass capsules in combination with the

Andrew-Beams probes.

The static band shape shows the typical powder pattern with a sharp peak at 4.6 ppm which has a broad base. This sharp peak is due to hydration of the complex as was already mentioned. The broad base of the peak contains the signals of the central transition line from the complex and the structure is lost due to the sharp peak. The outer transitions are clearly visible and centres at 9.06 and -8.88 kHz (116.5 and -114,2 ppm respectively). It is also possible to observe the outer steps from these transitions. It was possible to observe some structure in both outer transitions that may be attributed to the two possible complexes present in this sample. The positions of these maxima are 9.674, 8,453, -8.056 and -9.704 kHz. As in the previous two cases, the above information was used to calculate the ^{7}Li-Q_{cc}'s with values of 32.10 and 36.67 kHz. The SP/MAS/HPPD spectrum and the static powder patters are shown in Fig (**4.12**).

It is possible to observe the drastic drop in the value of Q_{cc} in going from the PMDETA to the Pyr complex. This shows an indication of higher symmetry around the lithium atom in the latter complex which reduces the interaction between the EFG and the quadrupole moment of the nucleus.

In the case of $LiBH_4HPMA_4$, the SP/MAS spectrum shows a sharp central transition band at 2.3 ppm and it has the narrowest linewidth of all the compounds presented in this work, with a value of $\Delta\nu_{1/2}$= 53.4 Hz. The spread of the ssb pattern is also the smallest one observed during this investigation, with a total breadth of less than 20 kHz. The

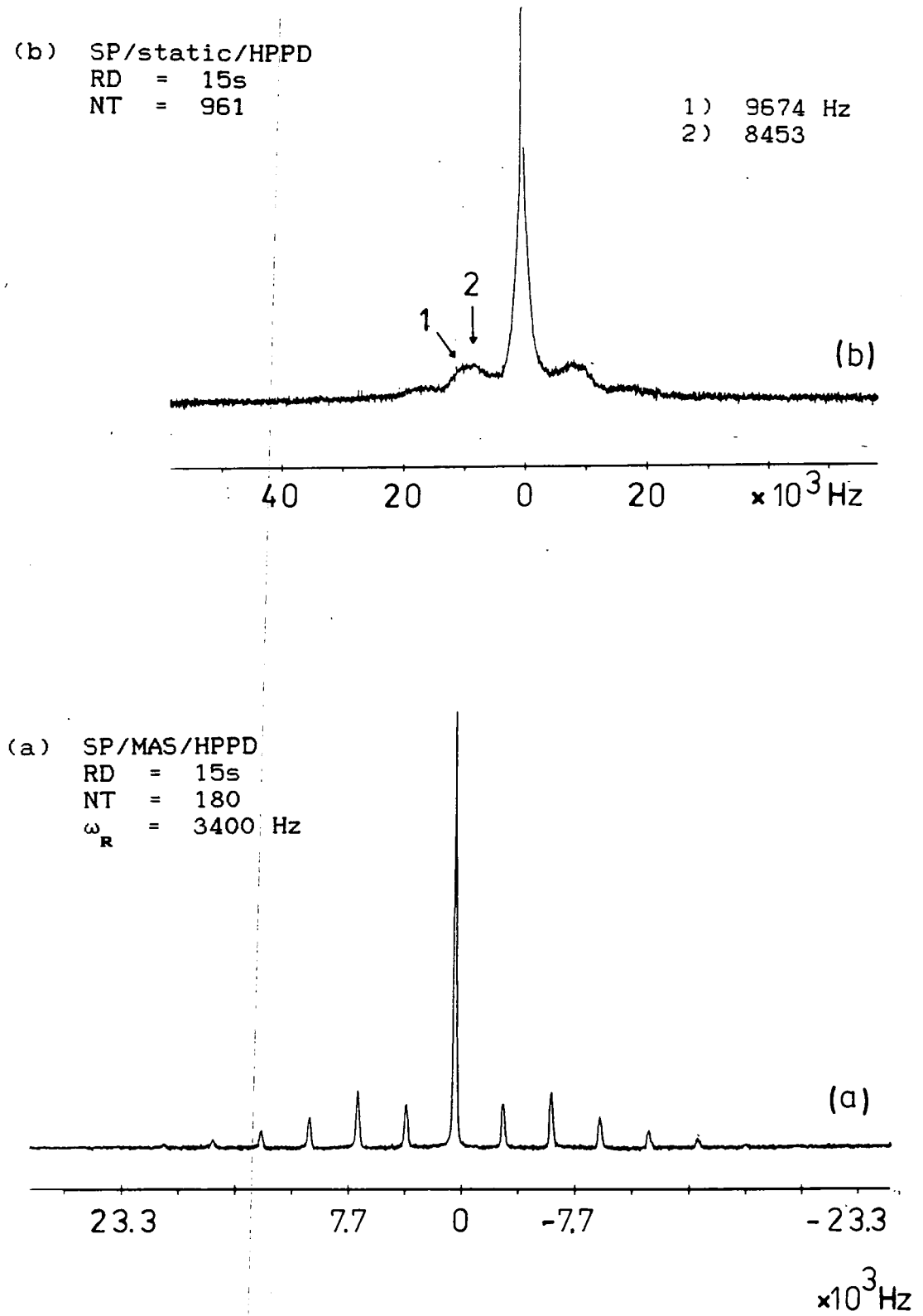

Fig (4-12) ^{7}Li SP/MAS/HPPD and SP/static/HPPD Spectra of $LiBH_4Pyr_4$ using glass capsule at 4.675 T.

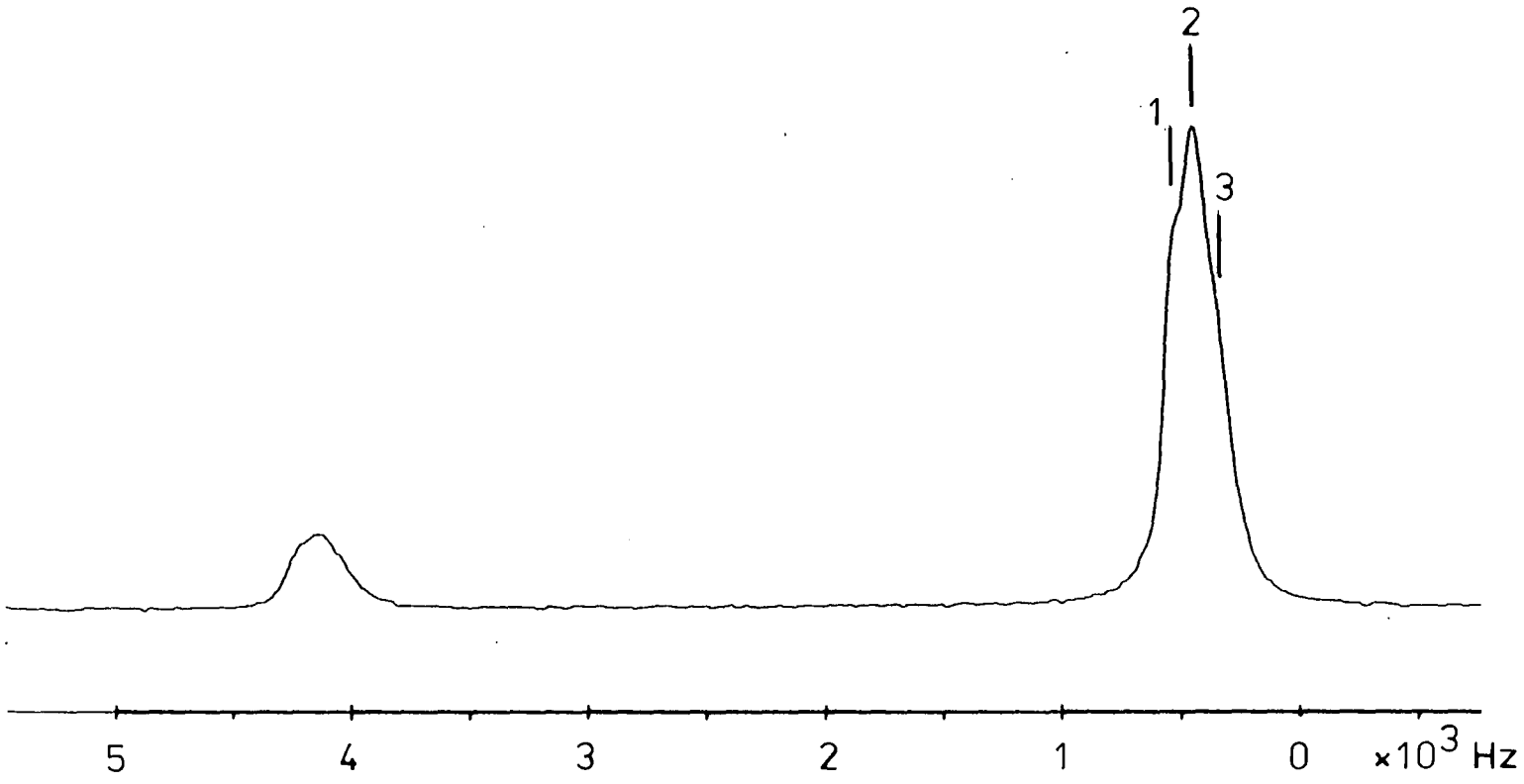

Fig (4-12c) $LiBH_4Pyr_4$ Spectrum; expansion of Fig (4-12(a)).

observation of the total ssb pattern was possible with the use of a very slow and stable rotation of the sample, i.e. ω_R = 500 Hz. As mentioned in chapter 3, the ability of producing this type of spectrum shows the type of stability that can be achieved when using the new rotor insert specially designed, during the period of this work, to handle this type of sample. No structure was observed in either the central band nor in the individual ssb's.

As in the case of the $[LiBH_4TMEDA]_2$, the static band shape shows the presence of a well resolved splitting in the outer transition signal. The separation of this splitting was equal to 0.92 kHz. The location of the maxima was measured to be at 3.3 and 2.38 kHz from the central transition signal. But in this case, this splitting seems to average as in the case of the PMDETA complex. The central transition band has a $\Delta\nu_{1/2}$ = 350 Hz and centre at 2.3 ppm. No structure was observed in this resonance.

If the average of the outer transition splitting is taken, it is possible to estimate the value for the quadrupole coupling constant for this complex which gives a value of 11.36 kHz, the smaller of all. The quadrupolar interaction has been further reduced in this complex but is still detectable. Fig (4.13) shows the MAS and static spectrum from this complex.

It is possible to draw some conclusions when comparing the values of $^7Li\text{-}Q_{cc}$ for the different complexes studied in this work. A summary of these values is presented in Table (4.3).

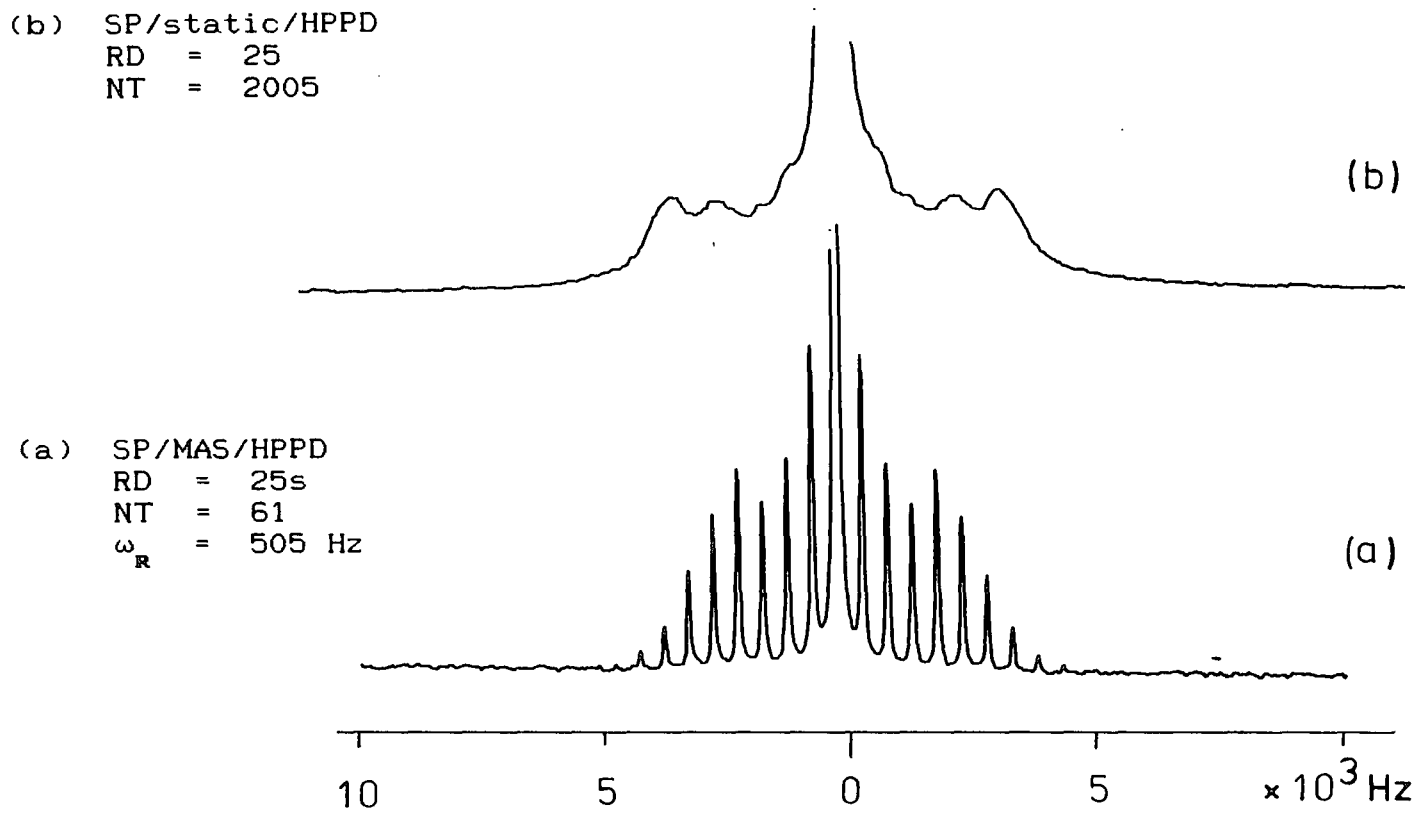

Fig (4-13) ^7Li (a) SP/MAS/HPPD and (b) SP/static/HPPD Spectra of $LiBH_4(HMPA)_4$ using new rotor insert at 4.6975 T.

It is possible to see from the table below that as the number of ligands increases around the lithium atom the value of the quadrupole coupling constant gets smaller and smaller. It goes from a probable maximum of 140 kHz to 11.3 kHz, i.e. the value is reduced by an order of magnitude. This observation suggests that the lithium environment is getting more and more symmetrical, closer to an octahedral one, reducing the interaction between the EFG and the quadrupole moment. As in the last two examples the ligands are uni-dentate, this means that the bonds are less distorted in these two cases.

$LiBH_4X_y$	$^7Li\text{-}Q_{cc}$ (kHz)
$[LiBH_4TMEDA]_2$	≥145.
$LiBH_4PMDETA$	124
$LiBH_4Pyr_4$	34
$LiBH_4HMPA_4$	11

Table (4.3) Comparison of the Q_{cc} values obtained for the different organolithium complexes.

It is possible to use the above information for the values of Q_{cc} and the results from the crystallographic studies to attempt to predict the possible structures for the last two complexes presented in this study. It is possible to postulate that the lithium atom could be in the centre of a square-bi-pyramid structure where two of the hydrogen atoms from the BH_4 unit form part of the square base and the

remaining four ligands will be two in base and one at the top and one at the bottom vertices of the pyramid. This will leave the lithium atom in an octahedral environment with the possibility of small distortion due to the Li-(H_2)-B bonds. These predicted structures are presented in Fig (**4.14**).

One of the most important conclusions from this study is the actual possibility of being able to observe NMR signals from air sensitive compounds thanks to the introduction of the new rotor insert design. This opens the opportunity to widen the understanding of organolithium compounds and their structures in the solid state. It is also possible to see that even for a small quadrupole moment nucleus like lithium complicated quadrupolar lineshapes can be observed and as in these cases are some times difficult to explain. The observation of all possible transitions is very valuable giving direct determination of the quadrupolar coupling constant. With lithium the possibilities are doubled due to the presence of the two isotopes from this nucleus.

4.3 INDIRECT QUADRUPOLAR EFFECTS

The particular effect that will be considered in this section is coupling between a spin 1/2 nucleus and a spin 3/2 nucleus for the case where the resonance lines arising from the 'scalar' (indirect) coupling between these two nuclei are modified by a combination of dipolar coupling and quadrupolar interaction between them.

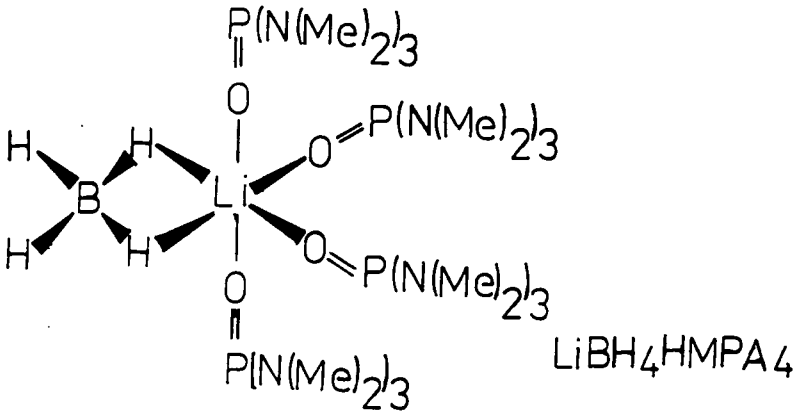

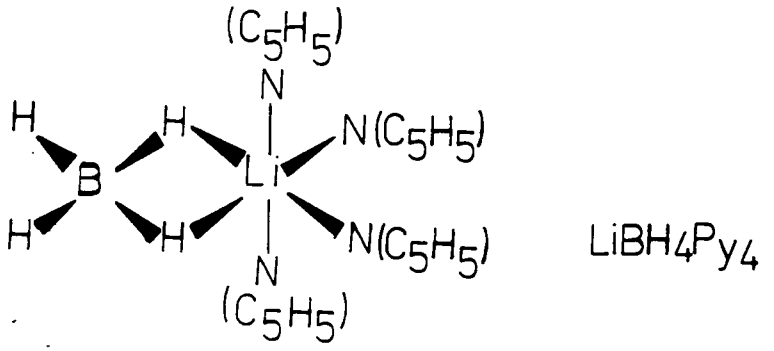

Fig (4-14) Predicted molecular structures for the $LiBH_4Pyr_4$ and $LiBH_4(HMPA)_4$ complexes.

As in the case of lithium, this effect has been observed in air and moisture sensitive organocopper samples[17] where ^{31}P and Cu^{I} are the nuclei of interest. These samples are: I) $[Cu_2(tBu)HP\text{-}CH_2\text{-}PH(tBu))_3]^{+2}2BF^{-4}$, and II) $(tBu)_3C_6H_2HPCuCl$. There are no crystallographic data available for any of these systems, but the suggested structures for samples I and II are presented in Fig (4.15). Again, the new rotor inserts play an important role the in acquisition of the NMR data. For this particular study ^{31}P is the spin 1/2 nucleus to be observed. All the spectra were obtained under CP/MAS conditions with the use of the double bearing probe for the Bruker CXP-200 at 4.6975 T at a frequency of 81.0141 MHz.

There are very detailed theoretical reports of this effect in the literature[18,19] as well as in terms of perturbation theory[20,21,22]. The present discussion will follow the latter description. In the presence of only 'scalar' coupling the spectrum from the spin 1/2 nucleus consists of four lines equally spaced and split by $|J_{iso}|$. When a dipolar interaction as well as a strong quadrupolar interaction are present the energy levels of the system are disturbed producing a frequency shift in the spin 1/2 spectrum. The magnitude of this shift has been determined, from perturbation theory[21], to be equal to $|\Delta\nu| = |(3/10)DQ_{cc}/\nu_s|$, where ν_s is the resonance frequency of the spin 3/2, and D is the dipolar coupling constant. As the magnitude of the quadrupolar coupling constant increases the four lines will be shifted by the same amount in pairs. The two outer lines will be shifted in one direction and the two inner lines in the opposite direction. The direction of this

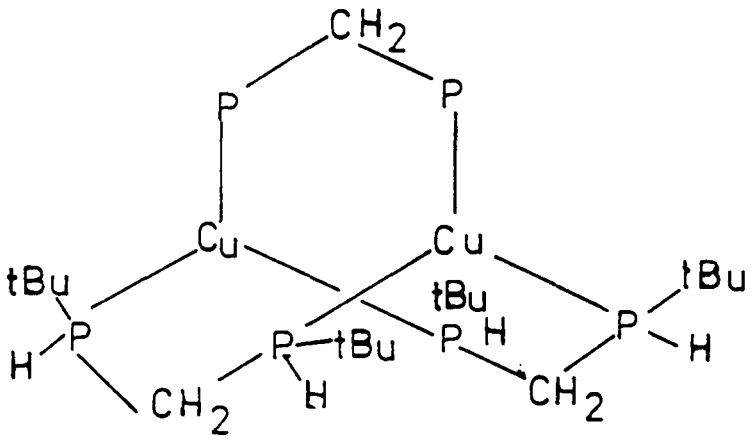

I

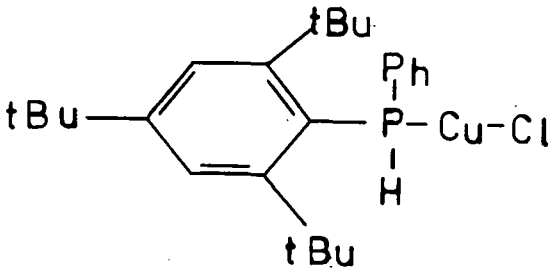

II

Fig (4-15) Predicted molecular structure for complexes (I) and (II).

shift is dependent on the signs of both D and Q_{cc}. Most of the cases reported in the literature show that the inner lines are shifted to right and the outer lines to the left.

For complex (I), it was very difficult to determine the true ^{31}P spectrum due to the superposition of ssb with the actual central bands and the spectrum had to be obtained at different values of ω_R between 1500 to 4016 Hz. The spectra obtained under these conditions are presented in Fig (4.16a). The spectrum consist of four lines at -10.7, -16.8, -28.6, and -45.1 ppm (in Hz at -868, -1356, -2312, and -3649 respectively). In contrast to cases presented in the literature, the two central lines have been shifted to the left whereas the two outer lines have been shifted to the right. The direction of the shift depends on the sign of the dipolar and quadrupolar coupling constant.

In this type of interaction there is a special case where the maximum of the shift is so that one of the outer lines will merge with the centre line closest to it[22]. Following this description, it was possible to conclude that in this case the lines were above the crossing point. This can be explained as follows: a) it is possible to see from Fig (4.16b) that the separation between lines 2 and 3 gives the value of the isotropic indirect coupling constant $|J_{iso}|$ = 956 Hz, b) at the crossing point the separation between the line are $|J_{iso}|$ and $2|J_{iso}|$ respectively[20], c) so, above the crossing point the separation between lines 3 and 4 will be $<2|J_{iso}|$ and below it will be $>2|J_{iso}|$. In this case the separation is equal to 1337 Hz, i.e the spectrum is above

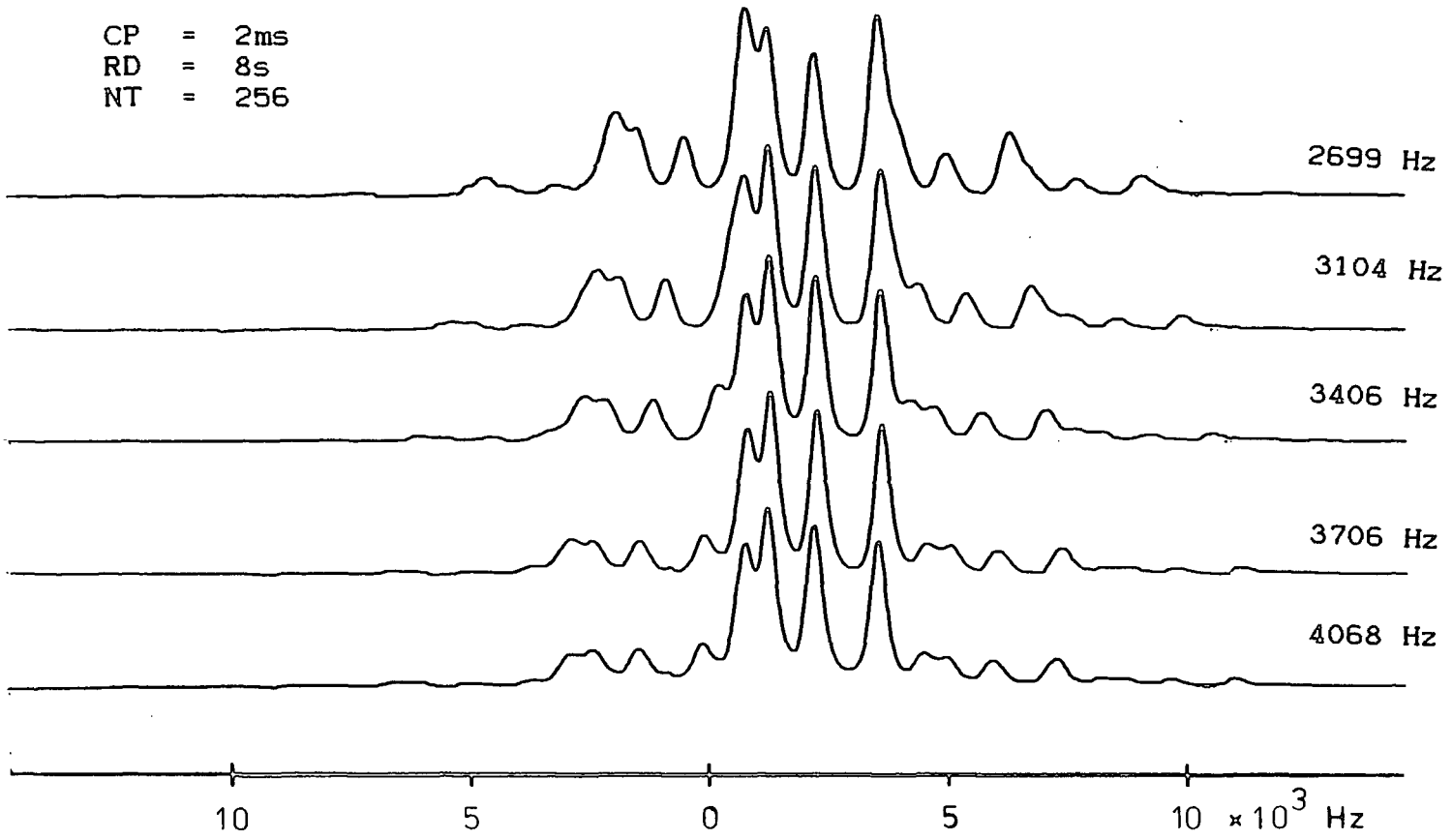

Fig (4-16a) ^{31}P CP/MAS/HPPD variable spinning spectra of complex (I).

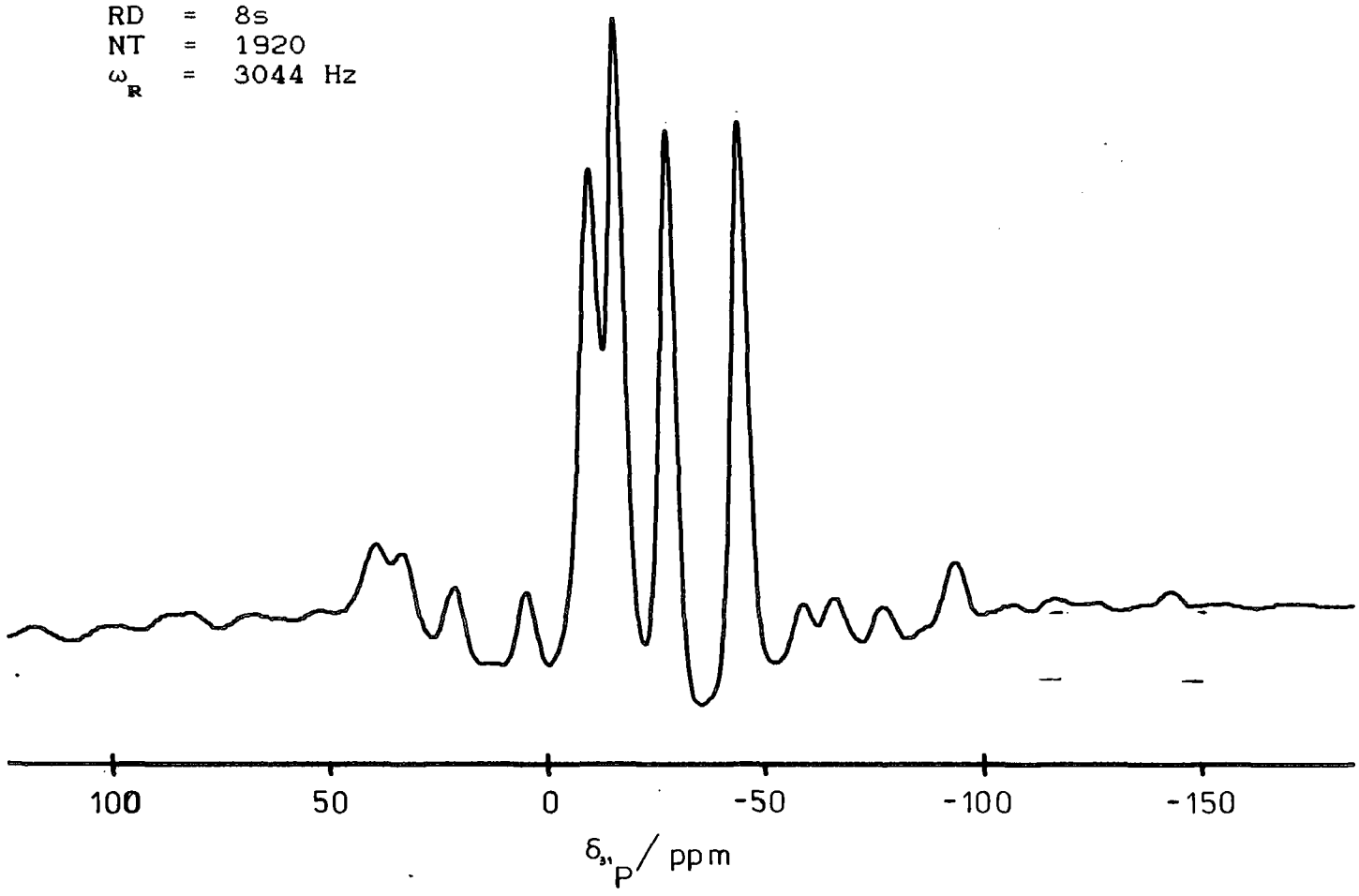

Fig (4-16b) ^{31}P SP/MAS/HPPD Spectrum at complex I.

the crossing point (see (a) in Fig (4.17)). It has been indicated that in the case when the two lines are merged the true chemical shift of the sample in the absence of 'scalar' coupling is given by the position of the central line of the 1:1:2 triplet. It is evident that this is not the case, nevertheless it is possible to give a good estimate of this value. The separation $|\delta_2-\delta_1|/2$ indicates how far way is the present spectrum from the crossing point. Therefore, this allows one to calculate a value of -25.6 ppm for σ_{iso}. As there are no crystallographic data it is not possible to calculate the dipolar coupling constant and therefore the value of the quadrupolar coupling constant. It was not possible to obtain reliable ^{65}Cu NMR spectra from any of the samples. So, it was not possible to obtain any information about D or Q_{cc}. But, it is possible to calculate the value of $|DQ_{cc}|$ to be equal to 4.2×10^{10} Hz^2.

The other complex II shows a pattern that seems to indicate the effects of scalar coupling between the ^{31}P and the Cu but it is not so clear if the combined dipolar-quadrupolar effect is also present in these cases.

For this complex the central bands of the ssb pattern obtained from the CP/MAS spectrum consists of four lines at -23.6, -42.5, -66.6 and -93.0 ppm (or -1879, -3448, -5402, and -7542 Hz respectively). The spectrum obtained from this sample is presented in Fig (4.18). If the spectrum is influenced by the same interaction as in the previous case, it is possible to conclude that the shift of the lines correspond to a situation above the crossing point. Therefore, it was also possible to estimated a σ_{iso} value of -57.2 ppm. and

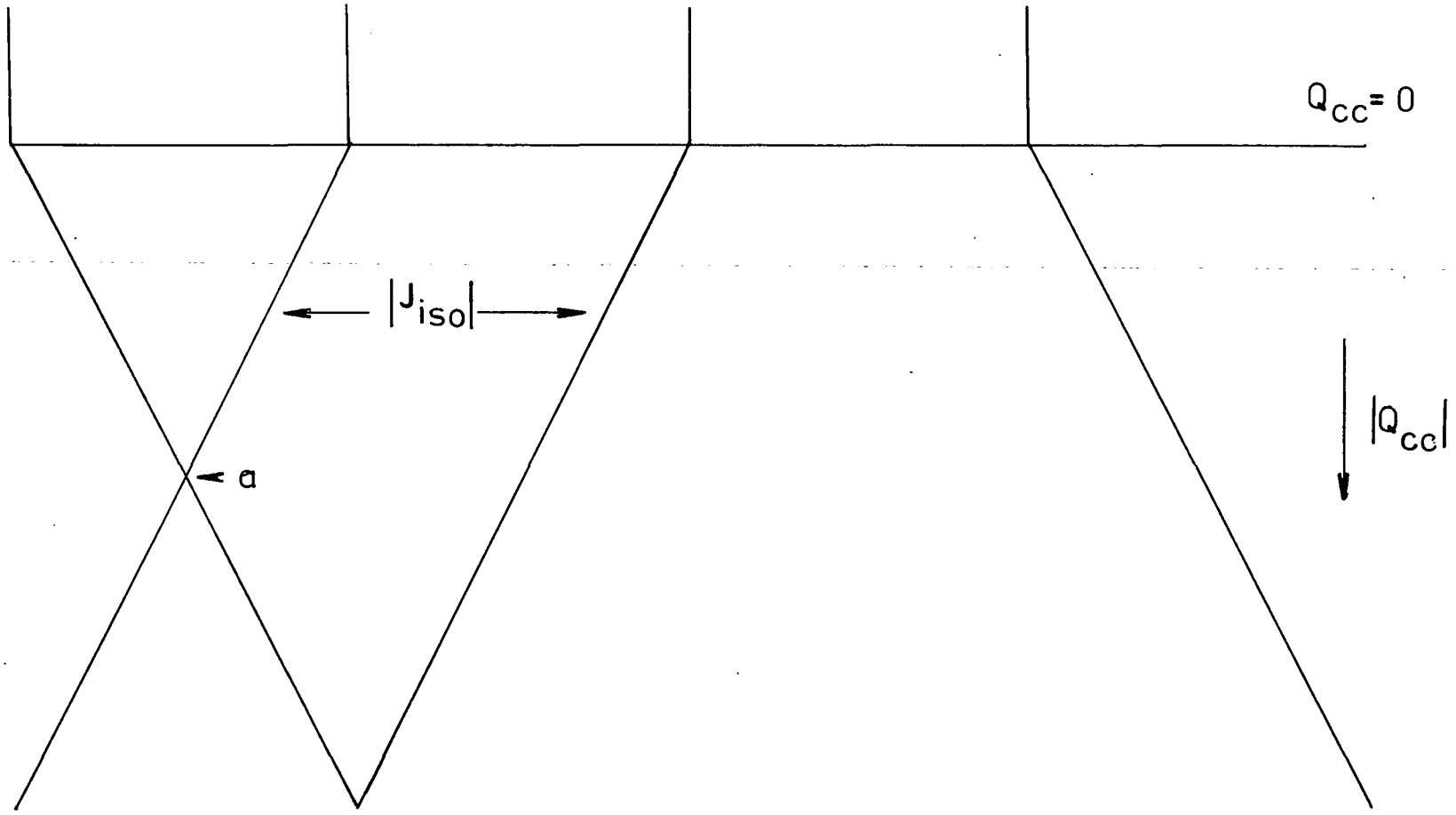

Fig (4-17) Diagramatic representation of the I = 1/2 Line position as a function of Qcc.

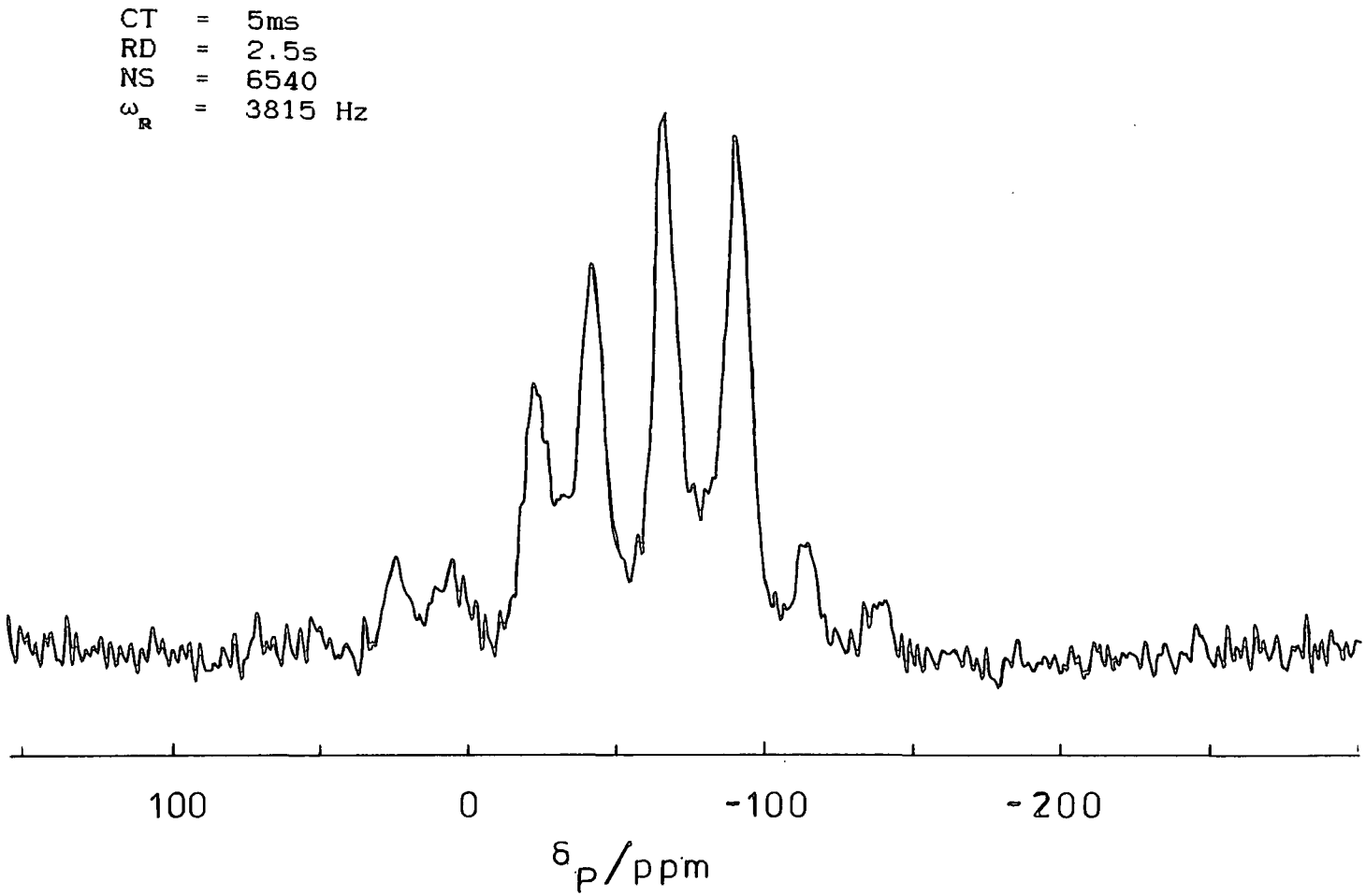

Fig (4-18) ^{31}P CP/MAS/HPPD Spectrum of complex (II).

$|J_{iso}|$ value of 1954 Hz. There is a degree of doubt about this interpretation due to fact that the lines do not extrapolate to their expected values under pure scalar splitting, i.e. the shift of the 4 line would be more negative that in the spectrum presented in Fig (4.18). It is not possible to fully explain these results with present information in terms of the above interaction, but the evidence seem to point very strongly in this direction.

4.4 CONCLUSIONS

It was possible to see the important role played by the new rotor insert in the investigation of organolithium complexes by means of solid-state NMR spectroscopy. It is a very simple system which allows the use of the same sample without repacking, as long as it is kept in a suitable container when not in used. The stability under MAS conditions has proved to be very good.

As far as the lithium complexes are concerned, their NMR spectra have proved to be very interesting and in some cases difficult to interpret. The $LiBH_4$PMDETA spectrum was very interesting from the point of view of its very typical quadrupolar ssb and powder pattern of a spin 3/2 nucleus. It has been possible to see the variation in the value of Q_{cc} in this series of complexes as the number of equal ligands increases around the lithium atom which indicates an increase in the symmetry around this nucleus. This gives valuable insight into the crystal structure of the compounds.

The organocopper complexes also proved to be interesting from the fact that the central band of the spectrum presented a shift due to the combined dipolar and quadrupolar effect in the opposite direction than those presented in the literature.

REFERENCES:

1- Merwin L. W., Sebald A., Espidel J., Harris R. K., J. Mag. Res. 84, 367, (1989).

3- Bray P. J., "Borate glasses: structure, properties, application", Eds. Pye L., D., Frechette V. D., Kreidl N. J., 321, Plenum Press, N. Y. (1970).

4- Oldfield E., Kuyng H., Timken C., Montez B., Ramachandran R., Nature, 318 (14), 163, (1985).

5- Jansen R., Veeman W. S., J. Chem. Soc. Faraday Trans. 1, 84, 3747, (1988).

6- Samoson A., Lippmaa E., Phys. Rev. B, 28, 6567, (1983).

7- Schmidt V. H., Ampere International Summer School, Yugoslavia, (1971).

8- Setzer W., Von Ragué Schleyer P., Adv. Organomet. Chem., 24, 353, (1985).

9- Wehrli F. W., Org. Magn. Res., 11, 106, (1978).

10- Fraenkel G., Fraenkel A. M., Geckle M. J., Schloss F., J. Ame. Chem. Soc., 101, 4745, (1979).

11- Günther H., Moskau D., Bast P., Schmalz D., Angew. Chem. Int. Ed. Engl., 26, 1212, (1987).

12- Gurak J. A., Chinn J. W., Lagow R. Jr., Steinfink H., Yannoni C. S., Inorg. Chem. 23, 3717, (1984).

13- All organolithium compounds presented in this work were prepared by Prof. K. Wade's research group at the Department of Chemistry, Durham University.

14- Armstrong D. V., Clegg W., Colquhoun H. M., Daniels J. A., Mulvey R. E., Stephenson I. R., Wade K., J. Chem. Soc. Chem. Commun 630, (1987).

15- Clegg W., Stephenson I. R., Wade K., unpublished work.

16- Fyfe C.A., "Solid-state NMR for Chemists", C.F.C. Press, P.O. Box 1720, Guelph, Ontario, Canada, N1H 6Z9

17- All organocpper compounds presented in this work were prepared by Prof. O. Stelzer of Bergische University, West Germany.

18- Naito A., Ganapathy S., McDowell C. A., J. Chem. Phys., **74**, 5393, (1981).

19- Zumbulyadis N., Henrichs P. M., Young R. H., J. Chem. Phys., **75**, 1603, (1981).

20- Olivieri A. C., Frydman L., Diaz L. E., J. Mag. Res. **75**, 50, (1987).

21- Harris R. K., J. Mag. Res., **78**, 389, (1988).

22- Apperley D. C., Bai H., Harris R. K., Mol. Phys., **68**, 1277, (1989).

CHAPTER 5

MATRIX ISOLATION

5.1 INTRODUCTION

Matrix isolation is a very powerful technique used to trap molecules, either in a stable form or in a unstable form, in very low concentrations, inside a host or inert substance called the matrix. In this way, it is possible to study isolated molecules without some of the interferences that dominate pure solids, liquids or solution samples. It is possible to suppress most of the intermolecular interactions, molecular diffusion, and in some cases rotation of the molecules of interest.

This technique was first applied to the study of phosphorescence of some aromatic molecules at very low concentrations in a glassy medium in work by Lewis et al[1]. The next report of its use was ten years later when independent studies by Pimentel[2] and Porter[3] with co-workers were presented (in 1954) in which they used noble gases, like argon, to trap and isolate materials to be studied by infra-red spectroscopy.

More to the interest of this work, the first matrix isolation study using NMR as the spectroscopic technique did not come until 1978 (almost 30 years later) with a publication by White[4] in which HCl and $(HCl)_2$ were isolated in an argon matrix in a range of different concentrations. This was quickly followed by a work from Grant and co-workers[5] where the first carbon-13 cross polarization (CP) NMR study of small organic molecules was presented, again in an argon matrix. Grant and co-workers have been the major contributors to matrix isolation studies in NMR, concentrating their

investigations on ^{13}C studies of a large number of organic molecular systems. These investigations have involved the determination of shielding anisotropy parameters for different types of carbon atoms as well as the study of heteronuclear dipolar interactions between carbon and other nuclei like H and N.

Matrix isolation is a very sophisticated technique which involves the mastering of different types of technologies. It needs the production of the very low cryogenic temperatures so the isolated species can be deposited and trapped. This can only be achieved in the presence of a high and dynamic vacuum which needs to be between 10^{-5} to 10^{-6} mbar. Finally, it is necessary to combine all the above facilities with the appropriate spectroscopic technique to study the samples of interest, which in this case is nuclear magnetic resonance.

The first part of the present chapter will be dedicated to the description and requirements of the matrix isolation technique in a general form[6,7]. This will include the description of different types of host materials used to form the matrices and the conditions needed for their deposition as solids, the minimum vacuum equipment needed for the isolation of the systems from ambient conditions, and a description of the crystallographic arrangements expected from the matrix materials. This appears to be the first attempt to review matrix isolation studies by NMR. So, the second part of the chapter will be dedicated to produce a summary of such a work in the areas of ^{1}H and ^{13}C NMR spectroscopy.

5.2 DESCRIPTION OF THE MATRIX ISOLATION SYSTEM

5.2.1 VACUUM SYSTEM

One of the most important factors needed to preserve and maintain the matrix-isolated materials is the presence of a high vacuum. Whether it is for IR, UV, Raman or NMR spectroscopy and using any type of cryogenic device, the sample deposition area, as well as the sample access to this area, needs to be at vacuum levels of the order of 10^{-5} mbar or less. It is necessary to construct the vacuum line with the widest bore of glass or metal pipe possible in order to increase the pumping speed. In the case of NMR, it is desirable to make it as short as possible. The use of glass has been recommended in construction but in NMR it is more practical to use metal lines in some areas of the system to make it more robust and less likely to break under handling. It is important to have a fine control of the matrix gas mixture in its approach to the cryogenic area and this can be achieved with the use of micrometer needle valves. Several large storage glass bulbs can be used to keep the gas pressure at low levels so its flow can be make easier to control. It is best to have them with a capacity of 2 litres or more to allow constant gas pressure during the whole period of deposition. This condition is very important because otherwise the quality of the matrix will be very poor.

Two types of vacuum pump are usually needed to achieve the high vacuum levels described above. A rotary pump is used for the initial evacuation and pumping down of the entire system, i.e. from atmospheric pressure to about 10^{-3} mbar.

They are also used as backing pumps when the more sophisticated diffusion pump is put into line. The latter is usually an oil type of pump capable of given vacuum levels of 10^{-7} mbar. These two pumps are also connected to a nitrogen trap which will help in increasing the pumping speed as well as to condense any undesired gases that may contaminate the oil inside both the diffusion and rotary pumps.

Several pressure-measuring devices are needed along the vacuum line to monitor the vacuum levels during the initial pump down of the system. They will also be used to follow the flow of gases during the period of deposition. So, it is important to have one such device near the pumps to check their performance, one as close as possible to the deposition area, and finally one at the entrance of the incoming gas. The first two need to be very sensitive and able to read pressures in the region between 10^{-5} and 10^{-7}mbar. A Penning-head gauge is recommended in this case. The last one is needed to monitor pressure between 10^{-3} mbar and atmospheric. So, a Pirani-head gauge is usually the best option.

The attachment of the sample bulbs to the inlet connection needs to be flexible enough so it is possible to interchange gas mixtures with little or no difficulties. It is also appropriate to have a practical number of sample ports so multiple deposition can be performed or to be able to keep a constant deposition pressure with the use of more than one sample bulb with the sample matrix concentration. In this situation, it is essential to have high vacuum isolation valves in each of the sample ports. In this way they can be

brought into line independently as well as be isolated from the system. It is also recommended to have an isolation valve between the end of the sample line and its outlet to the deposition area in case of accident or leaks in the sample line.

5.2.2 CRYOGENIC UNIT

There have been dramatic changes in the way cryogenic temperatures are produced for the benefit of matrix isolation. Early work was carried out on *single-dewar* cryostats. They are suitable for medium-range temperatures between 90 and 77 K using liquid air or liquid nitrogen as the refrigerant. They are usually made of stainless steel, copper or brass and consist of two compartments. The first one is a vacuum shield to minimise the heat exchange and the second is to contain the appropriate cryogenic liquid. The cell containing the deposition area, sample inlet, and windows located at the bottom of the dewar, is also surrounded by a vacuum jacket. This type of dewar are very limited in use.

The second step forward in cryogenic research is the use of *double-dewar* cryostats. In a similar way to the above, they consist of four consecutive compartments. Two of these are vacuum jackets of 10^{-3} and 10^{-5} mbar respective to prevent heat losses. The other two are for the use of liquid nitrogen and liquid helium. The liquid nitrogen is used to pre-cool the dewar to minimise the rate of helium boil off. The procedure for operation will be: first, to produce a medium

the vacuum in the first compartment and a hard vacuum in the third compartment; then the second compartment is cooled down with the use of liquid nitrogen, and when the temperature has reached 90 K the liquid helium is introduced to the dewar. Even in these carefully controlled conditions, the rate of evaporation of helium could be as high as 50% a day. So, re-fills are necessary in the case of performing long experiments. These types of systems were very popular in low-temperature work in IR and ESR. An example of a double-dewar cryostat is presented in Fig (5-1)[7] from work by Rowland Davies[8].

Matrix isolation was made very accessible to all techniques by the introduction of the *micro-refrigerator* unit. Two types of unit can be found under this classification. They are the Joule-Thomson effect type and the Solvary cycle type. They can attain minimum temperatures of 77, 20 and 4 K depending on the type of medium used to obtain the cryogenic temperature.

The principle of operation for the first type involves the used of compressed gas that is passed through a pre-cooling medium and to then allowed to expand when escaping through a nozzle, after which small droplets of liquids are produced. Temperatures of 4 K can only be obtained with this method when a two-stage process is used. In the first stage, liquid nitrogen is used to pre-cool compressed hydrogen to produce liquid hydrogen. The second stage uses the liquid hydrogen from the first stage to pre-cool compressed helium to form liquid helium in a third compartment. Normally, these types of refrigeration units are open-end systems i.e. the

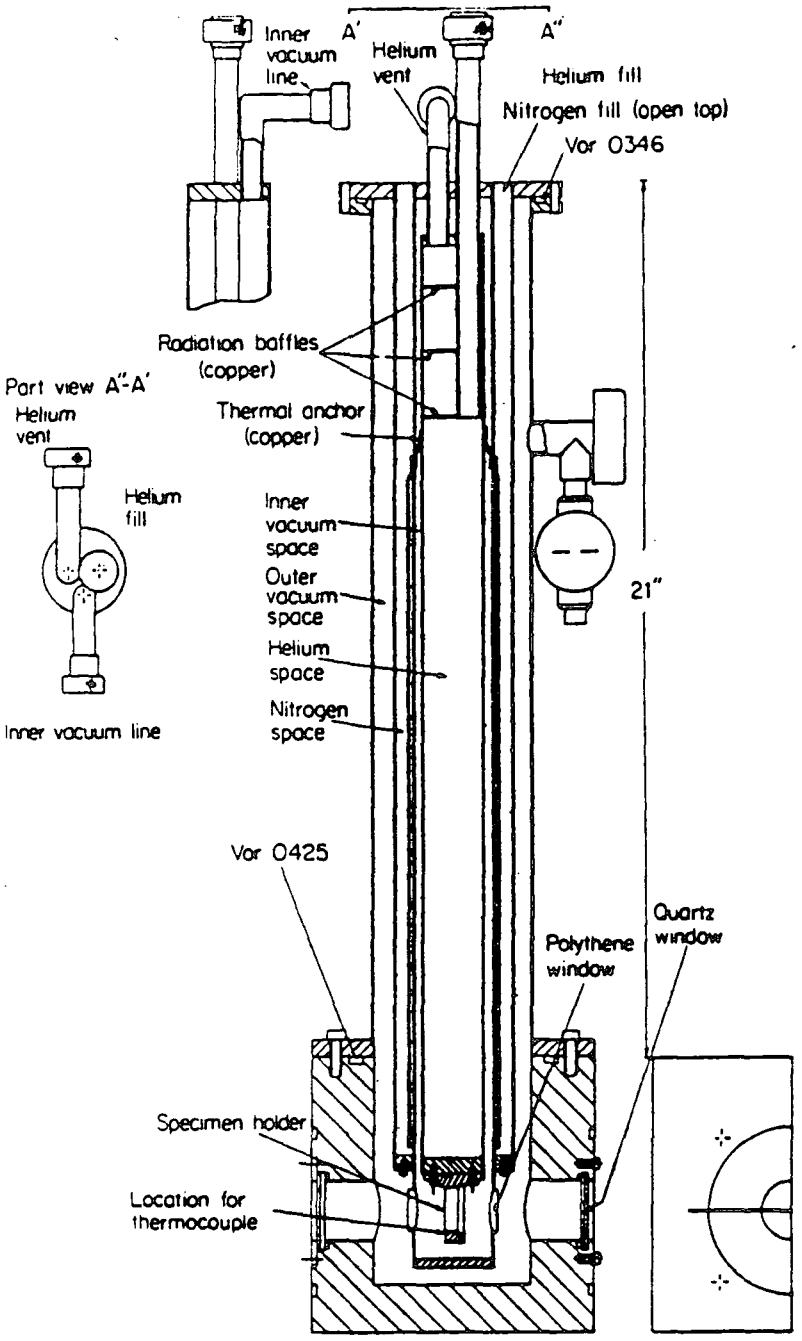

Fig (5-1) Double-Dewar cryostat typically used in past[7].

gases formed in the hydrogen and helium pools are allowed to escape to atmosphere. One of the greatest advantages of this system over the ones already presented is the fact that there is no need to keep large amounts of cryogenic liquids and that the prices of compressed gases are less than those of the corresponding liquid.

The second type of micro-refrigerator has the advantage from the previous one in that it only uses one kind of gas medium. The principle of its operation is based on the fact that a gas expanding at constant pressure produces work. In these conditions, a gas will produce cooling either above or below the Joule-Thomson inversion temperature. It is important to notice that high pressures are needed to produce the necessary low temperatures to avoid liquefying the working gas. These are usually in the region of 350 psi. Any type of gas can be used with this system. Another of its advantages is that when used in a closed-cycle form the gas is re-used an infinite number of times so reducing the costs, and the system can run for long periods of time allowing complicated experiments to be performed. A single-stage system working with nitrogen can go down as low as 100 K, whereas a two-stage system that works from very cool to cool and from cool to warm can use helium to give a temperature of 10 K. Control of the temperature is achieved by heating the coolest stage of the system with a small resistor, and this gives a very wide range of temperatures. A diagram of this type of cryostat is presented in Chapter 6, Fig (6-2), used for the experiments presented in this work.

5.2.3 TEMPERATURE MEASUREMENT

It is very essential to be able to measure accurately the working temperature during the performance of matrix-isolation experiments. It is also critical that, whatever measurement device is used, it is located as close as possible to the deposition area. This will help to determine if too much sample is introduced to the system and therefore if the cryostat is been over heated. It is also helpful when the annealing of the sample is carried out so that an even matrix can be produced.

The most reliable method is the use of thermocouples. Their qualities are: i) they have a very fast response to temperature changes. ii) they produce a very small heat leak due to the fact that long thin wires are used in their construction. iii) they are very sensitive and accurate at the low temperature range where they will be operating. Normally, the reference wire is held inside a vessel with ice water,i.e. at 273 K.

The working temperature is a determining factor in selecting the type of thermocouple used for a particular experiment. Copper/constantan and chromel/constantan are very adequate when measurements are done between 273 and 20 K. They become less reliable at the bottom end of the range. On the other hand, gold(cobalt) alloy or gold(iron)alloy/ copper or platinum thermocouples are best for this low temperature range, i.e. between 20 and 4 K. A table with the most important properties[7] from these types of thermocouple is presented as Table (5-1).

Thermocouple*	20 K	77 K
Au(0.07 at. per cent Fe doped)/Ag	768	378
Au(0.07 at. per cent Fe doped)/Cu	1500	923
Au(2.17 at. per cent Co doped)/Cu	8750	7279

*Reference temperature 273 K

Table (5-1) E.M.F (μV)values for different types of thermocouples

5.3 DESCRIPTION OF MATRIX MATERIALS

5.3.1 MATRIX CHARACTERISTICS

It is of great importance in matrix isolation to select an appropriate sample host in which to trap the molecules of interest. There are several characteristics that the matrix has to comply with and they can be summarized as follow:

i) The matrix needs to be transparent to the spectroscopic technique being used in the investigation or, as in the case of IR, the spectral band has to be in a region outside the one of interest. In the case of NMR, the matrix should not have a magnetically active nucleus in order to avoid dipolar interact with the molecule being studied. This fact limits the materials used to the inert gas family. In the case of ^{1}H NMR studies, it is possible to use CO_2 as the matrix for some applications due to the low natural abundance of both active nuclei (^{13}C and ^{17}O).

ii) One of the most obvious but critical characteristics of a matrix material is that it must be rigid at the particular

working temperature. If this requirement is not met there is a strong possibility that diffusion may occur. Recombination of reactive molecules will take place inside the matrix and pockets of aggregation or polymerization will then be present. This will result in achieving completely the opposite effect to what was intended to be produced. Pimentel[7] gave an important practical rule that can be used to ensure the rigidity of the matrix. It is essential that the temperature of the supporting material as well as the matrix during deposition is kept lower than 30 % of the melting point of the host matrix. Below the 30 % point the material becomes more and more rigid so matrix re-arrangement is not expected. When the temperature is kept between 30 and 50 % of the melting point the material is in the region called the *annealing temperature*. At this point there is some amount *of* movement in the matrix in order to reach a more stable configuration in its crystal structure. Most of this arrangement occurs in the *host* material and very little in the isolated sample, if this is a small molecule. This process of annealing is very important in order to get a well-isolated sample . Above 50 % total diffusion occurs and therefore the isolation of the material of interest will be lost and even reaction can take place. Table (5-2) shows some of the critical temperature for a selection of matrix materials relevant to NMR studies.

Matrix Material	Melting Point(Tm)	0.3Tm (K)	0.5Tm (K)
Ne	24.6	7.3	12.3
Ar	83.3	25	42
Kr	115.8	35	58
Xe	161.4	48	82
CO_2	216.6	65	108

Table (5-2) Critical Temperatures of Matrix Materials[6,7]

iii) Matrix materials need to be of high purity grade because this will have a decisive effect on the formation of the matrix crystalline structure during deposition.

iv) As the sample is being deposited, heat will be introduced to the system as the layers of material increase with time. This heat has to be removed as quickly as possible to avoid diffusion inside the matrix or in the worst case to prevent a total lost of the sample through evaporation. So, the matrix material has to possess a good thermal conductivity to be able to transfer the heat produced across the layer. The amount of heat removed has a direct relation to the cooling power of the cryogenic medium or the cryostat used. This power will limit the rate of deposition. Other factors determining the amount of material being isolated are the matrix concentration, and the total time taken in the operation. The first factor will determine how isolated the sample will be and therefore the resolution in the spectrum. The second one will be directly dependent on the refrigeration unit, and in the case of micro-refrigerators there is no limitation on this time.

When depositing non-reactive material it is possible to

reduce the deposition time by means of the technique known as *pulse matrix isolation*[6]. It involves the deposition of relatively large amounts of matrix in very short intervals of time that could be a second or less. Then, the system is allowed to cool down, and during this time some diffusion and re-arrangement will occur on a small scale. The process is repeated until enough material is present to carry out the necessary experiments. The pulsed volume can be controlled by having a set of two valves along the sample inlet line. One value is opened to allow an amount of sample to go from storage bulb into the pulse volume. Then, this valve is closed and the other one is opened to allow the sample to reach the cold finger for deposition. Samples deposited in this way give very sharp spectral lines.

5.3.2 STRUCTURE OF THE MATRIX MATERIALS

As was mentioned in the previous section, noble gases are the most common matrix materials used for the isolation of molecules. It is appropriate to have a clear picture of the crystalline structure formed when they are deposited on the supporting base.

Their molecules are spherical in shape and with no direct bonds. Three possible structures in the formation of the matrix may be expected. In one extreme, there is the possibility of producing a single crystal type of formation during deposition. If this is the case two types of arrangement can be expected, namely hexagonal and cubic close

packing. There are some difficulties in this idea due to the fact that it will involve the growth of a relatively large single crystal. At the other extreme, the atoms or molecules can arrange themselves in a totally random or glassy type of structure. This is also unrealistic because it would not be possible to get sharp narrow lines from matrix-deposited materials as has been shown to occur.

So, in the middle of these two extremes there is the possibility of a mixture in which there could be small areas of a crystalline type of formation where the matrix will be arranged in one of the above two close-packing formations. These crystalline types of formation will be separated up by a small random distribution of atoms possible due to the presence of small impurities or other factors.

In this discussion the matrix will be considered as a kind of single crystal. In this view, it is necessary to describe in a more detailed manner the matrix structures so suitable site can be identify for the location of the diluted guest sample.

As already mentioned, there are two possible types of packing for the arrangement of spherical molecules of the host to form a crystal. In both cases, a first layer of molecules will consist of one sphere hexagonally coordinated by six other spheres. Again for both cases of packing, the second layer has the same arrangement as before but with the spheres positioned to occupy the spaces left in the layer below. The difference between them comes in the third layer. For the hexagonal case this is directly above the number one layer. In the case of cubic packing, the next layer is staggered with

respect to the two layers below, i.e. this one is not directly above either of them. These arrangements are known as ababab and abcabc packing respectively. Most of noble gases crystallize in the cubic close packing form. The unit cell is known as face centred cubic (fcc). It has octahedral, O_h , symmetry.

As far as the possible natural vacancies in the structures are concerned, there are two such places one with four spheres around the empty space, a tetrahedral site, and the second location with six spheres around it, the octahedral site. From the two, the octahedral site is the bigger. Table (5-3) shows a summary of diameters for the noble gas family as well as the diameters for their tetrahedral and octahedral sites and the diameter of some small molecules. It is possible to see that these sites cannot be occupied even by the smallest of organic molecules.

Matrix Material	Diameter (nm)	O_h (nm)	T_h (nm)
Ne	0.315	0.131	0.071
Ar	0.375	0.156	0.085
Kr	0.399	0.165	0.090
Xe	0.433	0.173	0.094
CH_4	0.450	-	-
CCl_4	0.710	-	-
CF_4	0.476	-	-

Table (5-3) Site Diameters of Matrix Materials and Diameters of Small Organic Molecule[6,7].

It is obvious from the table above that in order to accommodate the isolated species inside the matrix it is necessary to make substitution of one or more matrix sites by the molecule of interest. The bigger the matrix-isolated molecule the greater the number of substitutions that have to take place in the matrix.

The number of substitution sites will have a significant effect on the mobility of the isolated molecule inside the host gas. It will also determine the amount of dilution needed to be able to completely isolate the molecule of interest. The larger the molecule the higher the ratio host/sample required. Cylindrical types of molecules will be the ideal species to be isolated without too much difficulty. Typical matrix dilutions are between 100:1 to 1000:1 of host vs. sample so that isolation is guaranteed. However, the low sensitivity of the NMR experiment is likely to cause problems at high dilutions.

5.4 LITERATURE REVIEW OF NMR MATRIX ISOLATION

As it had already been said at the beginning of the chapter, matrix isolation has been available since the middle 50's but it was only applied to NMR studies 10 years ago[2]. In the following section, a summary of the major advances of matrix isolation over this period of time for the different applications of the technique to NMR will be attempted.

5.4.1 PROTON MATRIX ISOLATION STUDIES

The introduction of this technique to NMR by White[4] opened up a completely new dimension to the study of solid materials and the removal of some intermolecular interactions. Initial attention was given to the study of proton-containing materials[4,10] at various concentrations. In the course of the investigation, two types of probe system were introduced, oriented to two different types of NMR magnet. The first design[4] was aimed for an 12 in. electromagnet with a 2.5 in. pole gap. The cryogenic temperature was produced by an Air Products Helitran and the sample was spread inside a CsI cylinder with a volume of 0.3 cm^3. The lowest temperature was reported to be 5 K, with the possibility of controlling the temperature over a wide range. The sample was introduced from the bottom of the probe through a small tube which stop a few mm before the CsI cylinder. A platinum RF coil was wound around the cylindrical sample container and the circuit was completed with a cylindrical, gold-plated, Pyrex tube capacitor. Typical 90° pulse durations were 6 μs; no mention was given about the dead time of the probe.

The second probe design[11] was intended to be used in superconducting magnets. It was a completely different design in all respects. It will not be described in full details but only its most important features will be given. It is possible to use this configuration on magnets with bore gaps between 7.6 and 10.2 cm. The only similarity with the previous design is in the use of a modified version of an Air Products Helitran which runs on liquid Helium. It needs very

high levels of vacuum, of the order of 10^{-6} Torr or less, to be able to maintain the very low temperatures. The temperature range of the system goes from 5 K to 350 K and this is achieved by controlling the helium flow and with use of a 80 Ω manganese wire heater. Its consumption of cryogenic liquid varied from 1 litre per hour at 5 K to 0.1 litre per hour at 100 K. The temperature was measured with two Au(0.07%Fe) versus chronel thermocouples located at the cold finger and at the RF coil respectively.

The probe could accommodate several kinds of arrangements for different types of sample which included single crystals, powders, samples in matrix form, and glasses. One of these configurations needed the sample to be glued to the RF coil, whereas in the case of single crystals a goniometer was used to allow rotation of the sample over one axis only. For the first case, each sample was mounted in a separate coil and glued to it. For the other cases, a CsI or sapphire cylindrical cold finger was used to contain the samples. The probe was described as dual channel with a wide frequency range, i.e. from 15.2 (^{15}N) to 250 (^{1}H) MHz.

The coil was made of either copper or heavy silver flat wire which was glued to give it greater mechanical rigidity. This allowed the probe ringdown to be reduced from 70 to 7 μs with a pulse duration of 5 μs for the 90° pulse. In the case of ^{13}C a 50 μs dead time was attributed to probe and receiver recovery.

The effect of matrix concentration and deposition rate in isolated HCl were investigated by White using his first probe design. All samples were diluted in Ar with molar

concentrations ranging from a molar fraction of 0.003 to 0.02. The rate of deposition was changed from 0.2 to 2.0 mmol/min.

As the concentration of HCl was increased the spectral line-shape goes from single Lorentzian to Lorentzian and a Pake doublet which were assigned to the monomer and a dimer respectively (see in Fig (5-2)[4c]). The half-separation of the doublet was in agreement with the predicted 2.41 kHz with a proton-proton distance of 0.33 nm. Line-width and doublet separation did not have a dependence on sample temperature or sample concentration but the line-width of the monomer was shown to have a dependency on the amount of impurity present in the matrix, going from 0.32 to 2.9 kHz. The interpretation of the data was based on theoretical calculations in which one of the dimer molecules has the H-Cl bond along the intermolecular axis and the other H-Cl bond is at an angle of 120° from the above axis. It was also concluded from the calculations that the reduced doublet separation comes from the rotation of the proton-dipolar vector about the intermolecular axis of the dimer with at least a threefold potential symmetry. The quadrupolar interaction was also very small or non-existent due to self-decoupling. The chlorine T_1 was estimated to be of the order of 150 μs. The calculations assumed a Cl-Cl distance of 0.37 nm.

More recently, and with aid of the second probe design, White et al. carried out an investigation on the effect that pulse separation in two and three pulse sequences[13] has to an I=3/2 spin system. In particular, it was applied to the case of CH_3CN, a very tightly coupled spin system. The samples

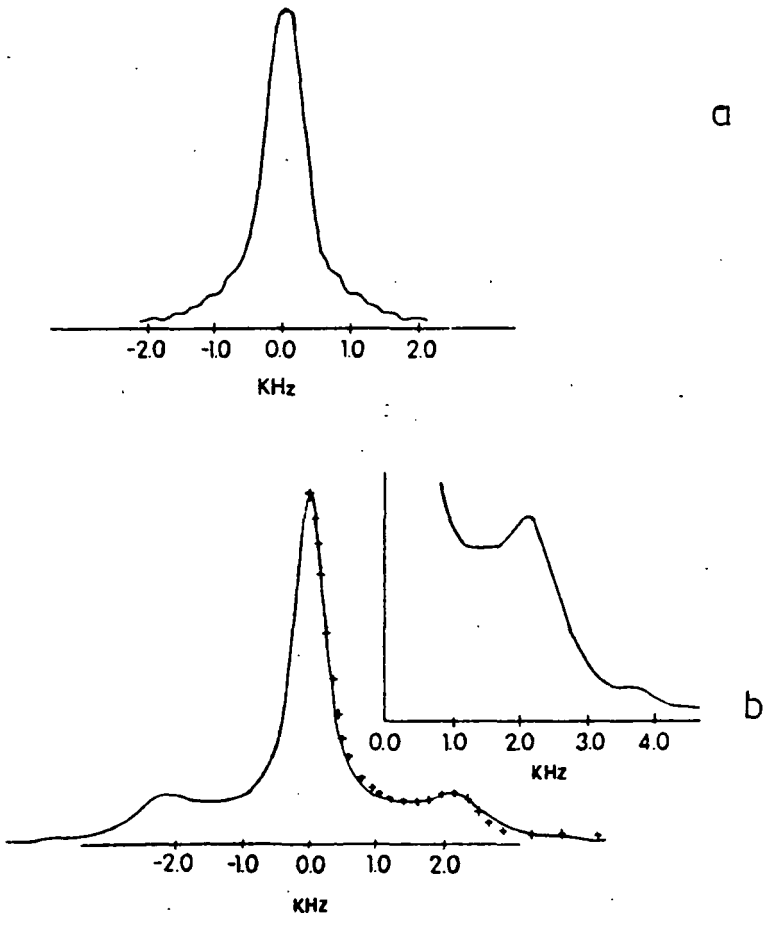

Fig (5-2) Comparison between α = 0.003 and α = 0.02 molar fraction spectrum from HCl. (a) the monomer Lorentzian Lineshape (b) Pake doublet[4c] from dimer and Lorentzian from monomer species.

were prepared in a Kr matrix with molar concentration ranging from 0.1 to 1.0 %. Several pulse sequences were used in the investigations of this system which included Hahn echo, solid echo, and Jeener-Brokaert. Theoretical expression using density matrix formulas were derived for the prediction of the NMR signal at the end of each of the above pulse sequences.

Homogeneous as well as inhomogeneous broadening was studied and determined using the Hahn echo sequence by looking at the exponential decay of the echo signal for different values of 2τ. The value of the homogeneous broadening was determined to be 50 Hz. The remaining width of the line was composed of ~ 200 Hz produced by the intramolecular ^{1}H-^{15}N dipolar coupling, 50 Hz due to ^{1}H-Kr dipolar coupling, and 200 Hz due to inhomogeneity in the static magnetic field. Information about the barrier of rotation for the CH_3 group was obtained from solid echo experiments resulting in a value of V_3/k= 50 K.

5.4.2 CARBON-13 MATRIX ISOLATION STUDIES

In an independent way and immediately after White published his first paper on this subject, Grant and co-workers[5] made another important contribution to the field of NMR when the first ^{13}C CP spectrum was presented from ethylene in an Ar matrix. Since then, a large collection of publications has been coming out of this research laboratory in an attempt to characterize the chemical shift tensor components for a variety of organic molecules (over 71

different molecular systems, stable and unstable compounds).

From then on, few authors have followed their initiative and presented work in these areas. This section will be divided into two parts. The first two will be concerned with the work of Grant et al. on matrix-isolation studies of small organic molecules. The second part will be dedicated to summarize the results presented by other workers.

5.4.2.1 C-13 MATRIX-ISOLATION STUDIES OF SMALL ORGANIC MOLECULES

First a few lines of description of the NMR-cryogenic system discussed by Grant et al.[14] in their investigations will be presented.

One of the major differences in the construction of the system is the fact that the probe detection unit was kept at room temperature rather than including it in the cryogenic system. The latter consists of an Air Products Model 202-B refrigeration unit using helium gas and not the liquid (see section 5.2.2 p.8) with a minimum temperature of 20 K. As the unit was outside the probe and because of the nature of the magnet used (a 12" gap Varian electromagnet) a 175 mm long HPOF copper rod was attached at the cold end of the cooling unit. Finally, a 75 mm long 2.37 mm o.d. sapphire rod was also attached to the copper rod where sample deposition was to take place. The cryogenic unit was shielded from room temperature by means of the non-magnetic vacuum shroud at the end of which a CAJON vacuum fitting was welded. The copper

rod was shielded with a glass tube whereas the sapphire one was shielded with a 12 mm NMR tube which in turn was attached to the vacuum line system. This arrangement means that the sample has to be deposited outside the probe area, then isolated from the vacuum system and finally inserted inside the probe. The great disadvantage of the system is the limitation of having to dismantle the entire sample area before another sample can be deposited, i.e. bringing the system to atmospheric pressure. It has to be mentioned that this configuration served as the basis for the design and construction of the cryogenic system presented in Chapter 6 of the present Thesis.

The type of carbon sites and molecules covered by Grant's studies on chemical shift parameters can be divided into: i) *olefinic carbons*[15], ii) *methyl carbons*[16], iii) CH_2 *types of carbon*[14,19,21], iv) *linear and pseudolinear molecules*[18], and v) *"trigonal" carbons*[17]. A compilation of all the molecules belonging to the above classification is presented in appendix A together with the experimental values of the shift tensor components.

A detailed description of the i type of carbon will be carried out as a typical representation of their work. This will be followed by a summary of the results from the other types of carbons. The study of i is the most extensive in terms of the number of molecules studied from the same family by means of cryogenic-NMR spectroscopy. A total of 24 molecules were isolated and analyzed having ethylene as the model compound for the description of the orientation of the tensor components. This type of carbon is the only one having

a well-defined division between the three principal components of the shift tensor. Their distribution is as follows: σ_{11} goes from 323 ppm to 200 ppm with the greatest density between 253 and 218 ppm, σ_{22} goes from 155 to 79 ppm concentrated between 133 and 113 ppm, and σ_{33} from 76 to -13 ppm with an almost uniform distribution. There are two exceptions which do not have tensor components close to those from the ethylene values: a) the methylenecycloalkane and b) the bicyclo[n.m.0]alkene families. They presented unusual values for their isotropic chemical shifts. In the case of (a), this was attributed to the values of σ_{11} and σ_{22}, which were relatively deshielded. The value of the σ_{22} component depends on the paramagnetic contribution to the C-H and C-C bonds, whereas for σ_{11} it depends on the changes of the carbon double bond. For the second family, (b), there are also two unusual components, namely σ_{11} and σ_{33} and again they were shifted to lower shielding. The main cause of the shift was determined to be the effects on the C=C and C-C bonds respectively.

There is no possibility of classification according to carbon substitution because there is no correlation between this factor and the shift positions of three components. The orientations of the principal axes were divided into three clear sub-groups. The first group consisted of those molecules that have their directions like that of ethylene. The theoretical calculations[20] indicated that σ_{22} was confined to the molecular plane in the direction of the carbon double bond. The direction of σ_{33} was assigned to be perpendicular to the molecular plane and therefore to the sp^2 plane, from experimental as well as theoretical evidence.

This component will depend very strongly on the circulation of the σ electrons. Finally, σ_{11} lies also in the plane of the molecule but perpendicular to the double bond. The representation of these orientations is given in Fig (5-3).

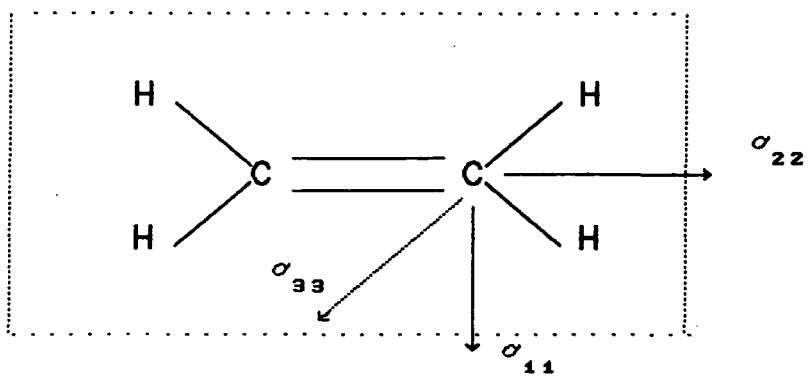

Fig (5-3) Orientation of the three principal axes for the ethylene molecule.

The second group is formed by those molecules (thirteen in all) in which only one component has the same orientation as that of ethylene, namely σ_{33}. The other two were allowed to rotate independently within the plane of the molecule. The size of the rotation was small in the majority of the cases with the exception of cyclopropane and 1,2- dimethyl-cyclopropane where the angles are 18.4° and 15.4° respectively.

Finally, the remaining molecules are those that do not have any relation with the ethylene reference and their orientations were described by directional cosines between them and the symmetry axes of ethylene. The symmetry of the π

bond plays an important role in determining the orientation of the principal axes in these molecules.

As far as the other types of system are concerned, the methyl carbons[15] have less clear division between the different tensor components and cover a range of 100 ppm. Theoretical calculations show the presence of two superimposed tensor patterns that were interpreted in terms of hydrogen bonding between monomeric units, and conformational differences. For all compounds σ_{33} was assigned in the direction of the C-X bond, whereas either σ_{11} or σ_{22} components were assigned in the CH_3-C-X-Y plane.

For the CH_2 type of carbon[14,19,21] the tensor components were found to be between 110 and 59 ppm and there was no real division between them. There was a good agreement between the $\langle\sigma\rangle$ values and that from the isotropic chemical shift in liquid (σ_{iso}).

The investigation of linear and near-linear systems showed the presence of both axially symmetric as well as non-symmetric shift patterns. There is an almost constant value for σ_{11} in the first case due to absence of paramagnetic contributions. There is no pattern at all between the different components for the second case[18].

Trigonal" carbons[17] can be regarded as a special type of aliphatic group. Their overall shift range is from 123 to 17 ppm. There is no clear distinction between components, and the majority of the compounds exhibit axial symmetry or very close to it. Half of the tensor orientations were fully described using the molecular symmetry, with the unique component in the direction of the C-H bond. For the other

half, theory was used to determine their direction. This resulted in using a symmetry plane to fix one of the components in a direction perpendicular to it and allow the other two to rotate with this plane.

Apart from all these extensive studies of non-reactive molecules, it is appropriate to mentioned the work done by Grant and co-workers in some less stable systems. In particular, there are two such studies[22,23] that involved the investigation of valence tautomerism and π-electron ring systems concerning radical species.

The interconversion of valence tautomers in ^{13}C-labeled cyclobutadiene was investigated by matrix isolation using both IR and NMR spectroscopy. Precursors were deposited and then irradiated to form a 1:1 mixture of the compound of interest with a matrix concentration of 1:100. From spectrum simulation it was concluded that the exchange mechanism was a nonrotating rapid interconversion. The rate governing this process was estimated to be in region of at least 10^3 s^{-1}

In studying the effects of π electrons in ring systems, Grant and co-workers emphasized the importance of the effect on individual tensor components of structural changes which could not be seen clearly when looking only at the values of the isotropic averages. This was put strongly for the series $C_7H_7^+$, $C_6H_6$and $C_5H_5^-$. The orientations of the three components were assigned as: σ_{11} is along the C-H bond, σ_{22} is in the plane of the molecule but perpendicular to the C-H bond, and finally σ_{33} is perpendicular to the plane of the molecule. Because the first two components are in the plane of the

molecules they will be affected very strongly by changes in the C-C bond and therefore changes in the π current, whereas σ_{33} will be more affected by changes in σ electrons. This can be clearly seen in the plot of individual components vs. π electron charge (see Fig (5-4)[23]). Two out of the three components experience big changes in shift is going from 7 to 6 to 5 member rings. It was also shown that the average of the two most affected components (σ') gave a better indication of this dependence than the isotropic value. Their relation is almost linear. The σ_{33} was the less-affected component.

5.4.2.3 OTHER CARBON-13 STUDIES

Apart from the authors already mentioned, there are two other groups that had given some attention to the study of ^{13}C matrix isolation by NMR. Their interest has been focused on the characterization of captive intermediate[24] and photochemically produced products[27]. Two different approaches were taken for the construction of the probe system and they will be briefly described. It is also interesting to note, though not surprising, that a member of one of these two groups was formerly a member of the Grant's team .

Zilm et al.[24-25] are the first to report a ^{13}C NMR spectrum of intermediate products isolated in a matrix. The probe system[26] used in this work was a modification of the one that has already been described in Chapter 3 of this thesis. It was designed to performed CP/MAS experiments, so in itself it is a very good step forward in the type of applications for

matrix isolated materials. The stability of the spinning system was not better than ±100 Hz, which could present problems when resolution is of importance. Their work was directed to complete characterization of the intermediate form when dimethyl furan-3,4 dicarboxylate- dicarboxy-^{13}C (98% enriched) was irradiated with a mercury arc lamp to produce the biradical 3,4-dimethylenefuran. It was possible to identify it as a singlet state radical with a shift at about 100 ppm, and the precursor was observed at about 60 ppm.

A second stage of the work with the same chemical system consisted in applying 2D magic angle spinning separate local field technique(MASSLF) for the determination of molecular structure information for the biradical. This experiment was used to separate the chemical shift (in F_2) from the dipolar interaction (in F_1). The shape of the ssb pattern in F_1 resembles the static dipolar spectrum, and by fitting it they were able to determine C-H distances (of 0.108 mm) for the labeled carbons, and the best fit was obtained with C-H-C angles of 120°.

Finally, Yannoni et al.[29] introduced in 1983 a different probe system to perform CP/MAS experiments. It used the traditional Andrew-Beams mushroom rotor mounted in a specially made stator. The whole assembly was enclosed inside a glass dewar through which cold nitrogen was passed to pre-cool the probe before the sample was introduced. Helium gas was selected as the cryogenic medium and it was introduced through a Be/Cu dewar fitted inside the glass one. This dewar was also provided with a goniometer facility to change the rotor

angles with respect to the magnetic field B_o. The disadvantage of the system is the way samples are introduced in the rotors. The initial reaction materials were introduced to the special dewar and deposited at its bottom, which it is kept at N_2 temperature. When the reaction had ended the top of the vessel was removed and then replaced with a top containing special tools to put the sample inside the rotors. This means that reactants and products must not be air-sensitive to be able to survive the top interchange.

Their interest has been directed to the understanding of the norbornyl cation in solids. Total characterization was achieved over the temperature range studied (200 to 5 K) under CP/MAS and static CP conditions (see Fig (5-5)[27,28]). It was possible to observe the exchange process that occurs between the carbons 6,1,2. An activation energy, (E_A), of 6.1 kcal/mol was calculated and an estimated of the exchange frequency of 10^5 s^{-1} was also given. The mechanism of interchange was interpreted in terms of a three-step process which goes through a σ bridged structure intermediate. This interpretation was supported by theoretical calculations using the isopropyl cation as a model compound.

5.5 CONCLUSIONS

It is hoped that this short review into the study of the chemical shift tensor, as well as the proton studies, has shown their great importance in the understanding of structural changes in molecular systems and the great help

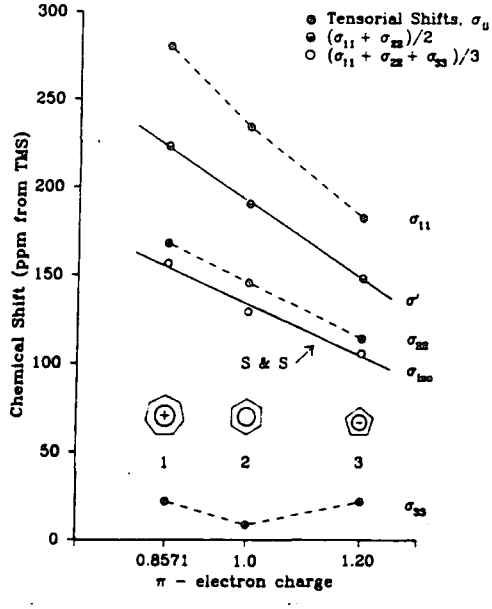

Fig (5-4) Plot of individual tensor components as a function of π electron charge[23].

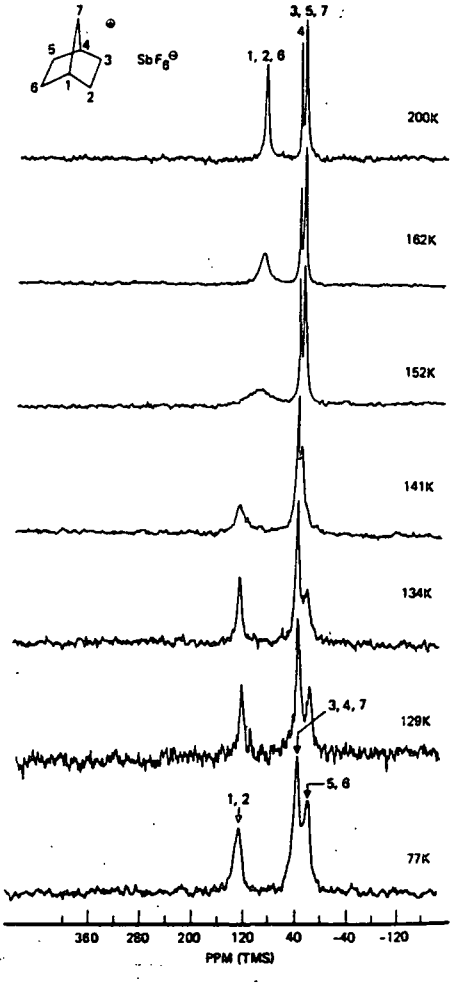

Fig (5-5) ^{13}C/CP MAR Spectra from 2-norbornyl cation.

that matrix isolation brings to the determination of the tensor components by the elimination of the intermolecular interactions.

REFERENCES:

1a- Lewis G. N., Lipkin D., Magel T. T., J. Amer. Chem. Soc., **63**, 3065, (1941). b- Lewis G. N., Lipkin D., J. Amer. Chem. Soc., **64**, 2801, (1942).

2- White E., Dows D. A., Pimentel G. C., J. Chem. Phys., 22, 1943, (1954).

3- Norman I., Porter G., Nature, London, **174**, 508, (1954).

4a- White D. E., 19th experimental NMR conference, Blacksbury, Va. April, (1978). b- 33th symposium on molecular spectroscopy, Columbus, Ohio, June, (1978). c- Kohl J. E., Semack M. G., White D., J. Chem. Phys. **69(12)**, 5378, (1978).

5- Zilm K. W., Conlin R. T., Grant D. M.,Michl J., J. Amer. Chem. Soc., **100(25)**, 8038, (1978).

6- Craddock S., Hinchclinkefe A. J., "Matrix isolation: a technique for the study of reactive inorganic species", Cambrige University Press, (1975).

7- Hallam H. E., "Vibration spectroscopy of trapped species: infrared and raman studies of matrix-isolated molecules, radicals and ions",London, Wiley (1973).

8- Rowland Davies P., Disc. Faraday Soc., **48**, 181, (1969).

9- White G. K., Experimental techniques in low temperature physics. Chapman and Hall Limited, London, (1968).

10- Kohl J. E., Semack M. G., White D., Phys. Rev. Lett., **42(16)**, 1072, (1979).

11- Carduner K., Villa M., White d., Rev. Sci. Instrum., **55(1)**, 68, (1984).

(12- Allavena M., Silvi B., Cipriani J., J. Chem Phys., **76(9)**, 4573, (1982).

13- Murphy M, Semack M, G., White D., J. Mag. Res., **73**, 143, (1987).

14- Zilm K. W., Conlin R. T., Grant D., Michl J., J. Amer. Chem. Soc., **102** (22), 6672, (1980).

15- Orendt A. M., Facelli J. C., Beeler A. J., Reuter K., Horton W. J., Cutts P., Grant D. M., Michl J., J. Ame. Chem. Soc. **110,** 3386, (1988).

16- Facelli J. C., Michl J., Grant D. M., J. Ame. Chem. Soc. **108**, 6464, (1986).

17- Facelli J. C., Orendt A. M., Solum M. S., Depke G., Grant D., Michl J., J. Amer. Chem. Soc., **108,** 4268, (1986).

18- Beeler A. J., Orendt A. M., Grant D., Cutts P. W., Michl J., Zilm K. W., Downing J. W., Facelli J. C., Schindler M. S., Kutzelnigg W., J. Amer. Chem. Soc., **106,** 7672, (1984).

19a- Facelli J. C., Orendt A. M., Beeler A. J., Solum M. S., Depke G., Malsch K. S., Downing J. W., Murthy P. S., Grant D., Michl J., J. Amer. Chem. Soc., **107,** 6749, (1985). **b-** Orendt A. M., Facelli J. C., Grant D., Michl J., Walker F. H., Dailey W. P., Waddell S. T., Wiberg K. B., Schildler M., Kutzelnigg W., Theor. Chim. Acta, **68,** 421, (1985).

20- Zilm K. W., Grant D. M.,Michl J., J. Amer. Chem. Soc., 103(11), 2913, (1981).

21- Zilm K. W.,Beeler A. J., Grant D. M., Michl J.,Chou T-C, Allred E. L., J. Amer. Chem. Soc., **103**, 2119, (1981).

22- Orendt A. M., Arnold B. R., Radziszewki J. G., Facelli J. C., Malsch K. D., Sturb H., Grant D., Michl J., J. Amer. Chem. Soc., **110**, 2648, (1988).

23- Strub H., Beeler A. J., Orendt A. M., Grant D., Cutts P. W., Michl J., Cutts P. W., Zilm K. W., J. Amer. Chem. Soc.,

105, 3333, (1984).

24- Zilm K. W., Merrill R. A., Greenberg M. M., Berson J. A., J. Amer. Chem. Soc., **109**, 1567, (1987).

25- Zilm K. W., Merrill R. A., Webb G. G., Greenberg M. M., Berson J. A., J. Amer. Chem. Soc., **111**, 1533, (1989).

26- Gay I. D., J. Mag. Res. **58**, 413, (1984).

27- Yannoni C. S., Macho V. Myhre P. C., J Amer. Chem. Soc., **104**, 1380, (1982).

28- Yannoni C. S., Macho V. Myhre P. C., J Amer. Chem. Soc., **104**, 907, (1982).

29- Macho V., Kendrick R., Yannoni C. S.,J. Mag Res., **52**, 450, (1983).

APPENDIX 5-A

SHIFT TENSOR COMPONENTS
(From references 14 to 23)

TABLE 5-A

Compound	σ_{11} exptl	σ_{22} exptl	σ_{33} exptl	σ_{av} exptl	σ_{liq}
methanol	76	68	6	50	49.0
dimethylether	88	88	6	61	59.7
formaldehyde	98	70	9	59	55.0
trimethoxy methane	80	65	11	52	51.1
dimethylsulfite	79	63	10	51	48.4
ethene	11	11	4	9	7.3
propane	30	15	4	16	15.4
isobutane	42	33	6	27	24.3
neopentane	50	50	5	35	33.0
acetone	49	47	-3	31	29.8
ethanol	35	19	4	19	18.2
ethylether	32	15	9	19	17.1
cis-butane2,3-epoxy	28	6	6	13	12.1
trans-butane2,3-epoxy	27	27	5	20	17.6
methylfluoride	105	105	15	75	74.1
methanethiol	14	12	2	9	6.5
dimethyl sulfide	43	20	4	22	18.2
dimethyl disulfide	48	16	6	23	22.1
dimethylsulfone	62	62	9	44	42.8
ethylene	234	120	24	126	123.3
propene C_1	226	97	[17]		113.4
propene C_2	253	133	[12]	0	132.7
cis-2-butene	232	119	22	124	124.6
trans-2-butene	232	113	37	127	126.0
isobutylene C_1	217	86	[29]		110.7
isobutylene C_2	268	152	[5]		141.7
tetramethylethylene	222	119	29	123	122.8
cyclopropene	239	79	5	108	108.7
cyclobutene	244	138	[30]		137.2
cyclopentene	235	118	39	131	130.8
cyclohexene	236	123	[23]		127.4
1-methylcyclopentene C_1	220	102	[51]		124.2
1-methylcyclopentene C_2	244	128	[48]		140.1
1,2-dimethylcyclobutene	235	131	[45]		137.0
1,2-dimethylcyclopentene	230	119	[46]		131.5
1,2-dimethylcyclohexene	214	117	[46]		125.6
methylenecyclopropane C_1	200	97	[12]		103.0
methylenecyclopropane C_2	220	185	[-13]		130.7

TABLE 5-A Continue

Compound	σ_{11} exptl	σ_{22} exptl	σ_{33} exptl	σ_{av} exptl	σ_{liq}
methylenecyclobutane C_1	208	90	[17]		105.1
methylenecyclobutane C_2	253	154	[44]		150.2
methylenecyclopentane C_1	220	82	[13]		104.9
methylenecyclopentane C_2	262	145	[52]		153.0
1,2-bismethylenecyclobutane C_1	204	95	[10]		103.1
1,2-bismethylenecyclobutane C_2	250	144	[55]		149.7
bicyclo[2.2.0]hex-1(4)-ene	323	128	[46]		165.8
bicyclo[3.2.0]hept-1(5)-ene	271	123	[56]		150.1
bicyclo[3.3.0]oct-1(5)-ene	244	118	[76]		146.0
bicyclo[4.2.0]oct-1(6)-ene	253	130	[43]		142.1
bicyclo[4.3.0]non-1(6)-ene	235	128	[41]		134.5
	Olefinic carbons				
ethylene	234	120	24	126	123.3
trans-2-butene	232	113	37	127	126.0
cis-2-butene	232	119	22	124	124.6
trans-cyclooctene	238	127	37±5		134.0
cis-cyclooctene	240	123	28±5		130.4
cycloheptene	245	126	27±5		132.7
cyclohexene	236	123	23±5		127.4
cyclopentene	235	118	39	131	130.8
cyclobutene	244	138	30±5		137.2
cyclopropene	239	79	5	108	108.7
acetylene	150	150	-90±5	70	72.1
	Aliphatic carbons				
trans-2-butene	27	27	5	20	17.6
cis-2-butene	28	6	6	13	12.1
cis-cyclooctene C_α					26.0
cyclopentene C_α	52	30	12	31	32.8
C_β	39	22	7	23	23.3
cyclobutene	43	33	23	33	31.4
cyclopropene	40	29	-59	3	2.3
isobutane	26	26	22	25	25.0
trimethoxymethane	123	116	99	113	115.2
bicyclo[1.1.1]pentane	42	42	17	34	33.57
bicyclo[1.1.1]pentanone	101	47	21	56	55.1
norbornadiene	58	56	32	49	50.9
cubane 6 K	71	35	35	47	47.3
cubane 20 K	62	35	35	44	
tetrahedrane					
ketene	265	239	77	194	194
ketene	39	4	-27	3	2.5
allene	158	54	23	78	74.8
allene	233	233	175	214	213.5

TABLE 5-A continue

Compound	σ_{AA} exptl	σ_{BB} exptl	σ_{CC} exptl	σ_{av} exptl	σ_{liq}
cyclopropene	40	29	-59	3	2.3
ethylene oxide	93	19	19	44	40.8
cyclopropane	22	2	-36	-4	-3.8
spiropentane	37	16	-23	10	5.9
ethylene sulfide	54	7	11	24	18.7
bicyclo[1.1.1]pentane	56	38	54	49	50.8
bicyclo[1.1.1]pentanone	87	47	1	45	35.6
cyclobutene	33	23	43	33	31.4
cyclobutane	23	14	39	25	22.1
oxetane C_{α}	93	15	104	71	72.8
oxetane C_{β}	22	4	41	22	23.1
norbornadiene	69	63	97	76	75.5
tetrahydrofuran C_{α}	75	21	110	68	67.9
tetrahydrofuran C_{β}	17	17	52	29	25.8
1,3-cyclopentadiene	39	33	51	41	42.2
cyclopentane	21	12	49	27	25.3
cyclopentene C_{α}	30	12	52	31	32.8
cyclopentene C_{β}	22	7	39	23	23.3
1,4-dioxane	81	37	86	68	66.5
malononitrile	11	-11	-6	10	8.7
tert-butylcyclohexane-4-^{13}C	57	25	9	30	27.0
1,4-cyclohexadiene	44	21	10	25	25.7
propane					15.9
1,3,5-cycloheptatriene	25	16	55	32	28.1
n-eicosane	39	18	51	36	

TABLE

Compound	$\sigma_{\perp}$	$\sigma_{\parallel}$	σ_{av}	σ_{liq}
carbon monoxide	305	-48	187	182.2
carbon dioxide	245	-90	133	132.2
carbonyl sulfine	275	-90	153	154.0
carbon disulfide	332	-92	191	192.8
carbon suboxide	235	-90	127	127.7
carbon suboxide	24	-90	-14	-14.6
acetylene	150	-90	70	71.9
propene	140	-74	69	68.4
propene	166	-93	80	79.8
2-butyne	152	-75	76	74.8

CHAPTER 6

MATRIX ISOLATION: EXPERIMENTAL

6.1 NMR-CRYOGENIC SYSTEM DESIGN CONSIDERATIONS

There are two main factors that influence the design of a matrix isolation system for NMR applications. The first is the access to an NMR magnet, i.e. the possibility of having a magnet totally dedicated to the matrix isolation work. This required because of the difficulty of frequently dismantling the cryogenic system for ordinary NMR work if the magnet is to be used for both purposes. The other factor is the amount of space available around the magnet area to accommodate the necessary equipment needed for this application.

It was possible to accomplish the first factor when a Varian XL-100 magnet became available which could be totally dedicated to this project. This is an open - gap electro-magnet designed to operate normally at a frequency of 100 MHz for protons. Due to its unique structure, this magnet provides excellent access to the pole faces from above, below, back and front. This factor alone was a major contributor in the final design of the probe system and in the total integration of the different parts that constitute this project.

The strength of the magnetic field at which the magnet operates was changed so that the proton resonance frequency is now at 60 MHz in order to make the interface with the home - built spectrometer successful.

The answer to the second factor mentioned above came with the first one. The fact that it was possible to have a magnet dedicated only for this application made it also possible to accommodate the equipment needed for both the cryogenic

requirements as well as the sample handling facilities very close together.

This chapter will describe the design and construction of an NMR matrix isolation system with such characteristics. The system integrates the capability to produce the cryogenic temperatures needed to freeze the sample, together with the high-vacuum facilities needed to introduce and deposit the materials to be studied, and the ability to perform the NMR experiments, all in one unit. One of the great advantages of this configuration is the reduction in the amount of time needed to produce the deposited sample from which NMR signals can be detected. This is due to the fact that the system does not have to be dismantled to go from one sample to the next. Another advantage of the system is the ability to detect the NMR signal from the sample during the period of deposition. This enables the concentration of the matrix sample to be determined, again helping to reduce time.

6.2 NMR-CRYOGENIC SYSTEM-DESCRIPTION OF THE COMPONENTS

6.2.1 CRYOGENIC SYSTEM

The cryogenic system is central as far as the matrix isolation technique is concerned. It is the part that provides the desired temperature at which the gaseous materials of interest can be properly deposited. It is a closed-cycle refrigerator known commercially as a Displex unit (Fig (6-1)), and it has been selected for this work due to its simplicity and flexibility during operation. This is an Air

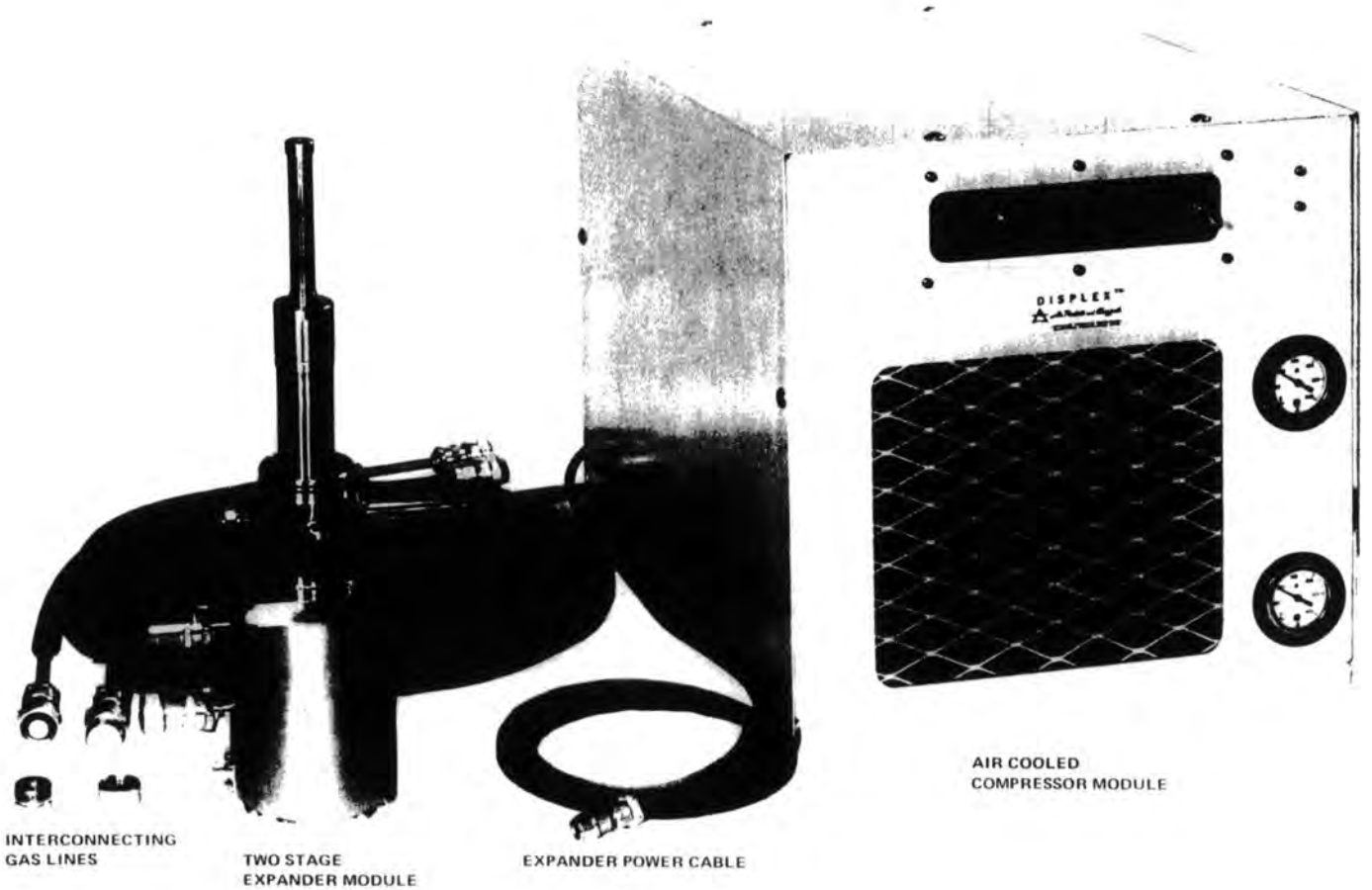

Fig (6-1) CSA-202 Cryogenic Refrigeration System[1].

Product CSW-202 model, which consists of a converted compressor (of the type used for air conditioners) and an expander module where the cryogenic temperatures are produced. The compressor uses high-purity helium gas as the working medium. These two components are coupled together by means of two flexible pipes, one for high-pressure and the other for low-pressure helium, together with a power lead from the compressor to the expander.

The compressor is a water-cooled type requiring a minimum of 0.4 gallons per minute of water under normal operating conditions. If the level of water flow drops below this, there is a safety mechanism valve that will sense the drop, and send a signal to turn off the compressor. It also has high-pressure and low-pressure gauges to monitor the helium pressure. The compressor should be pressured to 215±5 psig when the system is not in operation. The procedure for charging up the compressor is described in the operational manual provided by Air Products[1]. When the system is working, the compressor pressures should read 325±5 psig at the high-pressure gauge and 100±5 psig at the low-pressure gauge after the compressor has come to equilibrium.

The expander module is based on a design produced by Solvary and later improved by Taconis, Gifford, and Mcmahon[1]. A detailed description on the principles of operation of the expander is provided in the operational manual for the Displex[1]. In simple terms, the high-pressure helium gas provided by the compressor is passed through two expansion stages which cool the bottom end of the unit to the required temperature. A schematic diagram[1] of the expander unit is

presented in Fig (6-2). It is capable of covering the temperature range between 300 K and 10 K. This is achieved by cooling the system to the minimum temperature and then activating a heating resistor located at the end of the second-stage cooling part of the expander. A control system is provided to regulate the heat and maintain the temperature to within ±1 K of the set value.

In order to achieve this temperature range it is necessary to insulate the first and second stages of the expander from ambient temperature conditions. For this reason a vacuum shroud was designed and constructed in Durham according to the manufacturers' specifications. Copper was used in the construction of the shroud in order to minimize the amount of magnetic material around the area of influence of the magnet. A diagram of the vacuum shroud is presented in Fig (6-3). There is a very tight fit between the expander and shroud, and they are connected by means of two O-ring seals. These also play the important role of maintaining the essential vacuum seal between the cryogenic system and ambient pressures. This configuration allows rotation of the shroud around the expander while maintaining a very high vacuum. It is recommended to use sufficient amounts of vacuum grease on both O-rings to facilitate the coupling during assembly and to improve the vacuum seal. At the end of the vacuum shroud there is a 17.5 mm CAJON vacuum-fitting welded to the copper, which is used to connect the shroud to the NMR probe glassware.

The expander module has been provided with a Kp/Au-0.07 at % Fe thermocouple which is mounted at the coldest end of

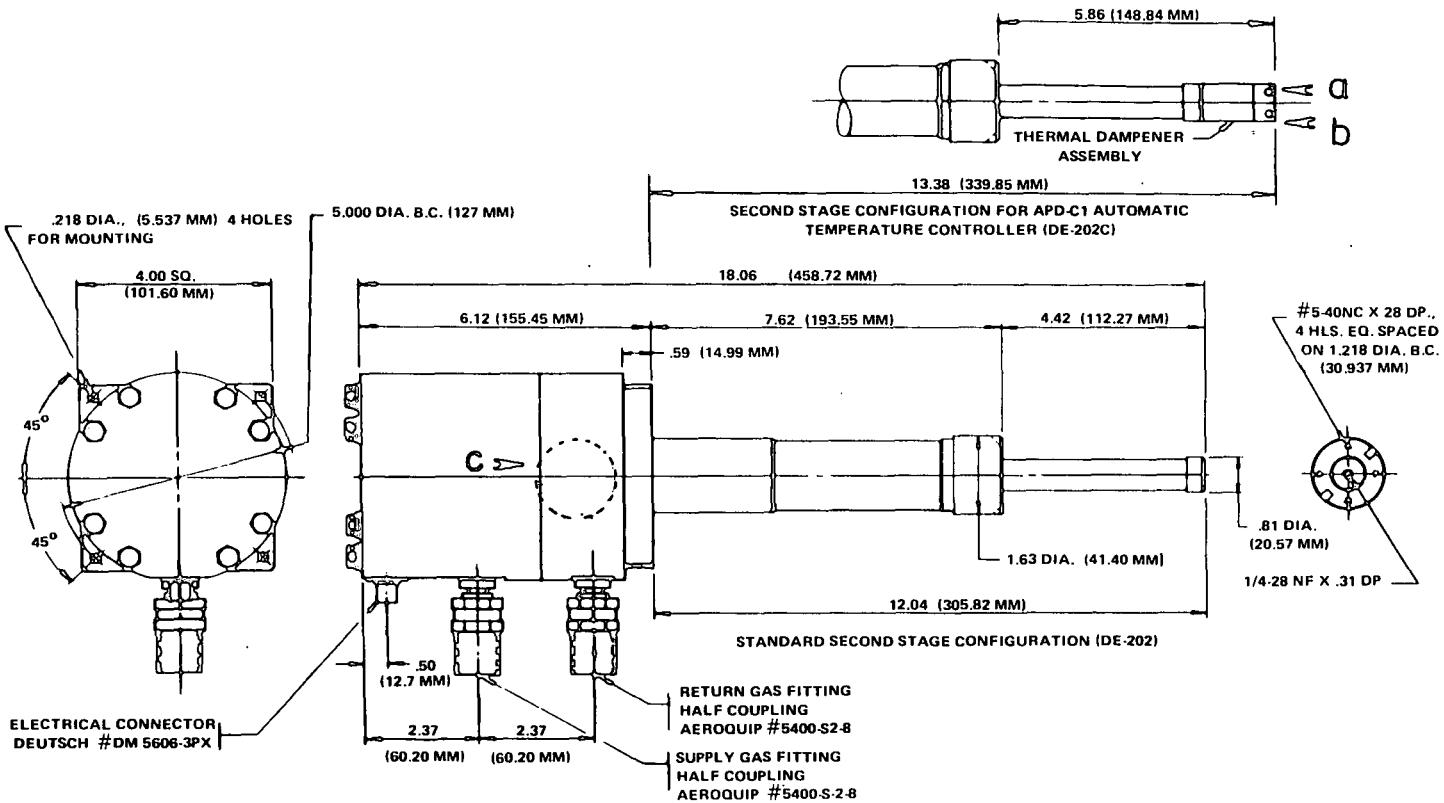

Fig (6-2) Schematic diagram of the expander module[1].

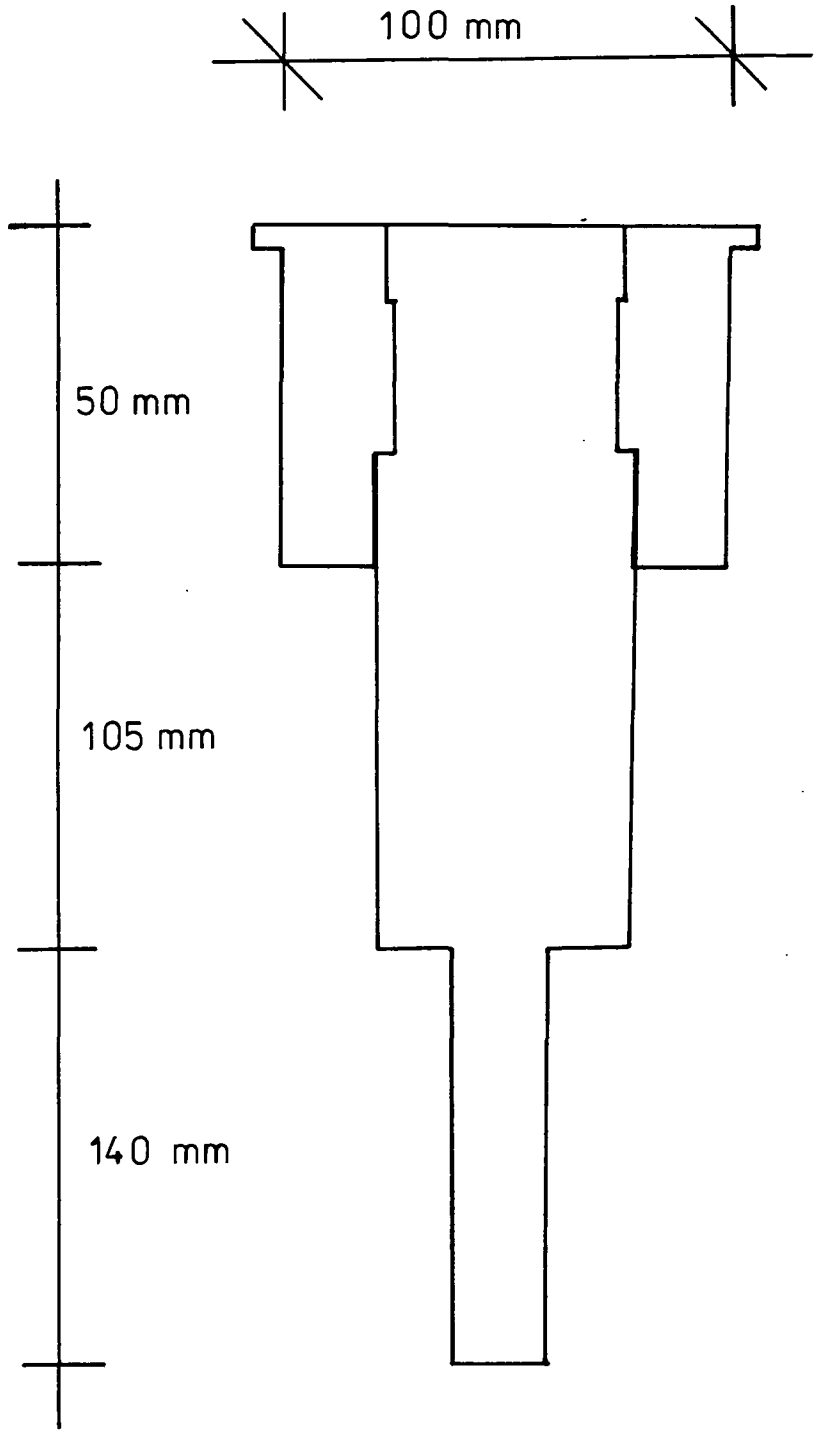

Fig (6-3) Schematic diagram of the Vacuum shroud.

the expander (see A in Fig (6-2)). This allows the possibility of monitoring the temperature of the system during the experimental period over the whole temperature range. The thermocouple is connected to a control unit model APD-B, also from Air Products, calibrated in such a way that it will give the system's temperature in Kelvin (K). This unit also provides the temperature control and necessary voltages for the heating resistor. An additional hydrogen vapour bulb thermometer is also provided with the expander, which is charged to 57 psi (see B and C in Fig (6-2)) . It provides a second way to monitor the temperature in the very low range between 10 and 25 K.

The first step in the construction of the integrated system was to bridge together the expander and the magnet, i.e. the expander needs to be located above the magnet gap. An aluminium table was designed and constructed for this task. The top face of the table presents an opening of 100 mm in diameter through which the vacuum shroud, together with the expander, can be lowered. A mounting jack is located on one side of this hole where the expander is clamped. The mount includes a vernier screw that allows the precise positioning of the expander in the vertical direction. This is very important during the assembly period. Four screws located on the top flange of the vacuum shroud serve as supporting legs. The assembly rests on them, releasing the pressure on the two O-rings. A diagram of the table is presented in Fig (6-4).

The separation between the magnet poles is 35 mm, and the external diameter of the Cojon fitting at the end of the vacuum shroud is 40 mm. It can be seen that there is

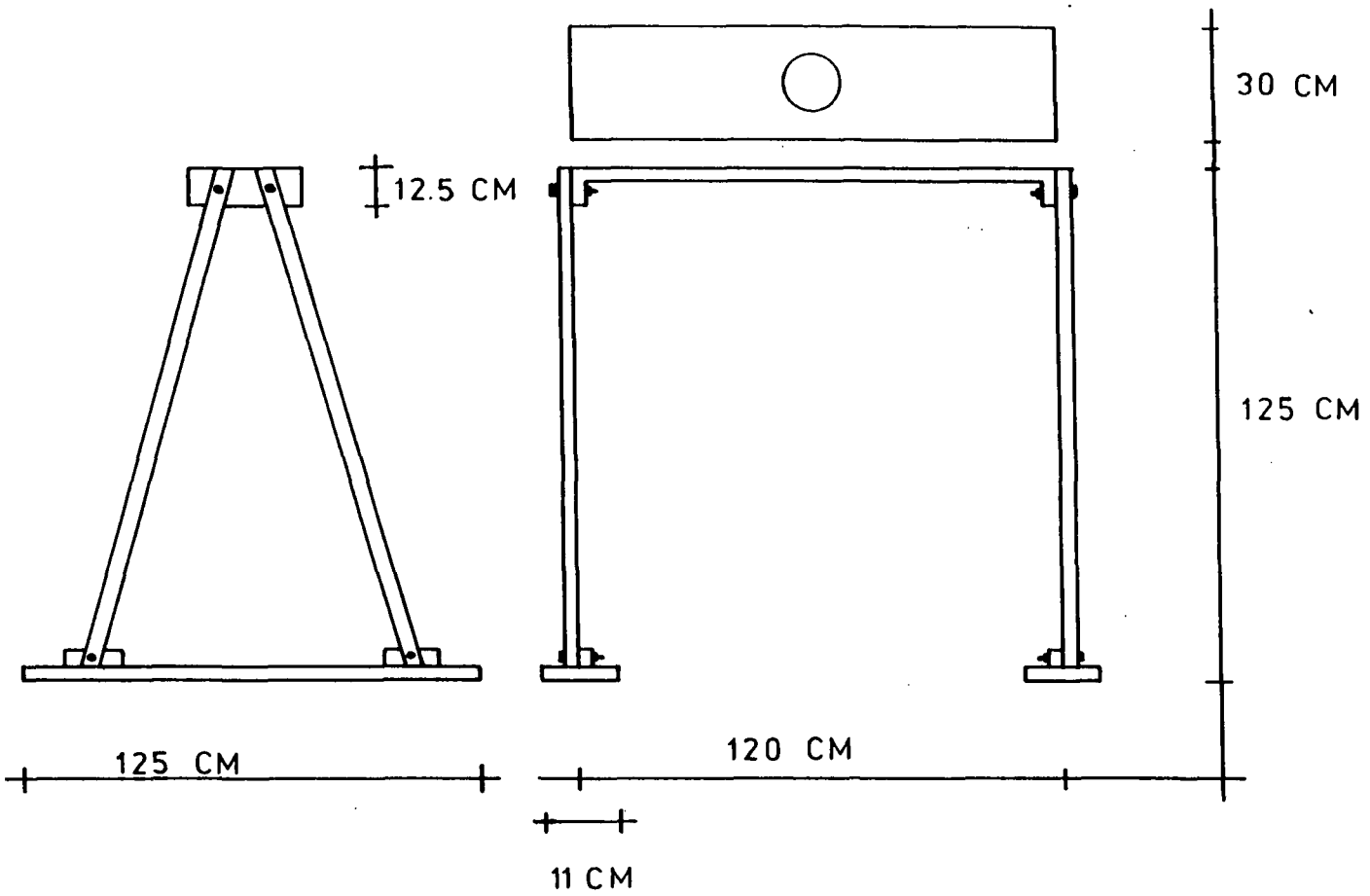

Fig (6-4) Schematic diagram of Aluminium Table

insufficient space to introduce the expander inside the magnet gap. It is therefore necessary to extend the effect of the cold end of the expander to where the sample will be located, i.e. the centre of the magnet poles.

First, a rod of oxygen-free, high-purity (OFHP) copper is connected to the end of the expander. It is 188 mm long and 12.7 mm in diameter. A screw thread was machined at one end, 6 mm long, so that it can be incorporated at the end of the expander. Thermal conductivity is increased at the joint by means of an indium solder disc place between then.

Second, a sapphire rod mounted on a copper base (OFHP) is screwed into the end of the copper rod. In this way the end of the sapphire will be at the centre of the magnet poles. It is at the end of the sapphire where the sample, either pure or in matrix form, will be deposited. The dimensions of the sapphire rod are 60.4 mm long and 2.08 mm diameter. The sapphire was selected as the matrix support due to its good thermal conductivity and because it is transparent in the frequency range at which the NMR spectrometer will be operating, i.e. it contains no protons. Again, indium solder was used to produced good thermal contact between the different parts. Fig (6-5) shows these two components joined together.

The sapphire is encased by a quartz tube which is also mounted on the copper base. The quartz glass has been cut at the end, leaving 16 mm of sapphire surface exposed. This portion will be the one inside the RF magnetic field in the probe. The quartz serves to protect the sapphire as well as to avoid deposition anywhere else but in the exposed area.

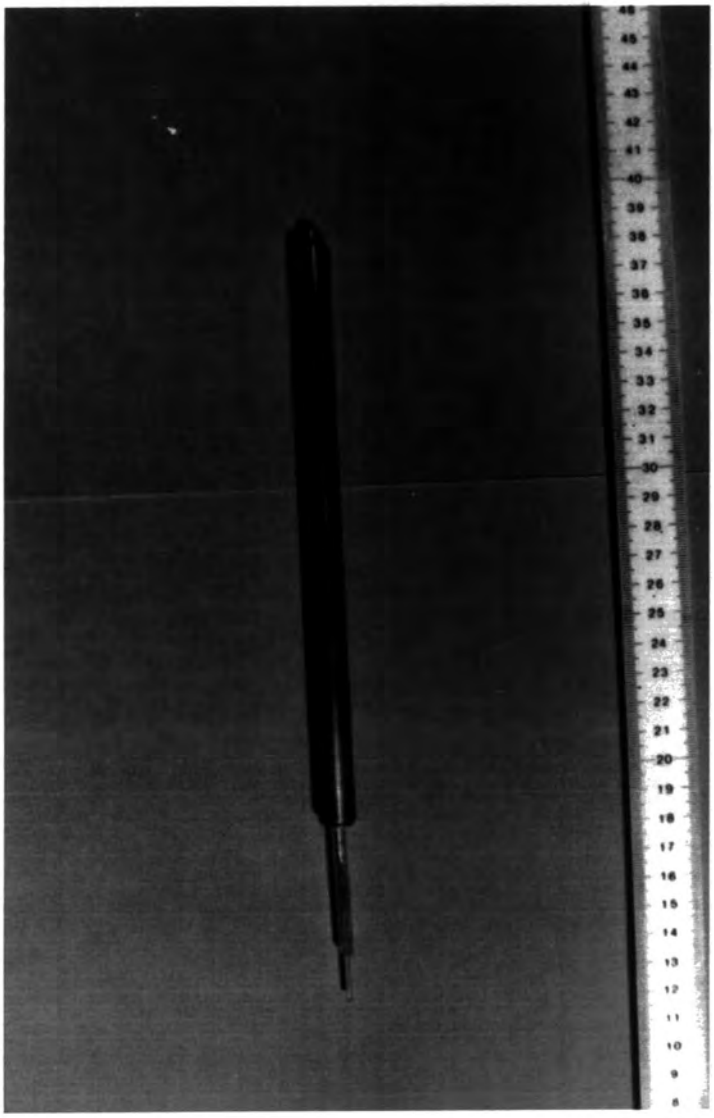

Fig (6-5) Copper rod and sapphire cool finger configuration.

6.2.2 VACUUM SYSTEM

In order to operate the expander module at the very low temperatures needed, and also to obtain the matrix samples, it is necessary to have the whole of the cryogenic system under a good, stable vacuum. Specifically, the expander needs a minimum pressure of 5×10^{-5} mbar in order to work at its maximum power.

There are several important considerations that need to be taken into account in the design and construction of a vacuum system for this particular application: i) the pipes used to construct the vacuum line must be of the widest possible bore to maintain a high pumping speed, ii) the vacuum line must be as linear as possible, with the least number of corners (These two features reduce the pumping speed dramatically), iii) the vacuum pumps and the expander need to be as close as possible to make the vacuum system effective where it is needed, i.e. close to the sapphire (This implies that the vacuum line needs to be as short as possible), iv) the instruments needed to measure the vacuum must be located close to the deposition area so that accurate readings are obtained, and v) two different types of pump are usually needed- a rotary pump and a diffusion pump. The pumping system has to work at a reasonable speed so that the time taken to produce the required vacuum can be minimized .

A combined pumping outfit provided by Edwards High Vacuum was chosen for this project. It consists of a rotary pump, model E2M5[2], capable of producing a vacuum of up to 8×10^{-4} mbar, and a 63 mm , water-cooled Diffstak[3] diffusion

pump. This has a pumping speed of 135 l s^{-1} and is capable of delivering a vacuum of 3×10^{-6} mbar. A diagram of the combined pumping system is presented in Fig (6-6).

The rotary pump is connected to the diffusion pump by means of a combined backing/roughing value (see 7 in Fig (6-6)). The "roughing" setting is used when it is necessary to operate the rotary pump independently from the diffusion pump to produce an initial vacuum to the system.

The diffusion pump is provided with a HV isolation valve positioned at the top of the pump (see 2 in Fig (6-6)). This valve has a connection to the rotary pump through the combined valve, by passing the diffusion pump.

A nitrogen trap[3] is fitted to the top of the isolation valve of the diffusion pump. This will condense water vapour and other gases coming from the vacuum line, so protecting the oil in the pump from being contaminated. It will also help in increasing the pumping speed. It has a capacity of 1 litre of liquid nitrogen and a charge life of 8 hours, making it very convenient for our use.

It would be ideal to maintain the wide bore of the diffusion pump for the whole of the vacuum line. Unfortunately, this is not possible due to the way the expander was designed. If the ideal conditions cannot be met, the next best possibility is to have the maximum diameter along the vacuum line. So a flexible stainless steel pipe of 25. mm diameter and 100 cm length was used in the construction of the vacuum line to link the vacuum pumps and the expander. An adapter was mounted at the top of the nitrogen trap to reduced the input to the diffusion pump from 63 mm to 25.5 mm.

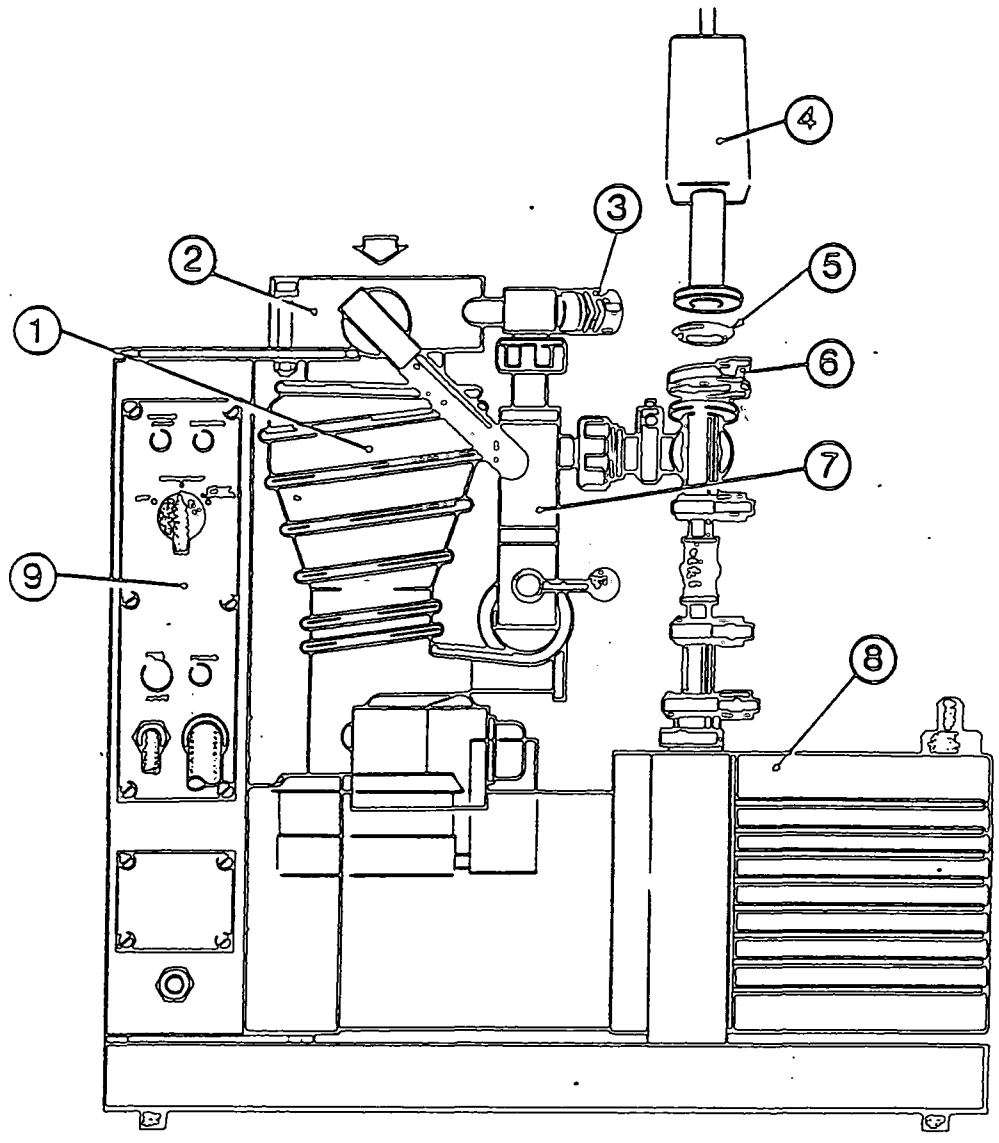

1..	Diffstak	6.	KF clamping ring
2.	HV Isolation valve	7.	Combined backing/roughing valve
3.	Air admittance valve	8.	Rotary backing pump
4.	Pirani gauge head (available as accessory)	9.	Switch box
5.	KF Centring ring (with O ring)		

Fig (6-6) Vacuum pump system.

This pipe connects to a T-joint which has one of the pressure gauges connected to it. The other end of the T-joint is connected to the expander module of the Displex. The expander is provided with its own isolation valve. This valve has proved to be very important during the leak testing of the vacuum line. The rest of the vacuum line consists of the NMR probe and inlet gas lines. They will be described in a later section of the present Chapter.

Two types of gauge were used to monitor the pressure of the vacuum system. The first is a Penning[4] gauge with a sensor head that is connected at the T-joint, as mentioned above. It covers the pressure range between 10^{-2} and 10^{-7} mbar. It is used to monitor the pressure during vacuum optimization and to detect any sample escaping from the probe area during deposition. The second is a Pirani gauge with a sensor head that is located at the gas supply inlets. It covers a range between 5 and 10^{-3} mbar of pressure. It is used to monitor the pressure of the incoming gases during the deposition time so that constant pressure can be maintained. All the connections between the different parts described above are made with high-vacuum O-ring seals. This approach allows easy dismantling and re-assembly of the vacuum line. The fact that most of the system is made of metal makes it very robust. Even so, great care must be taken when re-assembling the system to ensure that optimum high-vacuum performance is maintained: this will save long hours of leak-finding.

6.2.3 NMR PROBE AND SAMPLE ACCESS

In designing the matrix isolation system presented in this work, it was decided to deposit samples while the sapphire rod attached to the expander unit was inside the NMR probe. Therefore, the probe system has been constructed in such a way that it is possible to connect the vacuum system and sample supplies directly to it.

The body of the probe is a high-resolution Varian probe which has been specially modified for this particular application. It is made of aluminium with a width of 32 mm. This will fit very tightly within the magnet gap. The electronic circuit needed to both transmit the RF power and to receive the NMR signal is presented in Fig (6-7). It is a single-coil system operating at 60 MHz for protons. There are two variable capacitors, one for tuning and the other one for matching the circuit impedance to 50 Ω. The coil was made of tinned copper wire #16, with a length of 20 mm and an inside diameter of 11 mm , with a total of 9 turns. The probe is tuned and matched inside the Varian magnet gap using the facilities (a "wobbler") provided in connection with a Bruker CXP 200 NMR spectrometer located close by. It is possible to produce $\pi/2$ pulses of 1.5 μs duration. The dead time of the probe, i.e. the time needed for the electronics to recover after the pulse, has been measured to be 12 μs. This is a reasonably short value taking into account the size of the coil and the short $\pi/2$ pulse duration.

The problem of having the sapphire sample support inside the probe under permanent vacuum was solved by constructing a

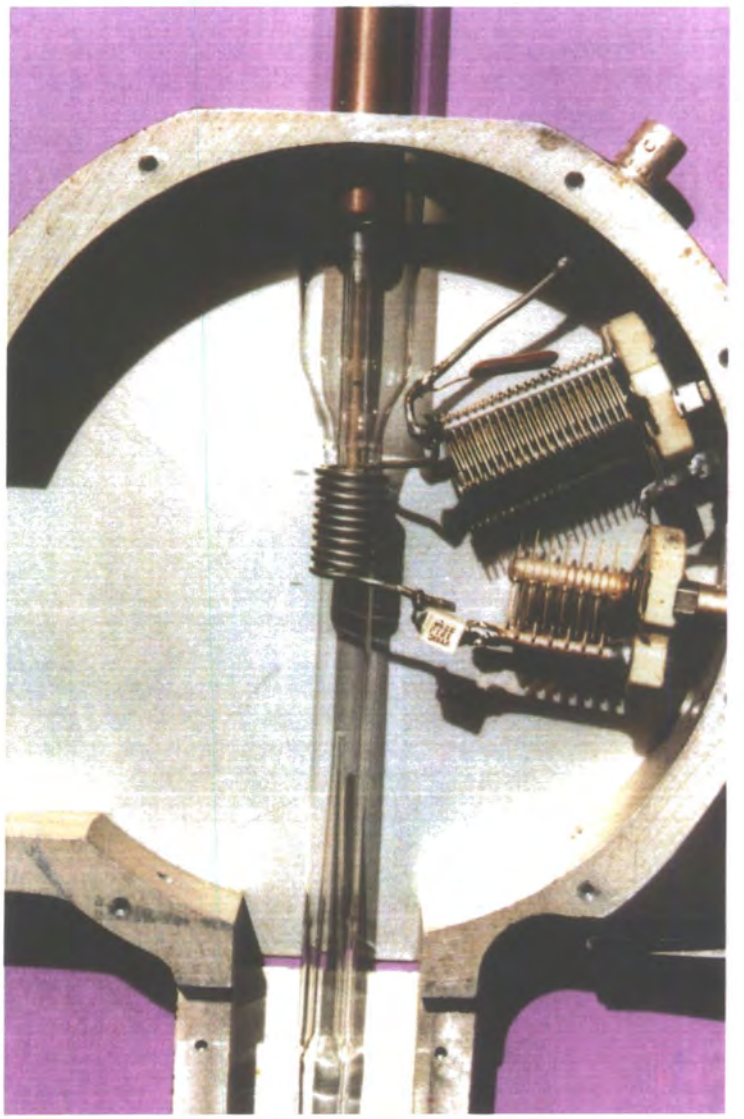

Fig (6-7) Electronic assembly of the NMR probe

glass dewar which runs along the whole of the probe body. The top of the dewar consists of a 25 mm diameter glass tube which has a ground-glass end joint. This couples to the CAJON vacuum fitting at the end of the vacuum shroud. A 10 mm diameter and 50 mm long thin-walled NMR tube is the next part of the dewar. For reasons of convenience and simplicity, the RF coil is located outside the NMR tube.

A nozzle is attached to the bottom of the NMR tube. It is a conical piece of glass about 50 mm long and 2.5 mm diameter at the small end. This narrow path ends 20 mm away from the coil and sapphire tip. This is used to limit the flow and direction of the incoming gases during the deposition period. It will guarantee that the incoming gases are directed and concentrated to the end of the sapphire inside the coil area. Below the nozzle is a 10 mm diameter glass tube which provides two gas inlets. These are at right angles to each other and can be used in a number of different ways. They have 5 mm diameter ground glass connectors and emerge from the probe body at the bottom and the front. This arrangement provides easy access to the inlet connections when the probe is located inside the magnet gap. A diagram of the probe assembly is presented in Fig (6-8). In practice, the dewar assembly was constructed before winding the RF coil around the 10 mm NMR tube section. The whole system was then placed inside the probe housing and the electrical connections were made.

There are several ways in which samples can be introduced into the probe, including the possibility of using samples in different initial phases. The most direct way will be to

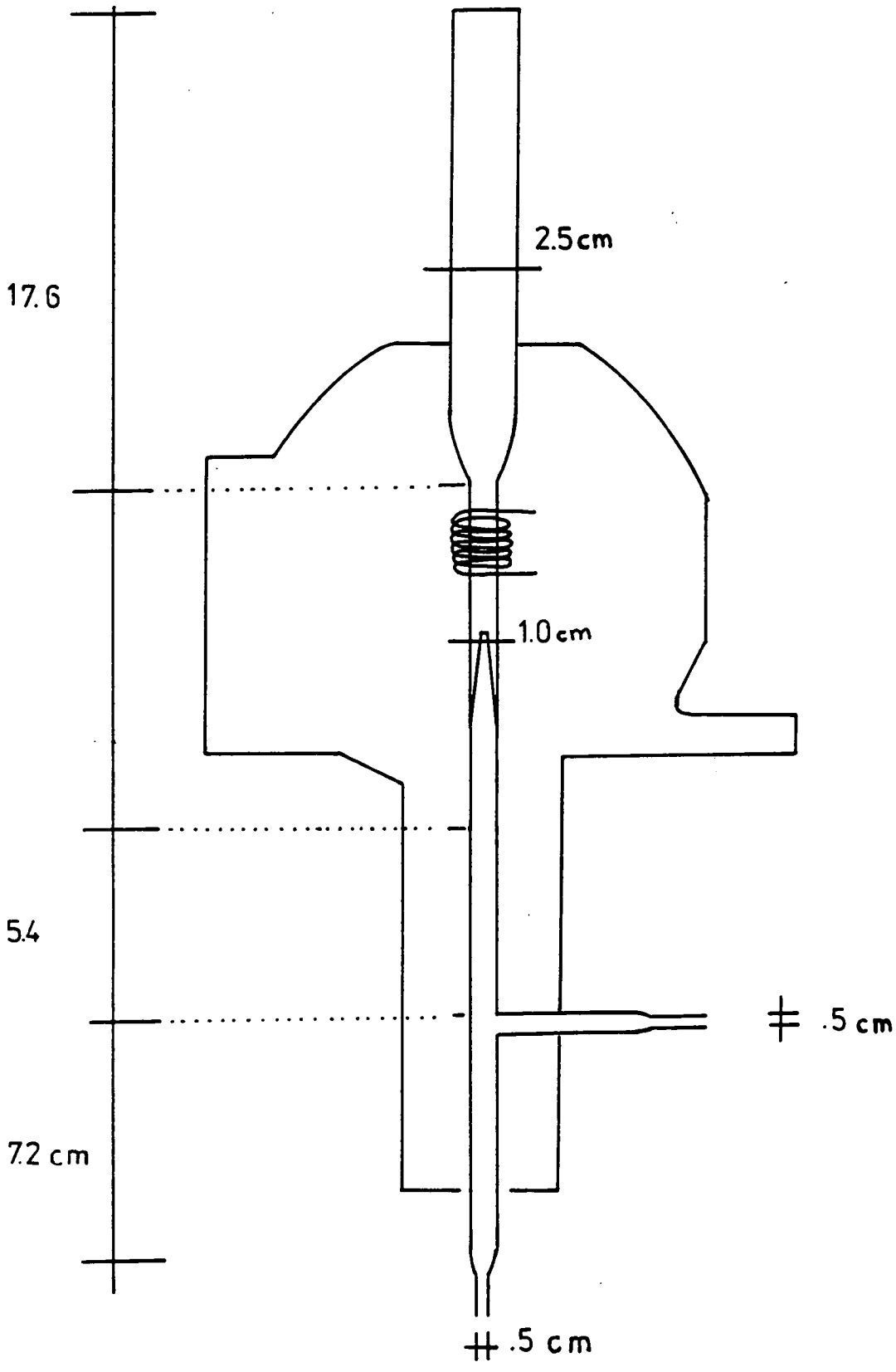

Fig (6-8) NMR probe and vacuum dewar Assembly.

connect gas bottles containing the sample and a matrix gas to the inlet ports. In this arrangement, two copper pipes of 3 mm o.d. are used to link the bottles to the probe. At the probe side of the lines, CAJON ultra-torr metal-to-glass connectors are welded to the copper pipes. At the other end the copper pipes, the connectors are fitted so that the gas cylinders can be attached directly to the lines. Regulating valves are placed between the cylinder and the copper pipe to allow coarse control of the gas flow. An extra needle valve, with a vernier, is also connected into each line. This allows fine control of the gases and the level of mixing between them. The lines also contain a pressure gauge head to monitor the gas flow rates. The method of operation of this configuration will be explained in a later section of this Chapter.

It is possible to have a second way of connecting the sample container to the probe which is more versatile and flexible. In this arrangement only one of the gas inlets at the bottom or at the front of probe is used to introduce a gas mixture. As before, a 3 mm o.d. copper pipe is connected to the inlet, and the line has the pressure-gauge detector head and a vernier needle valve. Then, a section of glass line is connected to the copper line using a CAJON adaptor. It has a teflon needle valve and a normal high-vacuum teflon valve which ends in a B10 grease-less connector. The two needle valves are used to control the flow of gases during deposition. The main teflon valve is used to isolate the whole of the vacuum system from ambient pressure during sample changes.

A length of vacuum line is joined to the B10 connector. It has three sample ports, each one with an isolation valve. The distance between them is 55 and 160 mm, with the connector to the vacuum line at the middle. As can be concluded, up to three samples can be present in the attached vacuum line at any one time. They can be initially in either liquid or gas form, in pure or matrix concentration. The sample container can be a test-tube or up to two, 3-litre round-bottomed flasks, with different gases or matrix concentrations. These should be located at the extremes of the line. So it is possible to see that this configuration gives a wider degree of flexibility and simplicity of operation as far as sample manipulation is concerned. It also helps to accomplish one of the aims of the system design, i.e. samples can be changed without taking the whole system apart after the sample has been evaporated from the sapphire. This is probably the greatest advantages of the system. Another advantage of this configuration is that it is possible to easily eliminate leaks in the system after they have been found. The small vacuum line together with the different sample containers is presented in Fig (6-9). The way in which this configuration operates will be described in a later section.

6.3 CRYOGENIC SYSTEM ASSEMBLY

The assembly of the cryogenic system is a very critical part of the whole experiment particularly the region where the probe and the expander are coupled together.

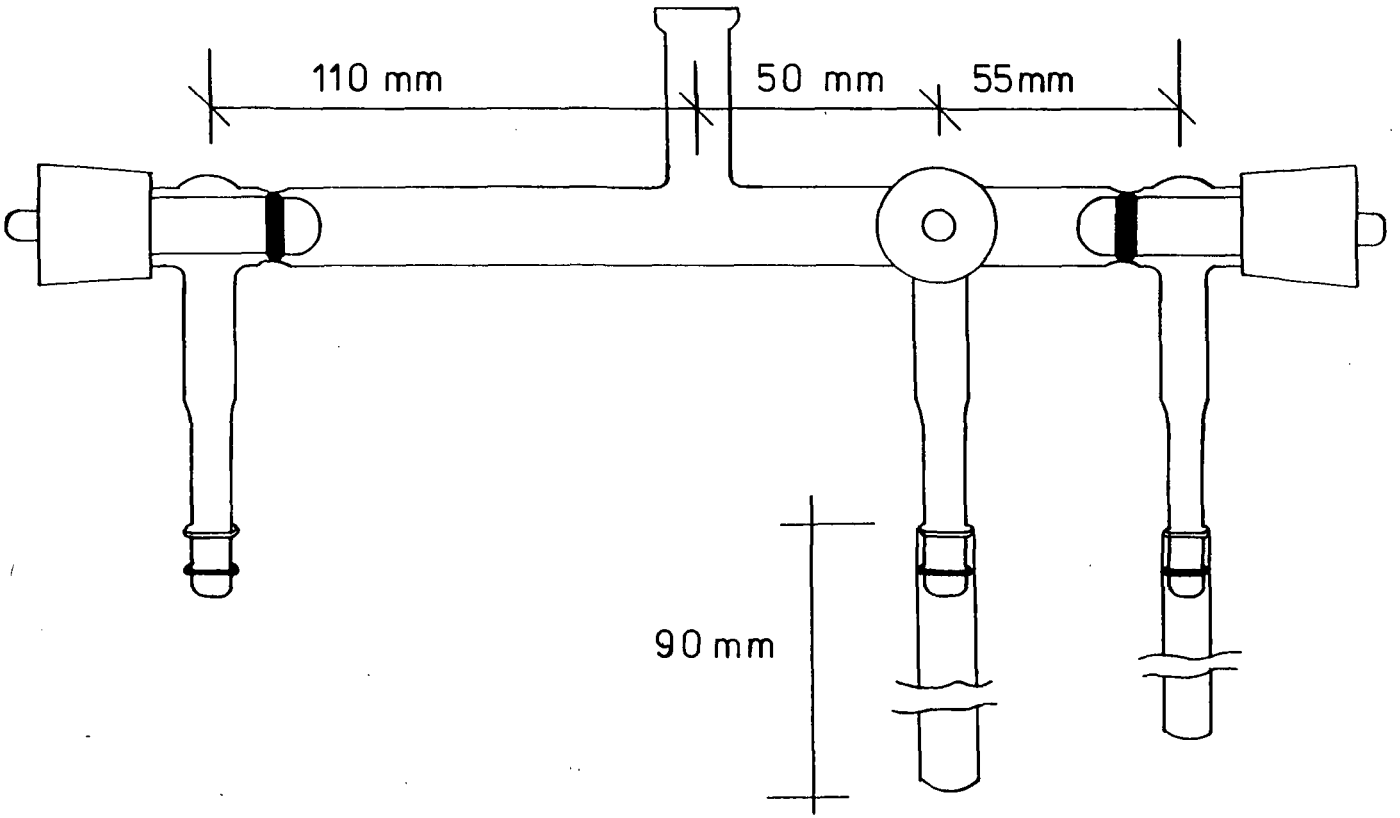

Fig (6-9) Schematic diagram of the small glass-vacumm line used for sample attachment.

The first stage is to put the aluminium table across the magnet in such a way that the hole in its middle is overlooking the magnet gap. At this point, the vacuum shroud is fed through the hole, with the four screws extended to hold it in position for the next stage of the assembly. The vernier screw in the expander's supporting base is extended to its most upright position. Now the expander can be introduced very carefully inside the vacuum shroud so that the thermocouple and heating wires are not damaged in the process. The expander is clamped down to the supporting base with two screws and nuts. The base has a degree of freedom in the horizontal direction. The position of the screws is adjusted in order to align the expander with the vacuum shroud. These will become very important when the two are coupled together. With the O-rings already greased, the expander is lowered down very slowly, with the aid of the vernier screw, towards the shroud. When the first O-ring is touching the shroud, a final adjustment can be made to its position. Then it is moved down even more slowly to allow the O-ring to be compressed evenly and to avoid damaging it with edge of the shroud. Failure in doing this will compromise the integrity of the necessary high vacuum. This process is continued until the top O-ring is also pressed between the two sections and the expander is resting properly inside the shroud.

The next step of the assembly is to place the NMR probe containing the vacuum dewar into position. This is done by locating the middle of the RF coil at the centre of the magnet poles. This is the region where the shimming coils are most effective. There is a mount for the probe located in front of

the magnet gap. This has two degrees of freedom: vertical and horizontal. The coordinates for the location of the probe were found to be 875 mm in the horizontal direction and 675 mm in the vertical direction. The bolt and O-ring from the CAJON fitting at the bottom of the vacuum shroud are removed at this point.

There are two more adjustments to be made to complete the operation. One is the precise horizontal position of the aluminium table so that the vacuum shroud can couple with the dewar. The second is the adjustment of the vertical position of the expander in relation to the top the dewar so that the sapphire cold finger will be in the middle of the RF coil.

For the first adjustment the expander is lowered so that the shroud is just touching the top of the dewar. At this point, the table is moved so that the dewar can easily be placed inside the CAJON fitting. Then, the table is secured using a pair of spacers and two stops underneath the top plate of the table. The stops are used to lock the table with the inside of the magnet poles. Next, the first pair of spacers is inserted between the magnet frame and the right hand side leg of the table. The second pair is inserted between the same leg of the table and the laboratory wall. These will present any sideways displacement of the table.

For the second adjustment, the screws on the vacuum shroud are raised all the way up without removing them. The expander is then lowered very slowly towards the dewar, checking if it has made contact with the end of the vacuum fitting. This is the most delicate part of the operation because if too much pressure is put onto the dewar there is

the possibility of breaking it. When the vertical position of the expander has been found, the four screws of the shroud can be lowered so they are in good contact with the table. These serve as stopping levels when the expander is moved down during future assembling of the system to prevent breakage of the dewar.

Now the copper rod, with the attached sapphire cold finger can be inserted into the system. This is an easy but delicate part of the assembly. The copper rod and the sapphire are screwed together with the indium solder between them. They are put inside the dewar, allowing them to rest at the top of the NMR tube. The bolt and O-ring of the CAJON fitting are fed through the dewar. With the expander in its most upright position, the probe is then placed in its mount and moved to the set position as indicated above. This will bring the probe right underneath the vacuum shroud, leaving a gap between them. The copper rod is manually lifted and screwed into the hole at the bottom of the expander, which already has indium solder around it. Now the expander is lowered down slowly until the dewar is about a centimetre inside the fitting. At this point, the O-ring and the bolt are attached to the fitting and the expander is lowered even more until the screws at the top of the shroud reached their set point. Then the bolt of the CAJON fitting is secured. Fig (6-10) shows the end result of the assembly in the area where the shroud and the probe meet.

The last part of the assembly around the probe area is to connect the sample supply lines to the probe inlets. As mentioned above, this is done by fitting the glass-to-metal

a) Displex unit
b) Aluminium table
c) Vacuum shroud
d) NMR probe
e) Magnet

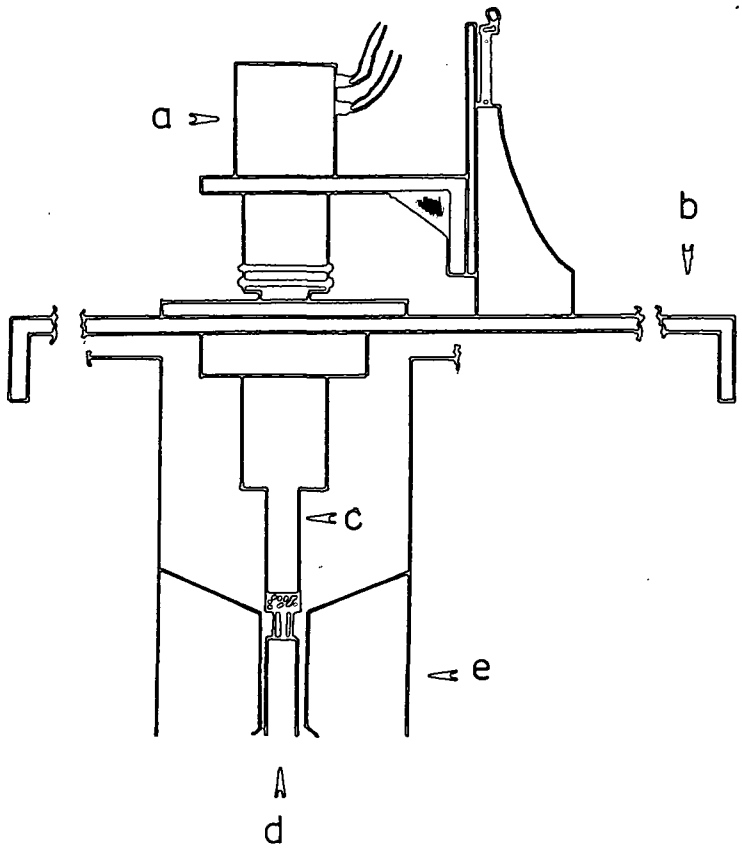

Fig (6-10) Schematic diagram of the coupling between NMR probe and vacuum shroud.

CAJON adapter at the end of the copper lines to the gas inlet from the bottom and/or from the front of the probe. First the bolt, spacer and the O-ring are introduced through the glass inlet and pushed along the glass (see in Fig (6-11a)). Then, the CAJON fitting is attached to the gas inlet, and the bolt and spacer are brought together, with the fitting, and the bolt is secured to the fitting. Final assembly is shown in Fig (6-11b). Care needs to be taken during this procedure because the inside of the fitting may break the glass joint. The coupling needs to be done as straight as possible. Fig (6-12) shows the fully integrated system .

Next, the sample configuration is selected and connected to the system. If the small vacuum line with the three ports is selected, the only essential part to connect is the teflon needle valve with the high-vacuum valve. The sample holder can be connected when the samples are safely attached to their respective ports. The procedure to connect this vacuum line will be described in the next section. If direct connection to gas bottles is selected, it is necessary to check that no leaks exist at the bottle end.

The time taken to complete the assembly of the system has been measured to be 3 to 4 hours. It does not take into account time needed for checking the vacuum or to produce the optimum vacuum pressure. This point will also be discussed in the next section.

a) bolt
b) spacer
c) O-ring

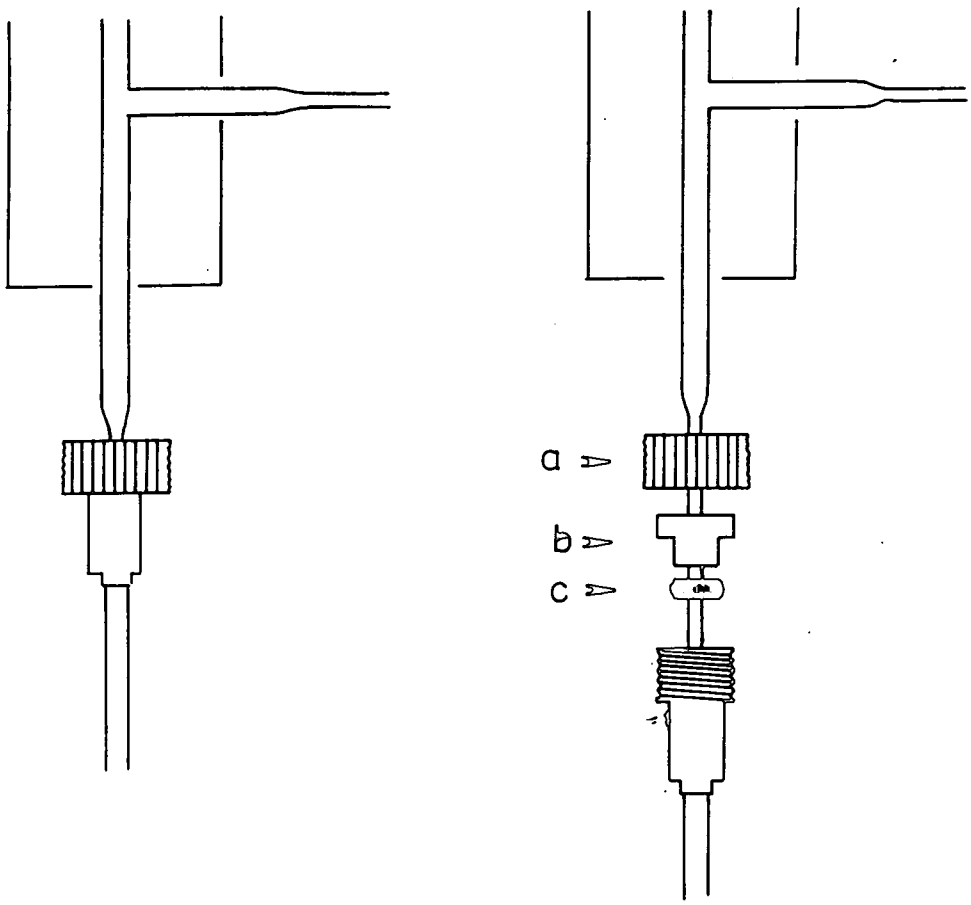

Fig (6-11) Schematic diagram showing the coupling between the copper gas lines and the probe inlet ports.

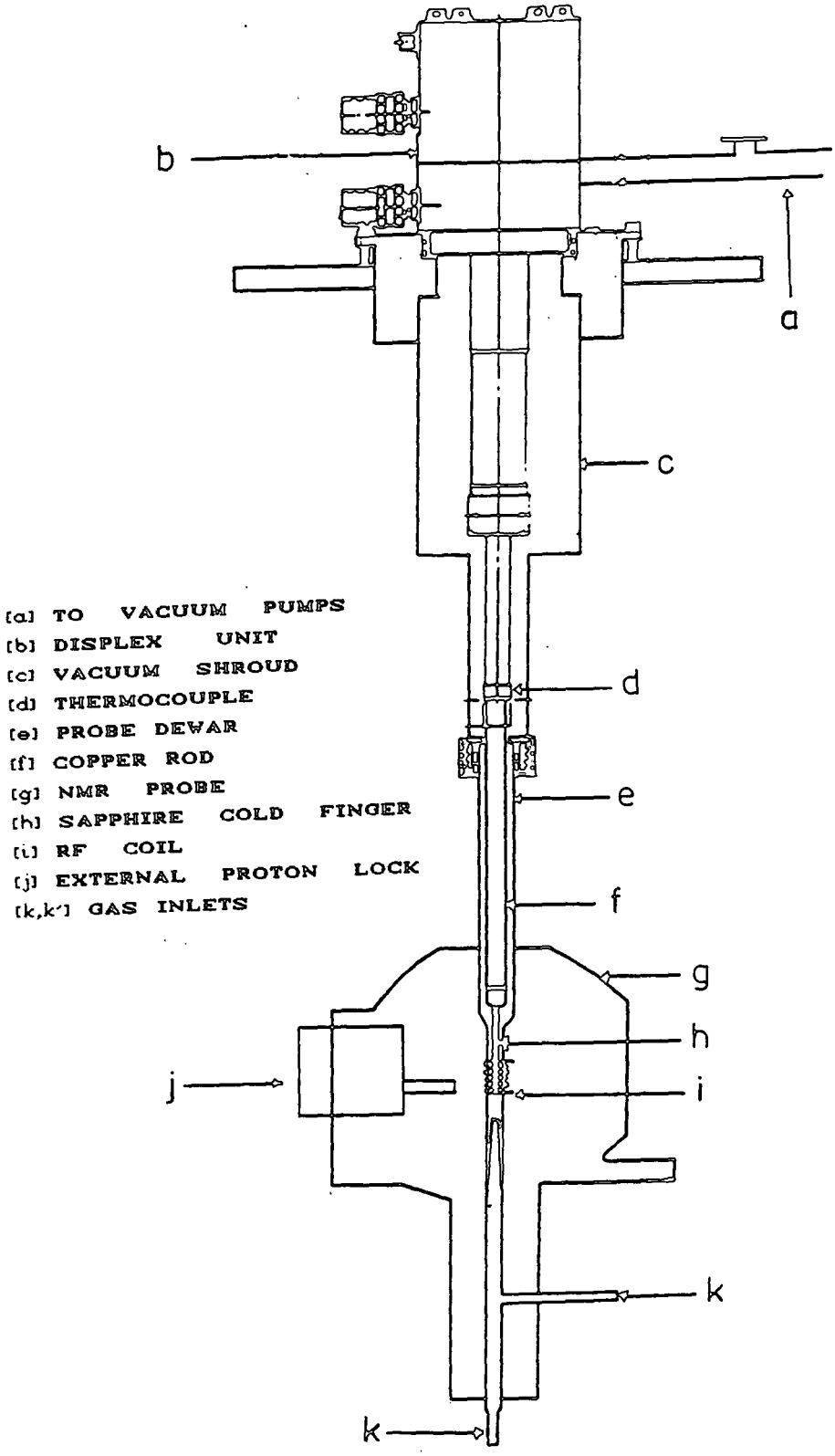

Fig (6-12) Schematic diagram of the final configuration of the NMR-Cryogenic system.

6.4 SYSTEM TESTING AND ROUTINE RUNNING

The importance of assembling and testing the vacuum system must be emphasied. This is because if it is done properly the first time the system can be used almost indefinitely without the need of dismantle any major part of it. In this section the testing of both the vacuum system and the cryogenic unit will be described.

6.4.1 VACUUM SYSTEM TESTING:

The assembly process allows the opportunity to make a complete check for leaks in the system. One section of the system is tested, and then the next one is added to it, and so on until the whole system is complete. The tests are carried out at: i) the reduction adapter on top of the diffusion pump, ii) at the end of the flexible metal pipe, and iii) at the end of the T-connector with the Penning gauge attached. All tests are done first with the rotary pump and then with the diffusion pump and the rotary pump. A pressure of 1×10^{-5} mbar can be obtained at the end of the T-joint. The shroud connected to the expander is tested without the probe by placing a blanking end instead. This test has a considerable importance because it is in this area that the cryogenic temperature will be generated. Problems were encountered with the copper-to-steel welding at the CAJON fitting which took some time to fix. The probe and the gas lines present no leak problems, meaning that all joints and welds are as required.

After assembly and leak testing of the system the nitrogen trap is filled and the HV isolation valve on top of the diffusion pump is in the closed position. The air admittance valve (see Fig (6-6)) is closed and the combined valve is then set to roughing and the rotary pump is activated. The only pressure gauge used at this point is the Pirani head at the end of the inlet line. The second gauge is activated when the system pressure reading at the Pirani is in the region of 5×10^{-2} mbar. This process continues until the Penning gauge reads a pressure of 10^{-3} mbar and the Pirani gauge reads 10^{-2} mbar. At this point, the combined valve is set to backing and the diffusion pump is turned on, allowing a period of 15 to 20 min for warming up. After this time the HV isolation valve is opened very slowly and the diffusion pump is brought into the line. When the system is being vacuumed for the first time it will take between 3 to 4 days to get a good vacuum pressure, i.e. 2×10^{-5} mbar. If this limit is not reached the procedure described in the previous section needs to be implemented to detect any possible leaks in the system. A longer period of time could produce a vacuum of 10^{-5} mbar.

As has already been mentioned, the strongest point of the system design is that when the optimum vacuum is obtained the system can be routinely used for different experiments.

6.4.2 CRYOGENIC SYSTEM TESTING:

The above section described how to get a good vacuum from this design. Once this is achieved, the necessary tests the

cryogenic system can be carried out. It is important to check the water is running through the cooling system of the Displex unit before it is turned on. Both the temperature readout and the Displex are turned on at this point and the temperature will start to fall almost immediately. A plot of ln T (in K) vs time (in min) was used to determine the performance of the Displex unit. Two such plots are provided by the manufacturer for typical loads and cooling times. These are shown in Fig (**6-13**). As indicated by the curves, the greater the load, the longer the time needed to obtain a very low temperature, so a substantial increase in time is to be expected in this application due to the presence of the long copper rod and sapphire cold finger. These measurements were carried out several times on this system and the results are presented in Fig (**6-14**) for two different cooling tests. One of the curves is from a system with a perfect vacuum in which the expected temperature of 16 K was achieved. The other is for a system with a very small leak. This stopped the Displex from reaching the lowest temperature.

It is possible to see that the rate of cooling is very nearly constant for most of the time. This steady change goes from room temperature down to 60 K. When 60 K is reached, the rate of cooling starts to increase rapidly. This process starts after 110 min from turning the Displex on, 60 min longer than in the curves presented in Fig (**6-13**). The system reaches the minimum temperature of 16 K after another 15 min. So the total time needed to produce the necessary low temperature is 130 min.

There is a very important point about safety that needs

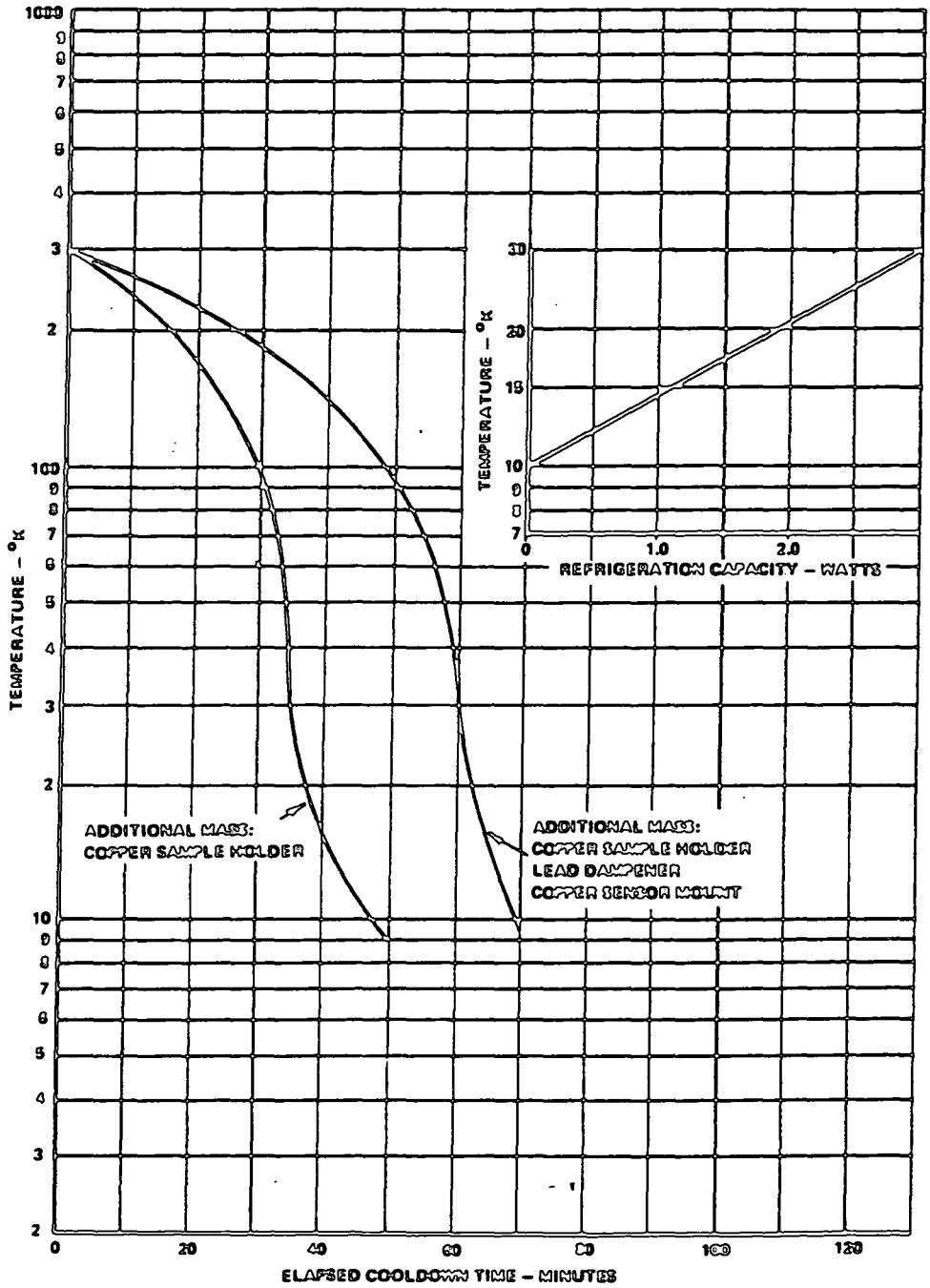

Fig (6-13) Standard cooling plot[1] of Temperature (K) vs. Time (min).

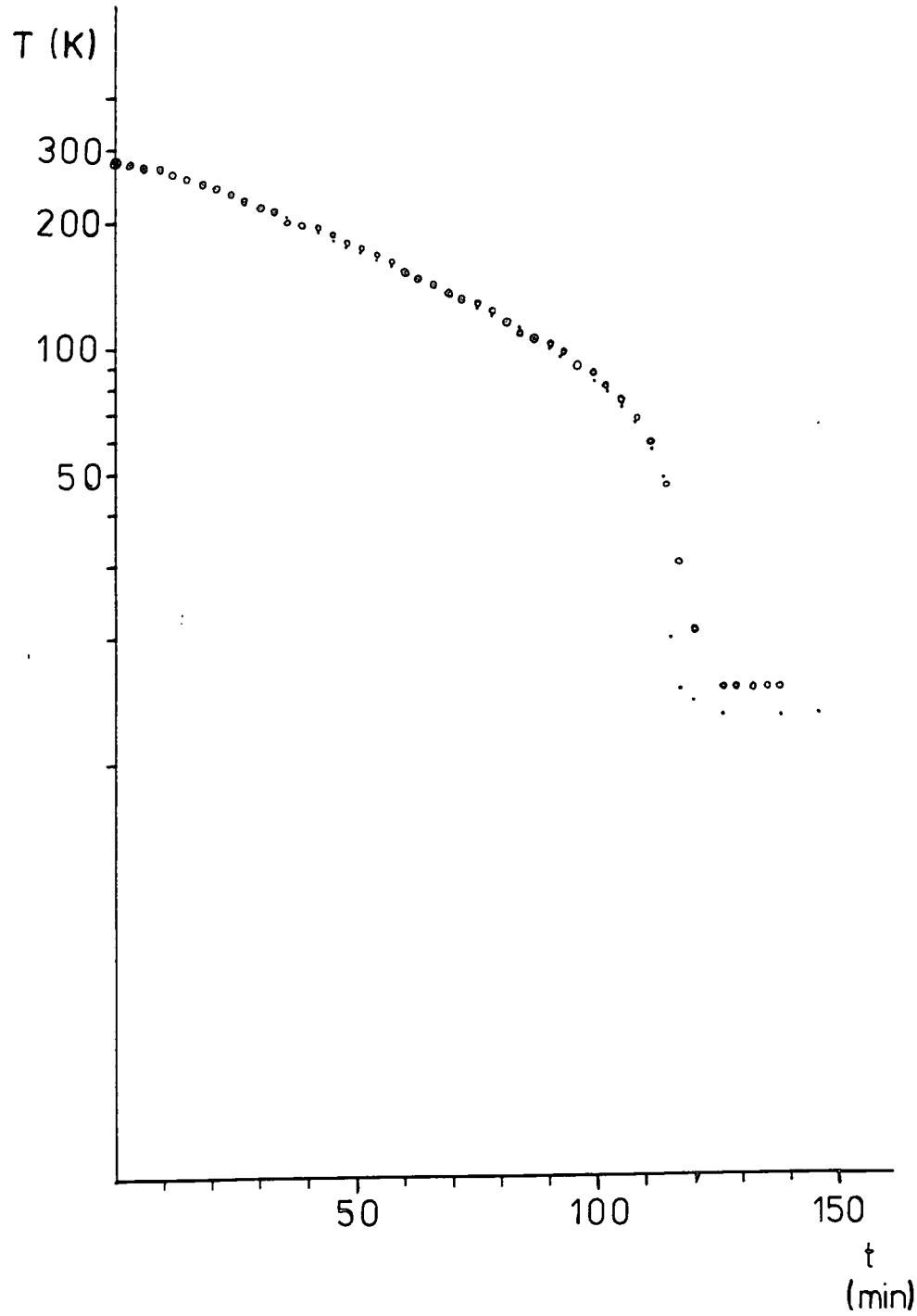

Fig (6-14) Typical cooling plot of Temperature vs. Time obtained with the present NMR-cryogenic configuration.

to be mentioned. In the case of power failure on both the vacuum system and the Displex unit the following course of action needs to be taken. First, isolate the expander from the rest of the vacuum system by closing the appropriate isolation valve. Second, the HV isolation valve of the diffusion pump is closed, and then the combined valve is set to its middle position and then the admission valve is opened fully. This will ensure that the cryogenic system will come back to room temperature at a steady rate, preventing any damage to the sapphire and quartz glass protection due to a very rapid increase in temperature when the admission valve is open at the vacuum pumps. The test has shown that the cryogenic system is capable of producing 16 K even with the large load presented by the copper rod.

The versatility of the system has been demonstrated going from one experiment to another or from one sample to another, reducing the time between sample depositions.

6.5 SAMPLE PREPARATION AND DEPOSITION

The way in which both gaseous samples at low pressure and liquid samples are prepared and handled will be described in this section.

All samples were used without extra purification, and liquid samples were degassed by the freeze-pump-thaw method before being used for deposition. After degassing, between 0.1 and 0.3 ml of liquid samples are introduced into one or more glass tubes 120 mm long, 20 mm diameter, and immediately

submerged in liquid nitrogen. Then they are connected to the small matrix system vacuum line which in turn is attached to another conventional vacuum line. With the glass tube still immersed in the nitrogen bath and all the valves open, the whole assembly is vacuumed down for about half an hour. Then the necessary valves are closed and the assembly disconnected from the normal vacuum line.

In the case of pure gas samples, a round bottomed flask of 3 litres capacity is connected to both the conventional vacuum line and a high-pressure gas cylinder containing the sample of interest. The flask is properly evacuated for an hour. After this period the pump is isolated from the vacuum line and one atmosphere of gas pressure is introduced to the flask. The flask isolation valve is then closed and the sample is transferred to the NMR-Cryogenic system for deposition. In the case of a dilute gas mixture, a procedure similar to the one above is used. For gaseous samples, the necessary small amount of sample is introduced into the flask and its isolation valve is closed. Then the matrix gas is connected to the vacuum line and the flask is filled to give a final pressure of one atmosphere. If further dilution is needed, a second flask (properly evacuated) is connected to the line, and the necessary amount of sample is transferred from one to the other, the pressure then being brought back to one atmosphere by further addition of matrix gas. Liquid sample are allowed to evaporate into the vacuum line to the required pressure, and then the procedure used for gas samples is repeated

Once the samples are ready to be used for deposition,

procedures have been established for the appropriate use of the matrix system.

A) **First, sample deposition:** when a new sample is going to be attached to the system it is important to first isolate the diffusion pump. This is achieved by closing the HV isolation valve. The combined valve is set to roughing and the sample holder is connected to the system. Next, the valve at the sample connection is opened and the system is evacuated with the rotary pump only. This is continued until the Penning gauge reads 10^{-3} mbar and the Pirani gauge reads 10^{-2} mbar. At this point the combined valve is set to backing and the HV isolation valve is opened to the line. Now it is necessary to wait until the system is at its optimum vacuum (see above section) before starting the deposition. The whole process of incorporating a new sample does not take longer than a couple of hours. This is a considerably shorter time than for other cryogenic NMR systems. The system is now ready for activation of the Displex unit.

B) **Subsequent depositions:** If all experiments have been carried out on a previously deposited sample, it is necessary to follow a similar sequence of steps to the one described above to eliminate the sample from the system. First, the Displex unit is turned off. This is followed by closing the HV isolation valve and turning off the diffusion pump. Then, the combined valve is set to roughing and the sample is allowed to evaporate. It has to be remembered that the nitrogen trap must be full of nitrogen during this procedure. When the system has reached room temperature, the diffusion pump is turned back on, following the procedure already

described, and put on line. After this, it will not be long before the system is pumped down to the required pressure.

It is clearly shown that the system has a considerable degree of flexibility once the difficulties of assembly have been overcome. It is also apparent that it is easy to change from one sample to the next with a saving of a considerable amount of time. It could be said that this is the most important feature of the design, taking a considerable amount of time to develop, test and to finally get into a satisfactory working order.

6.6 SPECTROMETER DESCRIPTION AND DATA ACQUISITION

The spectrometer system used for the study of matrix-isolated materials was a non-commercial type, designed and built at Durham University[4]. It has been configured to operate for the observation of proton resonances at 60 MHz. As mentioned, the magnet used for the cryogenic work is a Varian XL-100 with the magnetic field adjusted to operate at the above frequency. In fact, it is also possible to observe fluorine signals with a small adjustment of the field . This has a great advantage when looking at samples with both nuclei present in them.

The spectrometer console consist of a mixture of very efficient home-made as well as commercial components. Two computer systems are used for the control of the spectrometer. The first is an Archimedes computer used to produce the necessary pulse sequences in a high-level language form of

command, i.e. Basic. It is also used to store the final FID as well as to perform the Fourier transformation, phasing and plotting of the data. It has a special use in the analysis of T_1 and $T_{1\rho}$ data.

The second is a BBC computer which receives the set of information about a particular experiment from the above computer and sends it to the pulse programmer. During the execution of the experiment(s) the BBC computer takes control of the whole acquisition process, leaving the Archimedes free to do all the data manipulation. There is no real limitation on the number of steps in the pulse sequences.

The pulse programmer has four channels, so there is the possibility of performing phase cycling, giving flexibility when designing pulse sequences. It is also possible to perform quadrature phase detection. The pulses are fed to a four-channel modulator and its output is then sent to the high-power amplifier unit. This is a Bruker amplifier also capable of producing soft pulses. Signals from the probe are picked up by the pre-amplifier and then sent to the signal receiver, both of which are home built. The signal is digitized by the acquisition unit and accumulated in the BBC computer. At the end of the experiment the data is sent back to the Archimedes computer. An schematic diagram of the spectrometer configuration is presented in Fig (6-15).

Magnetic field stability is achieved using an external lock device. This external lock unit uses a small probe attached at the back of the main probe. This probe contains a solution of water and some amount of cupric nitrate to reduce the relaxation time. The proton signal obtained from this

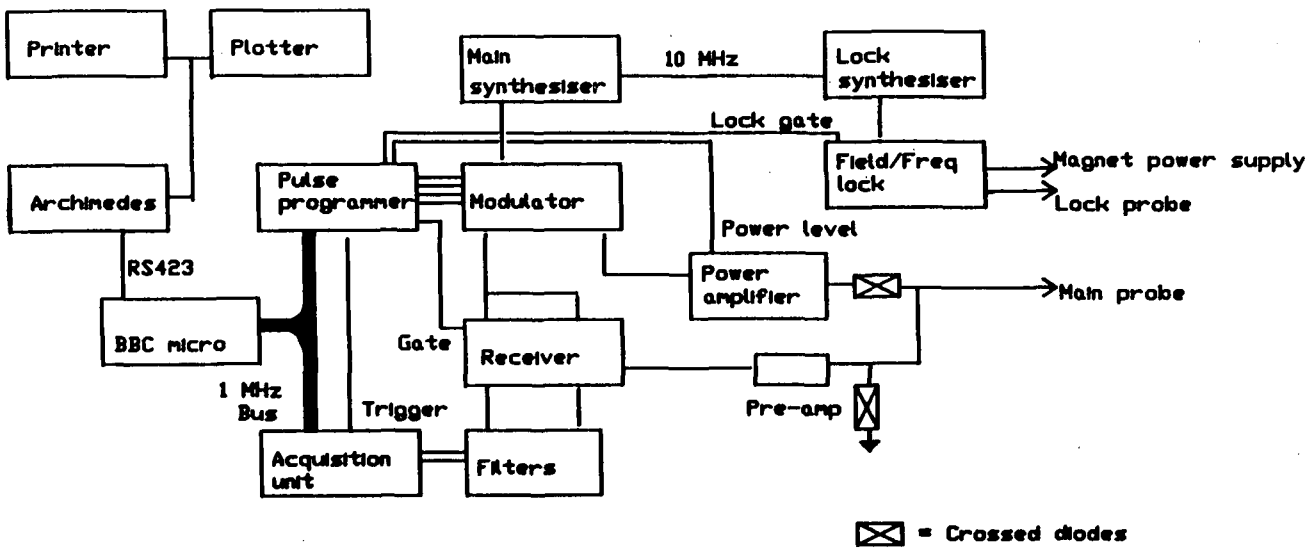

Fig (6-15) Diagramatic representation of teh spectrometer system.

probe is 4600 Hz off-resonance from the main probe signals. The FID is detected by the main lock unit, and this information is used to drive the flux stabiliser of the magnet. When observing fluorine, a sample containing this nucleus will replace the one described above.

The system has proved to be very reliable in its operation, very user-friendly and it is easy to design pulse sequences. There is no problem regarding the speed of data processing for Fourier transformation or relaxation analysis. Fourier transformation of a 4048 data-point FID takes 40 sec.

REFERENCES:

1- Technical Manual for Displex Closed-Cycle refrigeration system: Models CSA-20-2, CSW-202 and HV-202. Air Products and Chemicals, Inc. APD-Cryogenics, 1919 Vultee Street, Allentown, Pennsylvania 18103, USA.

2- Rotary vacuum pumps. Models E2M2,E1M5/E2M5, E1M8/E2M8. Installation and operating instructions. Edwards High Vacuum International. Manor Royal, Crawley, West Sussex RH10 2LW, England.

3- Series 500 vacuum measurement and control instruments. CP25 Penning gauge head. Edwards High Vacuum International. Manor Royal, Crawley, West Sussex RH10 2LW, England.

4- Harris R. K, Kenwright A. M., Royston A., Barry J. S., to be publish.

CHAPTER 7

MATRIX ISOLATION APPLICATIONS:

PROTON NMR STUDIES

7.1 INTRODUCTION

The present chapter will be dedicated to presenting the first experimental results obtained from the new spectrometer design, described in chapter 6, for the study of matrix isolated material by means of NMR.

It will include the description of the spectrometer experimental conditions like setting the homogeneity of the external magnetic field B_o, the proper set up of the resonance frequency and frequency lock, and the running of pulse sequences for the particular experiments.

It is very important to have an accurate knowledge of the real temperature of the sample to be studied. In the system here presented, this is especially so due to the fact that there is a temperature gradient between the location of the thermocouple and the actual location of the sample. This is because of the presence of the copper rod between the Displex unit and the sapphire cold finger where the sample is deposited. So, a description of how the sample temperature was measured is also presented.

Finally, two types of molecule were studied by matrix isolation. They were dichloromethene (CH_2Cl_2) and ethylene (C_2H_4) respectively. Their study also included some work with the samples in pure form, i.e. without dilution inside a matrix. These samples were studied under different conditions of matrix dilution and deposition rate. In the first instance, the work was concentrated on obtaining structural information, i.e. proton-proton distances, and comparing these results with those of the literature.

7.2 SPECTROMETER EXPERIMENTAL CONDITIONS

7.2.1 MAGNETIC FIELD HOMOGENEITY

Static line shapes from ^{1}H signals in pure samples can be as wide as 60 kHz depending on the strength of the dipolar interaction. But as already mentioned, it is expected that a significant reduction in the line broadening from matrix isolated species will be observed, and a better resolution of the transition lines will be obtained. So, it is important to reduce external broadening effects on the NMR signal of this type of sample. One of these external effects is the homogeneity of the external magnetic field B_o.

For the particular configuration used in the matrix isolation, it is necessary to set the static magnetic field homogeneity to its optimum value under the normal working conditions. These working conditions involved the presence of large pieces of metal (like the Displex unit and copper rod), probe configuration (including frequency lock probe, see Fig (6.12) in previous chapter), and expected shape and location of the sample. As many of these elements as possible need to be present during the period of homogeneity adjustment.

Silicone gum was chosen as the sample to be used for the setting up of the field homogeneity. It was shaped to the expected form of the deposited sample, i.e. in a drop like shape, at the end of a 3 mm glass rod. It was allowed to dry inside a desiccator under dynamic vacuum. After the probe has been assembled (as shown in Fig (6.8)), it was placed in the magnet gap in such a way as to have the RF coil as close as possible to the centre of the poles. This position was

determined to be 875 mm horizontally and 675 mm vertically. The silicone gum sample was introduced inside the probe and the Displex unit was positioned as close as possible to its final location during normal operation. The spectrometer was set to tune mode and the pulse program LFID (for long FID acquisition) was used during this operation (see spectrometer operating procedure in appendix A for more details). The fine setting of the resonance condition can be achieved by either changing the frequency of the main reference frequency synthesizer or by changing the frequency of the field lock unit. With the main reference frequency set at 60.00 MHz, the magnetic field was swept until the silicone gum resonance frequencies was observed on the monitor. At this point, the frequency lock unit was activated and the silicone gum signal was set off-resonance by changing the resonance frequency of the lock unit, to observe several oscillations in the full FID. The shimming of the magnet was performed under this condition until the narrowest line was obtained from this sample. The resulting resonance line obtained from the silicone gum sample is presented in Fig (7.1). The line-width of this signal was calculated to be 234 Hz, a very acceptable value under these conditions. This value gives enough confidence that there will not be instrumental line-broading influencing the signal observed from the matrix isolated material.

At this point, the silicone gum resonance was set back to the resonance condition by changing the frequency of the field lock probe. This gave a value of 29.99910 MHz. The value of 60.00 MHz for the main reference synthesizer and the above

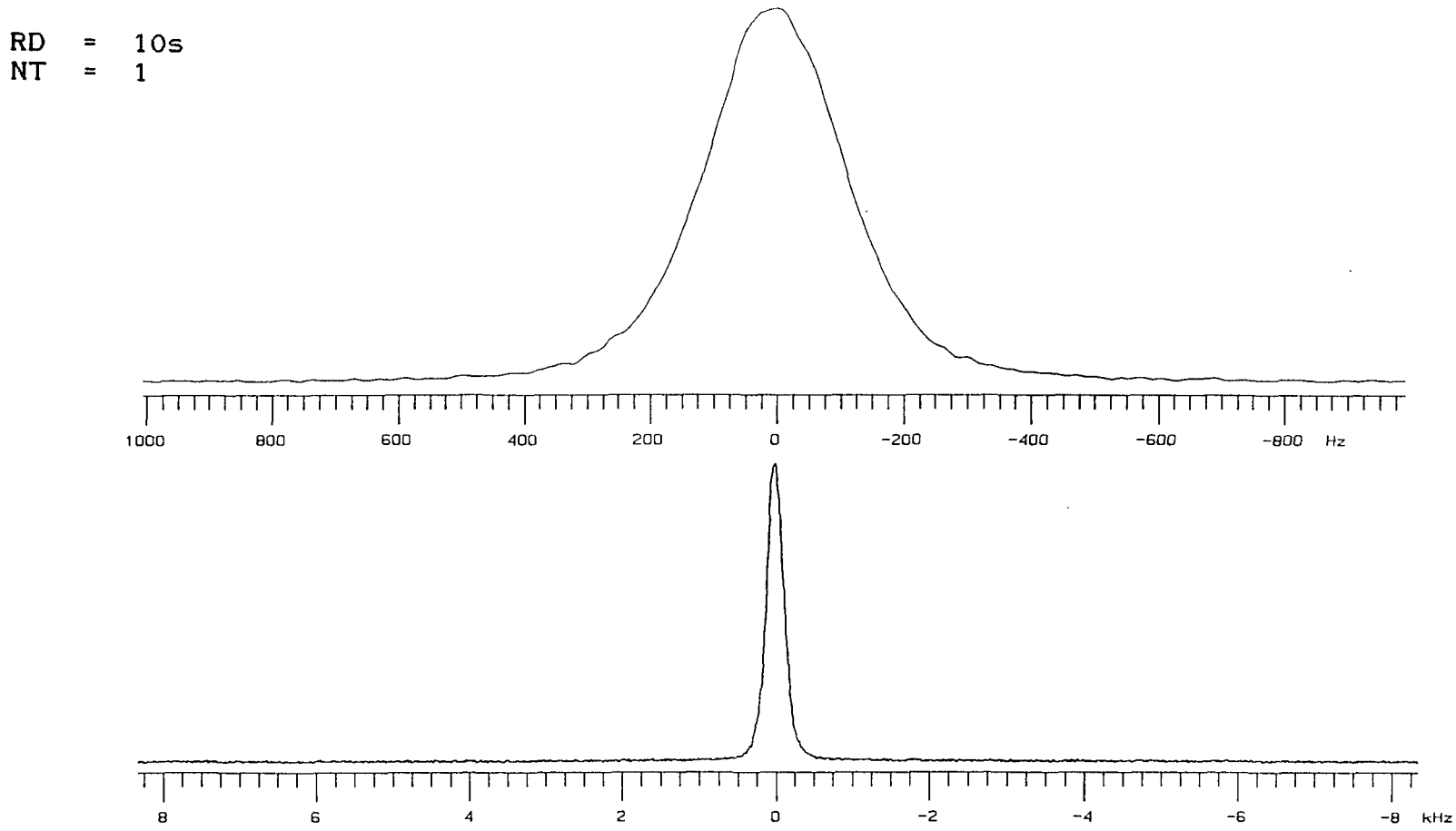

Fig (7-1) ^{1}H SP Spectrum of silicone gum: best shimming.

frequency for the lock unit are the ones to be used in the day to day running of the spectrometer. This completed the procedure of setting the field homogeneity.

7.2.2 PULSE SEQUENCES

The pulse sequences used within this system can be divided into two types. Those used to set the experimental conditions and those used to perform the actual experiments. The main difference between these two types is the fact that for the first one performs the pulse sequence, waits the recycle time and before executing the sequence again the memory is cleared, i.e. their is no accumulation of transients between acquisitions. Signal averaging is performed with the second type of pulse sequence.

The first type of sequence is very useful when selecting the optimum conditions of experiments like single pulse or echo sequences. It is easy to set the 90° pulse by determining the 180° pulse; it also helps in determining the dead time of the probe. In the case of the echo sequence, it helps to set the best tau, τ, value between the two pulses; the top of the induced echo is also determined which is very important for the start of the acquisition time in this pulse sequence. This type of pulse sequence can only be used from the tuning mode of the spectrometer operating system (see appendix A). It also proves invaluable during pure sample or matrix deposition. It was set to run during the deposition period helping to determine if any sample have been collected

at the sapphire. It was also possible to estimate the strength of the signal so that matrix dilution could be checked for suitability.

As far as the second type of sequences is concerned, four pulse sequences were used to obtained data from the different samples presented in this work.

A: SINGLE PULSE: As already described in chapter 2, this is the simplest type of pulse sequence. In this case, it was used to get the initial information about the observed signal. Data like total acquisition time needed, frequency spread of the resonance line, resonance condition, are the types of parameters selected with this pulse sequence.

B: SOLID ECHO: NMR signals from static solid samples are invariably very broad and with very short T_2 values. So, it is important to obtain as much information as possible from the initial part of the FID decay. This is very critical in the case of the dipolar interaction in strongly coupled spin systems. This is often very difficult due to restrictions imposed by the dead time of the probe. The solid echo pulse sequence[1,2] has been used to overcome this experimental difficulty. In this way it was possible to obtain reliable information about signal intensity and lineshape. This pulse sequence consisted of two 90° pulses, the second being 90° out of phase with respect to the first. The tau, τ,values separating the pulses are of the order of the dead time. Detection will start at the top of the formed echo at 2τ. A schematic representation of this sequences is presented in Fig (7.2a).

C: SATURATION RECOVERY: This pulse sequence was used for the measurement of T_1 values from the different samples studied. The values obtained in this way were used to calculate the appropriate recycle time for the above two sequences. The recycle time was made $5*T_1$ which will prevent any signal saturation. The sequence consisted of a saturation stage composed of 100 90° pulses separated by a 1 ms dephasing period. These are followed by a variable τ interval. The signal is detected with the aid of a solid echo sequence as described above. As the intensity is the only information needed, single point acquisition is used in this method, i.e. the top of the echo signal. In this way, it is possible to collect 1024 data points of intensity only using the same amount of disk space as for only one spectrum. The sequence is presented in Fig (7.2b).

D: T_1 INVERSION RECOVERY[3]: This pulse sequence was not used for the determination of the T_1 values. With the knowledge already gained with the saturation recovery method, the inversion recovery was used to observed the recovery of the entire resonance lineshape from the studied sample as the value of τ is changed. In this way, it is possible to determine if different parts of the resonance lineshape relax to equilibrium at different rates. The pulse sequence consists of a 180°_x followed by a τ delay time which is then followed by a 90°_x pulse. The signal is acquired after a solid echo sequence, so that the true lineshape can be observed. The pulse sequence is presented in Fig (7.2c).

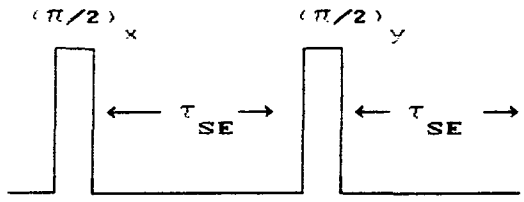

a) Solid Echo sequence

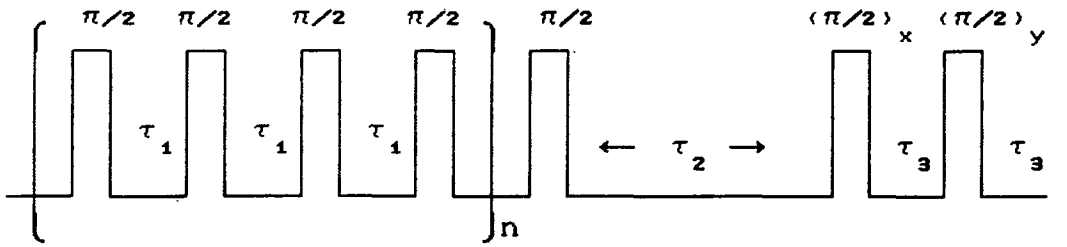

τ_1 = Dephasing delay

τ_2 = Relaxation delay

τ_3 = Solid echo delay

b) T_1 Saturation recovery single pulse acquisition

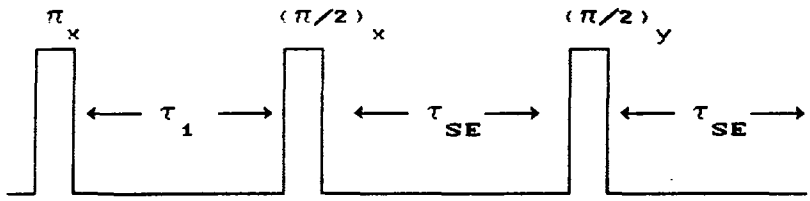

τ_1 = relaxation delay

c) T_1 Invertion recovery with solid echo acquisition

Fig (7.2) Schematic diagram of the different pulse sequencies used in this investigation.

7.2.3 SIGNAL INTENSITY AND LINE-SHAPE DISTORTIONS

In matrix isolation it is very important to detect as much signal intensity as possible from the deposited sample. It is also very important to guarantee that the frequency spectrum obtained after Fourier transformation is a reasonable representation of the true line-shape expected from the studied molecular system. This can only be done when the appropriate pulse sequence is being used.

As far as intensity is concerned, the solid echo sequence has already been mentioned as one way of obtaining the maximum signal intensity in comparison with the single pulse one. This can also be combined with a short probe dead time; the shorter the time between the two pulses the greater the intensity obtained from the observed echo. For the present study, the improvement in intensity was estimated to be between 20 to 25%. This is very welcome in matrix isolation where dilution can be 100:1 or higher. The detection of a strong signal will also help in reducing the total experimental time.

In investigating proton-proton dipolar interactions the interest is focussed on the separation of the lines in the Pake doublet[4] powder pattern. So, it is important to get a good representation of the line-shape from the observed sample. Again, the single pulse sequence is not suitable to obtain this type of information; very important information is lost during the dead time and in the present system this time can be as low as 15 μs.

As with the intensity, the solid echo experiment[5] is the

solution to obtain the most accurate line-shape information. This fact can easily be seen from Fig (7.3) where the line-shape from CH_2Cl_2 using the solid echo sequence is compared with that obtained using the single pulse one. The amount of distortion produced in the line-shape is obvious when the signal is detected with the SP sequence because it is impossible to record the beginning of the FID due to the dead time. The information obtained from the single pulse sequence can not be used to get an estimate of the line separation yet alone to be used in line fitting calculations. It is also shown in the figure that it is possible to transforme the solid echo line-shape into the single pulse with a succession of left shifts to FID before FT. These shifts are equal to the dwell time, and in this case they were of 1 μs. A total of eight shifts were needed to produce the change. The spectra were plotted in absolute intensity mode. This shows the effects of intensity loss from the single pulse in comparison with the one obtained when using the solid echo pulse sequence.

7.3 DETERMINATION OF SAMPLE TEMPERATURE

In chapter 5 (5.3.1) the effects that different temperatures regimes could have on the behaviour of the condensed matrix has been described, in particular to the motions of the isolated molecules inside the matrix and the possibility of forming aggregation and polymerization if the temperature is not kept within $0.3T_m^{\circ}$. This is even more

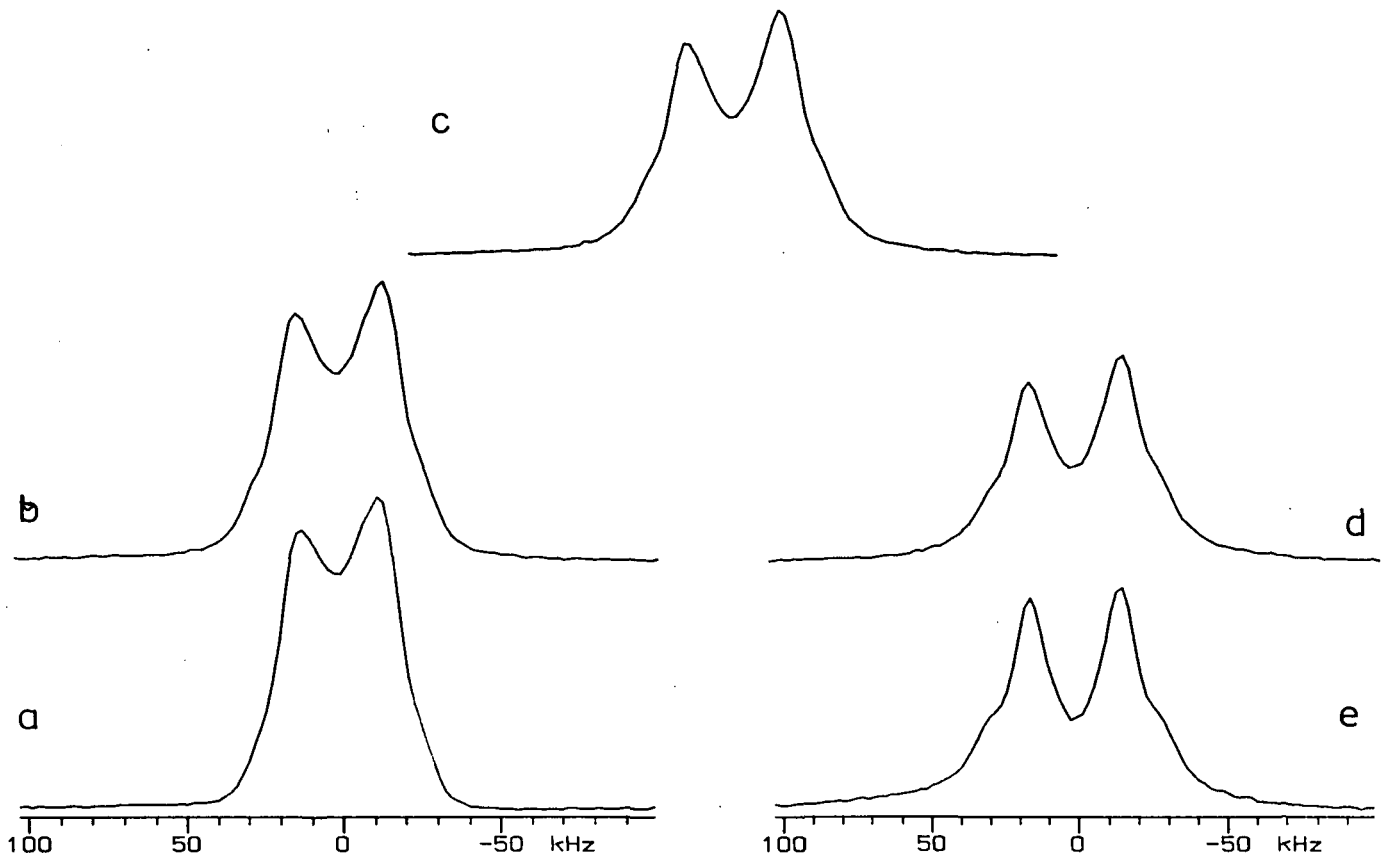

Fig (7-3) Typical lineshapes from a deposited sample of pure CH_2Cl_2 obtained using a solid-echo pulse sequence (a) and with a single pulse sequence (e). Spectra b, c and d were derived from left shifts to the SE (2 dwell times for b, 4 for c and 6 for d) before Fourier transformation.

important when rere gases are used as matrix material. For the particular case of this work, argon was selected as such material; the value of $0.3T_m$ is 25 K in this cases. So, it is very important to determine the temperature of the sample as accurately as possible.

In systems like the ones used by White[7,8] et al. or Zilm[9] et al. this determination has been achieved by locating a thermocouple directly in the sample holder or in the stream of cryogenic gases that pass through the sample.

The micro-refrigerator selected for this work can produce temperatures as low as 16 K (see Fig (**6-14**)). As indicated before, the magnet and probe configuration do not allow have the end of the Displex to get inside the magnet poles and near to the RF coil where the sample will be located. So, a copper rod had to be attached the end of the Displex to transfer the cryogenic temperature down to the sample area. It is obvious that this arrangement will introduce a temperature gradient between the minimum temperature produced by the Displex and the actual sample temperature. In practice, it is not possible to place the thermocouple near the sample area due to the difficulties that it will introduce during the assembly of the system. So, its location is at the end of Displex unit, i.e. in the joint between the coldest part of the Displex and the copper rod (see D in Fig (**6-14**)). A second measuring device is located in the same area, this being a hydrogen bulb thermometer which has an effective range between 14 and 25 K.

It was found that the practical use of the NMR-Cryogenic system produced a degrading factor in the thermocouple. Whereas at the beginning of the tests of the system both

thermometers were reading the same temperature, i.e 16 K (see Fig 6-14 in section 6.4.2 of this thesis). At the time of performing the final experiments for the temperature determination of the sample, the difference between the two was 9 K. This degradation is thought to be caused by the heating resistor needed to increase the temperature of the Displex and therefore that of the sample. This introduced an additional problem to be considered in this determination.

Grant and co-workers[10] have indicated that the temperature difference between the thermocouple and the sample is of the order of 6 to 8 K. This was determined by measuring the temperature when a particular sample evaporated with and without the presence of the copper rod.

An alternative method is proposed in this work, where the actual NMR technique is used to accurately measure the temperature of the sample. The total magnetization of an ensemble of nuclear spins under the influence of a strong magnetic field has an exponential dependence on inverse temperature[11]. With this in mind, two assumptions have been made in this determination of the sample temperature. For the case of I=1/2, the population difference between the two energy levels can be written as

$$n_{\alpha}-n_{\beta}=\Delta n \cong \frac{1}{1+\exp(-\Delta E/kT)} - \frac{1}{1+\exp(\Delta E/kT)} \qquad 7.1$$

$$\text{where} \Delta E = \gamma\hbar B_{o}$$

In the high temperature regime, where $kT \gg \gamma\hbar B_{o}$, a linear relationship is found between Δn, and therefore the total

observed intensity, and the inverse of the sample temperature[12], i.e.

$$M_o \propto \Delta n \propto \frac{\Delta E}{2kT} \qquad 7.2$$

Calculations performed using the two equations presented above, for the present case where B_o = 1.41 T, indicated that the magnetization should be proportional to T^{-1} to better than 1% for all temperatures above 1 K. The second assumption involves the degradation of the thermocouple. It was assumed that this effect and the temperature gradient of the sample with respect to the measuring device are approximately independent of temperature within the range covered by the experiments.

Under these conditions, the proposed method consists of depositing a controlled amount of sample and then measuring the NMR signal intensity obtained from it as a function of the temperature measured by the thermocouple. A plot of the intensity versus T^{-1} should give a straight line . A linear least-squares fit, constrained to pass through zero will be applied to the data and by adjusting the measured temperature by a constant amount it will be possible to minimize the differences between the experimental data and the fitted line as shown by the value of the correlation coefficient, τ. In this way, the lowest temperature point corrected, corresponding to the highest intensity from the sample, will be the actual sample temperature.

The sample selected for this determination was CH_2Cl_2

which comes in liquid form. Two 0.1 ml volumes were placed in separate glass tubes, attached to the small vacuum line and then degassed as described in section 6.4. They were transferred to the NMR-Cryogenic system and deposited onto the sapphire surface ensuring that the temperature did not rise more than 1 K during the sample condensation. The final temperature of the system was 25 K as measured by the thermocouple and it was not different from that prior to the deposition. It has to be indicated that the expected temperature of the thermocouple was 16 K as given by the hydrogen bulb thermometer.

After each deposition the spin-lattice relaxation time, T_1, was measured so that the appropriate value for the recycle time used in the solid echo experiment could be estimated. After total deposition, the temperature of the sample was changed with the help of the heating resistor and monitored with the thermocouple over a range between 25 to 126 K with a total of 24 temperatures. At each temperature the T_1 was measured and the signal intensity from the sample was also obtained for each temperature using the solid echo experiment. A plot of signal intensity versus T^{-1} is presented in Fig (7.4(a)) which also shows the initial linear least-squares on this data (fixed to pass through zero). The value of 0.99769 was obtained for the correlation coefficient under these conditions. It is clear from the plot that the first four points do not follow the linear correlation. These values were omitted from the fitting giving an improved value for τ= 0.99949. At this point, each temperature was corrected by a fix amount, ΔT, and this was followed by a least-square

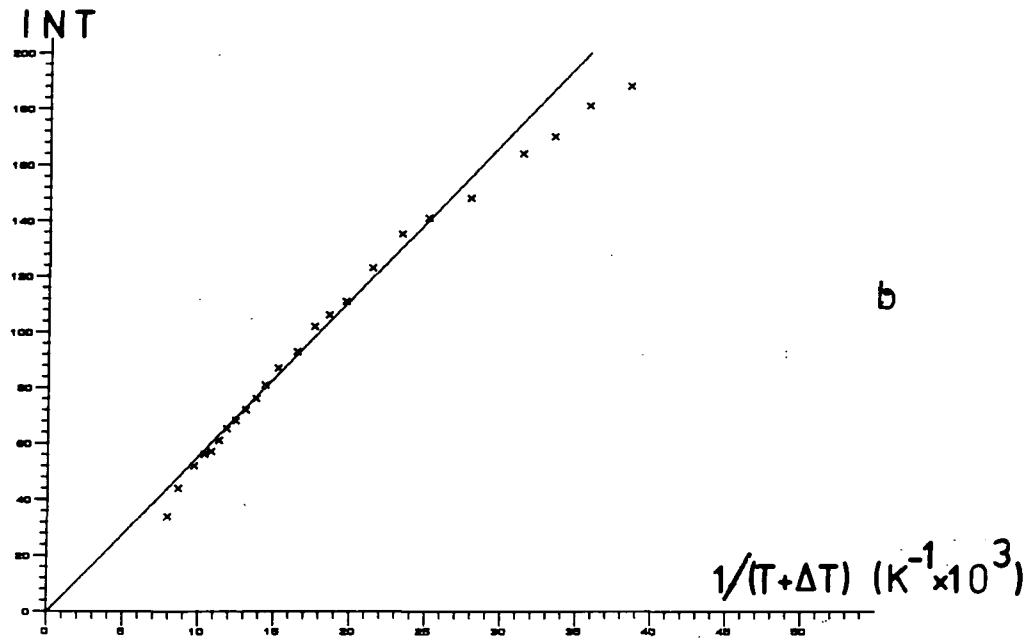

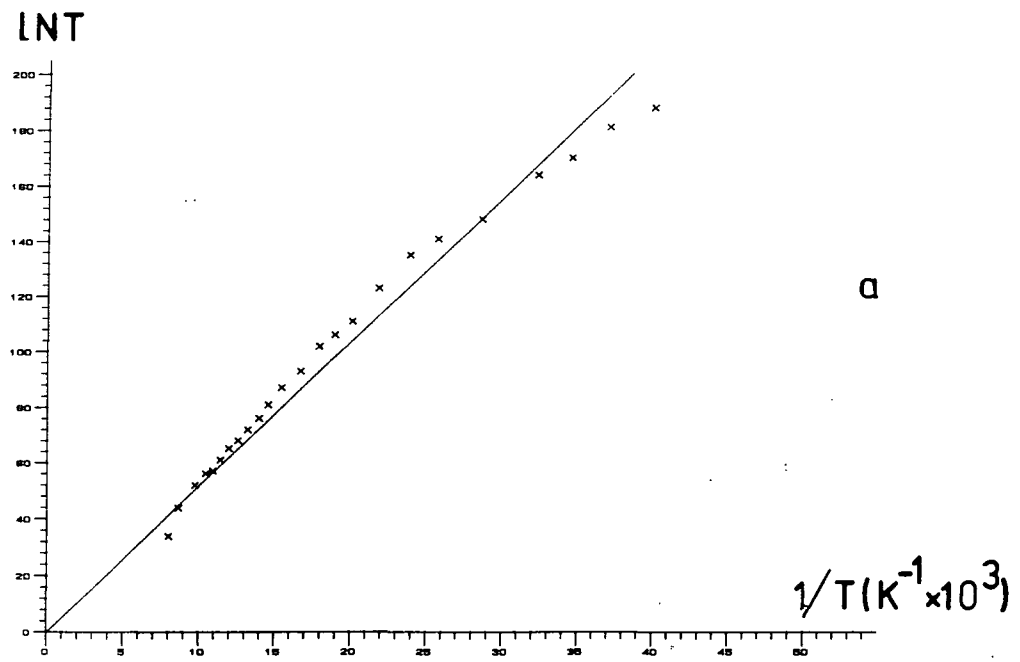

Fig (7-4) Linear least-squares fit of signal intensity vs. 1/T(K); (a) original data, (b) Best linear least-square fit after temperature correction.

fit of the new data taking note of the value of τ each time. A plot of τ versus ΔT gives a smooth curve with a minimum of 0.99951 at a value $\Delta t = +1$ K (see Fig (7.5(a)). The corresponding least-square fit of the plot Int vs T^{-1} for this value of τ is presented in Fig (7.4(b)). This result indicates that there is one degree difference between the sample temperature and that measured by the thermocouple. As indicated previously, the apparent error in the thermocouple reading is of 9 K which appears to make the sample temperature be at 26 K at the lowest temperature. This result seems to be in good agreement with the one already reported[10].

As far as the four initial points are concerned, there should not be any deviation from the linear correlation in this temperature region as has already been indicated. All precautions were taken to avoid or minimize the amount of bounce-off during deposition by carrying out this process at a very slow rate and by constant monitoring the pressure measuring devices and the temperature measuring devices which will indicate loss of sample and heating up of the deposition area, i.e. the sapphire.

In these conditions, the total measured intensity after the two depositions was only 146% of the one obtained after the first deposition. It is difficult to explain the big difference between the first and second depositions just on the grounds of sample loss. So, it appears that other factors than loss of sample during the period of deposition are responsible for the low initial intensity points. This comes from the fact that if the first measured intensity at the sample temperature of 26 K is corrected so that it will fall

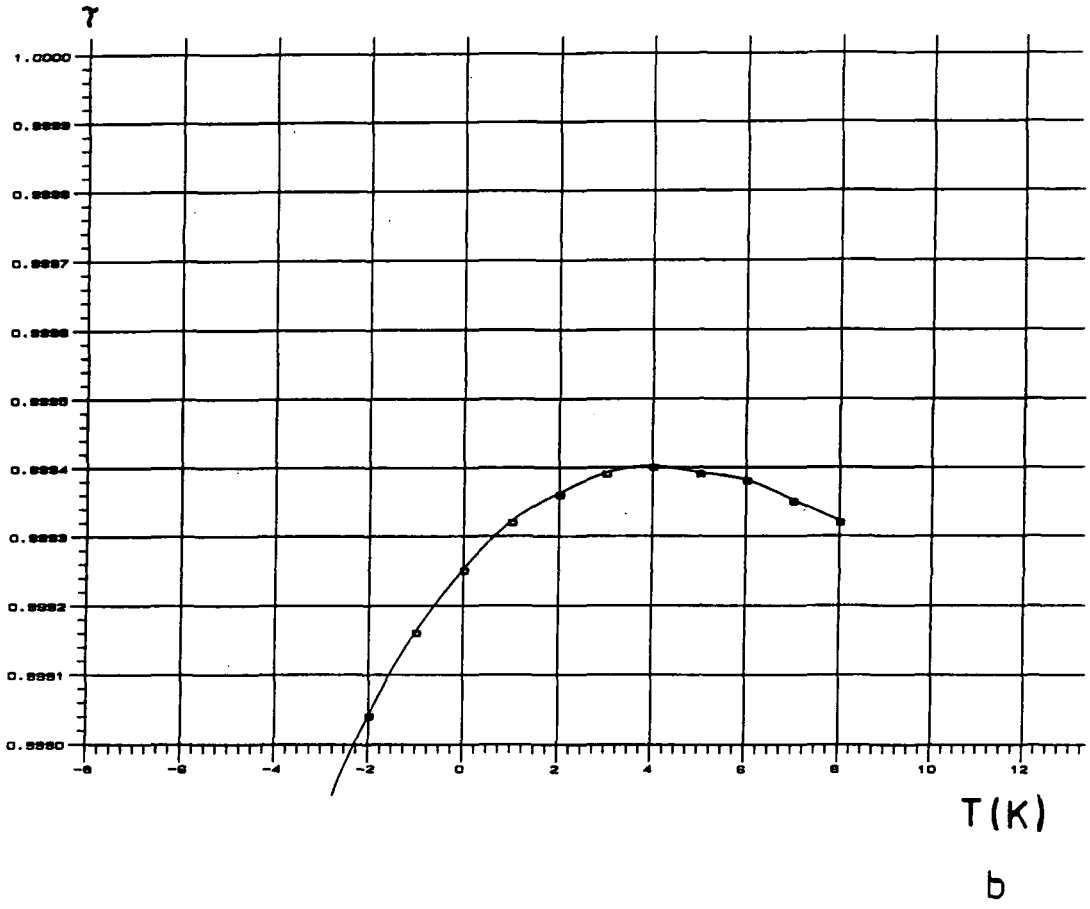

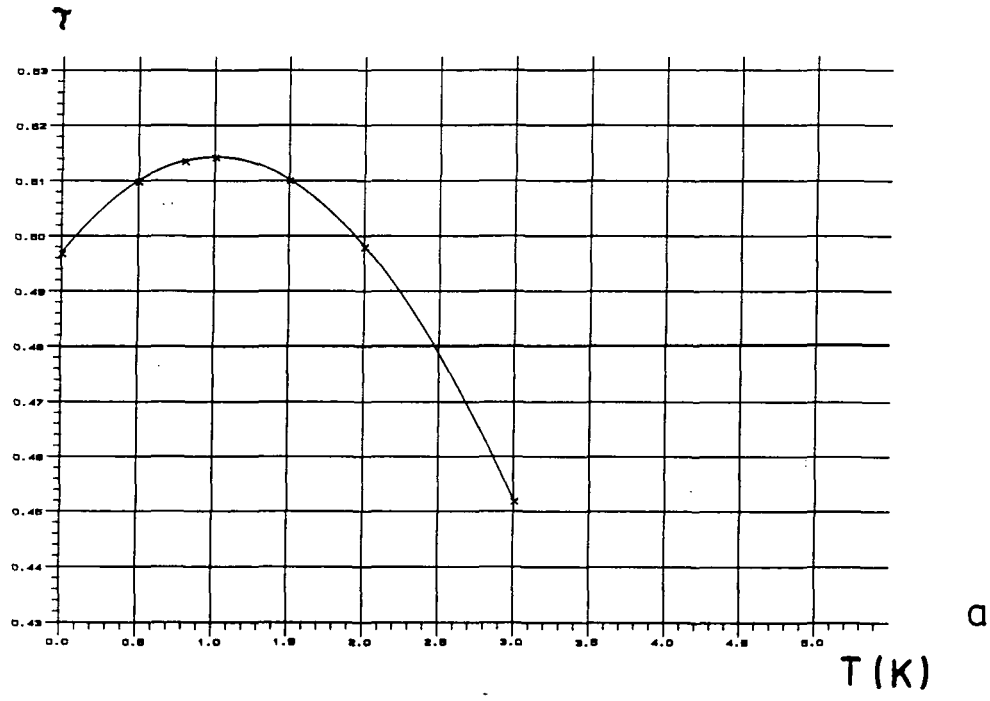

Fig (7-5a) Plot of correlation coefficient (τ) vs. ΔT.;
(a) from data in Fig (7-4a); ΔT = 1K, sample temperature 26K;
(b) from data in Fig (7-6a); ΔT = 4K, sample temperature 26K.

within the line of the fit, the total amount of deposited material will be of 162%, a value closer to the one expected from preliminary data. These data will be presented later in this section. Some of the factors that could contribute to this loss of intensity are: i) a non-linearity of the receiver in one of the amplification stages, or ii) an undetected saturation of the signal arising from an over-short recycle delay in the solid echo experiment.

As previously indicated, data obtained prior to the above final results were also treated with this method. In the first case about 2 ml of CH_2Cl_2 was placed inside the glass tube and prepared for deposition as in the above case. The sample was deposited on the sapphire surface at a very slow rate. This process was stopped by visually inspection to confirm that enough sample has been deposited. This can also be done by observing the actual NMR signal during deposition. It took 3 hrs. for the condensation to be completed. The initial and final temperature of the system was 22 K as given by the thermocouple. As before, the hydrogen thermometer gave a temperature of 16 K.

The temperature range was between 22 to 40 K in this case with only 9 data points. It can be seen that the apparent error in the thermocouple measurement is 6 K in comparison to that given by the previous temperature determination. T_1 measurements were also carried out for the determination of the recycle time. The plot of intensity vs. 1/T is given in Fig (7.6a). As before, if the first two points are included in the fit the value of τ is poor and equal to 0.99748. So, they were also excluded from the calculation. The

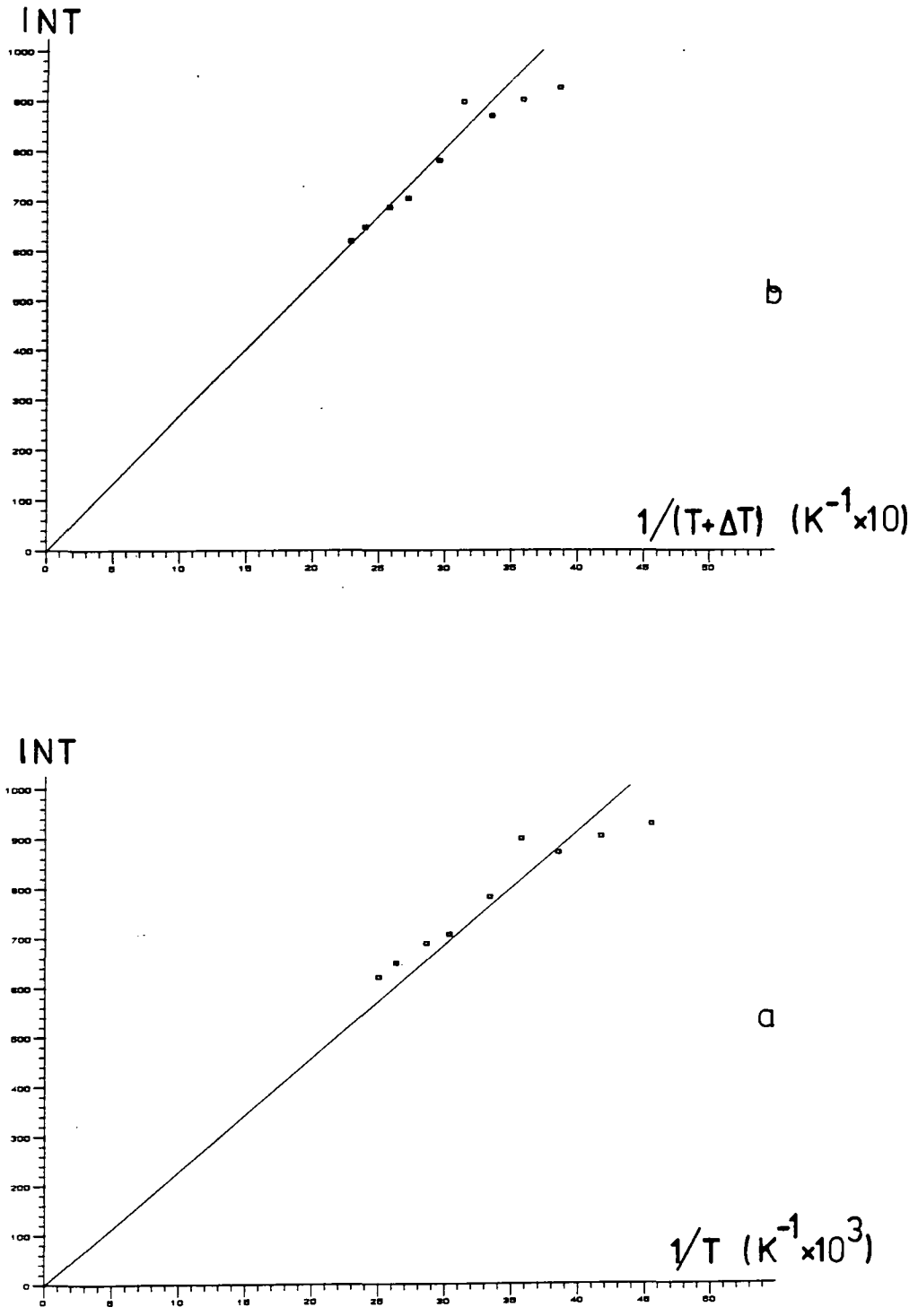

Fig (7-6) Linear least-square fit of signal intensity vs. $^{1}/T(K^{-1})$; (a) original data, (b) Best linear least-square fit after temperature correction.

determination of the Δt from the best fit of the data was done and the plot of τ vs. ΔT is also presented in Fig (7.5b). The value for Δt was equal to +4 K for the best fit. The plot of intensity vs. 1/T in this case is shown in Fig (7.6b). Under the same assumptions as in the first case, this determination gives a sample temperature of 26 K at the coldest point, a repeat of the first.

Two important conclusions can be deduced from these results. The first conclusion is related to the actual obtained temperature. The sample temperature can be reproduced with accuracy even though the apparent error in the temperature given by the thermocouple is less than in the previous case. The second conclusion comes from the actual sample. First, it was mentioned that all the deposit came from one liquid sample. So, sample loss was not really important because the amount of deposited sample was determined visually. Therefore, the deviation from linearity of the first two points in this case seems to confirm that most of the problem of detecting the right intensity signal comes from the spectrometer detection system. Finally, the most interesting and probably important conclusion is that the determination of the sample temperature can be done independently of the amount of sample deposited. It can easily be applied to determine the temperature of matrices. In these cases it is not necessary to go over a very wide temperature range as indicated in the last example. This has to be emphasized because the acquisition of the experimental data can be very time consuming depending on the range of T_1 for the particular system. For example, the data from the

first determination took 4 days to be obtained. The presence of a micro-refrigeration unit is a very important factor for the completion of this type of experiment because there is no time limit or complication in maintaining the right temperature.

The last sample treated in this way will show a result very different to the one obtained above. In this case three CH_2Cl_2 samples of 0.1 ml in volume were used in the determination. Conditions for the deposition were the same as the one described before for the first determination. The temperature range covered was between 25 and 48 K as indicated by the thermocouple with a total of 10 data points. Again, the apparent error in the thermocouple reading was in the order of 9 K. After the deposition of the first two samples the total intensity obtained from the solid echo experiment was 166% in relation to first deposition, in comparison with 146% obtained from the first temperature determination. This result supports the predicted initial intensity of 162% obtained from extrapolating that point to the best fitted least-square fit in the first temperature determination presented in this section. After three depositions the total intensity obtained was 237% in relation to the first one, and 210% in relation to the second one discarding the intensity of the first deposition. A plot of the solid echo signals obtained after each deposition is presented in Fig (7.7) with intensity related to the first deposition signal.

All data points were used to produce the ΔT from the best least-squares fit. A plot of intensity vs. 1/T and a plot of τ vs. ΔT are given in Fig (7.8). This gave a value of 14 K

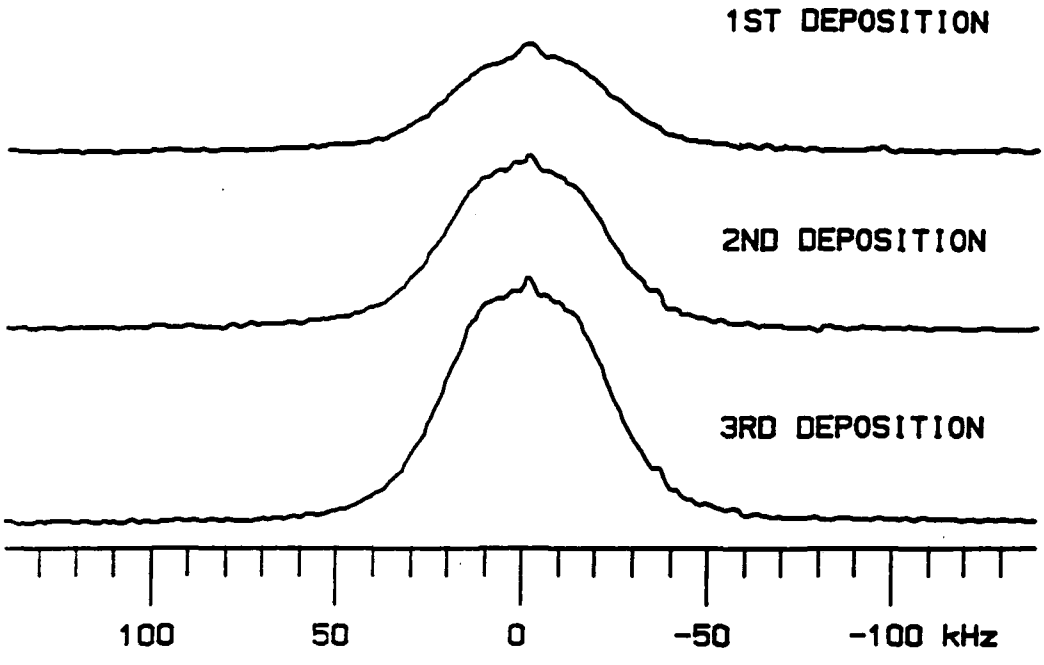

Fig (7-7) Absolute intensity plot of ^{1}H SE signal from the multiple deposition of three 0.1 ml of Ch_2Cl_2.

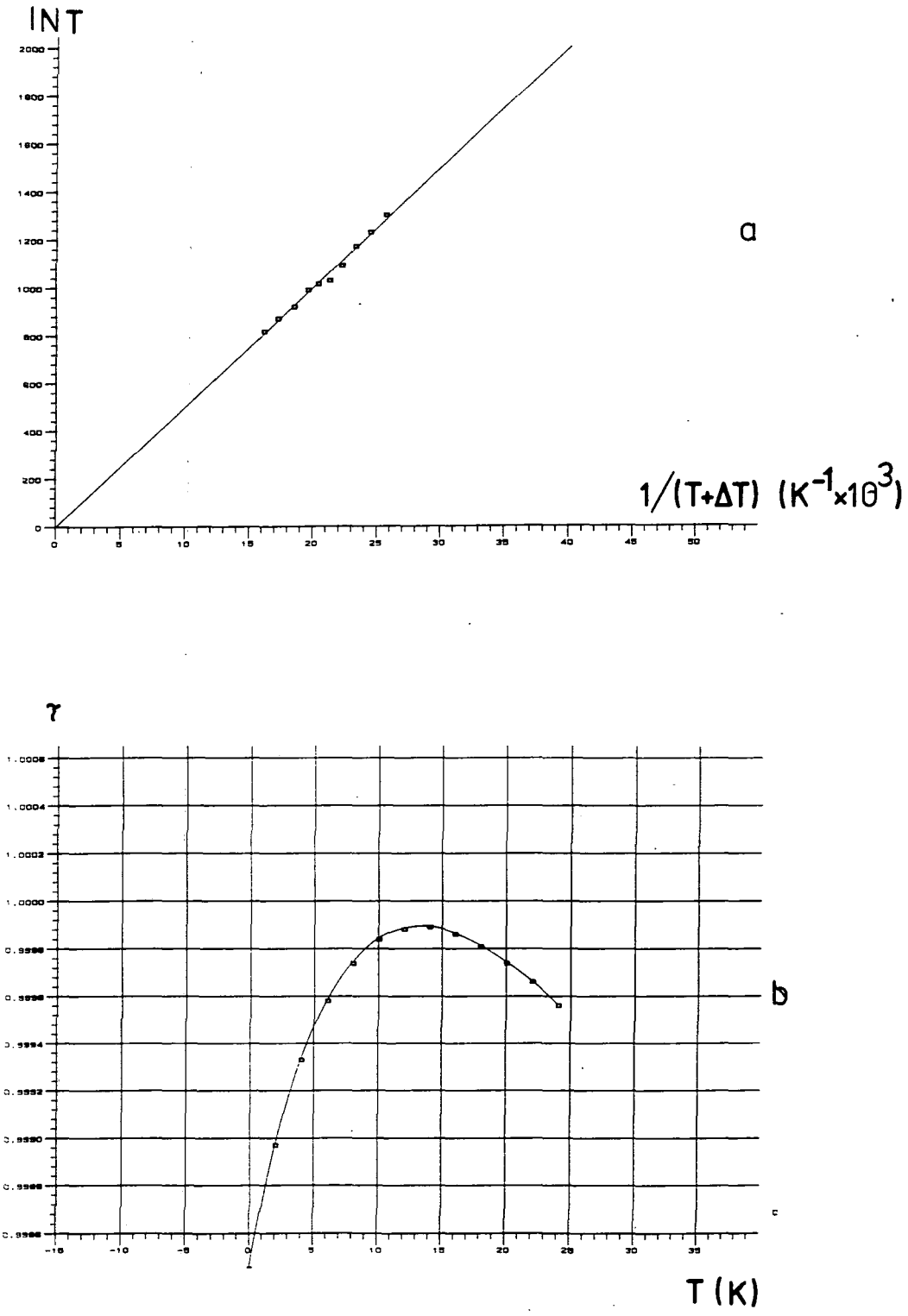

Fig (7-8) (a) Best linear least-square fit of signal intensity vs. 1/T (K^{-1}) from sample in Fig (7-7).

(b) Plot of correlation co-efficient (τ) vs. ΔT from data in Fig (7-8a); ΔT = 14K; sample temperature 39K.

for ΔT which puts the sample temperature at a value of 39 K. The reason for this increase was later trace to a reduction of thermal contact in the joins of the copper rod due to some contamination. This results indicates that it is absolutely important to get all conditions perfect to deposit the sample and even more important in the case of a matrix when using gases possessing just a narrow temperature range before it evaporates. It is clear that in this particular case the copper rod was not having good thermal contact with the Displex unit, producing such a big temperature gradient.

It has been shown that this is a very good method to determine the sample temperature in the case where no measuring device can be located very close to the actual sample. The method was also proved to be reproducible and it can be applied to pure samples as well as to matrix ones. It has been clearly shown that the method to determining the temperature does not depend on the amount of sample deposited in the sapphire cold finger. This is a very important fact because, as already mentioned, it will permit the temperature determination of any sample deposited with this system.

7.3.1 T_1 MEASUREMENTS AND MOLECULAR MOTION

As has already been described, the value of T_1 was measured at each temperature to guarantee the use of the proper recycle time during the determination of the sample temperature. In this way, it was possible to observed the

behaviour of the spin-lattice relaxation time, T_1, with respect to temperature. This effect is directly related to the molecular motion of the sample under study in the particular temperature range in the experiment carried out. It is not the intention of this section to go into great detail over this very complicated topic, but to present some general interesting results and show the potential that the present system has to carry out full investigations in this area.

The measurement of T_1 as a function of the temperature gives valued information about the rotational and translational diffusion of molecules which depend directly on the auto-correlation function, $G(\tau)$, a measurement of the memory loss of the system[13]. This is often assumed to be exponential with a characteristic decay time for this loss of memory known as the correlation time (τ_c), i.e $G(\tau) = \exp(-|\tau|/\tau_c)$[13,12]. Appropriate models of the molecular motion are needed to calculate $G(\tau)$ so that relations with the relaxation time can be made. In this way, if the motion is characterized by a single correlation time[14,15,16], it is possible to express T_1 as

$$\frac{1}{T_1} = K\gamma^4\hbar^2 \sum_j r_j^{-6} \left[\frac{\tau_c}{1+(\omega_o\tau_c)^2} + \frac{4\tau_c}{1+4(\omega_o\tau_c)^2} \right] \qquad 7.3$$

where K is a constant depending on the geometry of the molecular motion

$\omega_o = \gamma B_o$

It is assumed that the τ_c can be expressed as

$\tau_c = \tau_c^{\circ} \exp(\Delta E/T)$, where ΔE is the activation energy of the motional process and τ_c° is a constant of the system. In this way if the T_1 is measured as a function of the temperature and a plot of ln T_1 vs 1/T is carried out a curve is obtained that passes through at least one minimum[14,15]. This T_1 minimum corresponds to a molecular motion which has a correlation frequency that is proportional to the resonance frequency. The slopes of the straight lines at either side of this minimum give the value of ΔE.

Two examples were obtained from T_1 measurements done on CH_2Cl_2 during the temperature determination . These are presented in Fig (7.9). In both cases, it was not possible to define the linear part of the curve in the low temperature region. The values for T_1 change very rapidly in less than 6 K with values that go from 4 to 0.5 s in Fig (7.9a) and from 16 to about 7 s in Fig (7.9b). For this reason it is not possible to calculate the value of ΔE in this region. After this, the two plots go through a prolonged minimum which indicates a molecular motion having a correlation time in the region of 1.67×10^{-8}s. In this minimum area, the relaxation time average values are of 0.7 and 7.4 s respectively. Beyond this point, it is possible to observe the linear dependence with inverse temperature for both sets of data. It was possible to calculate the slope from these sets of data which gave values of ΔE= 1.58 kJ/mol for case Fig (7.9a) and of ΔE= 3.81 kJ/mol for case Fig (7.9b). These values may be related to energy barriers for molecular rotation as the temperature is increased.

These are only qualitative results that show the

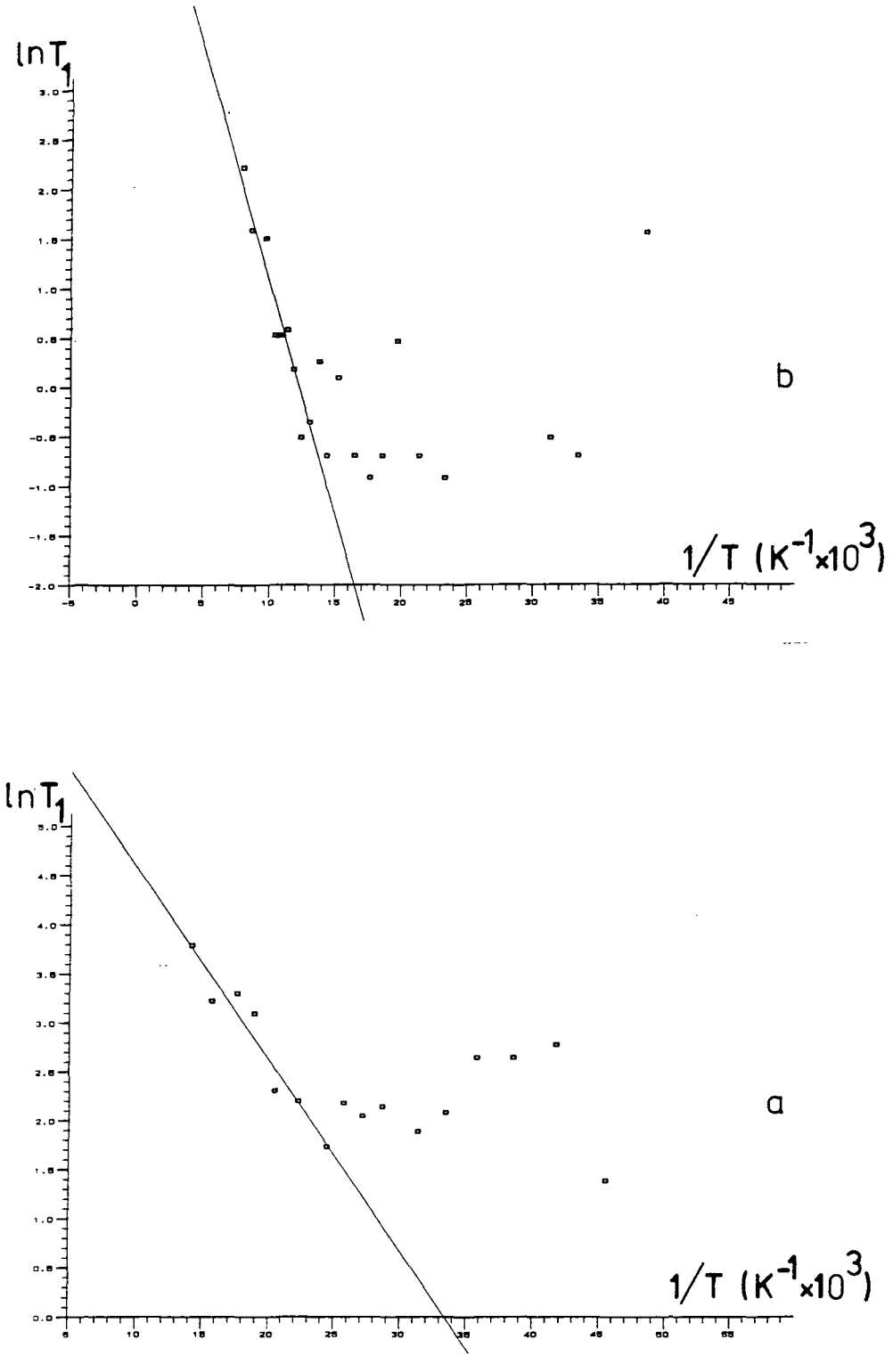

Fig (7-9) Plot of LnT_1 vs. 1/T for two different CH_2Cl_2 samples; (a) ΔT = 1.58 KJ/mol; (b) ΔE = 3.81 KJ/mol

potential of this spectrometer system for the study of motion in samples like CH_2Cl_2. The results give some indication of the type of rotational barrier that may involved in this spin system.

7.4 STUDY OF DICHLOROMETHANE AND ETHYLENE IN AN ARGON MATRIX

This section of the chapter will be dedicated to present the NMR data obtained from dichloromethene (CH_2Cl_2), and ethylene (C_2H_4) samples diluted in an argon matrix. Two different matrix concentrations were produced and deposited for the case of the CH_2Cl_2 samples. The results obtained from these matrices were compared with those obtained from the pure samples. The effects of sample deposition rate were also studied for the case of CH_2Cl_2. The spin-lattice relaxation times for the different samples were also measured using the saturation recovery method and the relaxation of the resonance line-shape was studied using the inversion recovery method.

7.4.1 MATRIX ISOLATION STUDY OF DICHLOROMETHANE

The results obtained in the temperature determination described in section 7.3 and the line-shape information mentioned in section 7.2.3 indicated that dichloromethene could be a very good sample to carry out NMR matrix isolation studied.

Data obtained from the literature[16] gives the value for

the C-H bond distance as 0.1075 nm with an H-C-H angle of 114.5°, and a C-Cl distance of 0.1770 nm with a Cl-C-Cl angle of 112°. It is possible to calculate the proton-proton distance and the proton-chlorine distance giving values of r_{H-H}= 0.1784 nm and r_{H-Cl}= 0.1766 nm respectively. With the information presented above and the use of equations 2.26 and 2.27, it is possible to calculate the expected value for the homonuclear and heteronuclear dipolar splitting, $2\Delta\nu$, for the intra-molecular interaction. In this way, it was possible to obtain a value of $2\Delta\nu_{H-H}$= 31.73 kHz and $2\Delta\nu_{H-Cl}$= 2.14 kHz respectively. These results seem to indicate that even in the pure sample the dominant interaction will be the proton-proton dipolar interaction.

Three different samples were prepared and deposited in this investigation, namely one in the pure form and two different matrix dilutions. Argon was selected as the matrix medium because it will not interact with the compound of interest and it does not have a NMR signal. The preparation of the pure sample has already been described in this chapter. As far as the matrix samples are concerned, they were prepared by evaporation of some CH_2Cl_2 from the liquid and allowing it to fill a 3 ℓ round-glass vessel up to the required pressure. Then, argon gas was injected into the vessel up to almost atmospheric pressure. In this way, two matrix dilutions were prepared with 8.4 and 2.9 % in pressure of CH_2Cl_2 in argon. These dilutions represent the equivalent of molar fraction, x, of 0.128 and 0.033 for each of the above cases. A summary of the matrix compositions is presented in Table (7.1).

CH_2Cl_2/AR	8.4 %*	2.9 %*
$P_{CH_2Cl_2}$ (atm)	1×10^{-1}	2.6×10^{-2}
P_{Ar} (atm)	7.8×10^{-1}	8.7×10^{-1}
$n_{CH_2Cl_2}$ (mol)	1.46×10^{-2}	3.8×10^{-3}
n_{Ar} (mol)	1.14×10^{-1}	1.16×10^{-1}
x (molar fraction)	0.128	0.033

(*) These values are expressed in terms of percentage of pressure measured in mm of Hg.

Table (7.1) Matrix composition for the two different dilutions.

The two matrices were deposited using the two methods of condensation already described, namely the pulse and the slow method. For the latter, the gas pressure was set to 2 mbar for the whole period of deposition and stoped when enough matrix has been condensed. The sample temperature was 26 K for all cases.

As far as the NMR measurements are concerned, saturation recovery experiments were performed for all samples to determine the T_1's so that appropriate recycling time could be used. Line-shape information was obtained from solid-echo (SE) experiments. T_1 inversion recovery experiments with full FID acquisition were also carried out for specific values of τ. The $\pi/2$ pulse was set to 1.5 μs with a dead time of 13 μs for all experiments. For the solid echo, the τ delay was set equal to the dead time of the probe and the dwell times were set to either 1 μs or 3 μs. The first was used in pure samples

and in the x = 0.128 case where the signal to noise ratio, S/N, was not so critical. The second dwell time was used for the x = 0.033 matrix concentration where better S/N is needed.

First, the results obtained from SE experiments will be presented and discussed which are concerned with line-shape and inter-proton distance information. This will be followed by the presentation of the relaxation data both from the intensity as well as from line-shape measurements.

7.4.1.1 LINE-SHAPE AND INTER-PROTON DISTANCE

The first sample to be studied was x = 0.128 molar fraction using the pulse method of deposition. A comparison of the spectrum from the pure sample and the one from this dilution is presented in Fig (7.10). No line-broadening was applied to the FID before FT transformation. The spike at 0 Hz is spectrometer artefact. At first sight, it is possible to see that the major difference between the two is the better resolution of the double minimum in the matrix isolated sample. In both cases, it is possible to see some indication of the position of the outer steps of the transition. It is also possible to detect a small asymmetry in the intensity height of the horns of the powder pattern, the one at negative frequency being the more intense.

The FID that gave rise to the spectra in Fig (7.10) were used to perform the fitting calculation to a theoretical dipolar function plus a gaussian broading. The theoretical dipolar function was calculated to be on-resonance,

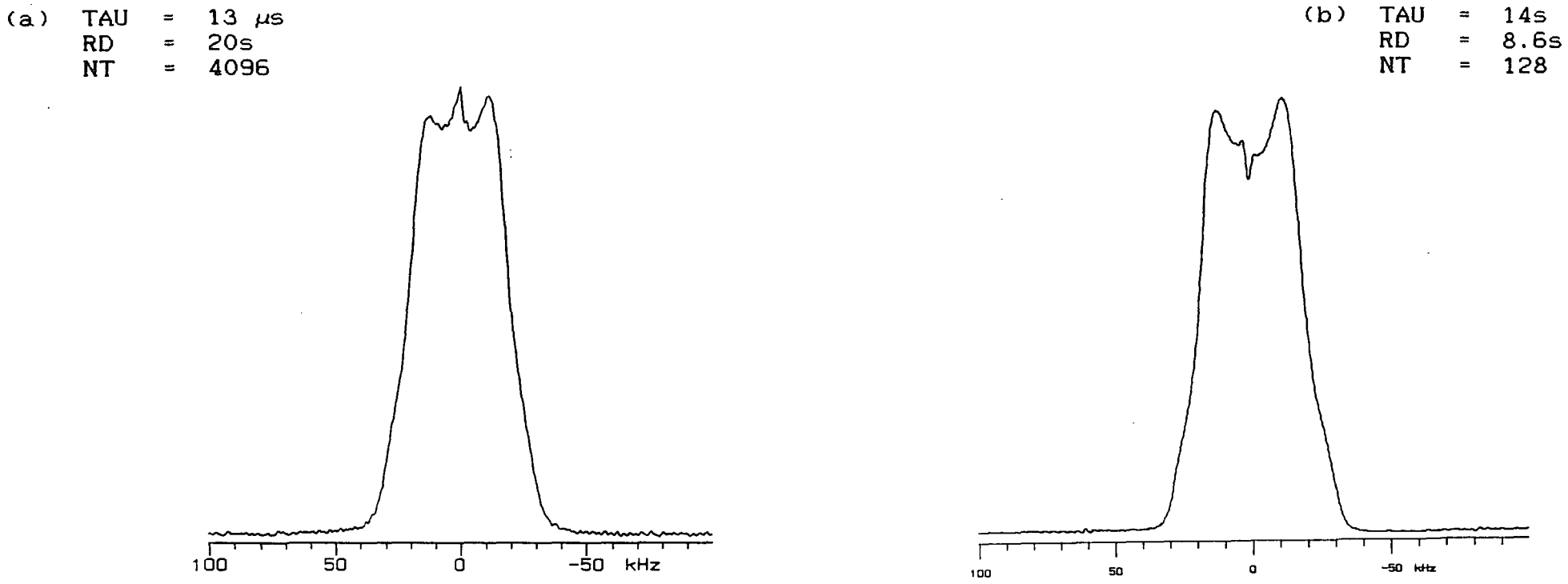

Fig (7-10) ^{1}H SE Spectrum from CH_2Cl_2; (a) pure sample; (b) Matrix-isolated CH_2Cl_2 in Ar, $\varkappa$ = 0.128, pulse deposition method.

symmetrical, and only the real part of the FID is fitted. The computer program used in this simulation was written at Durham University[17] and will be presented in afuture publication.

In the case of the pure sample the FID fitting gave a value of $2\Delta\nu$= 30.59 kHz for the peak separation and broadening of 27.36 kHz. For the matrix dilution, these values were equal to 29.73 kHz and 21.73 kHz respectively.

As has already been mentioned, it is not expected to see any big effect on the line-shape from the Cl-H interaction; the major effects are expected to come from the H-H interaction. From the above results, It is possible to see the decrease in the line-broadening factor in the matrix case. This can be attributed to a clear reduction in the inter-molecular interaction. If face centred cubic packing (fcc) will be considered each molecule is surrounded by 12 neighbours. In the case of the pure sample there is full occupancy of CH_2Cl_2 molecules introducing full inter and intra-molecular interactions. For the matrix sample with $\varkappa$ = 0.128 molar fraction and considering a single dichloromethene molecule, there is a probability of one to find another CH_2Cl_2 molecule in the first occupation shell around it. Even with this high probability to find two CH_2Cl_2 next to each other which will introduce a big inter-molecular interaction, it is possible to detect the reduction in this interaction on the value of the gaussian broadening used in the fitted function. A reduction of 6.24 kHz in the gaussian broadening is a significant one and it is outside experimental error. A comparison between experimental and fitted FIDs in the form of the FT of both FID is presented in Fig (7-11) for

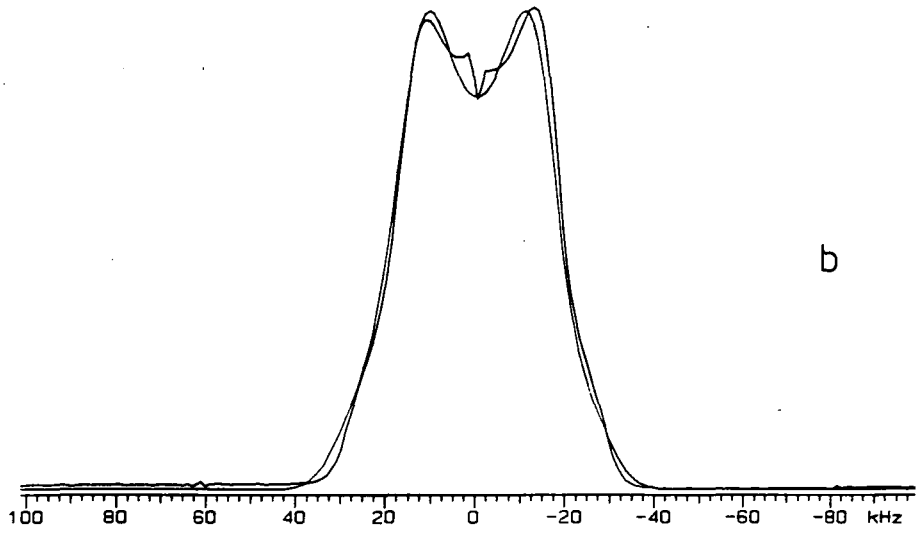

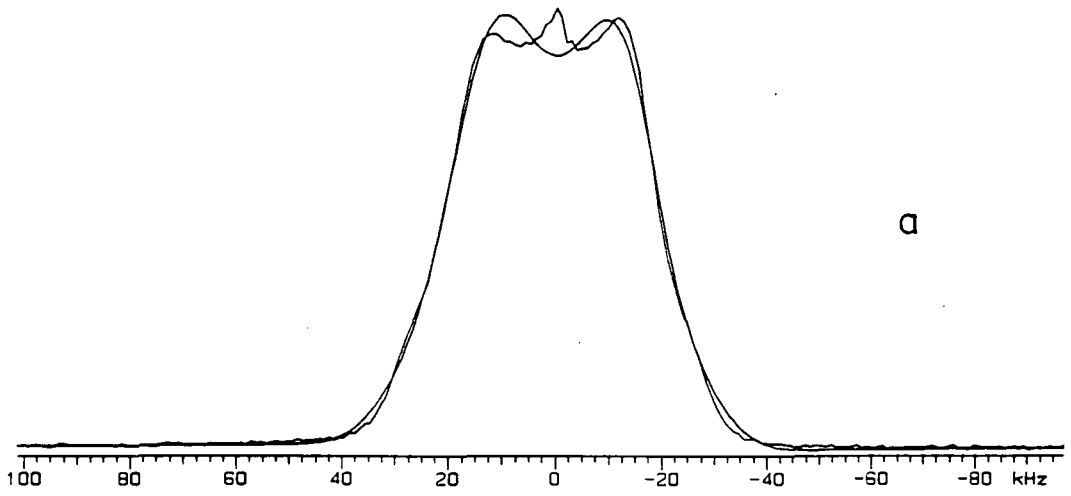

Fig (7-11) FIG-Dipolar fitting to the data in Fig (7-10);
(a) pure sample, $2\Delta\nu$ = 30.59 kHz, GB = 27.36kHz;
(b) x = 0.126 matrix, $2\Delta\nu$ = 29.73kHz, GB = 21.73kHz
pulse deposition method.

the pure sample as well as for the matrix isolated one.

In a comparison between the expected value for $2\Delta\nu$ obtained from the literature data and the one obtained from the FID fitting of both samples, it is possible to see a reduction in the value of the latter. In the matrix case the reduction is exactly 2kHz which gives a proton-proton distance of 0.1823 nm. In the pure sample the reduction in kHz is half of that from the matrix. There is a good agreement between the values for r_{H-H} from literature data and the one obtained in this work. The next step is to compared these results with the one obtained from the slow deposition of the same matrix concentration as above. The spectrum obtained from this type of deposition is presented in Fig (7.12). It is possible to see a great improvement in the resolution over the whole line-shape in comparison to the one presented in Fig (7.10). The doublet is sharper than before with a minimum between the two peaks increased considerable. One similarity between the spectrum from the different methods of deposition is the fact that the intensity of the two peaks is again not symmetrical. There is also a great improvement in the resolution of the outer steps from the individual transitions. In this respect, the one on the left seems to be higher and sharper than the one in the right, i.e. they do not look symmetrical.

In this case, the overall effect seems to indicate an even greater isolation of the CH_2Cl_2 molecules in comparison the other method of deposition for the same molar composition of the sample. This is a very significant result because it indicates that as far as NMR is concerned a slow deposition

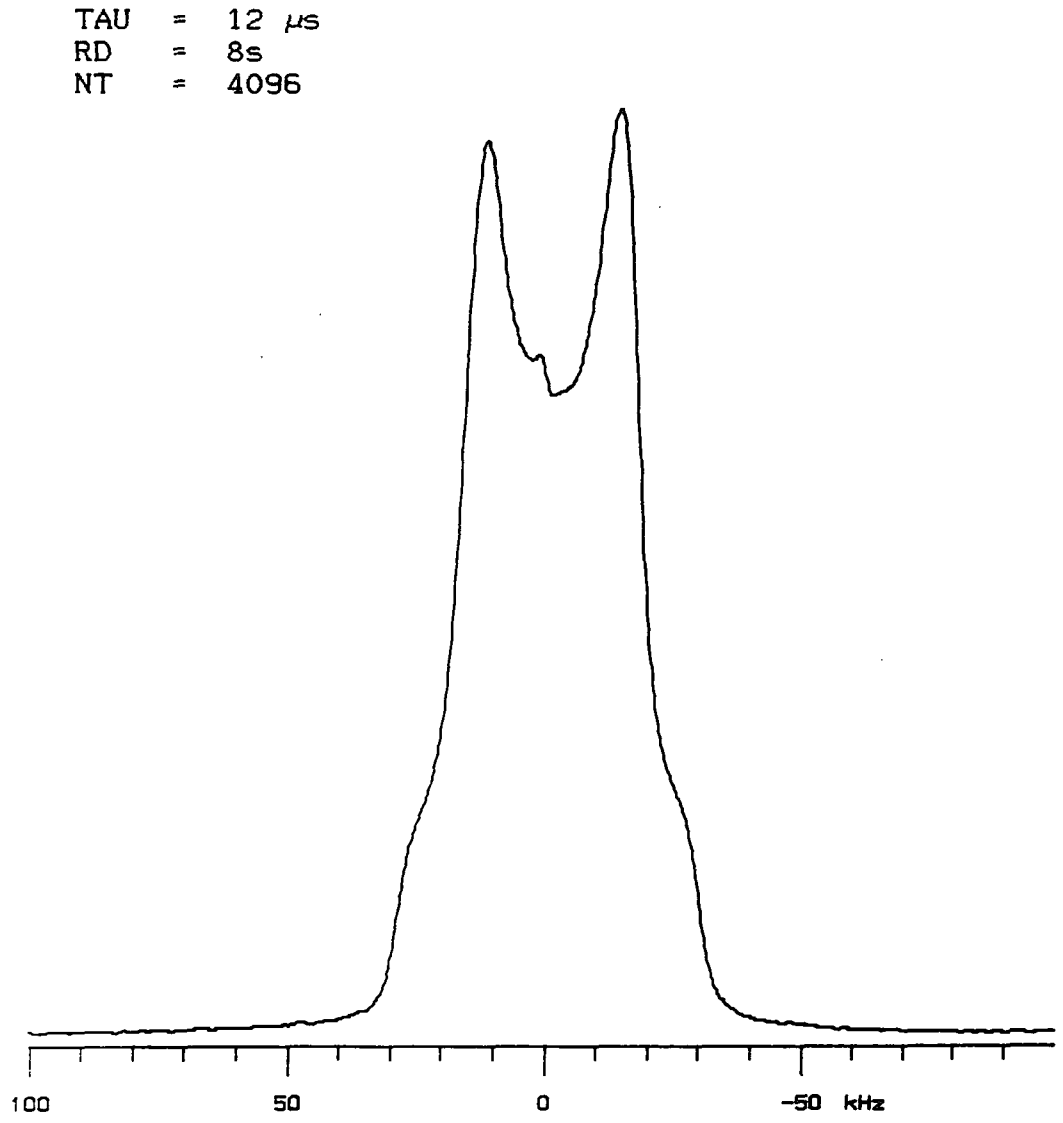

Fig (7-12) ^{1}H SE Spectrum from a Matrix-isolated sample of CH_2Cl_2 in Ar, α = 0.126, slow deposition.

of the matrix gives a better molecular isolation of the system of interest than in the pulse method. Another difference between the two methods is that the actual sample shape is different. In the pulse method the sample is arranged evenly along the sapphire surface almost in a cylindrical shape. In the case of the slow deposition the sample shape is almost concentrated at the end of the sapphire rod with a drop like shape.

As in the previous two cases, the FID obtained from this sample was used to produce a fitting. The doublet separation gave a value of 29.90 kHz and the gaussian broading was equal to 15.66 kHz. A comparative plot between the experimental line-shape and the one obtained from the fitting is presented in Fig (7.13). The dramatic change in the line broadening factor obtained in this fitting can be seen; a drop of 11.7 kHz in comparison with the pure sample. This result is in very good agreement with what was already indicated about the greater isolation of the molecules in this case. The fitted line reproduced very well the experimental one with good agreement in the intensity of the doublet and the position of the outer step but not with their intensities. The overall result indicates that even at this high concentration it is possible to produce a well resolved Pake doublet in which the inter-molecular broadening, expressed in kHz, can be reduced to half of the expected intra-dipolar splitting. There is no significant change in the doublet separation giving good reproducibility in the value of this parameter. This result seems to indicate that there is some advantages in using the slow method over the pulse method. This is due to a better

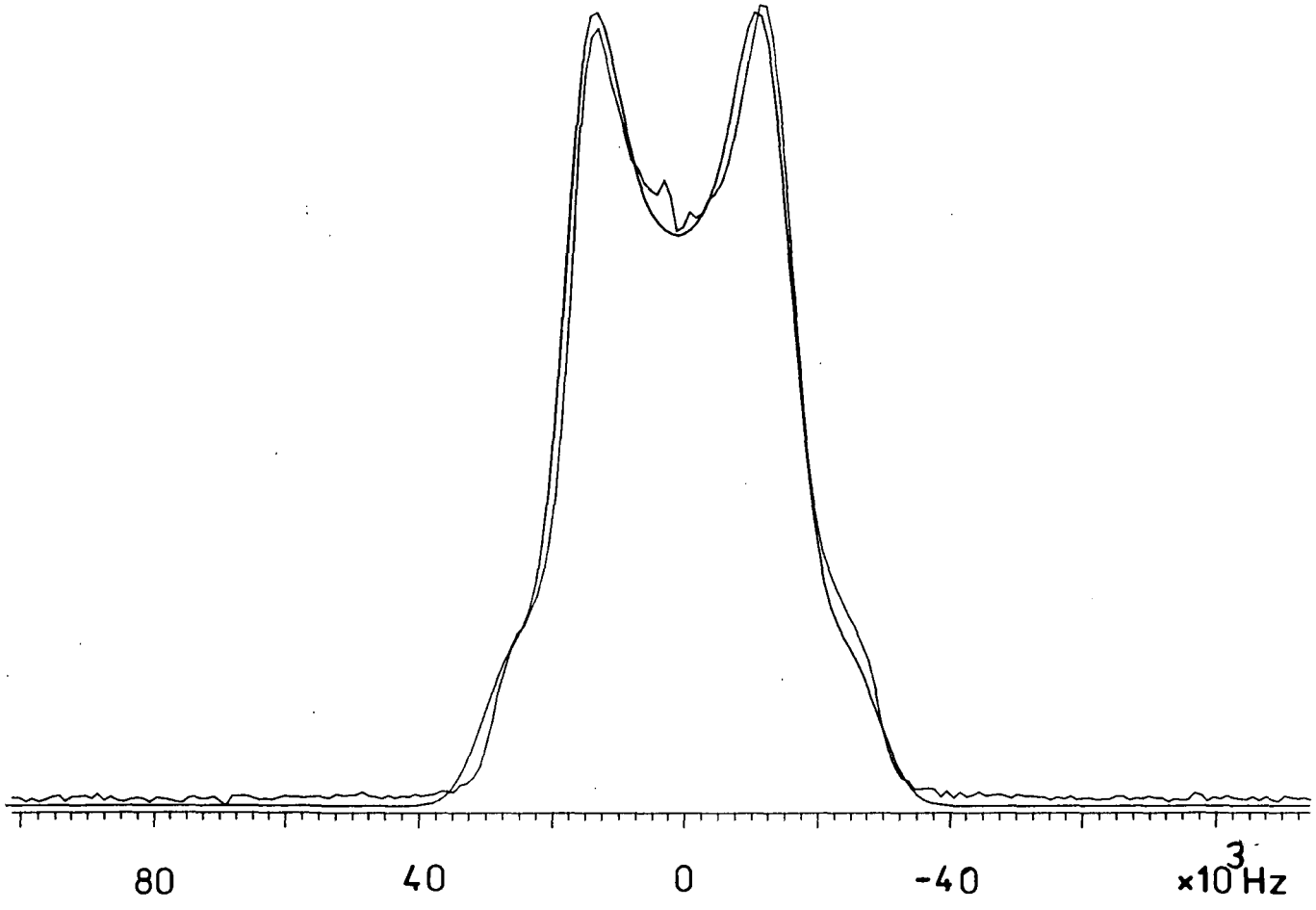

Fig (7-13) FID-dipolar fitting to the data in Fig (7-12).
$2\Delta\nu$ = 29.90 kHz , GB = 15.66 kHz

resolution of the Pake doublet.

The next step to follow was to reduce the molar fraction of the matrix and to observe the effects that produces on the line-shape and the parameters in the FID fitting. The molar fraction is equal to 0.033 in this case. This gives a probability 3/8 to find two CH_2Cl_2 next to each other. This probability is still high but from the previous result it is expected to see some changes in the line-shape from this sample. Again, consider the results from the pulse deposition first. The SE spectrum obtained from this sample is presented in Fig (7.14). Again the peak in the middle is a spectrometer interference that looks bigger due to the reduction in concentration.

Comparison with the one for the previous matrix reveals a big change in the asymmetry of the peak doublet, i.e. it has changed position. The peak at positive frequency is the more intense. Another difference between the two matrix sample is the increased resolution of outer steps from each transition. It also shows some amount of asymmetry between them. The fitting of the FID gives additional information with values of $2\Delta\nu$=31.51 kHz and a broadening of 24.80 kHz. A comparative plot of the best fit to the experimental data is presented in Fig (7.15). The first value seems to indicate that the molecules in this sample are in a more rigid environment whereas the value for the broadening seems to indicate a small increase in the inter-molecular interaction. It is also appropriate to say that this is not an ideal fitting because it does not produce a good matching in the intensity of the doublet and in the asymmetry of the outer steps.

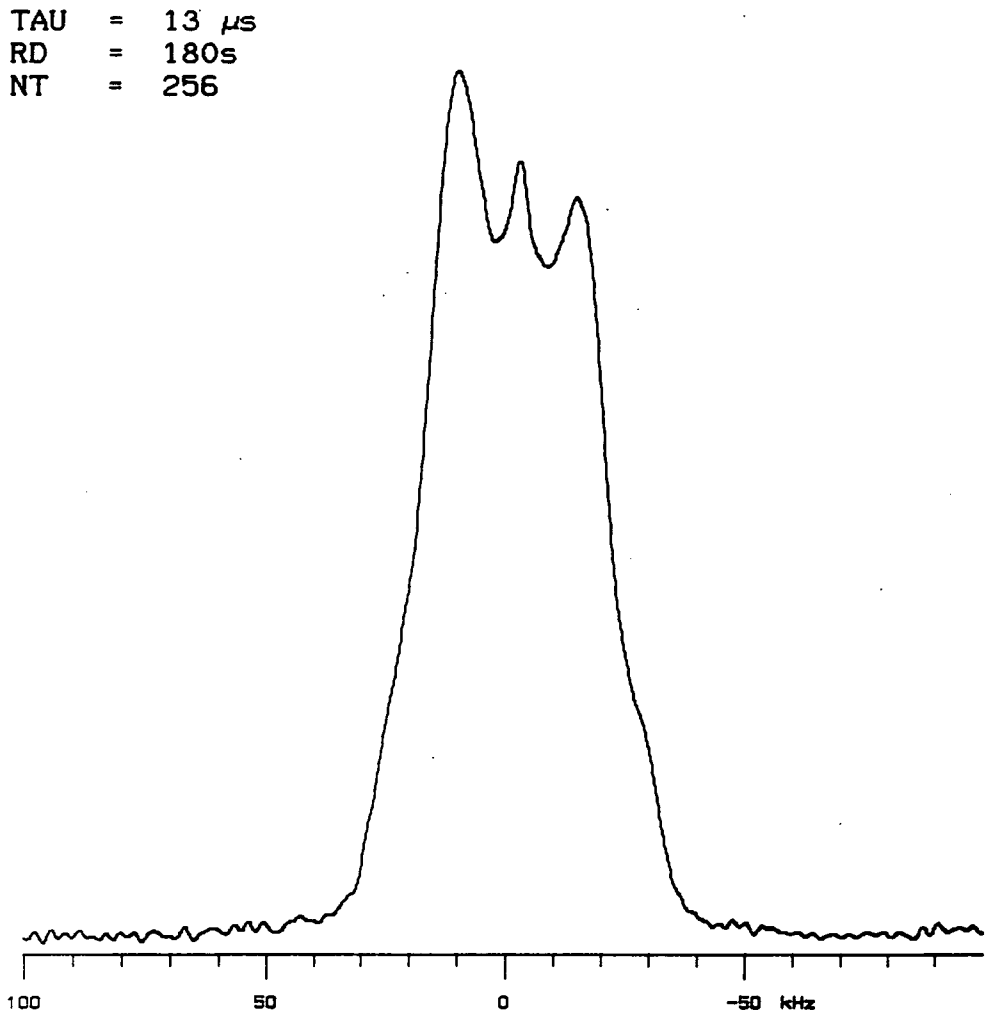

Fig (7-14) ^{1}H SE Spectrum from a Matrix-isolated sample of CH_2Cl_2 in Ar, α = 0.033, pulse deposition.

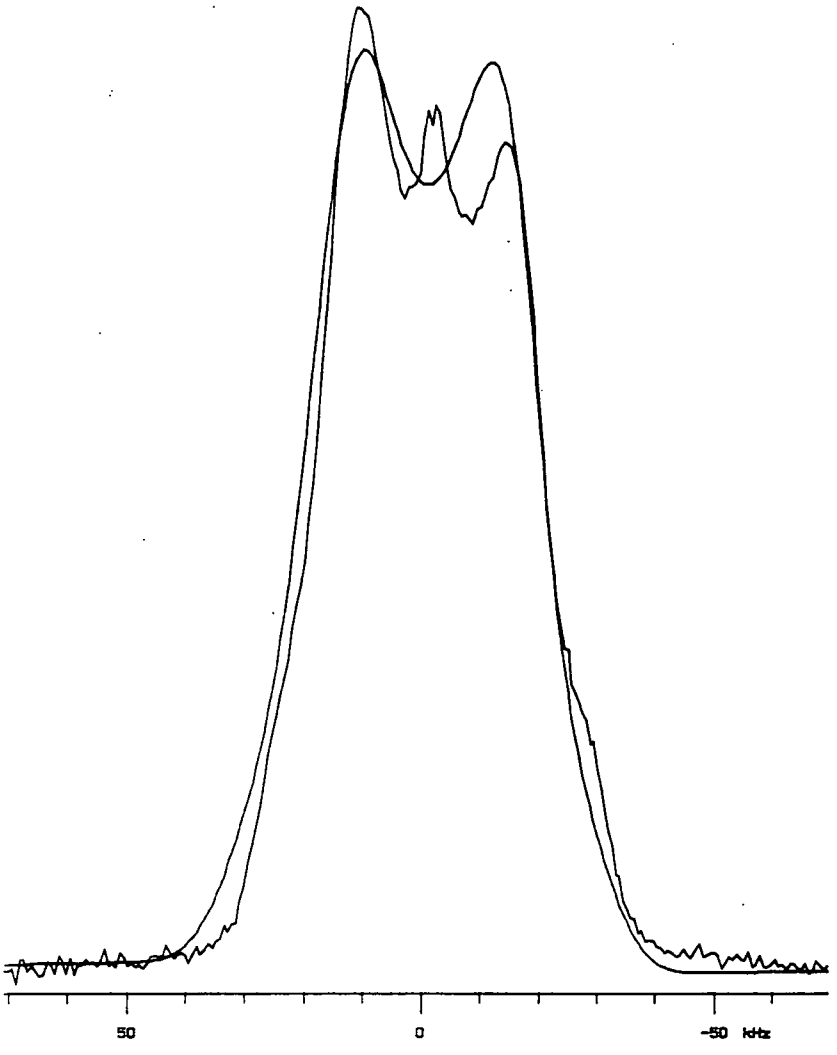

Fig (7-15) FID-dipolar fitting to the data in Fig (7-14); $2\Delta\nu$ = 31.51 kHz, GB = 24.80 kHz.

The conclusion reached from the first deposition gains more support when the comparison is made with a sample from the same matrix which has been deposited using the slow method. The spectrum from this sample deposition is presented in Fig (7.16). There is a sharp difference between this spectrum and that of previous sample deposition and even with that from the same sample deposition method from the previous molar fraction sample. The peaks from the Pake doublet are narrowed with a deeper minimum between them. The outer steps of the doublet are better resolved but still show asymmetry. The overall spectrum is in better agreement with the amount of dilution of the sample inside the argon matrix in complete contrast with the one from obtained the pulse method.

Again, the results of the FID fitting support this visual evidence of incease resolution of the Pake doublet and the result of the fitting is presented in Fig (7.17). The value for $2\Delta\nu$ is almost identical to the one obtained from the previous slow deposition with a value of 29.88 kHz. The broadening of the function was equal to 14.66 kHz. The intensity of the biggest peak is well matched considering the asymmetry in the line-shape and the location of the outer steps very good, again only failing the asymmetry. The value of 14.66 kHz is a small change in comparison with the previous slow deposition, but it is not that surprising because in this case the probability of finding two CH_2Cl_2 next to each other is still high, i.e. it is almost one in four.

It is possible to conclude from the results presented above that the slow deposition method is by far the best way

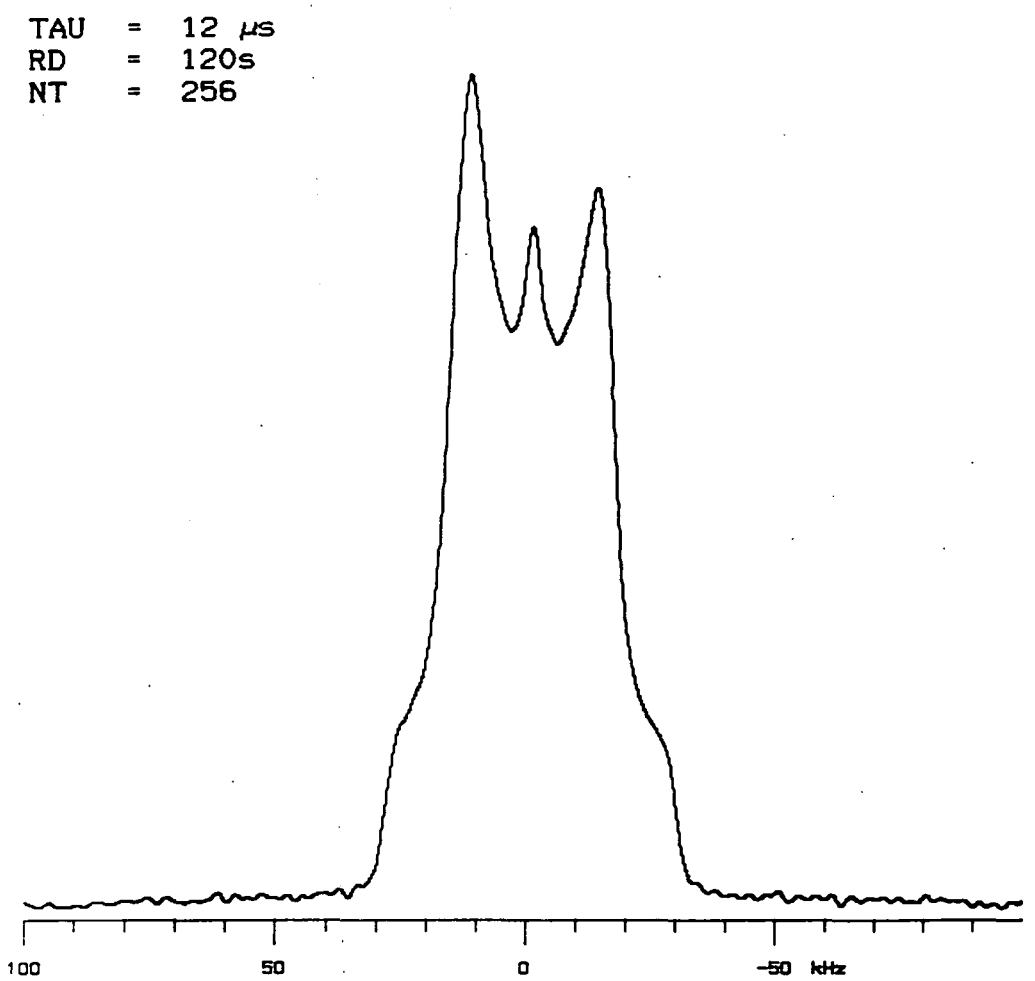

Fig (7-16) ^{1}H SE Spectrum from a Matrix-isolated sample of CH_2Cl_2 in Ar, $\varkappa$ = 0.033 slow deposition.

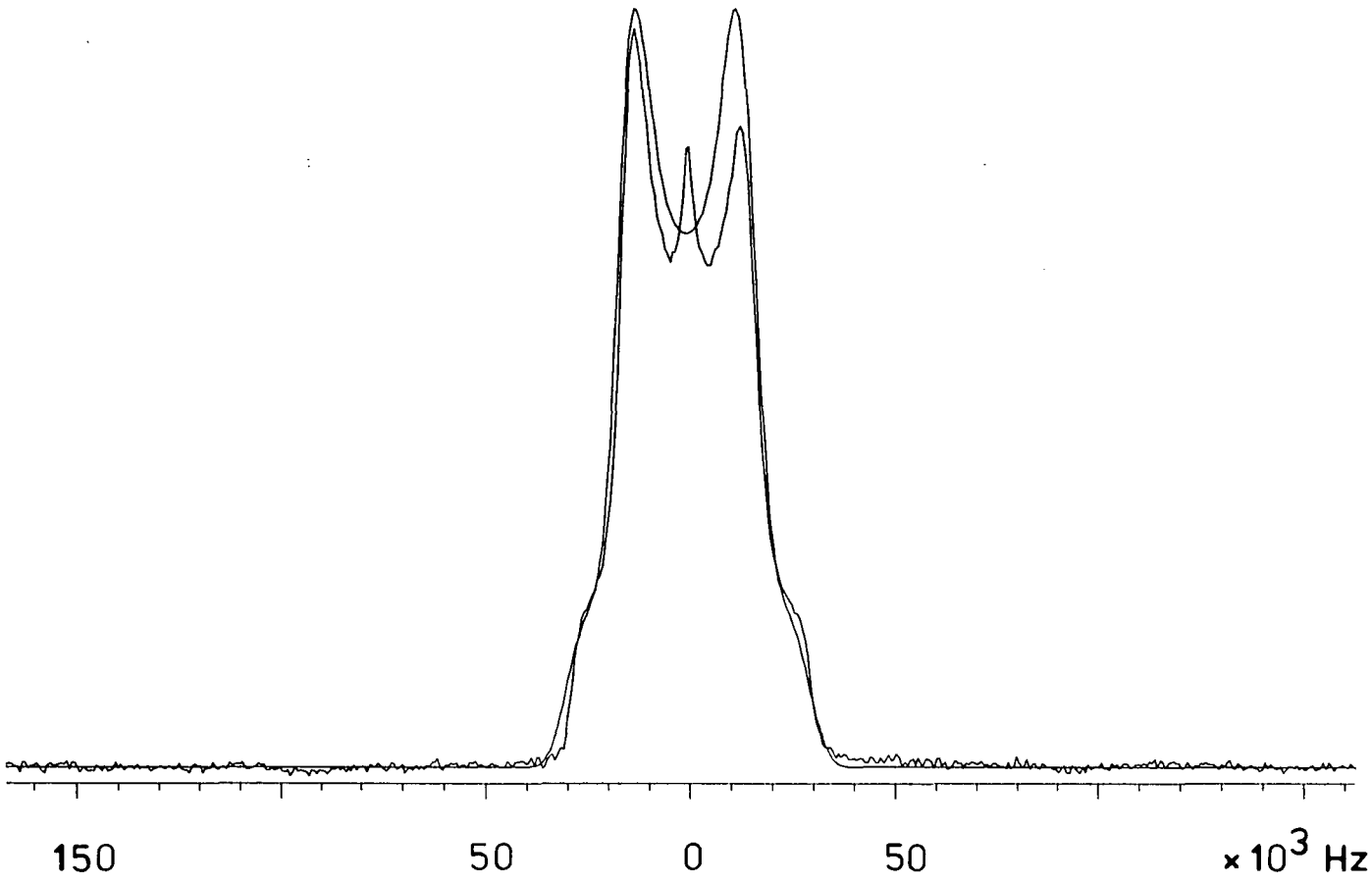

Fig (7-17) FID-dipolar fit to the data in Fig (7-16);
$2\Delta\nu$ = 29.88 kHz; GB = 14.66 kHz.

of ensuring a very good isolation of the sample under study. This is very clearly shown from the comparison of the two methods of deposition used in the $\varkappa = 0.033$ case. The increased resolution in the overall line-shape is very significant. It is also possible to say that the asymmetry in the overall line-shape is independent of the sample concentration, sample shape, and method of deposition. The reasons for this effect is not really understood, but it can be said that it is very difficult to interpret in terms of chemical shift anisotropy, i.e. for protons this is of the order of 10 ppm in comparison with the total spread of the line-shape in this cases that is of the order of 1000 ppm or more.

As far as line separationis concerned, it is possible to say that the value for the inter-proton distance obtained from these matrices is very reliable and it is in good agreement with those presented in the literature, within experimental error. The FID fits to the experimental data are not perfect but they are a very good representation of the data taking into account the asymmetry in some of the line-shapes obtained from the different samples.

7.4.1.2 SPIN-LATTICE RELAXATION STUDY

Two types of measurement were carried out as far as the spin-lattice relaxation time is concerned, namely saturation recovery measurements and inversion recovery measurements. In the first one the interest was concentrated in determining

the longest relaxation time of the sample and if the relaxation decay was single exponential. For this only single point intensity acquisition method was used in the experiment. This means that after the tau value only the first point of the FID is detected. This was done to both pure samples as well as matrices. In the second one the attention was focused on the behaviour of the full spectral line-shape with respect to the tau value. In this case the signal was detected with the help of the solid echo experiment to avoid distortions arising from the dead time of the probe. This experiment was only done to the matrix samples.

First consider the results from saturation recovery measurements to all the samples. They all show non-single exponential delay always expressed in terms of a 3 component T_1. This effect was also found for the pure samples. A summary of all the values obtained for the different samples as well as their relative populations is presented in Table (7.2). If this multi-component behaviour is associated with an orientation dependence of the molecules with respect to the external magnetic field it is expected to see its effect in the overall resonance line-shape. There are several examples in the literature[19,20] in which the dependence of the shielding tensor had showed this effect in powder samples. It shows that parts of the powder pattern relaxer fast than other parts . Inversion recovery experiments were carried out to three of the four matrix deposited samples in order to determine if this was the effect in this case. The results of these experiments are presented in Fig (7.18).

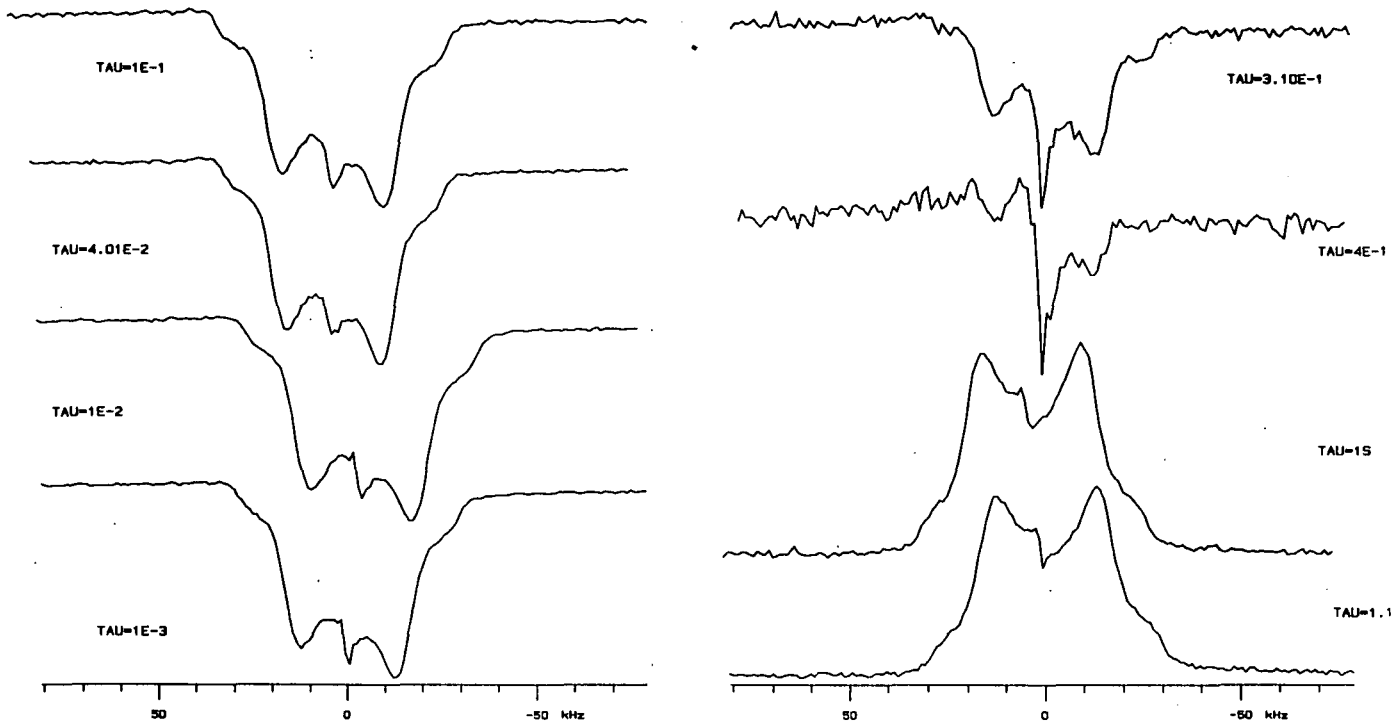

Fig (7-18a) Plot of signal recovery as a function of TAU in a T_1 inversion recovery experiment.

x = 0.128, slow deposition.

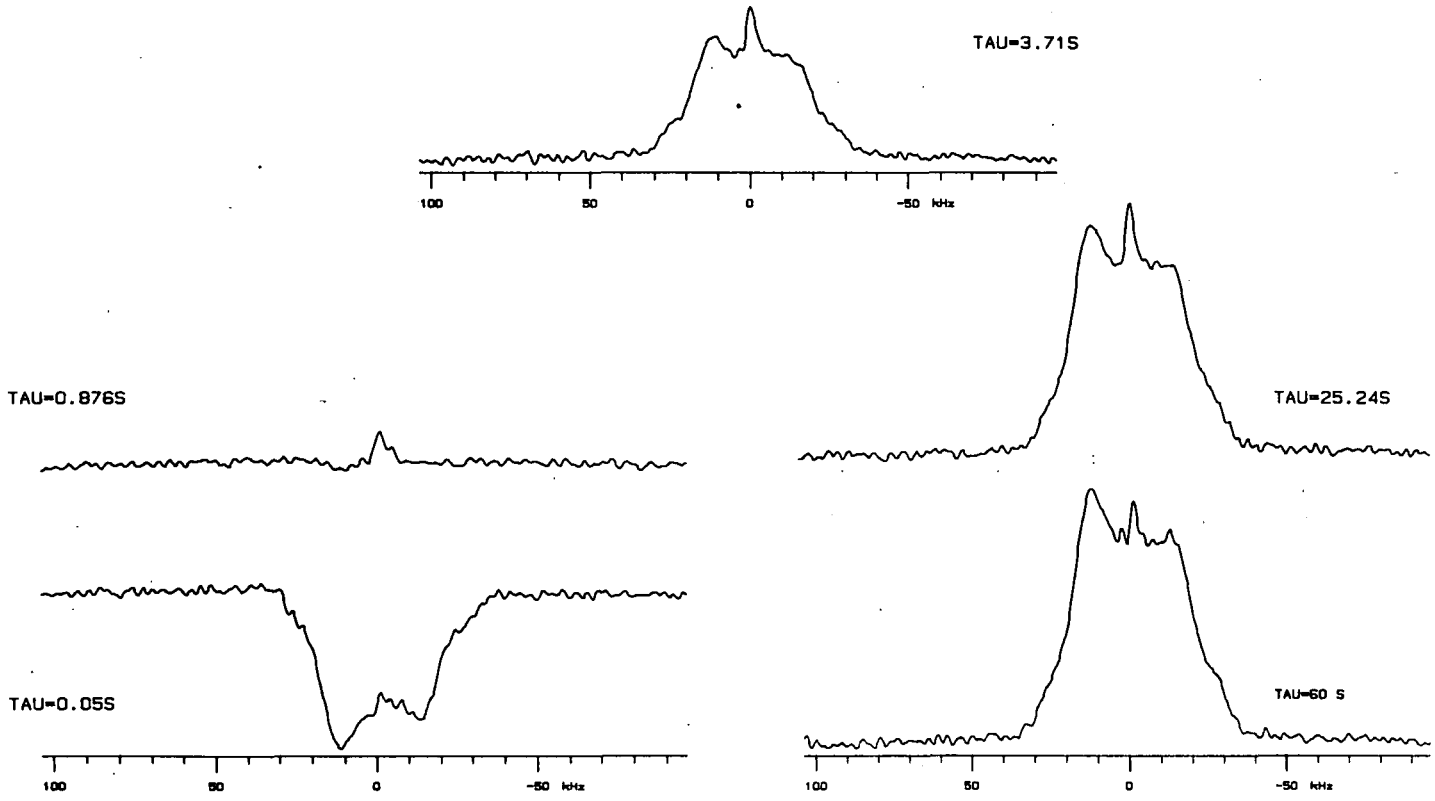

Fig (7-18b) Plot of signal recovery as a function of TAU in a T_1 inversion recovery experiment.

α = 0.033, pulse deposition.

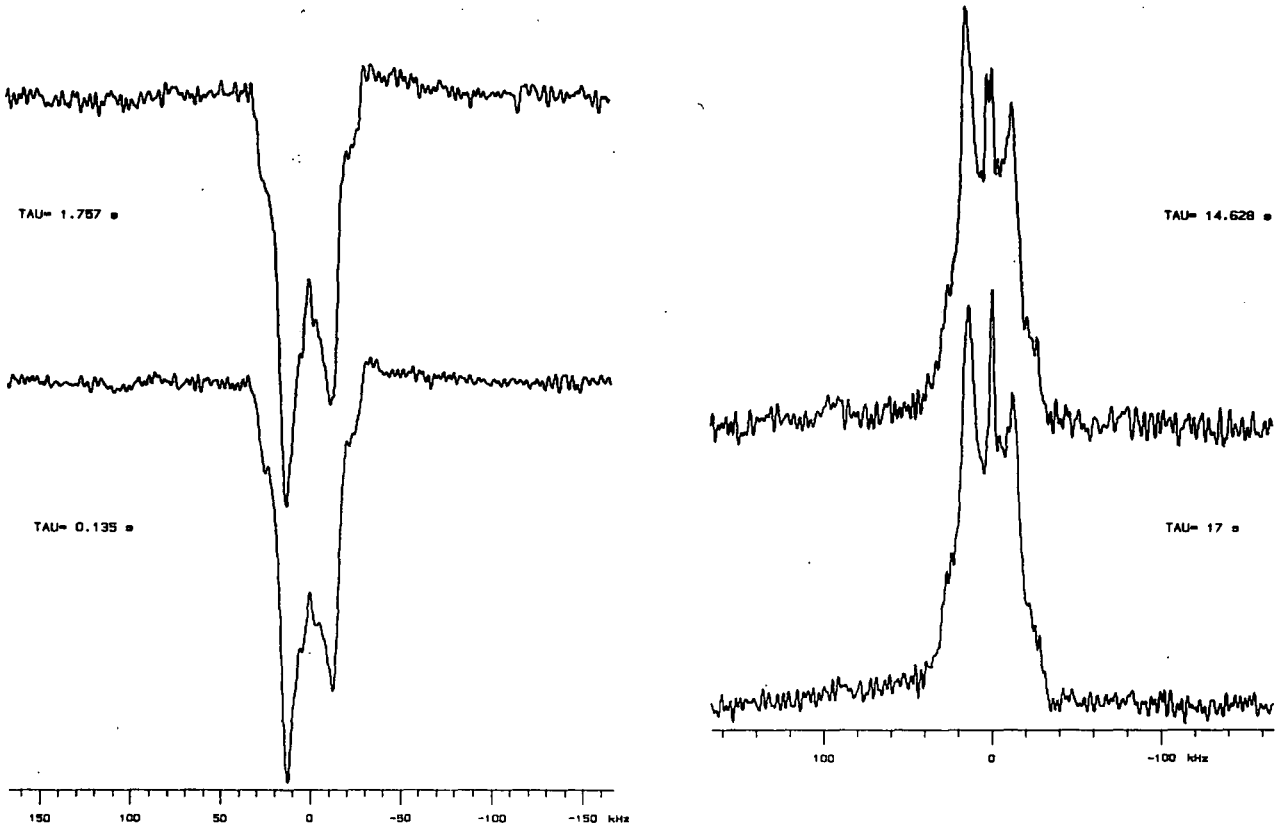

Fig (7-18c) Plot of signal recovery as a function of TAU in a T_1 inversion recovery experiment.

α = 0.033, slow deposition.

α	0.128		0.033		0.128		0.033	
DEP.	P^1		P^1		S^2		S^2	
	T_1 (s)[1]	Pop. (%)	T_1 (s)[1]	Pop. (%)	T_1 (s)[1]	Pop. (%)	T_1 (s)[1]	Pop. (%)
	1.76	36.4	36.58	33.7	1.64	55.4	21.20	79.6
	0.44	46.0	5.39	24.7	0.45	34.9	2.55	14.9
	0.06	17.54	1.27	41.63	0.06	9.64	0.20	5.5

1) Pulse deposition; 2) Slow deposition

Table (7.2) Multi-compounent T_1 values and the relative populations for the different matrices and sample depositions obtained from the saturation recovery experiment.

In none of the cases presented it is possible to say conclusively that the orientation dependence is the major factor dominating the multi-component patter observed in the T_1. There are no significant changes in the line-shape to support this conclusion. In all cases, the entire powder pattern seems to relax at the same rate to equilibrium.

Another possible explanation for this effect is a relation between the T_1 and the degree of isolation of individual molecules in the samples. From Table (7.2), the values for the three components are almost identical for both methods of deposition in the α = 0.128 samples. There is also a big difference between the relative proportions of the population of the three T_1 components obtained from the two methods. In the case of the pulse method, the second longest component is the one with the biggest population. For the

slow deposition, the populations keep the same relation as that of the relaxation values, i.e. the longest T_1 component has the biggest population and so on.

As mentioned, the slow deposition method is the most appropriate to guarantee isolation of the CH_2Cl_2 molecules inside the argon matrix. So, a close examination of the T_1 and population for the two depositions using this method gives a very interesting correlation. First, the T_1 values have an increase in going from the less to the more dilute matrix but the increase in the longest component is the biggest one going from 1.64 to 21.2 s. This is a clear indication of the increased isolation in the molecules inside the matrix, which correlates very well with what is observed for the powder pattern in these samples. At the same time, it is also possible to see that the relative population for this long components increase whereas the other two decrease. The population of the longest component goes from 55.4 to 79.6 %, whereas the other two are approximately half of the previous value. In this way, it is possible to relate the longest T_1 values and the biggest population to those molecules that have the least number of near neighbours, probably to the one with only one molecule as next neighbour. The other component can be related to molecules with increasing number of near neighbours.

In this way, it is possible to conclude that there is a relation between the multi-component effect on the T_1 and the degree of isolation of the studied molecule inside the argon matrix. The changes in the population seem to indicate that this is true and that no significant effect was found in the

line-shape behaviour in the inversion recovery experiment.

7.4.2 MATRIX ISOLATION STUDY OF C_2H_4

The results from the matrix isolation study of ethylene will be presented in this section where it will be possible to see the changes observed in the powder pattern when going from the pure sample to the matrix. Samples were prepared in a way similar to that described for the case of CH_2Cl_2 except for the fact that this sample is already in gas form. Two samples were studied namely a pure sample and matrix dilution of 2.17 % by pressure which is equivalent to a molar fraction, α = 0.022. The NMR data were obtained using the same pulse sequences as in the case of CH_2Cl_2.

This molecules can be regarded as a four spin system with at least six proton-proton dipolar interactions for the case in which all proton-proton distances were different. Due to the symmetry of the molecule and if it is considered that the four protons are located at the corners of a rectangle, it is possible to simplify the system to only three H-H dipolar interactions. Data obtained from the literature[16] give the C-H distance as 0.1085 nm with an H-C-H angle of 116.7°, and a C-C distance of 0.134 nmm.. Fig (7.19) shows a diagrammatic representation of the ethylene molecule with the relevant H-H distances. It is possible to use the molecular symmetry to reduce the number of dipolar interactions to those related to three H-H distances, i.e. $r_{1,2}$, $r_{2,4}$ and $r_{2,3}$. The other three will be equal to these as indicated in the figure.

These distances are 0.1847, 0.2478 and 0.3091 nm respectively. This information can be used to calculate the dipolar breadth of the interaction from these three types of proton. The values for the three interactions are 28.593, 11.840, and 6.101 kHz. All these interactions will introduce their effects into the line-shape obtained from this sample and none can be discarded.

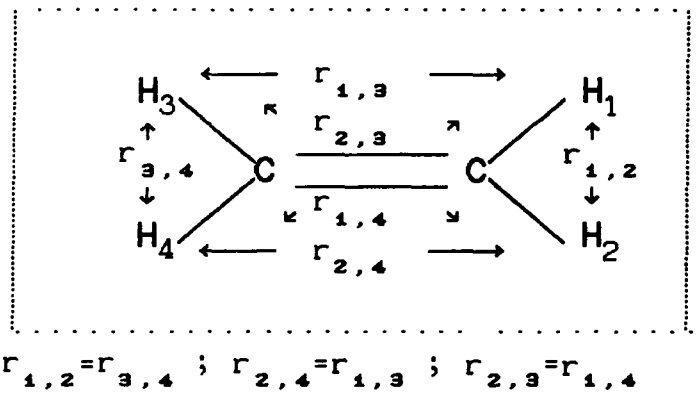

Fig (7.19) Inter-proton distances to be considered for the ethylene spin system.

As always, the first sample to be examined was the one from pure ethylene and the SE spectrum is presented in Fig (7.20). It is a very simple line-shape with no indication of the outer step as seen in the dichloromethene case and with just a small oscillation in an almost flat maximum. This is an expected result due to the multiple dipolar interactions expected in this system. This is clearly seen when the FID is

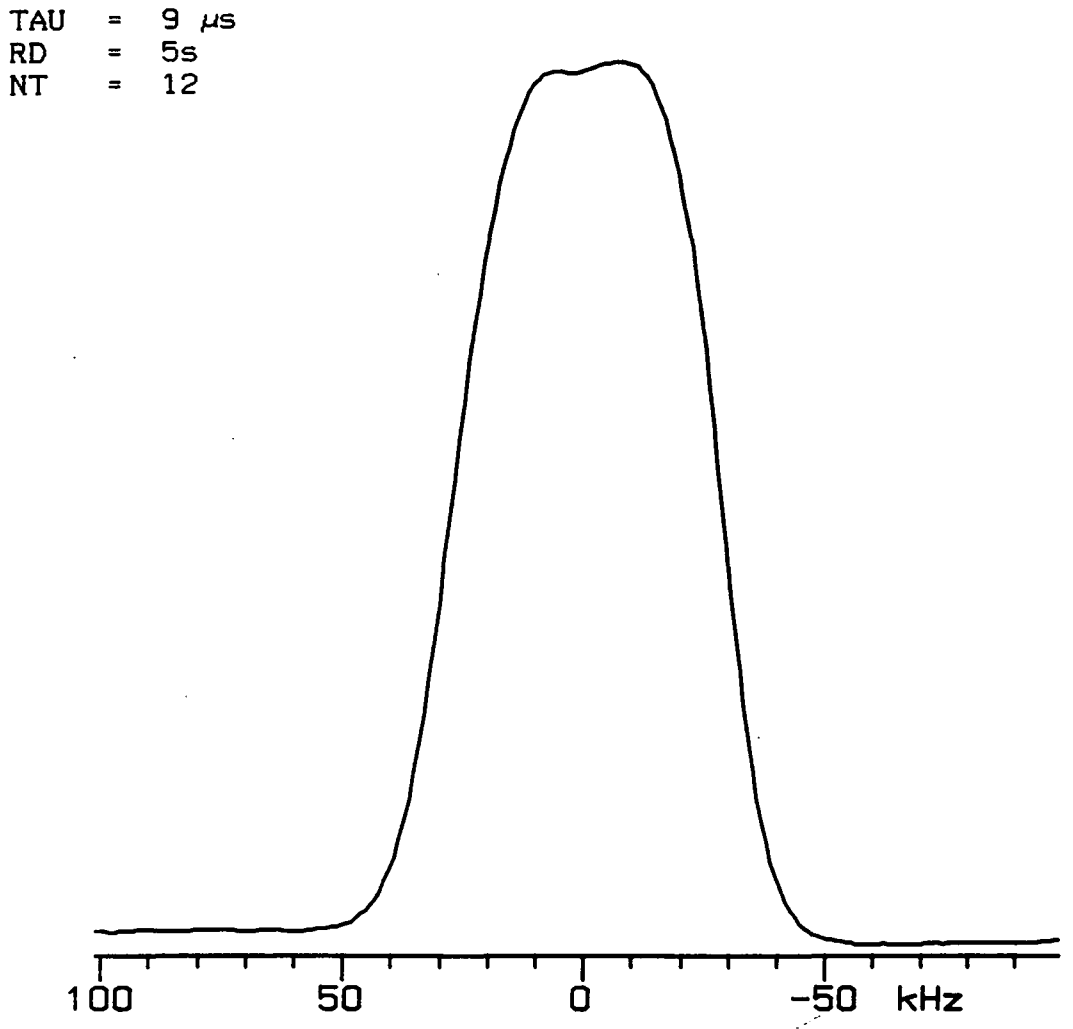

Fig (7-20) ^{1}H SE Spectrum of pure C_2H_4.

fitted to a normal Pake doublet which is presented in Fig (7.21a). It does not fit very well at the maximum nor in the base of the powder pattern; it is not due to a simple two symmetric pairs of spins. Small improvement in the fitting is observed if a function of a form[11]

$$F(t)= \exp[-(a^2t^2)](\sin bt)/bt \qquad 7.3$$

is used to fit the FID. This fitting is also presented in Fig (7.21b). The overall fit improves with only a mismatch in the intensity. There was no theoretical expression available in the fitting program which includes a four spin system.

Big changes can be observed when examining the powder pattern obtained from the deposition of the matrix sample. The SE spectrum using the slow method is presented in Fig (7.22). The first thing to notice is the total change in shape of the spectrum. It goes from a line with $\Delta\nu_{1/2}$ in the order of 50 kHz with a flat maximum to one with $\Delta\nu_{1/2}$ of about 30 kHz having a triangular type of shape. This big reduction in the line-broadening can be attributed to the reduction in the inter-molecular interactions between ethylene molecules. So, it is possible to say that what is observed in this case is mainly the intra-molecular interaction between the three different types of proton pairs. Attempts to fit the FID from this sample with a pure two pair dipolar function or with one as in eq. 7.3 gave no significant difference between the two fittings.

The results presented had shown the increase complexity of the ethylene system over the dichloromethene one. They also open the way for a more detailed investigation over this

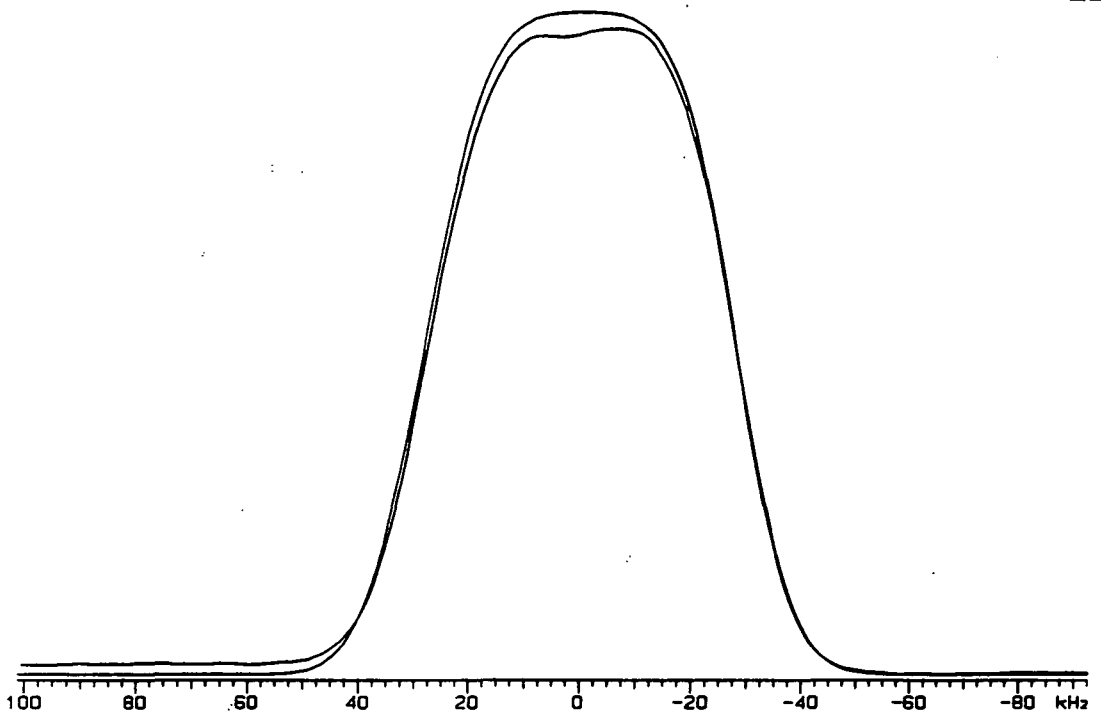

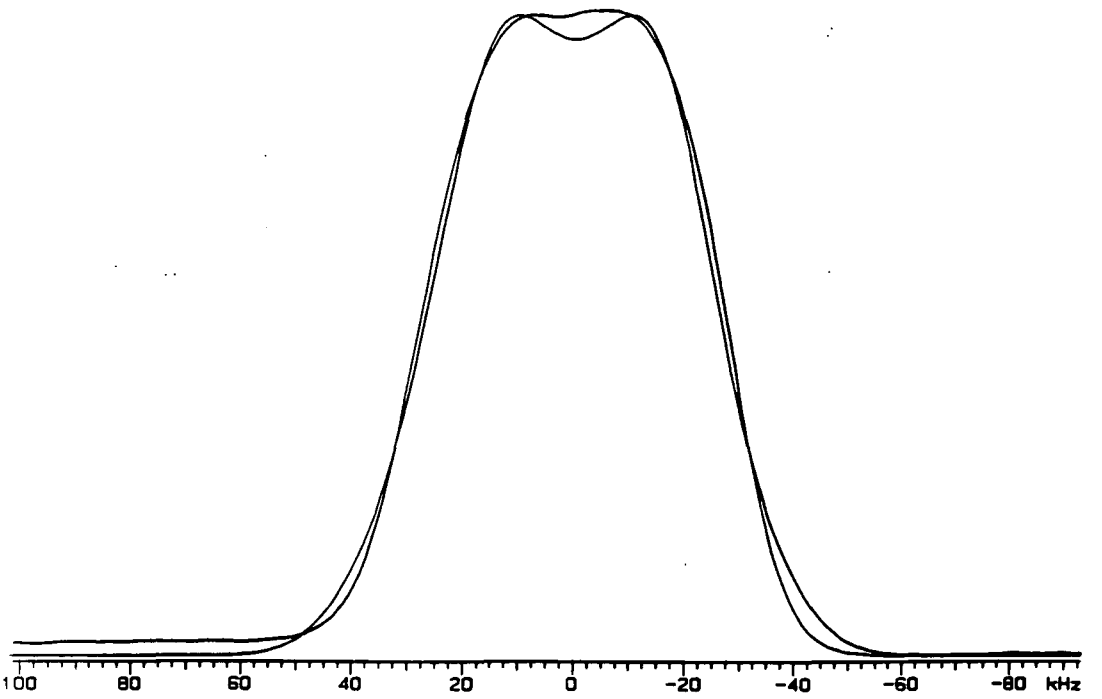

Fig (7-21) FID fit to the data in Fig (7-20) (a) Dipolar fit; (b) Fitting using expresion 7.3.

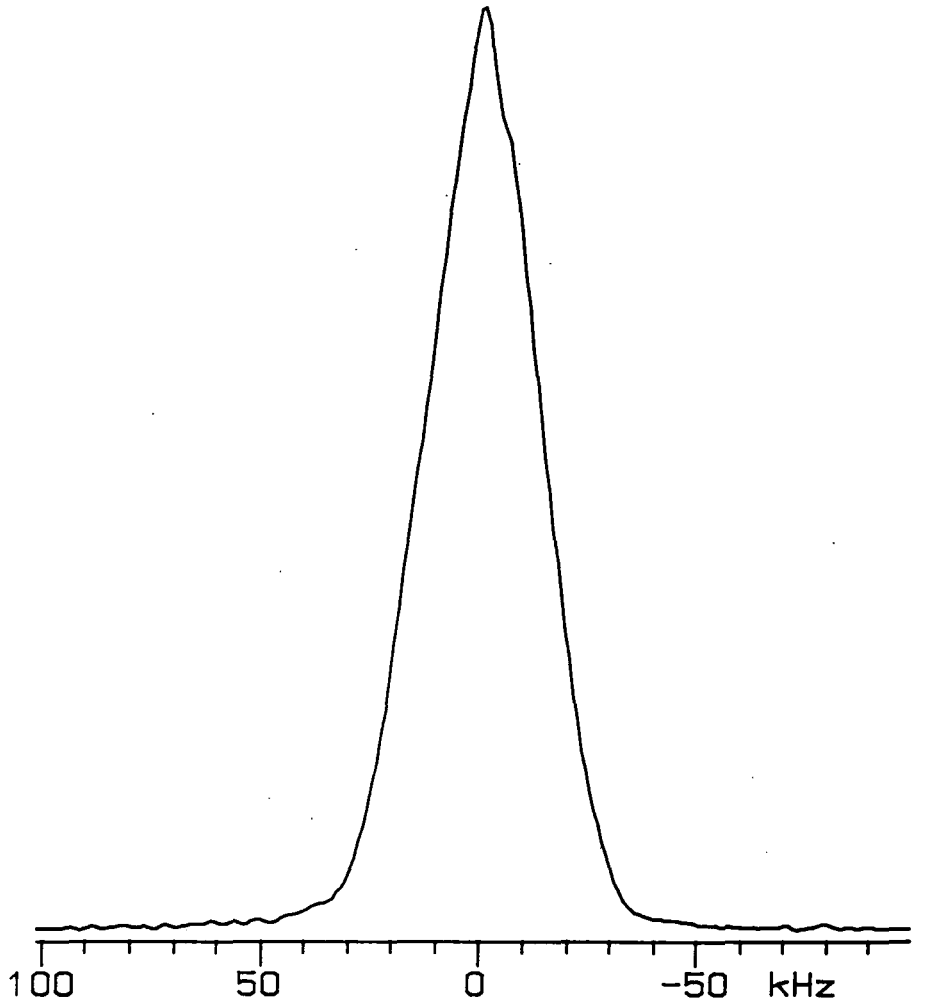

Fig (7-22) ^{1}H SE Spectrum from a Matrix-isolated sample of C_2H_4 in Ar, α = 0.022, slow deposition.

four spin system. It would also be convenient to step back and observed signals from a more simple system like $C_2H_2Cl_2$.

7.5 IMPROVEMENT TO THE NMR-CRYOGENIC SYSTEM

The design introduced in this work for the study of matrix isolated materials by NMR has proved to performed very well in the way it was planned. In particular, the system has been very efficient in reducing the time between two consecutive depositions. The system does not need to be taken apart as in other systems to make it ready for the next sample. The time is saved by avoiding the exposuse of the system to atmospheric pressure and moisture.

At the same time, it was also observed during the day to day operation of the system that there is still some room for improvement. Therefore, some new ideas will be presented in the next sections in this respect.

7.5.1 VACUUM SYSTEM MODIFICATIONS

There are two sections of the vacuum system that can be improved to reduce even further the amount of time needed to produce the high levels of vacuum. The first one is the main connection between the Displex unit at the vacuum pumps. it has been indicated in section 6.2 that in order to connect the diffusion pump with the Displex an adapter is used for the coupling. The big difference in the diameter of the vacuum

line connection and that of the diffusion pump increases the time needed to produce the high vacuum.

This limitation can be improved by modifying the vacuum shroud used to isolate the Displex unit. Fig (7.23) shows the schematic diagram of the system. It is possible to move the connecting vacuum line from A to C and increase the diameter of the line to meet the specifications of the diffusion pump. In this way, it is possible to use the maximum diameter in the vacuum line and therefore to increase the vacuum speed. This new connecting pipe can be made from copper with the appropriate connectors at both end so it can easily be dismantled.

Another section of the vacuum line that could be improved is the sample port. As was already mentioned, the NMR probe and the sample port are connected by a small diameter copper pipe. When samples are changed there is a small section of the vacuum line that is exposed to atmospheric pressure for a very short period of time. The process of evacuating this volume takes some time. This time can be reduced by modifying the sample port section. At the top of the diffusion pump there is a spacer section which includes several types of output connections. So, it is possible to run a vacuum line of appropriate diameter between one of these connections and the main isolation valve of the sample port. In this way, it is possible to isolate the small copper pipe from the sample port and evacuate the small volume exposed to air in a more direct and faster way. This will also help to reduce the time when the whole system has been exposed to air.

These two modification to the vacuum line will improve

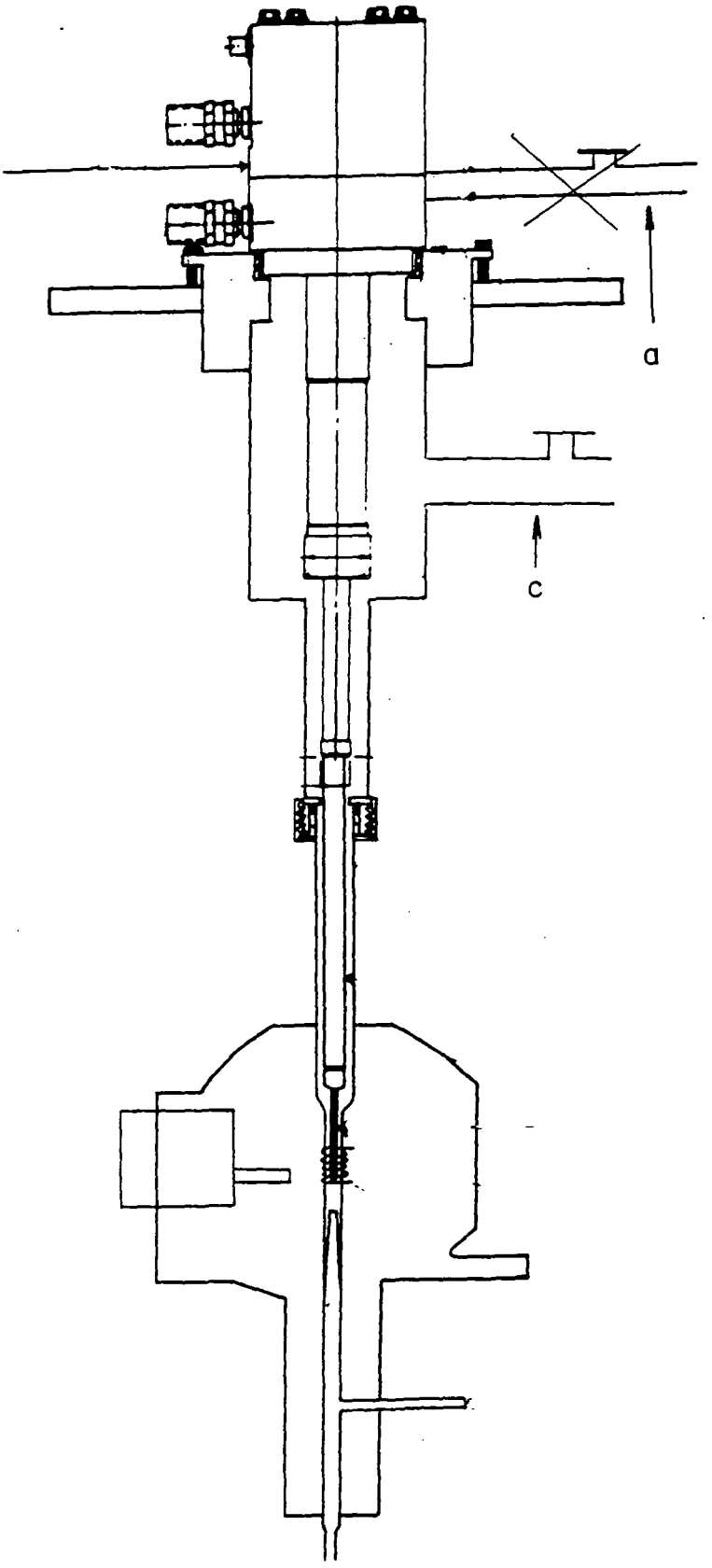

Fig (7-23) Schematic diagram of the NMR-cryogenic system.

the overall performance of the system and reduce even more the time between different sample depositions.

7.5.2 SAPPHIRE COLD FINGER MODIFICATION

As is known, the samples or matrices studied with the aid of this system are deposited in a cylindrical rod made from sapphire. The samples are blown to this area from a conical nozzle about 20 mm away from the end of the sapphire. It is possible to deduce and it has been shown in section 7.3 that a significant amount of sample can be lost from bounce off from the sapphire and from scattering from the spraying nozzle. It has also been indicated that the actual shape of the sample changes depending on the method of deposition. These effects can be minimized or eliminated by a change in the shape of the supporting surface from a sapphire rod to a sapphire with a hollow cylindrical shape having very thin walls. In this way, the spraying nozzle can be moved much closer to the supporting surface so reducing the amount of sample that could be lost. It will also guarantee a reproducible shape for the sample because it will always have to fill the cylindrical volume.

There are two disadvantages to this configuration. First, it will not be possible to visually observed the deposition process to determine if there is sufficient sample in the cavity. This problem case be overcome by observing the NMR signal from the sample as it is being deposited and determine by its strength if there is enough sample or not. Second, the fact that the sample will be inside the cylinder

will make it difficult to irradiate a mixture of samples with light in order to initiate reactions inside the matrix. For this special case, it will be necessary to use the original configuration of the sapphire to perform the experiments.

With these two arrangement it will be possible to have flexibility for different needs and types of samples. The advantage of the second configuration is that a better filling factor is used making it possible to have more sample. This will be very important if very dilute matrices are used with molar concentration below $\varkappa = 0.01$

7.5.3 OTHER NUCLEI

It has been the intention to be able to observed nuclei other than proton with this NMR spectrometer. In particular, the interest in other nuclei has been focused in the observation of signals from fluorine. As the Varian XL-100 electromagnet is not being used at the top of its range it is possible to change the field so as to detect the the fluorine signal. But, a field locking unit is still needed to avoid the drift of the frequency. Recent modification to the spectrometer has made it possible to have separate frequency sources for the lock unit and for the transmitter unit. So, it is possible to maintain all the tuning of the probe and transmitter as 60 MHz, sweep the field until the fluorine signal is detected and still use the proton lock to stabilize the field. This is done by increasing the frequency of the proton lock unit until the signal is observed from the locking

probe. This will allow the detection of the fluorine signal with the minimum of modification to the system. These modifications may involve the rebuilding of the main probe so that it would be possible to tune it between the two frequencies that at 1.4093 T are 3.554 MHz apart. It may also be required to build a second probe for the locking unit tuning and detection of a fluorine lock signal.

The suggested modification will not take much time to put in operation and will allow the detection of the signal from proton and from fluorines arising from the same deposited sample making very useful some types of investigation.

7.6 CONCLUSIONS

It was possible to complete the aim of this investigation, namely the deposition and study of matrix isolated samples by means of NMR. In particular, very interesting results were obtained from the dilution of CH_2Cl_2 in an argon matrix. It has been possible to see the reduction of the inter-molecular dipolar interaction to the benefit of a better resolution of the intra-molecular interaction. Good agreement was also shown between the inter-proton distance obtained by this method and that from the literature. The apparent dependence of the T_1 with respect to the degree of molecular isolation is an effect that needs to be followed by a further reduction of the molar fraction.

REFERENCES:

1- Powles J. G., Strange J. H., Proc. Phys. Soc., **82**, 6, (1963).

2- Mansfield P., Phys Rew., **137**(3A), A961, (1965).

3- Vold R.1, Waugh J.S., Klein M. P., Phelps D. E., J. Chem. Phys., **48, 3831,** (1968)

4- Pake G. E., J. Chem. Phys. **16** (4), 327, (1948).

5- Boden N., Levine Y. K., Lightowlers D., Squires R.T., Mol. Phys. **29,** 1877, (1975).

6- Hallam H. E., "Vibration spectroscopy of trapped species: infrared Ramman studies of matrix-isolated molecules, radicals and ions". Londom, Wiley (1973).

7- Murphy M., Semack M. G., White D., J. Mag Res., **73**, 143, (1987).

8- Kohl J. E., Semack M. G., White D., J. Chem. Phys., **69** (1), 5378, (1978).

9- Gay D., J. Mag. Res., **58**, 413, (1984).

10- Zilm K. W., Conlin R. T., Grant D., Michl J., J. Amer. Chem. Soc., **102**, 6672, (1980).

11- Abragam A., "The principles of magnetic resonance", Oxford University Press, (1978).

12- Harris R. K., "Nuclear magnetic resonance spectroscopy. A physicochemical view", Pitman books limited, 128 Long Acre, London WC2E 9AN.

13- Sherwood J. N., "The plastically crystalline state" John Wiley & Sons, Chichester-New york-Brisbane-Toronto.

14- Anderson J. E., Slichter W. P., J. Chem Phys., **41,** 1922, (1964).

15- McCall D. W., Douglass D. C., Polymer, 4, 433, (1963).

16- "Tables of interatomic distances and configuration in molecules and ions", special publication N• 11., London: The Chemical Society, Burlington House,W 1,

17- Say B., Kenwright A, Harris R. K., unpublished work.

18- Zilm K. W., Grant D., J. Amer. Chem Soc., 103, 2913, (1981).

19- Mehring M., Raber H., J. Chem. Phys., 59, 1116, (1973).

20- Gibby M. G., Pines A., Waugh J. S., J. Chem. Phys. Lett., 16, 296, (1972).

APPENDIX 7-A

OPERATOR'S MANUAL FOR WRAC ENVIRONMENT

written by Anita Patel, 1988
updated by Youssef Espidel, 1990

A. INTRODUCTION

All the commands in this manual are typed on the Archimedes Keyboard.

Before setting up the spectrometer, the first thing to be done is to create a directory specific to you into which all your results are to be recorded. For this operation consult any of the senior operators. If a directory has already been created under your name, you just type `Shift' and `Break' simultaneously.

The screen comes up with USER NAME?

Here you type your Christian name.

Then you are asked for a Results filename. Unless you are going to process some data already recorded in your directory, hit `Return'. If you wish to process data, then go to the later section on processing Results.

You will now be in WRAC.

The next stage is to tune the spectrometer, set the 90^{o} pulse and set the phases. To do this you must be in a higher level, ACQ (Acquisition).

Type ACQ.

You now have 7 options to choose from

F1 - Set up an Experiment

F2 - Show Queue

F3 - System Parameters

F4 - Tune

F6 - Process

F7 - Global

F9 - Exit

Some of these function are self explanatory. F2 will show

the list of experiments that will be executed automatically by the spectrometer. They way in which this queue is prepare can be see in section C step 3.

B. TUNING THE SPECTROMETER

1. FIND A SAMPLE.

   The first stage to tuning the spectrometer involves finding a suitable sample. In the past ethylene glycol has been used. A spinner must be placed around the tube at the correct height. This is done by measuring the tube on the marker near the magnet.

2. PLACE SAMPLE IN MAGNET.

   Lift the lid on the magnet, and place the sample-tube in the small hole.

3. SET ON RESONANCE.

   Now go back to the Keyboard.

   Type F4

   This puts you in Tuning.

   In front of you there is now a cursor flashing at SOURCE.

   Type LFID.

   Now hit `escape'.

   A screenful of parameters has appeared. You are now about to program the spectrometer.

   DEFINITIONS

   FIDLEN - Number of points in FID.

   DWELL - Time between each acquired point.

   PULSE - Length of pulse.

RECOVERY - Time allowed for instrument recovery.

RECYCLE - Time between cycles for magnetisation recovery in the sample.

Here you able to choose your own parameters. All the times are expressed in seconds, but the spectrometer will accept M(10^{-3}) and U(10^{-6}) as abbreviations. Hitting `Return' will take the cursor to each of the parameters in turn. Having chosen the parameters the next stage is to start the acquisition of the FID. To do this hit `escape'.

An FID will appear on the second monitor. This is the monitor on which the experiment is seen. If the signal is clipping, alter the two black knobs on the receiver (RH knob first) until the signal is no longer clipping.

The signal now has to be set on resonance. To your right you will find the synthesiser. Alter the frequency by turning the knobs until the signal is resonance. It may be easier to see the on resonance FID on the oscilloscope to your RHS top. Both the real and imaginary parts can be seen by typing B.

When there are no beats between the real and imaginary signal then the signal is on resonance.

To check if the signal being given is the best possible signal, take the a little way off resonance by turning the tens of Hz knob (on the synthesiser) by 1 turn. Then adjust the tuning knob on the `blue box' which is the power amplifier. The power amplifier is tuned when a maximum signal is obtained for the FID.

To stop the acquisition of the FID type H (Halt).

4. SET THE 90° PULSE.

You now have the 3 choices F1, F4 and F9.

Hit F4 again.

With the cursor on SOURCE

Type LFID

Hit `escape'.

Use the same parameters as before, but choose the pulse length to be whatever you wish the 180° pulse to be, and then hit `escape' again. The tuning experiment will start to run.

Type R.

This means that just the real part will be looked at on the 2nd monitor.

Increase the gain on the blue power amplifier until a null signal is obtained. This step may be a little tricky and take some time to do, however it is worth your while to get the best null signal possible. The best way is probably to start at gain 1, and SLOWLY increase the gain. The null signal is at the first minimum signal.

To check that this is a 180° pulse.

Type H.

Set up the same experiment again, but this time half the pulse length. Hit escape, to start the tuning experiment. If the signal is very large compared to the previous null signal you can say that you have set the 90° pulse. If there is not much difference between the null signal and the 90° pulse. If there is not much difference between the null signal and the 90° pulse -

try again!

Type H to halt the acquisition.

5. ADJUST SOFT PHASE.

Type F4, PROGRAM TP3, then escape.

Set the pulse length to the 90° pulse, and then escape to start up the experiment.

Type R.

Now only the real part is seen on the 2nd monitor.

Type P.

This enables the soft phase on the screen to be altered (i.e. the phase of the signal on the screen). The soft phase is given by the number in the top right hand corner of the screen. The two keys ↑ and ↓ change the values of the soft phase, and the keys C and F define whether you want coarse or fine adjustment. The soft phase must be altered so that the real signal starts 0 going positive.

6. ADJUST QUADRATURE.

Now Type B.

This enables both the real and imaginary parts to be displayed on the screen. The two waveforms should differ in phase by 90°. If they do not, then go to the modulator on your right-hand side. Alter the first left-hand knob marked ref-phase until the two waveforms do differ by 90°.

Now check the soft phase again to make sure that the real signal starts 0 → positive. If it does not, then adjust the soft phase as before until it does start 0 → positive.

Type H.

Now you need to check the phases of the other 3 pulses, to ensure that they are positioned 90° apart.

7. ADJUSTING PHASES.

Hit F4.

The program used is called TP0.

Hit escape, then fill in the parameters. Remember to set the pulse length to the 90° pulse length. Hit escape again to start the tuning experiment running.

Adjust the knob labelled Phase 0 on the modulator to give the real signal starting positive maximum. (Hint - it may be easier to look at the imaginary signal as well, and ensure that the imaginary signal starts on zero.)

Type H.

As before, hit F4.

This time the program used is called TP1.

Hit escape, fill out the parameters, then hit escape again. Use the knob labelled Phase I, and adjust until the real signal begins at 0 → negative.

Type H.

Similarly type F4, program TP2, etc.

This time adjust Phase II knob on the modulator to give a real signal beginning at negative maximum. (As before it is easier to adjust so that the imaginary signal starts at zero.)

Type H.

There is an extra pulse program call 'TSECH' which allows the possibility of setting the optimum parameter for the solid echo experiment.

C. SETTING UP AND RUNNING AN EXPERIMENT

STEP 1. Place your sample in the magnet as you did for the tuning sample.

STEP 2. Set the signal on resonance for your sample. In ACQ type F4 (tuning). As before, use SOURCE LFID. Hit escape. Change the parameters to suitable values, then hit escape again to set the experiment going.

Change the frequency using the knobs on the synthesiser to set the sample on resonance.

For fine adjustment there is a 3 digit counter next to the shims (top RH above power amplifier). This adjusts the frequency by small values to obtain a signal which is completely on resonance.

Check that the attenuation is not too high (i.e. the FID clips), or not too low (i.e. the signal is too low in intensity). This is done by altering the LH knob on the receiver to your right.

Type H.

Now you are really ready to go!

STEP 3. Now you must choose an experiment. A list of current pulse programs is available.

Type F9. This takes you out of ACQ back into WRAC.

Type PROGS.

The best way to get used to these pulse programs is to actually use them.

A self-explanatory list of programs should now be in front of you on screen.

As an example let us consider the measurement of ^{1}H

T1 by inversion recovery. The pulse program required is called INVREC.

We need to be in acquisition mode as before.

Type ACQ.

You now have 7 choices again.

Type F1.

Type INVREC in the program space, and hit `escape'. A list of parameters appears. As before you type in values for these parameters.

One new feature that you are now to meet is the concept of RESULTS. RESULTS needs a file name in which the data from the experiment is to be saved.

TYPICAL E.G. Let us consider an inversion recovery measurement on a sample X. Let us call the results file INVRECT1X.

SOURCE PROGRAM INVREC RESULTS INVRECT1X

SAMPLE X

COMMENT T1 BY INVERSION RECOVERY

TEMP (K) RT

	e.g. value	definition
AVERAGES	4	Number of averages
POINTS	350	Number of points acquired each average
PULSE	2E-6	Length of 90° pulse
TAU	0.027	Length of delay before Acquisition
RECOVERY	1.5 E-5	Delay to allow for instrument dead-time
RECYCLE	10	Delay for sample recovery (> 5T1)

As before `escape' reads in your values.

The program will then invite you to set up another experiment.

If you type No (N) to this question, you will then have a choice of F1, F4, F8, F9.

You may start the experiment whenever you choose by typing F8.

The system allows for stacking of experiments. this is a queue of experiments which will be executed one after another without you, the operator, having to be present.

To stack another experiment on top of the previous one, which we have just set up, Type Y to the Question `Another?'.

The program asks you if you want the experiment to be contiguous. If you type Y, then a queue will be formed. You will then be asked if you wish to set up another experiment. If Y, then the screen reappears blank. You may stack up as many experiments as you wish in this way.

Type F8 to stack the experiment or queue of experiments.

If at any time you wish to destroy the queue of experiments you have stacked up, you must type F9. This takes you out of ACQ and into WRAC.

Type Kill Q.

A question will be asked to ensure that you do really want to destroy your queue. If Y, then the existing queue is destroyed. To go back into ACQ, type ACQ.

One other point which it is important to mention is that it is possible to bring back old parameters from a previous experiment, to use in another experiment.

Let us say that you have run the T1 experiment on the sample X, and have stored the data in Results file INVRECT1X. Now you wish to run a T1 experiment on a similar sample Y. It is possible to recall the exact parameters which you used.

Type F1, to set up an experiment.

There is one part of the setting-up display you have not used yet, and that is SOURCE.

The source file is the old results file from which you have not used yet, and that is SOURCE.

The source file is the old results file from which you wish to recall the parameters.

For example if you typed INVRECT1X in the space provided for the source file, and typed 'escape', all the conditions used for the experiment on sample X would be displayed on the screen. All that would be left for you to do would be to type in a results file which you want the results of the experiment on sample Y to go into, so the top line on the screen would read:

SOURCE INVRECT1X PROGRAM INVREC RESULTS INVRECT1Y

The experiment is started in exactly the same way as before:

If at any stage you wish to exit from setting

up and experiment, type Ctrl Q.

Mission Control

Whilst the experiment is running, there is a function F5 called mission control.

Type F5, and you will be confronted with a lot of options. The best way for you to find what happens is to try them out for yourself.

APPENDIX 7-B

The Board of Studies in Chemistry requires that each postgraduate research thesis contains an appendix which lists:

a) all research colloquia and research seminars and lectures arranged by the Department of Chemistry and Durham University Chemistry Society during the author's residence as postgraduate student;

b) all research conferences attended and papers given by the author during the same period;

c) details of the postgraduate induction course.

UNIVERSITY OF DURHAM

Board of Studies in Chemistry

COLLOQUIA, LECTURES AND SEMINARS GIVEN BY INVITED SPEAKERS 1ST AUGUST 1986 TO 31ST JULY 1987

ALLEN, Prof. Sir G. (Unilever Research) Biotechnology and the Future of the Chemical Industry	13th November 1986
BARTSCH, Dr. R. (University of Sussex) Low Co-ordinated Phosphorus Compounds	6th May 1987
BLACKBURN, Dr. M. (University of Sheffield) Phosphonates as Analogues of Biological Phosphate Esters	27th May 1987
BORDWELL, Prof. F.G. (Northeastern University, U.S.A.) Carbon Anions, Radicals, Radical Anions and Radical Cations	9th March 1987
CANNING, Dr. N.D.S. (University of Durham) Surface Adsorption Studies of Relevance to Heterogeneous Ammonia Synthesis	26th November 1986
CANNON, Dr. R.D. (University of East Anglia) Electron Transfer in Polynuclear Complexes	11th March 1987
CLEGG, Dr. W. (University of Newcastle-upon-Tyne) Carboxylate Complexes of Zinc; Charting a Structural Jungle	28th January 1987
DÖPP, Prof. D. (University of Duisburg) Cyclo-additions and Cyclo-reversions Involving Captodative Alkenes	5th November 1986
DORFMÜLLER, Prof. T. (University of Bielefeld) Rotational Dynamics in Liquids and Polymers	8th December 1986
GOODGER, Dr. E.M. (Cranfield Institute of Technology) Alternative Fuels for Transport	12th March 1987
GREENWOOD, Prof. N.N. (University of Leeds) Glorious Gaffes in Chemistry	16th October 1986
HARMER, Dr. M. (I.C.I. Chemicals & Polymer Group) The Role of Organometallics in Advanced Materials	7th May 1987
HUBBERSTEY, Dr. P. (University of Nottingham) Demonstration Lecture on Various Aspects of Alkali Metal Chemistry	5th February 1987
HUDSON, Prof. R.F. (University of Kent) Aspects of Organophosphorus Chemistry	17th March 1987
HUDSON, Prof. R.F. (University of Kent) Homolytic Rearrangements of Free Radical Stability	18th March 1987

JARMAN, Dr. M. (Institute of Cancer Research) The Design of Anti Cancer Drugs	19th February 1987
KRESPAN, Dr. C. (E.I. Dupont de Nemours) Nickel(0) and Iron(0) as Reagents in Organofluorine Chemistry	26th June 1987
KROTO, Prof. H.W. (University of Sussex) Chemistry in Stars, between Stars and in the Laboratory	23rd October 1986
LEY, Prof. S.V. (Imperial College) Fact and Fantasy in Organic Synthesis	5th March 1987
MILLER, Dr. J. (Dupont Central Research, U.S.A.) Molecular Ferromagnets; Chemistry and Physical Properties	3rd December 1986
MILNE/CHRISTIE, Dr. A./Mr. S. (International Paints) Chemical Serendipity - A Real Life Case Study	20th November 1986
NEWMAN, Dr. R. (University of Oxford) Change and Decay: A Carbon-13 CP/MAS NMR Study of Humification and Coalification Processes	4th March 1987
OTTEWILL, Prof. R.H. (University of Bristol) Colloid Science a Challenging Subject	22nd January 1987
PASYNKIEWICZ, Prof. S. (Technical University, Warsaw) Thermal Decomposition of Methyl Copper and its Reactions with Trialkylaluminium	11th May 1987
ROBERTS, Prof. S.M. (University of Exeter) Synthesis of Novel Antiviral Agents	24th June 1987
RODGERS, Dr. P.J. (I.C.I. Billingham) Industrial Polymers from Bacteria	12th February 1987
SCROWSTON, Dr. R.M. (University of Hull) From Myth and Magic to Modern Medicine	6th November 1986
SHEPHERD, Dr. T. (University of Durham) Pteridine Natural Products; Synthesis and Use in Chemotherapy	11th February 1987
THOMSON, Prof. A. (University of East Anglia) Metalloproteins and Magnetooptics	4th February 1987
WILLIAMS, Prof. R.L. (Metropolitan Police Forensic Science) Science and Crime	27th November 1987
WONG, Prof. E.H. (University of New Hampshire, U.S.A.) Coordination Chemistry of P-O-P Ligands	29th October 1986
WONG, Prof. E.H. (University of New Hampshire, U.S.A.) Symmetrical Shapes from Molecules to Art and Nature	17th February 1987

UNIVERSITY OF DURHAM

Board of Studies in Chemistry

COLLOQUIA, LECTURES AND SEMINARS GIVEN BY INVITED SPEAKERS
1ST AUGUST 1987 to 31st JULY 1988

BIRCHALL, Prof. D. (I.C.I. Advanced Materials) Environmental Chemistry of Aluminium	25th April 1988
BORER, Dr. K. (University of Durham Industrial Research Labs.) The Brighton Bomb - A Forensic Science View	18th February 1988
BOSSONS, L. (Durham Chemistry Teachers' Centre) GCSE Practical Assessment	16th March 1988
BUTLER, Dr. A.R. (University of St. Andrews) Chinese Alchemy	5th November 1987
CAIRNS-SMITH, Dr. A. (Glasgow University) Clay Minerals and the Origin of Life	28th January 1988
DAVIDSON, Dr. J. (Herriot-Watt University) Metal Promoted Oligomerisation Reactions of Alkynes	November 1987
GRADUATE CHEMISTS (Northeast Polytechnics and Universities) R.S.C. Graduate Symposium	19th April 1988
GRAHAM, Prof. W.A.G. (University of Alberta, Canada) Rhodium and Iridium Complexes in the Activation of Carbon-Hydrogen Bonds	3rd March 1988
GRAY, Prof. G.W. (University of Hull) Liquid Crystals and their Applications	22nd October 1987
HARTSHORN, Prof. M.P. (University of Canterbury, New Zealand) Aspects of Ipso-Nitration	7th April 1988
HOWARD, Dr. J. (I.C.I. Wilton) Chemistry of Non-Equilibrium Processes	3rd December 1987
LUDMAN, Dr. C.J. (Durham University) Explosives	10th December 1987
McDONALD, Dr. W.A. (I.C.I. Wilton) Liquid Crystal Polymers	11th May 1988
MAJORAL, Prof. J.-P. (Université Paul Sabatier) Stabilisation by Complexation of Short-Lived Phosphorus Species	8th June 1988
MAPLETOFT, Mrs. M. (Durham Chemistry Teachers' Centre) Salters' Chemistry	4th November 1987
NIETO DE CASTRO, Prof. C.A. (University of Lisbon and Imperial College) Transport Properties of Non-Polar Fluids	18th April 1988

OLAH, Prof. G.A. (University of Southern California) — 29th June, 1988
New Aspects of Hydrocarbon Chemistry)

PALMER, Dr. F. (University of Nottingham) — 21st January 1988
Luminescence (Demonstration Lecture)

PINES, Prof. A. (University of California, Berkeley, U.S.A.) — 28th April 1988
Some Magnetic Moments

RICHARDSON, Dr. R. (University of Bristol) — 27th April 1988
X-Ray Diffraction from Spread Monolayers

ROBERTS, Mrs. E. (SATRO Officer for Sunderland) — 13th April 1988
Talk - Durham Chemistry Teachers' Centre - "Links Between Industry and Schools"

ROBINSON, Dr. J.A. (University of Southampton) — 27th April 1988
Aspects of Antibiotic Biosynthesis

ROSE van Mrs. S. (Geological Museum) — 29th October 1987
Chemistry of Volcanoes

SAMMES, Prof. P.G. (Smith, Kline and French) — 19th December 1987
Chemical Aspects of Drug Development

SEEBACH, Prof. D. (E.T.H. Zurich) — 12th November 1987
From Synthetic Methods to Mechanistic Insight

SODEAU, Dr. J. (University of East Anglia) — 11th May 1988
Durham Chemistry Teachers' Centre Lecture: "Spray Cans, Smog and Society"

SWART, Mr. R.M. (I.C.I.) — 16th December 1987
The Interaction of Chemicals with Lipid Bilayers

TURNER, Prof. J.J. (University of Nottingham) — 11th February 1988
Catching Organometallic Intermediates

UNDERHILL, Prof. A. (University of Bangor) — 25th February 1988
Molecular Electronics

WILLIAMS, Dr. D.H. (University of Cambridge) — 26th November 1987
Molecular Recognition

WINTER, Dr. M.J. (University of Sheffield) — 15th October 1987
Pyrotechnics (Demonstration Lecture)

UNIVERSITY OF DURHAM

Board of Studies in Chemistry

COLLOQUIA, LECTURES AND SEMINARS GIVEN BY INVITED SPEAKERS
1ST AUGUST 1988 to 31st JULY 1989

ASHMAN, Mr. A. (Durham Chemistry Teachers' Centre) — 3rd May, 1989
The Chemical Aspects of the National Curriculum

AVEYARD, Dr. R. (University of Hull) — 15th March, 1989
Surfactants at your Surface

AYLETT, Prof. B.J. (Queen Mary College, London) — 16th February, 1989
Silicon-Based Chips:- The Chemist's Contribution

BALDWIN, Prof. J.E. (Oxford University) — 9th February, 1989
Recent Advances in the Bioorganic Chemistry of Penicillin Biosynthesis

BALDWIN & WALKER, Drs. R.R. & R.W. (Hull University) — 24th November, 1988
Combustion: Some Burning Problems

BOLLEN, Mr. F. (Durham Chemistry Teachers' Centre) — 18th October, 1988
Lecture about the use of SATIS in the classroom

BUTLER, Dr. A.R. (St. Andrews University) — 15th February, 1989
Cancer in Linxiam: The Chemical Dimension

CADOGAN, Prof. J.I.G. (British Petroleum) — 10th November, 1988
From Pure Science to Profit

CASEY, Dr. M. (University of Salford) — 20th April, 1989
Sulphoxides in Stereoselective Synthesis

WATERS & CRESSEY, Mr. D. & T. (Durham Chemistry Teachers' Centre) — 1st February, 1989
GCSE Chemistry 1988: "A Coroner's Report"

CRICH, Dr. D. (University College London) — 27th April, 1989
Some Novel Uses of Free Radicals in Organic Synthesis

DINGWALL, Dr. J. (Ciba Geigy) — 18th October, 1988
Phosphorus-containing Amino Acids: Biologically Active Natural and Unnatural Products

ERRINGTON, Dr. R.J. (University of Newcastle-upon-Tyne) — 1st March, 1989
Polymetalate Assembly in Organic Solvents

FREY, Dr. J. (Southampton University) — 11th May, 1989
Spectroscopy of the Reaction Path: Photodissociation Raman Spectra of NOCl

HALL, Prof. L.D. (Addenbrooke's Hospital, Cambridge) — 2nd February, 1989
NMR - A Window to the Human Body

HARDGROVE, Dr. G. (St. Olaf College, U.S.A.) — December, 1988
Polymers in the Physical Chemistry Laboratory

HARWOOD, Dr. L. (Oxford University) — 25th January, 1988
Synthetic Approaches to Phorbols Via Intramolecular Furan Diels-Alder Reactions: Chemistry under Pressure

JÄGER, Dr. C. (Friedrich-Schiller University GDR) — 9th December, 1988
NMR Investigations of Fast Ion Conductors of the NASICON Type

JENNINGS, Prof. R.R. (Warwick University) — 26th January, 1989
Chemistry of the Masses

JOHNSON, Dr. B.F.G. (Cambridge University) — 23rd February, 1989
The Binary Carbonyls

JONES, Dr. M.E. (Durham Chemistry Teachers' Centre) — 14th June, 1989
Discussion Session on the National Curriculum

JONES, Dr. M.E. (Durham Chemistry Teachers' Centre) — 28th June, 1989
GCSE and A Level Chemistry 1989

LUDMAN, Dr. C.J. (Durham University) — 18th October, 1988
The Energetics of Explosives

MACDOUGALL, Dr. G. (Edinburgh University) — 22nd February, 1989
Vibrational Spectroscopy of Model Catalytic Systems

MARKO, Dr. I. (Sheffield University) — 9th March, 1989
Catalytic Asymmetric Osmylation of Olefins

McLAUCHLAN, Dr. K.A. (University of Oxford) — 16th November, 1988
The Effect of Magnetic Fields on Chemical Reactions

MOODY, Dr. C.J. (Imperial College) — 17th May, 1989
Reactive Intermediates in Heterocyclic Synthesis

MORTIMER, Dr. C. (Durham Chemistry Teachers' Centre) — 14th December, 1988
The Hindenberg Disaster - an Excuse for Some Experiments

NICHOLLS, Dr. D. (Durham Chemistry Teachers' Centre) — 11th July, 1989
Demo. "Liquid Air"

PAETZOLD, Prof. P. (Aachen) — 23rd May, 1989
Iminoboranes XB≡NR: Inorganic Acetylenes?

PAGE, Dr. P.C.B. (University of Liverpool) — 3rd May, 1989
Stereocontrol of Organic Reactions Using 1,3-dithiane-1-oxides

POLA, Prof. J. (Czechoslovak Academy of Sciences) 15th June, 1989
Carbon Dioxide Laser Induced Chemical Reactions - New Pathways in Gas-Phase Chemistry

REES, Prof. C.W. (Imperial College London) 27th October, 1988
Some Very Heterocyclic Compounds

REVELL, Mr. P. (Durham Chemistry Teachers' Centre) 14th March, 1989
Implementing Broad and Balanced Science 11-16

SCHMUTZLER, Prof. R. (Technische Universitat Braunschweig) 6th October, 1988
Fluorophosphines Revisited - New Contributions to an Old Theme

SCHROCK, Prof. R.R. (M.I.T.) 13th February, 1989
Recent Advances in Living Metathesis

SINGH, Dr. G. (Teesside Polytechnic) 9th November, 1988
Towards Third Generation Anti-Leukaemics

SNAITH, Dr. R. (Cambridge University) 1st December, 1988
Egyptian Mummies: What, Where, Why and How?

STIBR, Dr. R. (Czechoslovak Academy of Sciences) 16th May, 1989
Recent Developments in the Chemistry of Intermediate-Sited Carboranes

VON RAGUE SCHLEYER, Prof. P. (Universitat Erlangen Nurnberg) 21st October, 1988
The Fruitful Interplay Between Calculational and Experimental Chemistry

WELLS, Prof. P.B. (Hull University) 10th May, 1989
Catalyst Characterisation and Activity

CONFERENCES ATTENDED:

1) "Air sensitive sample insert", Bruker users' meeting, Coventry, England, 14th of November, 1988.

2) "Spectrometer design and NMR studies of matrix isolated materials", Poster presentation, Ninth international NMR meeting, University of Warwick, England, July, 1989.

PUBLICATIONS

1) "An airtight, inexpensive, easy-to-use MAS rotor insert", Merwin L.W., Sebald A., ESPIDEL, J., Harris R.K. J. Mag. Res. 84, 367, (1989).

2) Cryogenic NMR: spectrometer design for studies of matrix-isolated materials", ESPIDEL J., Harris R.K. to be published.

POSTGRADUATE INDUCTION COURSE, OCTOBER 1986:

1) Departmental organasation.
2) Safety matters.
3) Electrical appliances and infrared spectroscopy.
4) Chromatography and microanalysis.
5) Atomic absorptiometry and inorganic analysis.
6) Library facilities.
7) Mass spectroscopy.
8) Nuclear magnetic resonance spectroscopy.
9) Glassblowing techniques.